

# Synthesis, Functionalization, and Design of Magnetic Nanoparticles for Theranostic Applications

Jalal Mosayebi, Mehdi Kiyasatfar,\* and Sophie Laurent

In order to translate nanotechnology into medical practice, magnetic nanoparticles (MNPs) have been presented as a class of non-invasive nanomaterials for numerous biomedical applications. In particular, MNPs have opened a door for simultaneous diagnosis and brisk treatment of diseases in the form of theranostic agents. This review highlights the recent advances in preparation and utilization of MNPs from the synthesis and functionalization steps to the final design consideration in evading the body immune system for therapeutic and diagnostic applications with addressing the most recent examples of the literature in each section. This study provides a conceptual framework of a wide range of synthetic routes classified mainly as wet chemistry, state-of-the-art microfluidic reactors, and biogenic routes, along with the most popular coating materials to stabilize resultant MNPs. Additionally, key aspects of prolonging the half-life of MNPs via overcoming the sequential biological barriers are covered through unraveling the biophysical interactions at the bio–nano interface and giving a set of criteria to efficiently modulate MNPs' physicochemical properties. Furthermore, concepts of passive and active targeting for successful cell internalization, by respectively exploiting the unique properties of cancers and novel targeting ligands are described in detail. Finally, this study extensively covers the recent developments in magnetic drug targeting and hyperthermia as therapeutic applications of MNPs. In addition, multi-modal imaging via fusion of magnetic resonance imaging, and also innovative magnetic particle imaging with other imaging techniques for early diagnosis of diseases are extensively provided.

## 1. Introduction

Nanotechnology as a promising strategy has successfully allowed for an unprecedented resolve of a wide range of impasses incurred in science. Surprisingly, intersection of nanotechnology with biology has enabled a superb thrust for active developments in an emerging field, termed as nanobiotechnology.<sup>[1]</sup> To this end, nanoscale particles have been considered as an important class of biomaterials to unleash

the potential of nanobiotechnology in the form of various functional agents for biomedical applications. In particular, by exploiting the unique properties of nanoparticles the ideal notion of simultaneous therapeutic and diagnostic applications has been made practical on a single so called "theranostic" agent.<sup>[2]</sup>

Among the broad spectrum of nanoparticles, magnetic nanoparticles (MNPs) have attracted a significant attention to be investigated as an appropriate and practical theranostic platform.<sup>[3]</sup> To this end, MNPs have to embark a long journey from the first steps of synthesis and functionalization to the final modulation for biomedical applications (Figure 1). Synthesizing MNPs, magnetic cores with appropriate coating shells are the undoubtedly primary components. Superparamagnetic iron oxide nanoparticles (SPION) have received a wide range of attentions due to their unique properties of being biodegradable and biocompatible to serve as scaffolds for building theranostic agents. Such magnetic cores render the theranostic agents trackable which come in handy for mapping and steering them to the specific site of disease.<sup>[4]</sup> While magnetotactic bacteria contain biogenic MNPs in the form of iron oxide and greigite,<sup>[5]</sup> there are chemical<sup>[6]</sup> and mechanical<sup>[7]</sup> routes to prepare synthetic MNPs. In particular, state-of-the-art microfluidic reactors have been extensively exploited to produce suitable MNPs with appropriate physicochemical properties for biomedical applications.<sup>[8]</sup> The presence of a coating shell on the surface of MNPs is a prerequisite to stabilize them in the colloid during their maintenance and promotes favorable interactions between the MNPs and the biological system. Different organic and inorganic coatings including silica, gold, small molecules, synthetic and natural polymers, or copolymers have been investigated.<sup>[9]</sup>

Furthermore, since such nanoparticles are implemented within a very complex system of body, a set of design criteria should be fulfilled to engineer MNPs for both prolonging the blood circulation time and promoting better interaction with the vascular wall.<sup>[10]</sup> In fact, the physicochemical properties of MNPs, such as size, shape, surface charge, and hydrophobicity should be greatly modulated to evade the immune system of the body and undergo a successful endocytosis process.<sup>[11]</sup> In the matter of evading the body immune system, large nanoparticles

J. Mosayebi, Dr. M. Kiyasatfar  
Department of Mechanical Engineering  
Urmia University  
Urmia 5756151818, Iran  
E-mail: m.kiyasatfar@gmail.com

Prof. S. Laurent  
Laboratory of NMR and Molecular Imaging  
University of Mons  
Mons Belgium

DOI: 10.1002/adhm.201700306

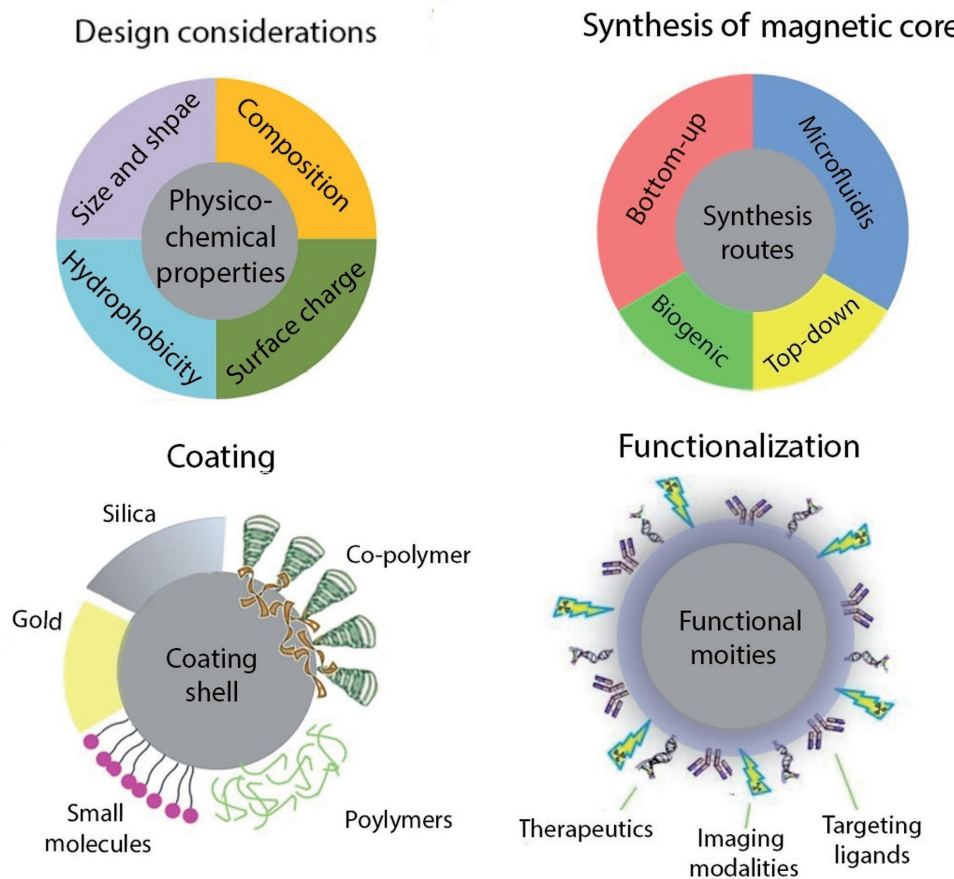


**Figure 1.** Different steps to design magnetic nanoparticles for theranostic applications.

are readily taken by the reticuloendothelial system (RES), and also increase the chances of vessel embolism.<sup>[12]</sup> On the other hand, very small nanoparticles can be renally excreted from the body due to small pores of the basal lamina of kidney,  $\approx 10$  nm sized.<sup>[13]</sup> Furthermore, hydrophobic and negatively charged surface of nanoparticles make them prone to the adsorption of opsonin proteins which alters their chemical identity and makes them more visible to phagocytic cells and removal of the body. Hence, a wide range of polymeric and biomimetic coatings as well as zwitterionic molecules have been shown promising to reduce the hydrophobicity of nanoparticles and inhibit the formation of protein corona.<sup>[14]</sup> In addition to evading the RES, cellular internalization of nanoparticles is also highly affected by their size and shape. Although larger nanoparticles increase the propensity of migration near the vascular wall, their chance to be taken up by tumor cells may be decreased.<sup>[15]</sup> Additionally, compared to spherical nanoparticles, elongated and disk-like nanoparticles have shown better cellular uptake due to exhibiting larger lateral drift velocities and lowering the hydrodynamic forces.<sup>[16]</sup>

Within this last step, functionalization of MNPs to prepare a practical theranostic agent takes place by loading targeting ligands, imaging modalities and also therapeutics via conjugating them on the surface of MNPs by encapsulating them within the coating shell.<sup>[10,17]</sup> The presence of targeting ligands is beneficial to increase the MNPs affinity toward the specific

site of disease.<sup>[18]</sup> Types of specific coating as well as diagnostic and therapeutic payloads highly depend on the end therapeutic and/or diagnostic applications which not only determine the nature of surface coatings and the final size of the MNPs, but also have a great impact on biokinetics and biodistribution of MNPs in the body.<sup>[14]</sup>

In the matter of diagnostic applications, MNPs can serve as potential contrast agents for MRI,<sup>[19]</sup> as well as novel tracers for magnetic particle imaging (MPI).<sup>[20]</sup> Furthermore, MNPs enable a successful dual/three-modal imaging by serving as workhorses to load other imaging modalities, such as positron emission tomography (PET),<sup>[21]</sup> optical,<sup>[22]</sup> single photon emission tomography (SPECT),<sup>[23]</sup> computed tomography (CT),<sup>[24]</sup> and photoacoustic<sup>[25]</sup> imaging techniques. On the other hand, numerous therapeutic applications of MNPs have been widely investigated during the last decades. Thermal ablation and hyperthermia,<sup>[26]</sup> targetable drug delivery,<sup>[27]</sup> tissue engineering,<sup>[28]</sup> gene delivery (transfection),<sup>[29]</sup> cell or DNA purification and separation<sup>[30]</sup> are of some most important therapeutic applications facilitated by the novel MNP theranostic agents.

In this review, the most recent advances to prepare theranostic agents will be described. The review will start with a conceptual framework of a wide range of synthetic routes classified as wet-chemistry, microfluidic reactors, and biogenic routes along with the recent examples of the literature which is, to the best of our knowledge, provided for the first time. This section

will be followed by describing the exigencies and approaches of coating MNPs as well as pros and cons of different types of coating materials. Within the next section, we will provide a better understanding of the *in vivo* behavior of MNPs along with a set of criteria to overcome the biological barriers in order to prolong their blood circulation time. This section will be followed by unraveling the fundamentals of passive and active targeting by taking advantage of EPR and targeting ligands to increase the propensity in going through the cell's gate to perform their designated function. Finally, we will provide information on magnetic drug targeting and hyperthermia as two of the most popular therapeutic applications of MNPs. Furthermore, extensive information on the superb potential of MNPs for state-of-the-art multi-modal imaging via fusion of MRI and MPI with other imaging techniques will be described in detail.

## 2. Synthesis of MNPs

Numerous synthetic routes have been developed to produce MNPs with good control of shape, size, and distribution. Furthermore, the synthesis method determines the way of coating MNPs, whether by an *in situ* or a post processing method.<sup>[31]</sup> Broadly speaking, the batch production of magnetic core of MNPs, which is iron oxide in most cases, can be performed either by top-down or bottom-up techniques. Lots of different mechanical and physical techniques such as ultrasonication, irradiation, laser ablation, microwave and electrochemical, and physical vapor deposition are used in top down approaches to produce MNPs by "green" methods.<sup>[32]</sup> In particular, these environmental friendly methods consist of transforming the bulk phase material into nanometer sized.<sup>[33]</sup> Top-down options are preferred in industry because they are simpler, less expensive, and easy to scale up the production. Although it is a viable green technique and requires limited manual operation,<sup>[34]</sup> particles functionalization will be more problematic and the resultant NPs through these inexpensive routes will be in a wide distribution of size and shapes<sup>[35]</sup> which directly limit their utilization for biological applications. On the other hand, bottom up techniques (also known as wet chemistry routes) refer to the chemical synthesis of nanoparticles wherein the primary nucleation of nanomaterials followed by growth and aggregation will finally result in desired nanoparticles with specific size and shapes.<sup>[36]</sup> In addition to batch production by conventional top-down and bottom-up approaches, microfluidic reactors and biogenic synthesis have also been widely exploited to improve the quality of MNPs (Figure 2).

A qualitative comparison of these three synthetic routes is provided in Table 1. Wet chemistry routes lead to the batch production of nanoparticles by exploiting macro-scale equipment to perform the reaction process. These conventional routes are more energy consuming compared to microfluidics (MF) and biogenic synthesis of MNPs. Furthermore, controlling the determining factors of size, shape, and morphology are also more difficult. In contrast with batch synthesis, with microfluidic manipulations, all the laboratory is miniaturized on a single small chip that handles whole reaction process for the synthesis of nanoparticles. These novel systems offer a good mixing of reagents in microchannels to produce high quality

MNPs with controlled shape and size. Continuous production parallel to the automation of the process is of the distinct advantages offered by microfluidic systems.<sup>[37]</sup> Last but not least, a lot of efforts have been directed to biogenic synthesis of MNPs by exploiting magnetotactic bacteria, its pioneering protein (Mms6), fungi, and ferroxidase to produce nanoparticles under mild conditions. These routes are advantageous in terms of being very low energy consuming and providing high qualified MNPs with narrow size distribution.<sup>[38]</sup>

Practical manipulation of bio-nanomaterials in theranostic applications highly owes to fulfilling a range of prerequisites related to their shape, size, and crystal structure. To this point, a series of anatomical size restrictions exerted by renal ultrafiltration in kidney, and other organs such as spleen and liver makes it compulsory for the nanoparticles to have a narrow size distribution for eluding such physiological barriers. On the other hand, since magnetic property of MNPs render them trackable and capable for therapeutic applications such as hyperthermia and magnetic drug targeting, it will be necessary to ensure the uniformity of all nanoparticles for a predictable and concordant respond to the magnetic field. In the matter of MNPs nanoparticles which comprise transition metals such as iron, a self-assembling process occurs wherein metal solutes nucleate, grow and agglomerate into nanoclusters (Figure 3a).<sup>[39]</sup> For a better control of reaction, understanding both kinetics and thermodynamics of the reaction is critical.<sup>[40]</sup> Reagent concentration, reaction temperature and residence time are of the most critical factors in controlling the size, crystallinity, and shape of the resultant nanoparticles (Figure 3b).<sup>[41]</sup> Following the primary nucleation of nanoparticles, critical growth parameters such as surface energy and growth rate along with the factors mentioned determine the final shape of the resultant nanoparticles during the crystal growth.<sup>[42]</sup> Presence of a homogenous reaction environment followed by ultrafast mixing along with controlling the mixing time of reagents can lead to the fabrication of nanoparticles desired properties.<sup>[43]</sup> Despite the widespread utilization of wet-chemistry routes, they still suffer from some inherent properties to control the mentioned factors which results in uneven mixing and local temperature fluctuations.<sup>[44]</sup> For instance, although the coprecipitation method offers a good control over the shape and phase uniformity of nanoparticles,<sup>[45]</sup> maintaining and controlling the product homogeneity is problematic and needs multipurification steps for obtaining stable monodisperse nanoparticles.<sup>[46]</sup> However, pH, the ratio of salts and the nature of the base can be regulated for a better control over the reaction.<sup>[47]</sup> On the other hand, type of precursor and surfactant, their relative ratio and solvent within the thermal decomposition have significant effects on the quality of the final product, nevertheless, tuning of the nanoparticles' shape is still remaining.<sup>[48]</sup> Moreover, confined growth due to the use of surfactants and polymers is one drawback of these methods and is an area for improvement.<sup>[49]</sup>

In contrast, microfluidic devices offer a potential controlling ability over the mixing time, reaction temperature, and concentration of reagents which directly results in preparation of nanoparticles with narrower size distribution.<sup>[50]</sup> In fact, by performing the reaction by means of fluid flows that are geometrically constrained within microenvironments, smaller volumes of reagents will be used in a continuous safer process which

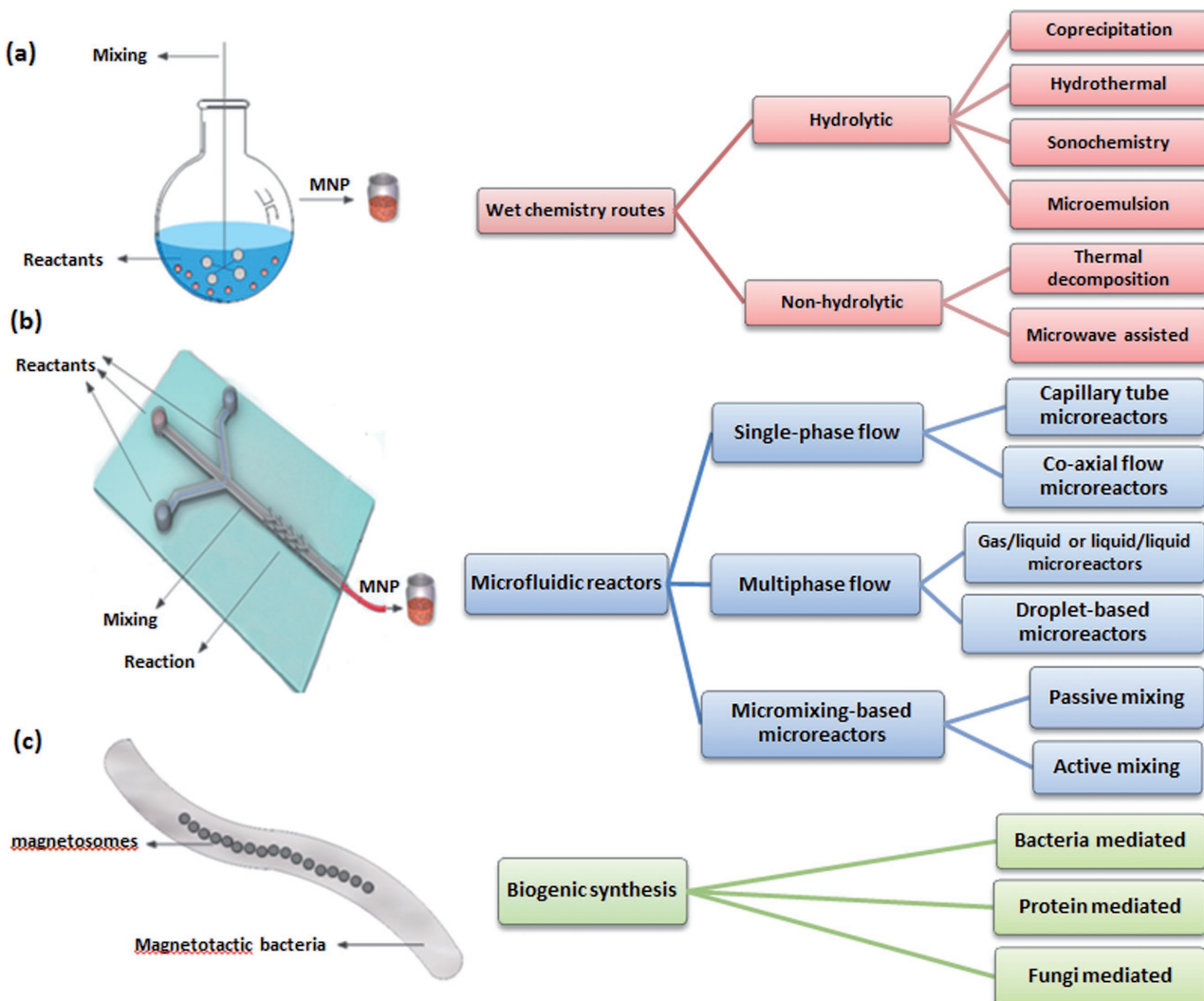


**Figure 2.** Different strategies for MNPs preparation: a) wet chemistry routes, b) microfluidic reactors, and c) biogenic synthesis.

can be easily scaled up. In the first place, an accurate control over the synthesis process is attainable owing to large surface areas of microfluidic devices and their unique ability for fast heating/cooling of the reaction mixtures which prevents the formation of large temperature gradients.<sup>[51]</sup> More importantly, different modules of single-phase and multiphase microfluidics devices, combined with optimized designs geometrical channels networks ensure the homogeneity of the reaction through enhancing the continuous mixing of reagents toward a uniform heating and mixing.<sup>[52]</sup> Furthermore, by tuning the channel length and regulating the flow of reagents a precise control over the reaction time is achieved for quenching the reaction whenever the nanoparticles reach the appropriate size and shape.<sup>[53]</sup>

## 2.1. Wet-Chemistry Routes

Bottom up approach synthesis which generally uses wet chemistry routes, is grouped into hydrolytic and non-hydrolytic approaches both having some advantages and disadvantages

(Figure 4). Table 2 compares different bottom up synthesis approaches. In this section, we provide common chemical routes which have been mostly used for the synthesis of MNPs and some of experimental works related to them.

### 2.1.1. Hydrolytic Approaches

**2.1.1.1. Coprecipitation:** The most commonly used way to produce MNPs in a large scale is hydrolytic coprecipitation which relies on Massart method,<sup>[55]</sup> where iron oxide nanoparticles are synthesized by alkaline coprecipitation of  $\text{Fe}^{2+}/\text{Fe}^{3+}$  salt solutions at room temperature or elevated temperature (Figure 4a). Within this process, NPs are synthesized by the quick increase of monomers over critical supersaturation followed by a slower growth phase.<sup>[11a]</sup> Then the nuclei growth take place at the same rate to produce monodisperse NPs.<sup>[56]</sup> Although this quick method offers excellent shape and phase uniformity control, it suffers from poor size control.<sup>[45]</sup> The size and shape of the produced nanoparticles are highly affected by experimental

**Table 1.** Qualitative comparison between bottom-up (wet-chemistry), top-down, microfluidic reactor-based, and biogenic synthesis of magnetic nanoparticles.

Properties	wet-chemistry routes	Mechanical routes	Microfluidic reactor	Biogenic synthesis
Minimal practical size	Small	Small	Very small	Very small
Practical size distribution	Large	Very large	Small	Very small
Reproducibility	poor	Good	Good	Poor
Yield	High	Very High	High	Low
Mixing quality	Good	–	Very good	–
Mass and heat transfer	Moderate	–	Very good	–
Scale up efficiency	Good	Very good	Very good	Poor
Surface area to volume ratio	Small	Small	High	High
Operational stability	Very good	–	Good	Poor
Automation	Poor	Good	Very good	Poor
Safety of operation	Good	Poor	Very good	Very good
Continuous synthesis	Poor	Good	Very good	Poor
Energy consumption	High	Low	Low	Very low
Control over reaction time	Poor	–	Good	Poor
Control over shape and size	Good	Very poor	Very good	Poor

parameters such as the temperature of the reaction, pH value, types of salts used, the ratio of  $\text{Fe}^{2+}/\text{Fe}^{3+}$  and the nature of the base. Among them, pH is a key parameter that has an impact on MNP size.<sup>[47]</sup> Specifically, as the pH of the reaction increases, the induced repulsion among primary MNPs leads to smaller magnetite nanoparticles. Overall, this process takes advantage of cheap chemicals and mild reaction conditions,

with the possibility to be performed for the direct synthesis of nanoparticles in water.

Iron chlorides, nitrates or sulfates are generally the ferrous and ferric salts used in the reaction. Such salts are combined with an acidic material (hydrochloric acid as an example). Subsequently desired iron oxides will precipitate upon addition of a base with strong alkaline nature (such as ammonia or sodium

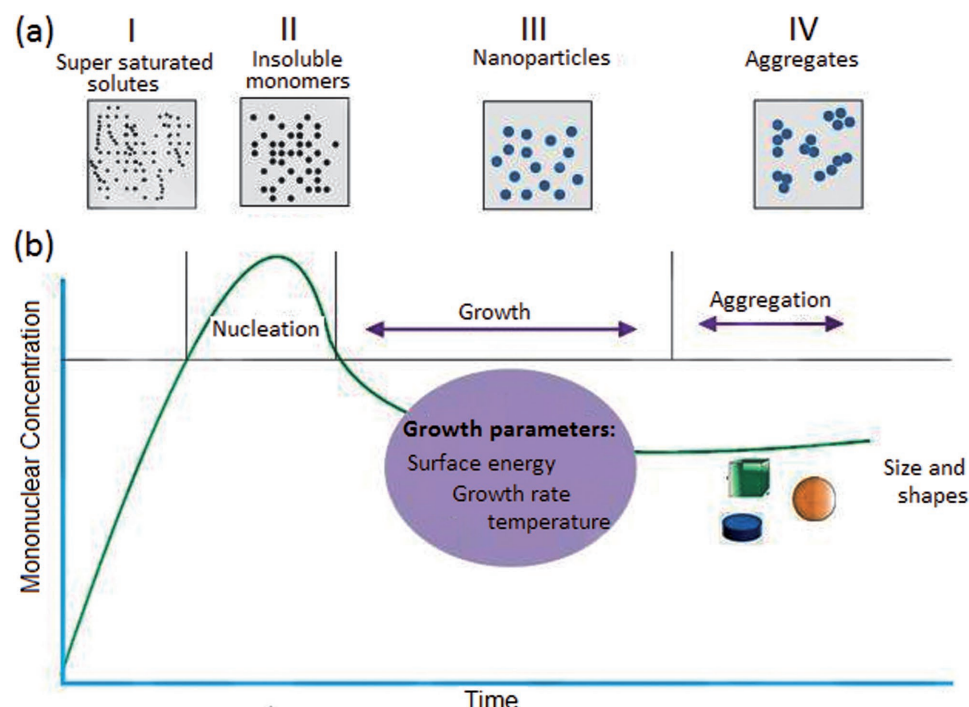


**Figure 3.** Diagram of the self assembly, nucleation, and growth of nanoparticles. a) Individual molecules first nucleate (I and II), followed by aggregation of nuclei into nanoparticles (III). If the reaction is not quenched or stabilized, nanoparticles tend to agglomerate into bulk material (IV). b) Surface energy, growth rate, and temperature of the reaction highly control the final size and shapes of the nanoparticles.

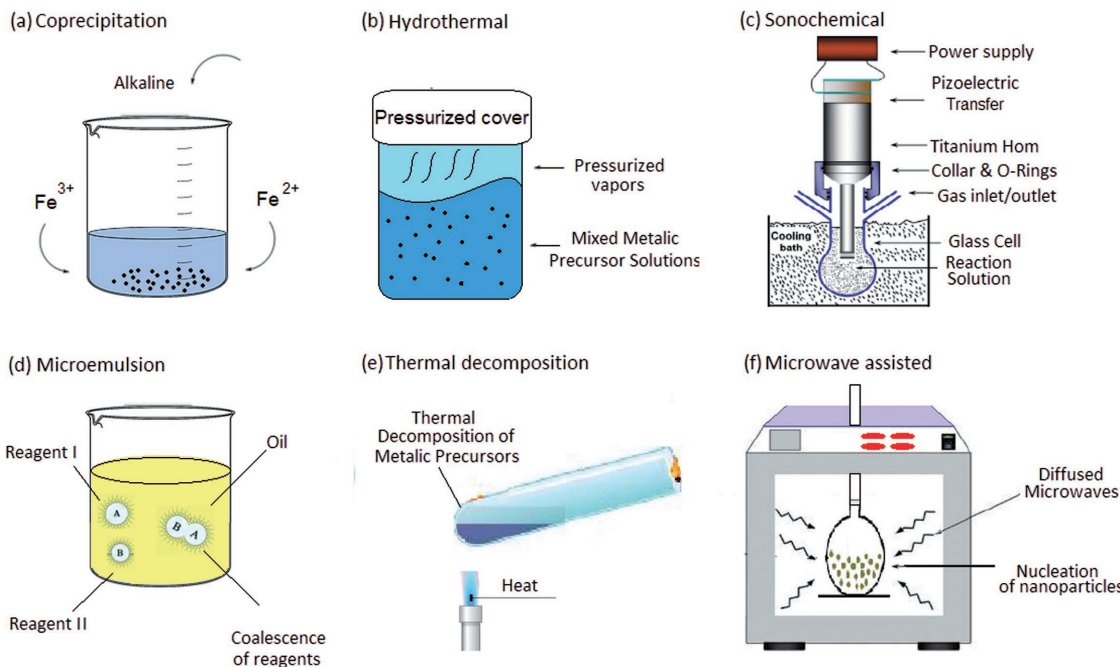


**Figure 4.** Schemes of different types of hydrolytic and non-hydrolytic wet-chemistry routes for the synthesis of nanoparticles. c) Reproduced with permission.<sup>[32]</sup>

hydroxide). Finally a centrifugation procedure in the presence of ethanol and water takes place to wash unreacted chemicals. Coprecipitation process has the potential of producing highly concentrated ferrofluids thanks to the high density of hydroxyls groups on the surface. In contrast with thermal decomposition method, surfactants are not added to the solvent until the coprecipitation process is finished. However, this step should be done precisely with great care to avoid any further oxidation of the resultant MNPs in ambient conditions.<sup>[57]</sup> A good dispersity and size stability maintenance of the resulting MNPs can be achieved by adding hydrophilic polymers such as polyvinylalcohol (PVA) during the process to act as coating agents or stabilizing matrixes.<sup>[58]</sup> MNPs with either of these surface coating materials can disperse at high concentration in water or oil to form stable ferrofluids. Such ferrofluids contain small enough MNPs, due to which neither magnetic nor gravitational fields can cause their precipitation.<sup>[59]</sup>

In a pioneering study performed by Cabuil and co-workers nickel–zinc ferrite particles were synthesized by coprecipitation of an aqueous mixture of metallic salts (nickel chloride, zinc chloride and iron (III) chloride) in an alkaline medium. Studies of the magnetic properties of resultant particles revealed that the saturation magnetization can be varied through modifying the zinc amount.<sup>[60]</sup> Another study by the same group produced superparamagnetic liposomes as highly efficient MRI contrasts for in vivo imaging.<sup>[61]</sup> In the first place, magnetite nanoparticles were fabricated by alkaline coprecipitation of iron (II) chloride and iron (III) chloride salts. Subsequently, a thin film hydration method coupled with sequential extrusion was used to encapsulate the resultant nanoparticles within large unilamellar liposomes sterically stabilized by polyethylene glycole (PEG) chains. These magnetic micelles presented long-circulating behavior in blood among with proper potential for in

vivo magnetic resonance (MR) imaging. In a study performed by Chen et al. MnFe<sub>2</sub>O<sub>4</sub> particles were synthesized through coprecipitation of FeCl<sub>3</sub>·6H<sub>2</sub>O and MnCl<sub>2</sub>·4H<sub>2</sub>O salts and using NaOH as the reaction agent to study the size effects on the magnetic properties of the resultant nanoparticles. Their results showed that the curie temperature and saturation magnetization decrease relative to the bulk as size decreases.<sup>[62]</sup> Another group synthesized superparamagnetic MgFe<sub>2</sub>O<sub>4</sub> nanoparticles by coprecipitation of FeCl<sub>3</sub>·6H<sub>2</sub>O and MgCl<sub>2</sub>·6H<sub>2</sub>O by adding NaOH to study their superparamagnetic relaxation of magnetization. It was obtained that the relaxation time was correlated with the particle size and temperature and is consistent with Neel theory.<sup>[63]</sup> Kang et al. synthesized Fe<sub>3</sub>O<sub>4</sub> iron oxide nanoparticles with a narrow size distribution through coprecipitation method without using surfactants.<sup>[64]</sup> In contrast, many researchers have reported efficient routes for the synthesis of monodispersed MNPs by adding surfactants such as dextran or PVA in the reaction media to have better control of the size distribution.<sup>[65]</sup> Influence of surfactants on the structural and magnetic properties of NPs have been studied<sup>[66]</sup> and it was concluded that the estimated average particle and crystallite size distributions depend on the choice of the surfactant. This method allows coating the produced MNPs to make them stabilized and biocompatible especially for biomedical applications.<sup>[67]</sup> Salunkhe produced superparamagnetic iron oxide nanoparticles from ferrous chloride and ferric chloride salts by applying a new generation base diisopropylamine, which electrostatically complexes with iron ions, reduces them and subsequently caps the nanoparticle.<sup>[68]</sup> A comprehensive study was performed by Hauser et al.<sup>[69]</sup> to investigate the chemical properties of dextran coated iron oxide nanoparticles via four variations on the coprecipitation method. The time of the addition of dextran into the reaction mixture was the varying parameter

**Table 2.** Qualitative comparison between different types of hydrolytic and non-hydrolytic approaches of wet chemistry routes for synthesizing MNPs.

Precursors	Hydrolytic Approaches						Non-hydrolytic approaches		
	Ferrous and ferric salts, mainly iron chlorides, nitrates, and sulfates			Sonochemistry			Iron containing organometallic compounds		
Synthesis route	Coprecipitation	Hydrothermal	20–90 hours	20–90 minutes	Microemulsion	20–50 hours	Thermal decomposition	Microwave assisted	160–210 minutes
Reaction temperature	20–90 °C	180–220 °C			Water	Water	Organic compound	Organic compound	
Reaction period	Minutes								
Solvent	Water	Water, ethanol							
Production	High	Medium			Low		High	High	
Advantages	Mild reaction conditions Synthesis in H <sub>2</sub> O Easy surface modification Ease conversion to magnetite Ease scale up	Improved size control Narrow size distribution Synthesis in H <sub>2</sub> O Tunable magnetic properties Applicability for continuous synthesis	Accelerated reaction time Enhanced mixing by non-invasive source of energy	Relatively narrow size distribution Good dispersivity High crystallinity	Improved size control Relatively narrow size distribution Ease of size tunability Uniform magnetic properties	Narrow size distribution High crystallinity High size control Tunable magnetic properties	Narrow size distribution High crystallinity Tunable magnetic properties	Narrow size distribution, high crystallinity, water dispersible, Rapid processing, high reaction rate, reduced reaction time, high yield of product along with simplicity and high energy efficiency	
Disadvantages	Broad size distribution Polydispersity Low reproducibility Uncontrolled oxidation Difficulty in adjusting the pH of the reaction	High temperature High pressure Need for special reactors or autoclaves	Need for ultrasound wave irradiation equipment	Low reaction yield Poor crystallinity Difficulty to remove surfactants	Toxic organic solvents High temperature Need for phase transfer	Need for large amounts of organic solvents	Need for organic solvent Limited penetration depth of the microwave		

in the methods named as: two step, semi-two-step, simultaneous semi-two-step, and one-step synthesis. They reported the greatest batch-to-batch reproducibility of nanoparticles and the least variation in nanoparticles synthesized by a simultaneous semi-two-step method. In this method the reducing agent and dextran solution were injected into the reaction vessel at the same time. On the other hand, their results showed that one-pot synthesis resulted in significantly smaller MNPs, very stable in phosphate buffered saline (PBS), with lower specific adsorption rate (SAR) values. In another comparative study, Roth et al. investigated the impact of synthesis parameters on the coprecipitation process SPIONs.<sup>[70]</sup> They reported synthesis of MNPs with diameters between 3 and 17 nm by variation of iron salt concentration, reaction temperature, ratio of hydroxide ions to iron ions and ratio of Fe<sup>2+</sup>/Fe<sup>3+</sup>. Their results also revealed that employment of high iron salt concentrations and molar ratio of Fe<sup>2+</sup>/Fe<sup>3+</sup> below 2:1 can enhance the saturation magnetization of resultant MNPs. On the other hand, higher iron salt concentrations and a hyperstoichiometric normal ratio of hydroxide ions to iron ions of 1.4:1 can increase the size of MNPs. Kumar et al. also elucidated the effects of precursors in the formation of different forms of iron oxide and oxyhydroxide by using trioctylamine as the reducing agent in a coprecipitation process.<sup>[71]</sup> Their results showed that the constitution, shape, size, and properties of phases significantly changed by changing the cations.

Topel el al. performed a modified coprecipitation method to produced functionalized polyethyleneimine (PEI) coated Fe<sub>3</sub>O<sub>4</sub> nanoparticles, with a diameter of around 10 nm, covalently conjugated with fluorophore molecules.<sup>[72]</sup> Their investigation from in vitro tests on two human cancer cells showed the easy penetration of the resultant MNPs into cell cytoplasm in the living cells to be very promising for bio-imaging applications. In a very recent study performed by Bhandari et al.,<sup>[73]</sup> a simple coprecipitation method was used to produce curcumin functionalized magnetite nanoparticles and they were analyzed for cell viability assay against an inflammatory agent. Pereira et al.<sup>[74]</sup> prepared small sized ferrites by using alkanamines as the alkaline source and as complexing agents which resulted in better magnetic properties. In a recent study, block copolymers were used in a coprecipitation process, where iron salts (1:2 molar ratio of FeCl<sub>2</sub>/FeCl<sub>3</sub> at 0.065 M) were pre-mixed with different amounts of diblock copolymer in aqueous solutions, to make magnetic nanoparticles for use as MRI contrast agents.<sup>[75]</sup> In other study performed by Mireles et al.,<sup>[76]</sup> three differently functionalized magnetite iron oxide nanoparticles were prepared by the alkaline coprecipitation of FeCl<sub>2</sub> and FeCl<sub>3</sub> in diethylene glycol (DEG). The heated mixture of the salts under N<sub>2</sub> at 170 °C was followed by the addition of NaOH to obtain black precipitates of bare MNPs. Two additional samples were prepared by further functionalization of the produced MNPs via direct reaction with silanes. Their results indicated of weak surface functionalization due to the catalytic effect of the magnetic cores. In addition, unavoidable contaminations which could possibly cause problems in biomedical applications were obtained.

Coprecipitation method can also be used for the synthesis of shape-controlled iron oxide nanoparticles. Recently, Shen et al.<sup>[77]</sup> have reported the synthesis of monodispersed

magnetite ( $\text{Fe}_3\text{O}_4$ ) nanoparticles with high saturation magnetization, including nanospheres, nanoneedles, and nanocubes by changing the amount of sodium dodecyl sulfate through coprecipitation method. Transmission electron microscopy (TEM) showed that by varying the amount of sodium dodecyl sulfate the morphology of magnetite nanoparticles changed from nanospheres to nanoneedles and to nanocubes.

In summary, mild reaction conditions, as well as cheap chemicals for direct synthesis in water and easy surface modification are of the advantages of coprecipitation method. Types of salts, the ratio of  $\text{Fe}^{2+}/\text{Fe}^{3+}$ , reaction temperature and pH value highly affect the size and shape of nanoparticles. However, despite the excellent control over shape and uniformity, controlling the size of nanoparticles is problematic through synthesis strategy. MNPs produced by the coprecipitation approach tend to be polydisperse. In particular, the blocking temperature depends on the particle size, hence a wide particle size distribution results in a wide range of blocking temperatures. In this regard, in order to produce monodisperse MNPs, a short burst of nucleation and slow controlled growth are required and also in most cases, it requires a consequent size sorting procedures to reduce the polydispersity index of the batches.<sup>[67]</sup> In addition, adjusting the pH value of the reaction mixture in both steps of synthesis and purification faces this approach with some difficulties. Furthermore, subsequent treatments are required for protecting the environment from the generated wastewaters with very basic pH values.<sup>[78]</sup>

**2.1.1.2. Hydrothermal/or Solvothermal Synthesis:** General problem related to all hydrolytic approaches is that various numbers of parameters deal with the complex aqueous chemistry and rich phase diagram of iron oxide phases must be monitored to control the synthetic outcome.<sup>[47]</sup> An old accessible way termed as solvothermal synthesis has been devised to produce MNPs with various morphologies, narrow size distribution, and good shape control.<sup>[9]</sup> This method involves a sealed container or an autoclave within which the chemical reaction is performed under high temperature (130–250 °C) and high vapor pressure (0.3–4 MPa).<sup>[79]</sup> The process is called hydrothermal synthesis in case of using water as the solvent of the reaction. Performing the reactions in such aqueous solutions at high temperature and pressure conditions produces high crystalline MNPs with uniform small size. A review on hydrothermal synthesis of metal oxide nanoparticles has been published,<sup>[80]</sup> which gives detailed information on what exactly happens within hydrothermal process. Herein we briefly explain the basic mechanism behind this method. A diagram of the solvothermal synthesis method is shown in Figure 4b. The ions or molecular groups to be nucleated at initial stage are formed in a solvent or mixture dissolving metallic precursor and surfactants.<sup>[81]</sup> Subsequently, the entire setup is placed into a constant temperature vessel until the materials are “pressure cooked” at elevated temperatures.<sup>[57]</sup> In particular, a driving force produced by the intense convection effects due to temperature difference between the bottom and top of the sealed container is in charge of transporting these ions or molecular groups to the low temperature area. This phenomenon continues until a critical supersaturated solution for nucleation is generated, which subsequently leads to a large amount of

magnetic nuclei. Eventually, high crystalline nanoparticles will be resulted by repeated dissolution and recrystallization processes induced in the growth of MNPs.<sup>[82]</sup>

There are numerous reports in the literature on exploiting the hydrothermal synthesis for producing iron oxide MNPs, either in the presence or absence of stabilizing surfactants.<sup>[83]</sup> In 1980, a comprehensive study conducted by Sapiszko et al., utilized the hydrothermal decomposition of metal chelates in mixture with different additives for producing colloidal solids of different chemical compositions and morphologies.<sup>[84]</sup> Specifically, ferric oxide colloidal particles of a variety of morphologies were prepared under the hydrothermal aging of strongly alkaline solutions of ferric salts and triethanolamine at 250 °C. In another work, magnetite nanoparticles with fairly uniform size were produced by precipitating  $\text{Fe}^{2+}$  ion with ammonium hydroxide in the absence of surfactants.<sup>[85]</sup> The reaction was performed under hydrothermal conditions at a temperature of 134 °C and a pressure of 2 bars for 3 h. The average size of the produced MNPs was  $31.1 \pm 6.1$ , which was dependent on concentration of the reactants and the reaction solvent composition. In a very recent study, iron oxide nanoparticles containing nanosized cavities were produced by developing a surfactant free hydrothermal method.<sup>[86]</sup> The prepared samples were calcined in air and nitrogen, resulting in MNPs with cavities of diameter 7–15 nm and 5–12 nm, respectively.

Hydrothermal synthesis can also be performed under a continuous process wherein micropumps are employed to flow the reagent within tubes.<sup>[87]</sup> Xu et al.<sup>[88]</sup> conducted a pioneering study to investigate the factors that affect the size, size distribution, and morphology of iron oxide nanoparticles obtained in the presence and absence of PVA, via continuous hydrothermal synthesis. Temperature and residence time increased the average particles size. Presence of PVA significantly limited the aggregation of resultant MNPs. Their results also showed narrow particle size distribution with increasing the PVA concentration. In a very recent study, iron oxide nanoparticles were synthesized within a low temperature hydrothermal approach by using two series of iron precursors, sulfates, and chlorides.<sup>[89]</sup> MNPs with a mixture of both spherical and rod morphologies were obtained when iron sulfate was used as the precursor of the reaction at 180 °C. While spherical MNPs with size range 5–20 were obtained in the case of using iron chlorides. On the other hand, by increasing the temperature up to 190 °C, spherical MNPs were resulted from both types of precursors.

Gyergyek et al.<sup>[90]</sup> also presented a study to investigate the influence of the temperature and the concentration of ricinoleic acid on the size and magnetic properties of iron oxide nanoparticles produced by coprecipitation from aqueous media and hydrothermal treatment of the media. Their results showed that at high temperatures (180 °C) the growth of MNPs becomes more pronounced, while they have broader size distribution. In addition, presence of ricinoleic acid surpassed their growth under the hydrothermal conditions. A relatively good control over the average size of the MNPs was achieved by varying the concentration of ricinoleic acid.

A method introduced by Li and co-workers<sup>[91]</sup> involves use of liquid–solid–solution (LSS) reaction. The system consists of metal linoleate (solid), an ethanol linoleic acid liquid phase, and a water–ethanol solution at different reaction temperatures

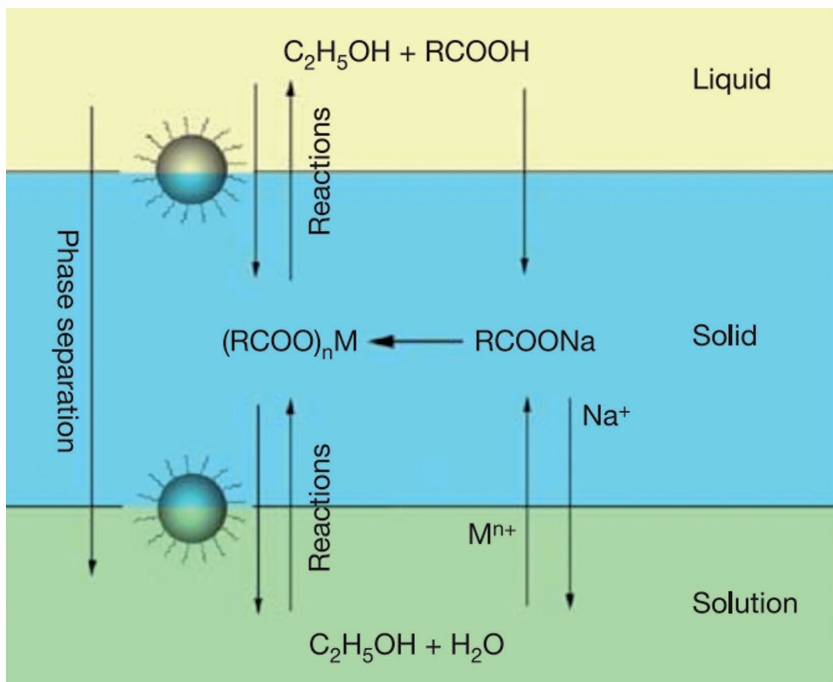


**Figure 5.** The liquid–solid–solution (LSS) phase transfer synthetic strategy. Reproduced with permission.<sup>[91]</sup> Copyright 2005, Nature Publishing Group.

under hydrothermal conditions. As illustrated in Figure 5, in this process, a general phase transfer and separation occur at the interfaces of the ethanol linoleic acid liquid phase (liquid), metal linoleate (solid), and the water–ethanol solutions (solution) of the present phases during the process.<sup>[92]</sup> Through this approach, reaction conditions, such as solvent, temperature, and time have great impacts on the properties of the synthesized nanoparticles. The competence between the rate of process of nucleation and particle growth can control the MNP size in crystallization. By maintaining other parameters at constant values, these rates are highly dependent on the temperature of the reaction. At higher temperatures the nucleation process takes place faster than MNP growth which results in a decrease of MNP size. In contrast, prolonging the reaction time would favor MNP growth.<sup>[47]</sup>

Chen et al. were inspired by this method and used pre-synthesized iron–oleate and zinc–oleate precursors to produce zinc-doped iron oxide MNPs as  $T_2$ -weighted MRI contrast agents.<sup>[93]</sup> They transformed the resultant hydrophobic MNPs into hydrophilic ones by strong ultrasonic treatment in the presence of cetyltrimethylammonium bromide (CTAB) surfactant. Li et al.<sup>[94]</sup> reported a PEI-mediated approach to synthesizing folic acid (FA)-targeted magnetic iron oxide nanoparticles ( $\text{Fe}_3\text{O}_4$  NPs) for *in vivo* MR imaging of tumors. A hydrothermal synthesis method was applied through their study and MNPs with a spherical shape and quite uniform size distribution with a mean diameter of 15.0 nm were obtained.

Overall, improved size control within hydrothermal synthesis method directly leads to narrow size distribution of MNPs. More importantly, this strategy is applicable for continuous synthesis to improve the production yield of nanoparticles. However, the need of high temperature and high pressure

of the reaction makes along with the need for special reactors or autoclaves makes this strategy not be energy efficient compared to other synthesis methods.

**2.1.1.3. Sonochemistry:** Ultrasound refers to acoustic fields at frequencies greater than those audible to humans. Despite the applications of ultrasound radiation in medicine, mainly for diagnosis, ultrasound has also paved its path in chemistry.<sup>[95]</sup> Currently, ultrasound is a laboratory tool used to dispersing nanoparticles and colloids, as well as driving chemical reactions.<sup>[96]</sup> Ultrasound offers a non-invasive control over the fabrication process of materials by generating localized heating and/or mechanical forces.<sup>[97]</sup> It was in 1996 when Suslick<sup>[98]</sup> published a review on the application of ultrasound radiation for producing nanomaterials. Sonochemical synthesis has merged the hydrolysis, and thermolysis with radiation of ultrasound to prepare nanostructured materials under non-equilibrium conditions under cavitation induced by acoustic waves.<sup>[96]</sup> Subjecting the reacting bath to ultrasound irradiation will result in concentrated spots

of extremely high temperatures. These “hot spots” which are produced by acoustic cavitation can significantly accelerate the rate of hydrolysis of metal ions.<sup>[99]</sup> Figure 4c illustrates a typical laboratory-scale sonochemical apparatus. As it is shown, a piezoelectric transducer drives a high-intensity ultrasonic titanium horn which directly introduced into a thermostated glass reactor.<sup>[54]</sup> In particular, applying powerful ultrasound radiation (20 kHz–10 MHz) to a mix of reagent dissolved in a solvent, the alternating expansive and compressive acoustic waves result in oscillation of the unseen particles, or microscopic gas bubbles generally present in the liquid which indeed enable the creation of the bubble.<sup>[54]</sup> Since the bubbles are created, they accumulate ultrasonic energy effectively and a vacuum induces diffusion of solute vapor into their volumes which leads to the growth of bubbles. This growth continues until the collapse of bubble occurs upon reaching to the maximum size to release the stored energy.<sup>[99]</sup> Specifically, chemical bonds are broken upon a very localized cavitation implosion wherein extremely high temperatures (5000–25 000 K) are obtained.<sup>[100]</sup> Nanosized particles are resulted due to extremely short duration of the process.<sup>[96]</sup> Although, the high cooling rates of the collapsed bubbles lead to amorphous nanoparticles in the case of volatile precursors, nanostructured products can be produced from non-volatile precursors.<sup>[100]</sup> In the case of non-volatile precursors, a 200 nm liquid phase ring surrounding the collapsing bubble is in charge of housing the reaction.<sup>[101]</sup> The macrostream produced due to collapse of bubbles creates a relatively uniform reaction condition for atomic mixing in the synthesis process.<sup>[102]</sup>

Kim et al. performed a sonochemical synthesis of superparamagnetic iron oxide nanoparticles coated by oleic acid and with high crystallinity.<sup>[103]</sup> An aqueous solution of  $\text{FeCl}_2$  and  $\text{FeCl}_3$  salts was irradiated by ultrasonic waves and black nanoparticles

(65 nm in size) were resulted by rapidly adding NH<sub>4</sub>OH to the mixture. A ferrofluid was prepared by dispersing the resulted MNPs in chitosan to be used for MR imaging. Their results showed that the contrast of MR images prepared by their ferrofluids were similar to those of Resovist. Islam et al.<sup>[104]</sup> also developed a sonochemical synthesis of magnetite nanoparticles with a relatively narrow size distribution and moderate monodispersity.

Well crystallized MNPs with good dispersivity and thermo-stability were also produced by enhancing the coprecipitation of iron salts by ultrasonic.<sup>[105]</sup> The resultant MNPs were subsequently modified by anionic surfactant sodium dodecyl sulfate. Abbas et al.<sup>[106]</sup> synthesized uniform ferromagnetic magnetite nanocubes by applying a sonochemical method in the absence of any surfactants. They enhanced the crystallinity of the magnetic nanocubes by annealing treatment up to 600 °C. However, further increase in annealing temperature decreased the saturation magnetization due to the presence of a thin magnetic dead layer at the surface. Bang et al.<sup>[107]</sup> reported a preparing of nanosized hollow iron oxides by using carbon nanoparticle templates. The produced hollow iron oxide nanoparticles were thermodynamically stable crystalline hematite with very weak ferromagnetism. Pectin coated magnetite nanospheres were synthesized via using a sonochemical method by Dai et al.<sup>[108]</sup> The produced MNPs had high saturation magnetization and superparamagnetic property along with high biocompatibility and biodegradability. Dang et al. exploited an ultrasonic irradiation to coat magnetite nanoparticles with silica by preventing the agglomeration of magnetite nanoparticles and accelerating the hydrolysis and condensation of tetraethyl orthosilicate (TEOS).<sup>[109]</sup> In a recent study, aqueous solution of ferrous salts were coprecipitated in a basic aqueous solution of ethylene glycol under irradiation of ultrasound to prepare iron oxide nanoparticles loaded by folate and cisplatin. Results of the study showed that cisplatin loading on MNPs were proportionally increased with ultrasound frequency.

Overall, despite the need for ultrasound irradiation equipment, the sonochemistry method highly accelerates the reaction time by enhancing the mixing through a non-invasive source of energy. As a matter of fact, not only nanoparticles with relatively narrow size distribution are produced, but also they possess high crystallinity and good dispersity.

**2.1.1.4. Reverse Micelle (Microemulsion):** The main drawback to hydrolytic approaches is their limited ability in controlling the size distribution of the produced nanoparticles. Thus, amphiphilic molecules (surfactants) were exploited to enhance the reaction condition through providing nanoreactors wherein coprecipitation process can occur within confined environments, either as micelles<sup>[110]</sup> or reverse micelles.<sup>[111]</sup> Specifically, capability of amphiphilic molecules with hydrophilic tail and hydrophilic heads to undergo a self-organization process of forming spheroidal aggregates is the key factor contributing to the formation of such nanoreactors.<sup>[112]</sup> By dissolving surfactants in polar solvents (e.g., water) strong interactions of hydrophilic heads lead directly to the formation of a normal micelle with a hydrophilic core and a hydrophobic outer layer. On the other hand, using organic solvents results in stronger affinities with the hydrophobic tails to form spheroidal

aggregates which are structurally reverse of normal micelles, that is having an external shell of hydrophobic hydrocarbon chains and hydrophilic polar cores capable of solubilizing polar solvents.<sup>[113]</sup> In fact, such a reverse micelle (also named as microemulsion) is an isotropic dispersion of two immiscible liquids within a thermodynamically stable condition in which microdomain stabilization of either or both liquids is performed by an interfacial film of surfactant molecules.<sup>[92b]</sup> Eicke et al. were the first to study the physical properties of the reverse micelles as water-in-oil (w/o) microemulsions in a comprehensive manner.<sup>[114]</sup> The same group also demonstrated that exchange of material between the reverse micelles was feasible for the Aerosol OT (sodium bis(2-ethylhexyl) sulfosuccinate) system.<sup>[115]</sup> Additionally, transfer of small ions between reverse micelles was investigated by using flow methods.<sup>[116]</sup> Fletcher et al. also provided a detailed investigation of the temperature, oil solvents and additives on the exchange kinetics in AOT systems.<sup>[117]</sup>

By the superb advantages of such interfacial film of surfactants to split the confined nanoreactors of the encompassing solution as well as its ability for exchanging material, microemulsions (typically 1–50 nm in diameter)<sup>[118]</sup> can serve as a proper asset to stabilize the entire solution<sup>[119]</sup> and offer excellent control over shape, size and phase of the produced nanoparticles.<sup>[57]</sup> Synthesis of MNPs under microemulsion process entails simple stages as follows:

In the first place, two separate microdroplets, one containing the metal precursors and the other containing the precipitating agent are required. Subsequently, a continuous collision, coalescence and break of microdroplets happen as two w/o microemulsions are mixed (Figure 4d).<sup>[120]</sup> These phenomena lead to the faster mixing of the reactants to be nucleated and grown in the form of a precipitate within the microemulsions. Finally, a demulsifying agent such as acetone or ethanol is added to extract the resultant nanoparticles by filtering, centrifuging or exploiting a magnetic field. Temperature, kind of counterion and microstructure of microemulsion are among the parameters which affect the nanoparticles size. The sizes of nanoparticles which are prepared with the microemulsion are easily controlled and consequently particles tend to be very homogenous in size. Determination of the size of the reverse micelle depends on the molar ratio of water to surfactant and type of surfactants.<sup>[121]</sup> The radius of the spherical droplets made in a system of water and surfactant dispersed in oil is given by  $R_w = 3V_{aq}[\text{H}_2\text{O}]/\sigma[S]$ , where square brackets indicate concentration, S refers to surfactant,  $\sigma$  is the area per head group of the surfactant molecule and  $V_{aq}$  is the volume of a water molecule.<sup>[57]</sup>

Historically, Pilani and co-workers were of the first groups attempting at exploiting the reverse micelles for nanoparticles synthesis.<sup>[122]</sup> They synthesized copper metallic clusters by mixing two micellar solutions, one containing the reducing agent and sodium AOT and the other mixed copper and sodium AOT.<sup>[122f]</sup> Through a similar approach, cadmium sulfide nanoparticles were synthesized by mixing two AOT reverse micelle solutions, containing cadmium nitrate and sodium sulfide, respectively in the presence and absence of sodium hexametaphosphate.<sup>[122e]</sup> In addition, numerous researches in the literature have exploited the microemulsion process for producing high quality MNPs, mainly coated by silane

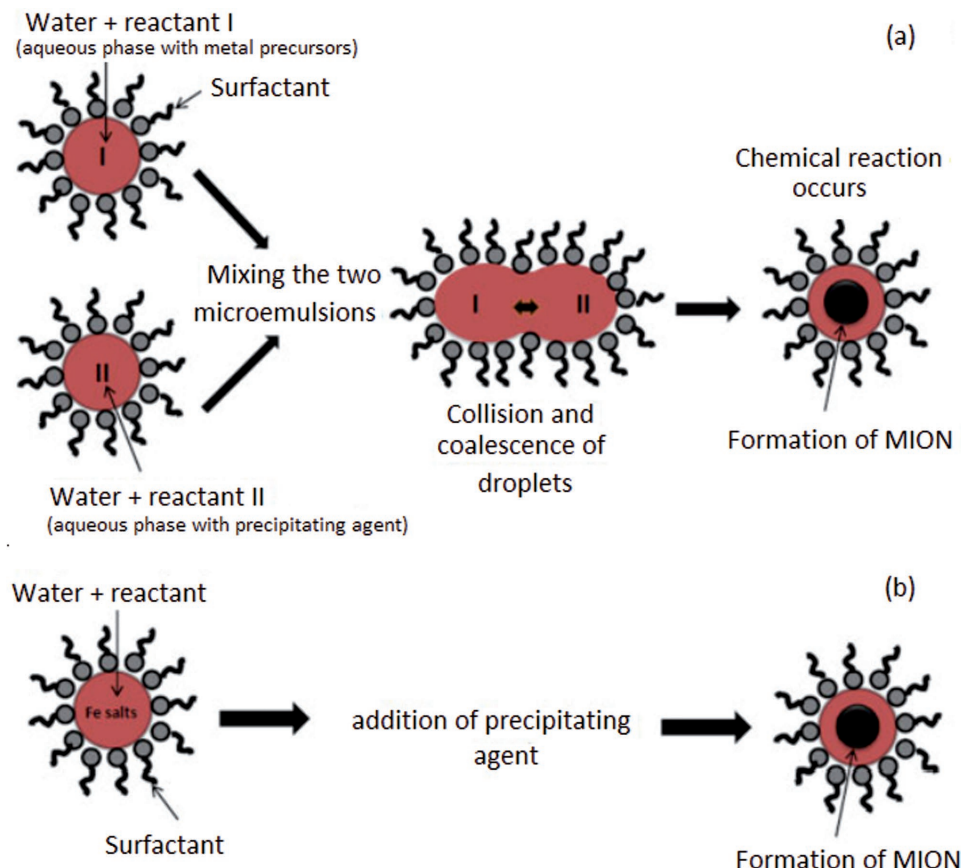


**Figure 6.** Schematic representation of synthesizing magnetic iron oxide nanoparticles (MION): a) two water/oil (w/o) microemulsion solutions, one containing the metal precursors and the other containing the precipitating agent are mixed. b) one w/o microemulsion containing metal precursors will be added by the precipitating agents. Reproduced with permission.<sup>[124]</sup>

groups.<sup>[123]</sup> Okoli et al.<sup>[124]</sup> reported fast synthesis of MNPs for water purification with two different microemulsion compositions (Figure 6). In the first approach they synthesized MNPs by mixing two w/o microemulsion solutions. Microemulsion I was obtained by adding  $\text{FeCl}_2$  and  $\text{FeCl}_3$  iron precursor solutions to the mixture of the surfactant, and for microemulsion II a precipitating agent solution was added to the mixture. Subsequently formation of MNPs was indicated by black coloration as both microemulsions were combined with each other. Finally an external magnetic field was applied to separate the produced MNPs. In the second approach a single-step preparation route was applied wherein only one type of microemulsion is required for formation of nanoparticles. Through this approach, formation of magnetic nanoparticles was achieved by adding  $\text{NH}_3$  as precipitating agent to the microemulsion containing the precursor upon vigorous stirring until the required pH was achieved. Finally, the obtained MNPs were washed with a mixture of chloroform, methanol and water to remove all the surfactant and oil left in the system.

In a more recent study, w/o microemulsion route was used to synthesize magnetite nanoparticles by using different kinds of surfactants to investigate the morphology, size, size distribution and crystalline feature of the resultant MNPs.<sup>[125]</sup> They used *n*-heptane as the oil phase, conventional single-chain surfactants and novel Gemini surfactants, and *n*-hexanol as

the co-surfactant phase. Their results showed that nucleation and growth of the nanocrystalline are significantly affected by the film flexibility of the reverse micelles and life time of a surfactant molecule in the micelle. In addition, temperature of samples played an important role in regulating the crystal defects, where the hydrophobic chain length of the surfactants showed a great influence on the lattice defect against the temperature variation.

Microemulsion method can be also used for the post processing of the produced MNPs to be functionalized, mainly by silica coatings.<sup>[126]</sup> In this strategy, the solid structure of the produced MNPs is exploited as a seed or templated for the growth of silica shell.<sup>[127]</sup> Addition of silica precursors to the dispersion of MNPs which are under continuous stirring leads to the growth or coating of the silica shell via increased interaction between silica source and MNPs. Single core MNPs which are uniformly coated with silica are resulted through this process.<sup>[128]</sup> Zhao et al. performed a modified reverse microemulsion synthesis to prepare MNPs coated by silica, with average size of 40 nm. TEOS molecules were immediately added to the resultant MNPs and the reaction was continued for 24 h at room temperature. The core-shell MNPs were finally modified by alcohols and emulsifier pair.

Overall, thanks to improved size control offered by microemulsion route, it has considerable potential in synthesizing

MNPs with a narrow size distribution and uniform magnetic properties. However, MNPs with lower yields and poor crystallinity are produced by microemulsion route compared to the coprecipitation one. However, it has been shown that as the reverse micelle is heated up, improvement of the crystallinity of iron oxide and other ferrite is achieved.<sup>[129]</sup> In addition, scaling up is complicated due to the sensitivity of preparation conditions, the need for large amounts of organic solvent, and difficulty to remove the surfactants.

### 2.1.2. Non-Hydrolytic Approaches

**2.1.2.1. Thermal Decomposition:** In contrast with hydrolytic routes, wherein complex aqueous chemistry is applied to form hydroxyl and oxyhydroxy species as intermediates, high quality ferrite MNPs have been synthesized by more recent and faster non-hydrolytic routes, specially thermal decomposition.<sup>[130]</sup> Actually, this non-hydrolytic method has been devoted to the fabrication of uniform MNPs by inspiration from semiconductor nanocrystals and oxide formation in non-aqueous media.<sup>[46a,131]</sup> As its name implies, it involves breaking down of materials to form new compositions at various temperatures.<sup>[57]</sup> If one starts with low-valent complexes bound with olefinic ligands, a decomposition reaction which would leave behind the metal oxides can be envisaged.<sup>[99,132]</sup> The process consists of decomposition of metal precursors in boiling organic solvents<sup>[133]</sup> in the presence of surfactants to produce stabilized MNPs with well-defined magnetic properties thanks to their high crystallinity, controlled size and narrow size distribution (Figure 4e). Quick burst nucleation followed by crystal growth is the main reason to make this approach successful. This process can be controlled through the involved parameters such as type of precursor and surfactant, their relative ratio, solvent, temperature of the reaction and the reaction time.<sup>[92b]</sup> However, despite the controlled size synthesis of the MNPs with desirable magnetic properties,<sup>[48]</sup> tuning of the MNPs shape for substituted ferrites is still remaining.

Versatile ligands such as cupferron (*N*-nitrosophenylhydroxylamine), cyclooctatetraene, cycloocta-1,5-diene, acetylacetone, and carbonyls bound with Fe can form practical iron containing organometallic compounds as initiating precursors to produce iron oxide nanoparticles.<sup>[57,132]</sup> An effective crystal nucleation and growth can be achieved by surfactants to produce MNPs with stabilizing coatings which prevents their fouling and aggregation. Fatty acids,<sup>[134]</sup> oleic acid,<sup>[135]</sup> and hexadecylamine<sup>[136]</sup> and oleylamine are of the common surfactants which enable clear dispersions of MNPs in non-polar media. Octyl ether, phenyl ether, 1-octadecene, or benzyl ether often serves as the high boiling point organic solvents. After mixing all organometallic compound, surfactants and solvents in one flask, oxygen is purged from the container. Subsequently, upon heating the flask for a short period of time, MNPs will form through thermal decomposition of metal precursors. Finally, MNPs are washed and any excess chemicals are removed by centrifuging the sample in the presence of ethanol for several times.<sup>[57]</sup>

Iron (III) oleate ( $\text{Fe}[\text{C}_{18}\text{H}_{33}\text{O}_2]_3$ ), iron oxyhydroxide  $\text{FeOOH}$ , or iron pentacarbonyl ( $\text{Fe}[\text{CO}]_5$ ) are of the very common

precursors in the synthesis of nanoparticles due to their high levels of reactivity and solubility.<sup>[137]</sup> Additionally, type of solvent in which produced MNPs can be well dispersed is directly determined by the type of surfactant used.<sup>[138]</sup> Although a well dispersion of such MNPs can make ferrofluids in non-polar media such as toluene, hexane or chloroform, a phase transfer into aqueous media of the nanocrystals is required before their *in vivo* injection.<sup>[139]</sup> In particular, a surface functionalization with biocompatible material is essential to enable their dispersion in polar solvents such as water. Two basic strategies are ligand addition and ligand exchange, where the former involves addition of a biocompatible coating on top of the original coating,<sup>[140]</sup> while the latter strategy involves removal of the original coating and replacing it by another biocompatible coating.<sup>[141]</sup> As an alternative strategy, a very simple synthesis of water-soluble magnetite nanoparticles was reported. Maity et al. also reported direct synthesis of water-soluble magnetite nanoparticles by thermal decomposition of iron (III) acetylacetone,  $\text{Fe}(\text{acac})_3$ , in tri(ethyleneglycol).<sup>[142]</sup>

In 2001, an elaborate study performed by Hyeon et al. a thermal decomposition method led to the synthesis of highly crystalline and monodisperse maghemite nanoparticle through two different approaches.<sup>[143]</sup> Within the first approach, mono-dispersed  $\gamma - \text{Fe}_2\text{O}_3$  nanoparticles were synthesized through the oxidation of iron nanoparticles. At first, iron oleate complex was prepared by adding  $\text{Fe}(\text{CO})_5$  to a mixture containing oleic acid and octyl ether at 100 °C. As reported by Wongterghem et al.,<sup>[144]</sup> decomposition of iron pentacarbonyl resulted in the production of iron(II) complex at this stage. Subsequently, by heating the resultant iron complex aging for 1 h at 300 °C, iron nanoparticles were being generated as the solution color gradually changed to blacked. In the final step,  $\gamma - \text{Fe}_2\text{O}_3$  nanoparticles were produced by oxidizing the resultant iron nanoparticles with trimethylamine oxide (( $\text{CH}_3$ )<sub>3</sub>NO) as a mild oxidant. The produced MNPs demonstrated an excellent uniformity of the particles size (Figure 7a) and highly crystalline nature (Figure 7b). Within the second approach,  $\gamma - \text{Fe}_2\text{O}_3$  were prepared through the direct oxidative decomposition of iron pentacarbonyl in the presence of surfactant and oxidant. Specifically,  $\text{Fe}(\text{CO})_5$  was injected into a solution lauric acid, octyl ether and trimethylamine oxide in an argon atmosphere followed by vigorous stirring. Subsequently, MNPs started being formed by stirring the solution for 1 h at 120 °C and heating it to reflux. Finally, upon adding excess ethanol and centrifuging process black precipitates of maghemite nanoparticles were obtained. TEM images of the resultant nanoparticles through this approach also demonstrated very uniform and highly crystalline MNPs with a diameter of 13 nm (Figure 7c).

Peng and co-workers have reported a general thermal decomposition approach in which MNPs could be synthesized with a narrow size distribution over a wide size range (from 3 to 50) with great control over their shape to be whether in the spherical or cubic form.<sup>[134]</sup> Nogues et al. also applied thermal decomposition method for the synthesis of highly monodisperse cubic and spherical maghemite ( $\text{Fe}_2\text{O}_3$ ) nanocrystals.<sup>[145]</sup> In a recent study, Hufschmid et al. evaluated and compared synthesis of iron oxide nanoparticles from decomposition of different precursors for their capability to produce iron oxide nanoparticles with specific size and phase-purity requirements.<sup>[130]</sup> It was

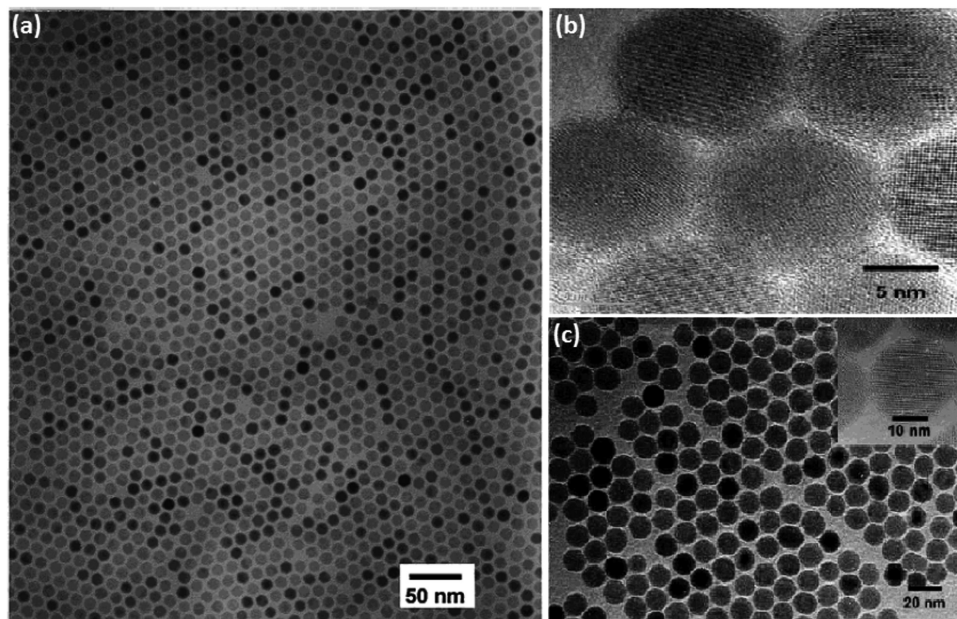


**Figure 7.** a,b) TEM and high resolution TEM images of a 2D hexagonal assembly of 11 nm  $\gamma$ - $\text{Fe}_2\text{O}_3$ , showing the uniformity of particle size and crystalline nature of MNPs produced by oxidation of iron nanoparticles. c) Low-resolution and high-resolusion TEM image of a single nanocrystallite (inset) of 13 nm MNPs produced through the oxidative decomposition of iron pentacarbonyl Reproduced with permission.<sup>[143]</sup> Copyright 2001, ACS.

concluded that pentacarbonyl synthesis is suited for synthesis of small (<10 nm) SPIONs, while both iron oleate and oxyhydroxide surpass the thermal decomposition method for production of larger (10–30 nm) particles.

Particle size plays an important role on the blocking temperature of nanomagnets, thus a narrow size distribution of magnetic particles prevents polydispersion in a resulted sample.<sup>[92a]</sup> In addition to the ratio of precursors and ligands to start with, shape and size of the formed MNPs by thermal decomposition approach are governed by the rate of heating, the final temperature of the reaction and the annealing time.<sup>[146]</sup> In a study performed by Herman et al.,<sup>[147]</sup> they studied the effect of altering the symmetry and metal-ligand bond dissociation energy of the organometallic precursor on controlling the size and size distribution of iron oxide nanoparticles within a thermal decomposition synthesis. Three iron sandwich compounds having different decomposition profiles were decomposed in 1-octadene solvent in the presence of oleylamine as a capping agent. Their results showed that organometallic compounds with optimal symmetry and bond dissociation energy give narrower decomposition temperature range which directly results in monodispersed nanoparticles. However, the importance of thermal control during the reaction has hampered a facile scale-up of this process.<sup>[148]</sup> In particular, it is more difficult to control the reaction temperature as the batch becomes larger, which indeed leads to less consistent particles with wider size distributions. To overcome such hindrances, Glasglow et al.<sup>[149]</sup> reported the first continuous synthesis of iron oxide nanoparticles via thermal decomposition. They constructed a high-temperature continuous flow reactor which offered a precise control over flow rate, temperature and precursor composition (**Figure 8**). A precursor solution consisting of iron oleate, oleic acid, and trioctylamine was stored in a sealed flask. As the

solution flew within the tubes, iron oleate underwent a rapid decomposition in a nitrogen atmosphere at 300 C. Their results showed the iron oleate/ligand ratio in the precursor to play an important role in the final particle size.

Overall, drastically opposite to coprecipitation method, thermal decomposition offers good control over the size of MNPs, but suffers from tuning their shape for substituted ferrites. Specifically, monodisperse MNPs with high crystallinity and tunable magnetic properties are resulted due to quick burst nucleation followed by crystal growth. Surfactants can also be added as stabilizing coatings to prevent the aggregation and fouling of nanoparticles. However, this strategy suffers from the need for phase transfer, toxic organic solvents, and high temperature. In the matter of former, thermal decomposition method results in MNPs which are dispersable in non-polar media, which entails a phase transfer into aqueous media needed for *in vivo* applications.

**2.1.2.2. Microwave Assisted Synthesis:** Same as ultrasound, microwaves can also be exploited to accelerate the reaction synthesis of nanoparticles. Specifically, electromagnetic waves with wavelengths in the range of 1 mm–1 m (frequency range 0.3–300 GHz) are termed as microwaves. Also microwaves have been extensively used in the food industry since 1940s, it was in 1986 that they paved their way to applications in chemistry, especially through works published by Baghurst and Mingos.<sup>[150]</sup> In fact, microwaves can be used as an alternative source of heat, individually or in assisted with other synthesis routes (Figure 4f).<sup>[151]</sup> Since microwave assisted technique is mostly combined by thermal decomposition, we have categorized this method as a non-hydrolytic approach. However, hydrolytic approaches such as hydrothermal,<sup>[152]</sup> sol-gel<sup>[153]</sup> can also be accelerated upon utilizing microwaves. This method

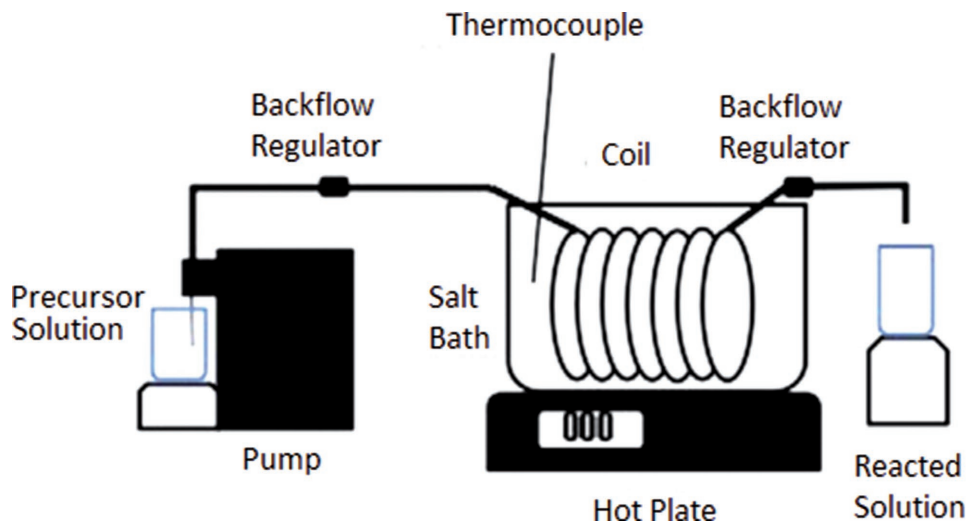


**Figure 8.** Diagram of the continuous flow reactor via a thermal decomposition synthesis route. Reproduced with permission.<sup>[149]</sup> Copyright 2016, Elsevier.

uses microwave radiation for heating materials containing electrical charges for instance polar molecule in the solvent or charge ion in the solid. Rapid processing, high reaction rate, reduced reaction time, high yield of product along with simplicity and high energy efficiency are some advantages of this method. However, its expansion in the area of organic chemistry has been much faster than that of inorganic chemistry. Overall, iron oxide nanoparticles have gained considerable attention to be synthesized by microwave assisted method.

Wang et al. synthesized magnetite and hematite by using microwave radiations during 10 min. They used  $\text{FeCl}_3$ , polyethylene glycol, and  $\text{N}_2\text{H}_2\text{H}_2\text{O}$  as precursors and found that controlling the final phase of  $\text{Fe}_3\text{O}_4$  is highly dependent on the amount of  $\text{N}_2\text{H}_2\text{H}_2\text{O}$ .<sup>[154]</sup> In a recent study, FITC-dextran coated iron oxide nanoparticles were synthesized by the hydrazine mediated reduction of iron (III) chloride salts in the presence of dextran under continuous stirring and microwave irradiation.<sup>[155]</sup> Subsequently, a gel filtration chromatography was used to perform the purification of the sample and removing unreacted iron salts and the excess of hydrazine. MNPs with small size (21.5 nm) and an excellent reproducibility were synthesized. They also showed good performance as a positive contrast agent for MRI as well as optical probes for fluorescent imaging. Microwave assisted method is very capable for scaling up the synthesis of nanoparticles.<sup>[156]</sup> Gonzalez-Moragas et al. have also recently reported the scale-up synthesis of water-dispersible iron oxide nanoparticles by microwave assisted thermal decomposition.<sup>[157]</sup> They utilized multimode equipment and increased the reaction volume from 4.5 to 50 mL (tenfold scale up) whose vessels were simultaneously irradiated with microwaves and notably reduced the time and energy cost for production of large amounts of MNPs (3 g per reaction in less than 1 h).

In summary, the rapid processing and high reaction rate within this strategy leads to reducing the reaction time for the production of narrow sized distribution MNPs with high crystallinity and water dispersibility. Although the penetration depth of the microwave is limited, high yield of production

within a high energy efficient and simple process can be achieved.

## 2.2. Microfluidic Synthesis of Nanoparticles

Manipulation of magnetic nanoparticles needs to fulfill some requirements in exhibiting physical and chemical properties to make them efficient for their utilization in biological applications. These properties of nanoparticles are highly determined by their size, shape, and crystal-structure. Therefore, a better control of reaction, both kinetic and thermodynamic, is critical in order to synthesize nanomaterials of required properties.<sup>[40]</sup> Hence, fabrication of nanoparticles with small size and narrow size distribution need a homogenous reaction environment followed by ultrafast mixing.<sup>[43]</sup> A number of these challenges, particularly in the size control have been overcome by the batch synthesis routes<sup>[158]</sup> presented in the previous section. Although wet-chemical methods have been widely used, they are still suffering from some of their intrinsic properties. Conventional batch routes are time-consuming, mostly involving thermo-decomposition (requiring a long reaction time, up to several hours) or a coprecipitation (requiring a short, usually within less than half an hour).<sup>[159]</sup> Within these processes, controlling the product homogeneity is difficult and requires multipurification steps in order to obtain stable monodisperse nanoparticles.<sup>[46b]</sup> Furthermore, when it comes to physical fabrication techniques, greater challenges in fabrication of high quality nanoparticles are faced.<sup>[160]</sup> The resulted nanoparticles are “bare,” hence, they require post processing in order to prevent their intensive oxidation and agglomeration that decrease their ability for post-synthesis processing and manipulation in practical applications.<sup>[160]</sup> On the other hand, both expensive equipment and small production rates limit their commercialization.<sup>[161]</sup>

MF is an intrinsically interdisciplinary field of science that provides a powerful tool for better researches in physics, chemistry, biology, and materials science.<sup>[162]</sup> As with many new

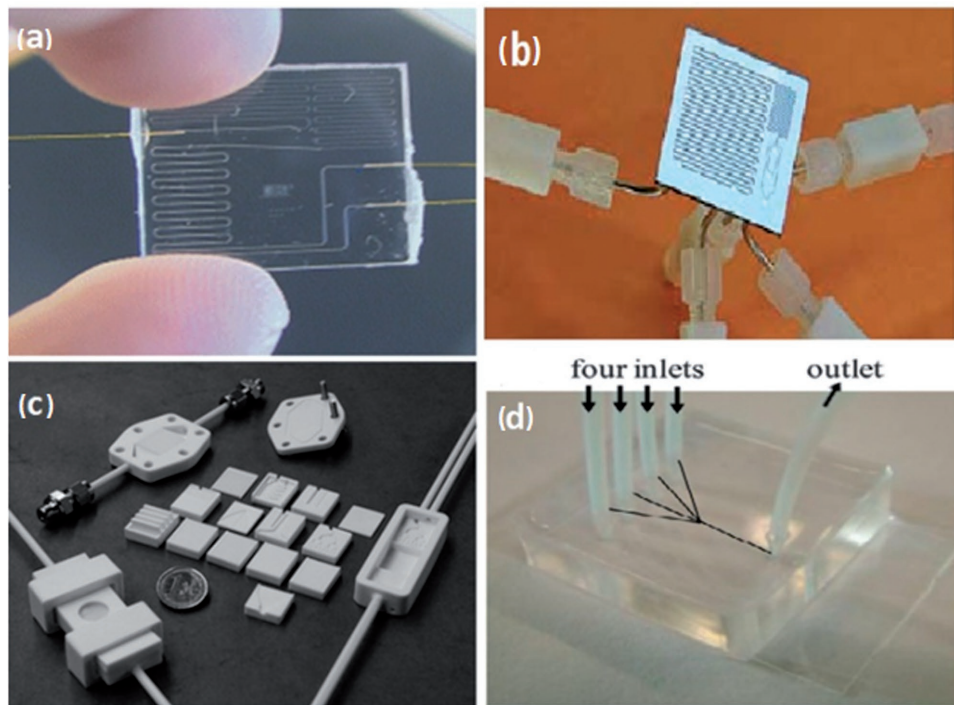


**Figure 9.** Micromixing based reactors made of a) glass, b) silicon, c) ceramic, and d) PDMS. a) Reproduced with permission.<sup>[190]</sup> b) Reproduced with permission.<sup>[188]</sup> Copyright 2009, RSC. c) Reproduced with permission.<sup>[191]</sup> Copyright 2004, RSC. d) Reproduced with permission.<sup>[192]</sup> Copyright 2014, RSC.

techniques, initial claims regarding performance, uniqueness, and applicability were optimistic and wide ranging.<sup>[163]</sup> The utilization of MF systems has found many applications in chemical industries for applications such as chemical synthesis, diagnosis, and crystallization due to their state-of-the-art developments in recent years. The first use of MF devices dates back to 1940,<sup>[164]</sup> for the fabrication of a chip-based chromatography.<sup>[165]</sup> Later in the early 1990s, with the development of MF reactors which are the key components of a lab-on-a-chip (LOC) for use in synthetic chemistry, MF devices were used for chip-based separation.<sup>[166]</sup> Such MF reactors have played a significant role in improving the reaction conditions and production of chemicals.<sup>[167]</sup>

In contrast with conventional batch systems, the use of MF to study and optimize the fabrication of a wide range of nanoparticles is attracting more and more attention<sup>[167]</sup> and their use for chemical synthesis gained a quick development with notable contributions from researchers at GlaxoSmithKline (UK),<sup>[168]</sup> Massachusetts Institute of Technology (USA),<sup>[169]</sup> the Institut für Mikrotechnik Mainz (Germany)<sup>[170]</sup> and Imperial College London (UK).<sup>[171]</sup> Since the first use of MF to prepare Cd nanoparticles on a lab-on-a-chip device,<sup>[172]</sup> advancement in the area of chemical synthesis of nanomaterials has been accelerated over the past decade.<sup>[39]</sup> Since then, various nanoparticles such as metal,<sup>[173]</sup> metal oxide,<sup>[174]</sup> semiconductors,<sup>[175]</sup> organic,<sup>[176]</sup> inorganic, etc., have been synthesized in MF systems, for example CdSe, Cds, Ti<sub>2</sub>O, boehmite, Au, Co, Ag, Pd, Cu, BaSO<sub>4</sub>, and CdSe – ZnS core–shell nanoparticles.<sup>[177]</sup> In nearly all cases MF synthesis has demonstrated clear advantages over conventional batch methods in terms of monodispersity and shape control.<sup>[178]</sup>

MF systems offer a versatile range of advantages over fabrication of nanoparticles due to the manipulation and controlling fluid that are geometrically constrained within environments having internal dimensions on a scale of micrometers.<sup>[163]</sup> Generally, shrinking entire chemical and analytical laboratories on a single microchip would be the ultimate goal.<sup>[179]</sup> Different types of materials, such as glass,<sup>[180]</sup> silicon,<sup>[181]</sup> ceramic,<sup>[182]</sup> polymers (PVC and PEEK), and stainless steel can be used to make MF devices. Operating conditions, ease of fabrication, and type of chemistry process define what construction material to be selected.<sup>[183]</sup> Glass microreactors (Figure 9a) enable the reaction process to be visualized, but difficulty in creating high aspect ratio structures makes them to be limited.<sup>[184]</sup> Microreactors made of silicon (Figure 9b) can be fabricated through photolithography, deep reactive ion etching and wet etching techniques.<sup>[185]</sup> Transparent reaction channels can be created through capping silicon structure by anodic bonding to Pyrex which enables process at high temperatures and pressures. Silicon also has a high coefficient of heat transfer that enables a precise control over temperature. Ceramic-based microreactors (Figure 9c) are chemically inert and can withstand high temperature but they have a complicated microfabrication process.<sup>[186]</sup> Polydimethylsiloxane (PDMS) is an interesting material for the fabrication of polymer-based microreactors (Figure 9d) for low temperature applications. This material takes advantage of being cheap, flexible, and transparent.<sup>[187]</sup> Metal microchannels can be created through mechanical micromachining, stamping, and Lithographie, Galvanoformung, Abformung (LIGA) techniques.<sup>[188]</sup> Such microchannels can sustain high pressure and temperature, but are vulnerable to strong acids.<sup>[189]</sup>

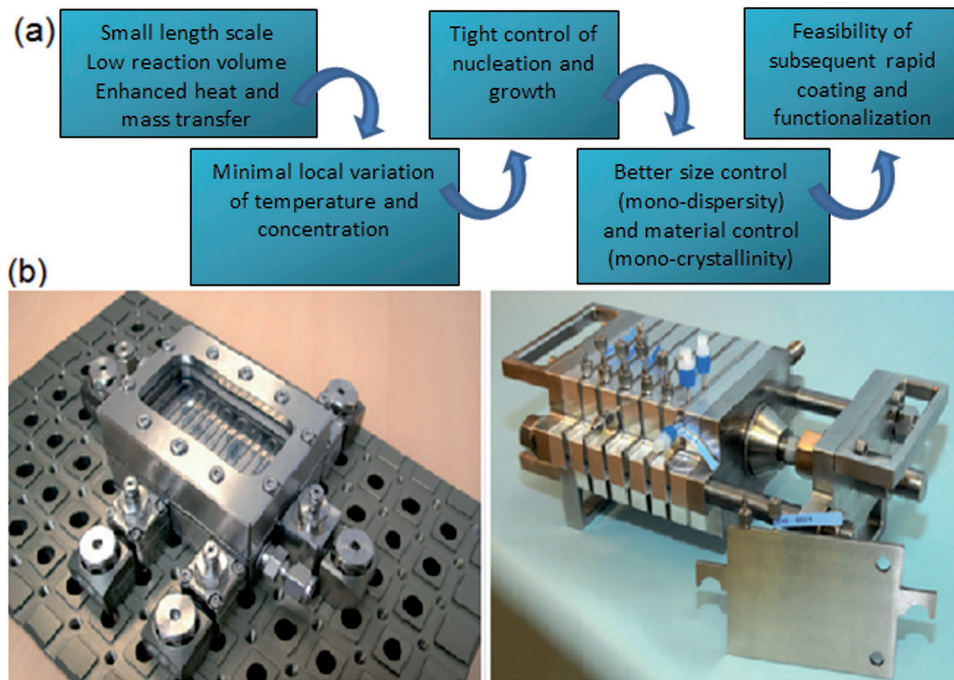


**Figure 10.** a) Potential advantages offered by the state-of-the-art microfluidic reactors for synthesizing nanoparticles. b) Photographs of two microfluidic reactors for process development kg production and also viewing the chemistry. Reproduced with permission.<sup>[193]</sup> Copyright 2012, de Gruyter.

By all the advantages offered by MF systems, better size control (mono-dispersity), and material control (monocrystallinity) can be easily achieved. In addition, produced nanoparticles are highly capable for a subsequent rapid coating and functionalization without need of surfactants or other primary stabilizing and capping agents (**Figure 10**).

The most highlighted advantages offered by MF systems are as below:

a. Small reagent volumes:

The inherent small reactor volumes required to process reagents in micro/nanoliter volume result in minimal reagent consumption.<sup>[194]</sup> Hence, it is economically beneficial in processing or testing where minimal amounts of precious reagents are available.<sup>[195]</sup> Particularly when used for informatics rather than for product synthesis, MF reactors consume far less reagent than bulk systems to gather the same (and in most cases more) chemical information.<sup>[42]</sup>

b. Process screening:

MF devices provide a high chemical detection that enables an efficient screening of chemical process and formulations under controlled conditions that can't be achieved in conventional macroscopic systems.<sup>[196]</sup> This *in situ* monitoring of chemical reactions comes in handy for time-resolved analysis or mechanistic studies.<sup>[42]</sup>

c. New concepts production:

Producing new concepts are possible by using MF. In particular, new compounds can be synthesized by integrating large numbers of independent chemical reactions on a

single chip with microfabricated networks having individually addressable microchannels and reservoirs.<sup>[197]</sup>

d. Automation:

MF devices are also capable of automating multi-step processes, such as combining analysis, reactions, and purification in a single microchip, thus becoming the LOC systems or micro total analysis systems.<sup>[42]</sup> In this case, MF devices culminate in "black box" techniques to completely automate the synthetic process which afford quality and product of materials with specific properties (Figure 10b).<sup>[177a]</sup>

e. Selectivity:

In process of chemical and biological reactions in a same reactant pool, more than one product can be generated depending on local conditions. This phenomenon is often ascribed to kinetic versus thermodynamic control of the reaction pathway.<sup>[198]</sup> By such a high degree of control over local conditions that are provided by MF devices, selection of one product over another with a high precision is possible.

f. Continuous synthesis:

Unlike the bulk synthesis routes, the flowing mechanism of reagents in MF channels offers the possibility of a continuous synthesis of nanomaterials by running up to 24 h d<sup>-1</sup> and carrying out analyses on-line.<sup>[199]</sup>

g. Safer operation:

Since the process consumes much reduced hazardous chemicals and reagents, complications in bulk synthesis associated with safety issues such as explosion and leakage of toxic and flammable solvents are minimized resulting

in a safer operation and environmental friendliness.<sup>[175,200]</sup> Furthermore, by eliminating the need to store and transport potentially hazardous materials, flexibility for tailoring complex functional nanomaterials is provided.<sup>[201]</sup>

h. Easy Scale out:

MF devices can be easily transformed into industry based on the concept of parallel processing of reactor systems combined with their continuous synthesis ability. It should be noticed that in this case microfluidics are scaled out by numbering up the devices rather than to be scaled up by increasing the characteristic dimension of channels.<sup>[202]</sup>

i. Small footprints:

Due to more efficient heat transfer, the need for heat-exchange equipment is minimized which leads to smaller footprint per kilogram of product in MF systems than in macroscale reactors.<sup>[203]</sup>

j. Green credentials:

Microreaction technology takes advantage of the large surface area-to-volume ratios within microchannels which can afford a high heat-exchanging efficiency compared to that of traditional ones. Hence, the amount of energy consumed per unit temperature rise can be made extremely small, resulting in environmental benefits.<sup>[204]</sup>

k. Rapid reactions:

Higher area to volume ratios accelerate heat and mass transport and lead to rapid changes in reaction temperature and concentrations. Thus, more uniform heating and mixing take place which dramatically impacts the synthesis process for higher space-time yields (product formed per reactor volume and time).<sup>[197b]</sup> It is, however, difficult to make direct comparisons, as bulk reactions are rarely optimized to terminate exactly at the final equilibrium position of the reaction (reaction completion or endpoint), but often incorporate extra time to ensure completion has been reached. Reactions in MF reactors are rarely run for longer than required to reach the reaction endpoint, as they can be closely monitored to determine reaction completion. Accordingly, reaction times from literature syntheses are almost always incompatible with times associated with MF formats.<sup>[163]</sup>

l. Precious control over temperature and concentration:

The ability to manipulate reagent concentrations in both space and time within the channel network coupled with large area to volume ratios in MF systems facilitate fast and accurate temperature control for synthesis process of nanoparticles, that is actually not attainable in bulk stirred reactors where concentrations are generally uniform.<sup>[197b]</sup> These properties with intrinsic ones of MF, like very small reaction volumes, make microreactors suited for synthesis of nanoparticles that requires fast reactions with a large heat effect, in nearly isothermal conditions at high reactant concentrations. Furthermore, the possibility of fast mixing of reactants and fast heating and cooling of reaction mixtures enables precise control of the reaction temperature and preventing large temperature gradients, thus improving the yield of reaction intermediates while reducing

by-product formation. In general, it takes only seconds or sub-seconds to raise a solution in a microchannel from room temperature to hundreds of degree °C.<sup>[201]</sup>

m. A precious control over reaction time:

As reagents flow through microchannels, a potential control over the reaction time in MF systems is achieved by varying reagent flow rates or channel geometry. In particular, the reaction time relates to the distance that continuous flows of reagents have traveled through channels.<sup>[176]</sup> This way, the reaction can be controlled and quenched through the channel length tuning or reagents adding at precise downstream locations during the particle formation process.<sup>[39]</sup>

n. A precious control over the shape and size of resultant nanoparticles:

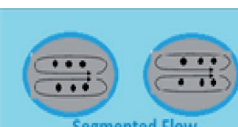
Two important properties of nanoparticles used in biological applications are the size and shape of nanoparticles. Nanoparticle synthesis process involves nucleation, growth, and agglomeration.<sup>[205]</sup> Inorganic nanoparticles undergo self-assembly where metal solutes nucleate, grow, and agglomerate into nanostructures.<sup>[206]</sup> The critical factors effecting the preparation of nanomaterials are reagent concentration, reaction temperature, and residence time for the size of nanoparticles, and crystalline surfaces for their shape.<sup>[41]</sup> Since MF systems provide a potential controlling ability over reaction time, reaction temperature, and concentration of reagents, particles with better narrow size distribution can be achieved by quenching the reaction whenever the desired size of the NPs is reached.<sup>[207]</sup>

### 2.2.1. Microfluidic Strategies for Synthesizing Nanoparticles

Microfluidic approaches for nanoparticle synthesis can be generally classified into two categories: continuous-flow (single-phase flow) approach and segmented-flow (multiphase) approach.<sup>[50,196]</sup> Table 3 compares these two microfluidic strategies by their advantages and disadvantages. This section will summarize these two approaches with focus on introducing some basic concepts and their applications in the synthesis of MNPs.

**2.2.1.1. Continuous Flow Microreactors (Single-Phase Flow):** Continuous flow microreactors have attracted significant interest in applications of material synthesis by virtue of their unique properties, such as simple and controllable operation, high throughput, and easy separation. Reaction time, temperature, efficiency of mixing, and concentration of the reagents are among the factors which determine the product quality.<sup>[42]</sup> The homogeneity of reaction solutions can be highly improved by this more productive method, leading to a more uniform product.<sup>[208]</sup> These systems enable facile and rapid change of conditions by decreasing flow channels to micron size.<sup>[209]</sup> Furthermore, continuous variation in the chemical composition of the mixture can take place since numerous kinds of reagents can be added along the microfluidic channels.<sup>[210]</sup> As mentioned previously, one advantage of microfluidic devices is its easy scaling-up. These continuous synthesis platforms are able to simply run reactions in parallel that shortens their transition

**Table 3.** Comparison of single-phase and multiphase microfluidic reactors.

Micromreactor categories	Type of micromreactor	Flow Pattern	Production	Advantages	Disadvantages
Single-phase micromreactor	Capillary tubes		High	Simplicity High temperature adaptability	Longer channel lengths Wide RTD and broad size distribution of produced nanoparticles Contamination of channel wall Channel clogging
	Coaxial flow micromreactor		High		
Multiphase micromreactor	Gas–liquid or liquid–liquid		High	Enhanced mixing Reduced RTD Narrow size distribution Reduced risk of fouling	Difficulty in subsequent addition of reagents
	Droplet-based		High		

from lab scale to industrial scale.<sup>[210]</sup> One of the other advantages of these systems is their ability to link individual reactions into multistep sequences wherein one reaction flows into another resulting in combining multiple synthetic steps.<sup>[211]</sup> This way, reliable kinetic information for chemical process design can be extracted through online monitoring of complex transformations.<sup>[202a]</sup>

However, some limitations still remain in synthesizing multiple functional and high-quality nanoparticles. In these systems, the mixing and reaction of the reagents take place under diffusion-based laminar flow conditions. In the continuous flow systems the parabolic velocity profile limits the reaction into slow diffusive mixing. Thus, wider residence time distribution (RTD) occurs that results to a wider particle size distribution. In most cases, the laminar flow is disturbed by both mass transfer and growth of nanoparticles resulting in a hard control of mixing conditions and residence time.<sup>[50,213]</sup> Moreover, when it comes to the selection and design of micro-reactors using single-phase flow, great caution must be carried out due to the probability of channel clogging and blockage.<sup>[213]</sup> Based on the internal microchannel networks, continuous flow microreactors are grouped into capillary tubes which are constructed through mechanical assembly and chip-based microfluidics.

**2.2.1.2. Capillary Tubes Microreactor:** The simplest microreactor used for synthesizing nanoparticles is made of capillaries at the micrometer length scale. A typical capillary microreactor is illustrated in **Figure 11a**. Two streams of reagents flow within two separate capillaries and subsequently pass through a micro-mixer. In the next step, the reaction temperature is controlled by entering a single capillary submerged in a heated water or oil bath. Finally, the synthesis of nanoparticles starts with their nucleation and growth within the heated capillary. A facile improvement in size and composition control in the synthesis of nanoparticles along with an accurate temperature control can be easily achieved due to the microscale diameter of the capillaries. Nakamura et al. showed that only 0.4 s was needed for heating a 200 nm diameter channel from 20 to 300 °C.<sup>[214]</sup> Hence, the temperature of the reaction ranges from below room temperature to several hundred degrees.

Structural and magnetic properties of the spinel structure of materials can be significantly varied by substituting various transition metals into them. It has been reported that the saturation magnetization value of iron oxide nanoparticles increases with partial substitution of them with zinc.<sup>[217]</sup> With respect to this improvement, a study was conducted by Simmons et al.<sup>[215]</sup> to synthesize zinc doped iron oxide nanoparticles within a continuous microreactor. They modified the same procedure reported in their previous work.<sup>[218]</sup> While the precursor solution (consisting of iron and zinc salts) was pumped into the central microchannel, the basic solution (sodium hydroxide) was pumped through two lateral microchannels to focus the precursor solution between the two flows of base (Figure 11b). This strategy greatly reduced the amount of precipitating nanoparticles upon the microreactor walls and prevented blocking of the channel. Resultant  $Zn_xFe_{3-x}O_4$  superparamagnetic MNPs had an average size of 5 nm. Their results also showed a linear increase of the saturation magnetization with increasing Zn content.

Recently, a simple natural-rubber-based microfluidic device has been proposed to prepare controlled amounts of magnetite nanoparticles decorated with Au nanoparticles.<sup>[216]</sup> Within this process, magnetite nanoparticles were produced by a conventional coprecipitation method. Subsequently, two inlets of the microfluidic device were used to introduce concentrations of magnetite nanoparticles to the suspension of gold nanoparticles (**Figure 12a**). TEM images highlighted that the resultant Au nanoparticles were homogenous in terms of their size and their distribution on the surface of magnetite nanoparticles (**Figure 12b**). The histogram also shows that the average size measured for the Au nanoparticles was around 6.3 nm (**Figure 12c**).

In a very recent study, Thu et al.<sup>[219]</sup> have developed a convenient approach to combine the traditional coprecipitation method and microfluidic devices for producing iron oxide nanoparticles. They designed a microfluidic reactor and exploited soft-lithography techniques to build it out of PDMS. Their results confirm the production of MNPs with narrow size distribution and more controllable behaviors. Ma et al.<sup>[220]</sup> reported the synthesis of magnetic nanohybrids with the formula of  $Sn_{(1-x)}Fe_x@Fe_ySn_{(1-y)}O_z$  via a simple programmed microfluidic

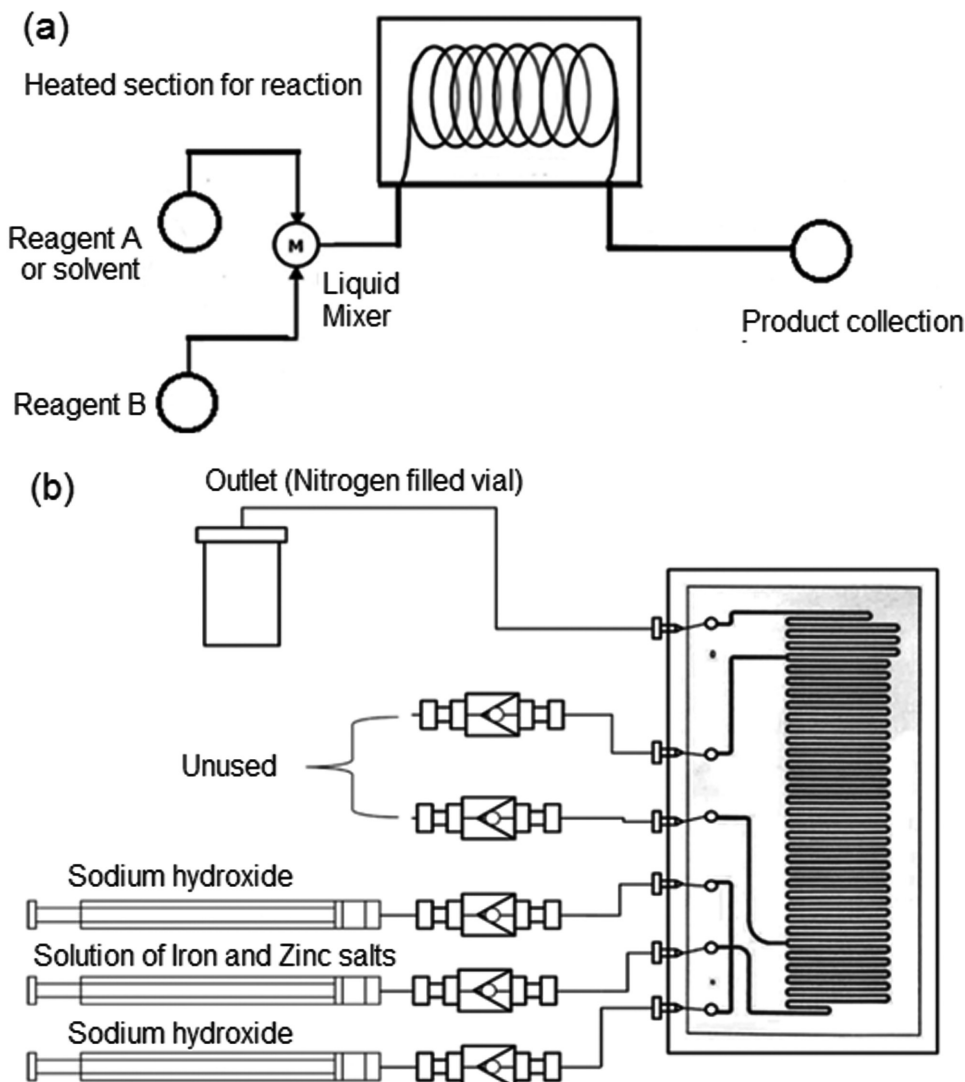


**Figure 11.** Capillary microfluidic reactors for the synthesis of nanoparticles. a) Schematic illustration of a typical capillary microreactor. b) Schematic diagram of a microreactor set up used in the synthesis of  $Zn_xFe_{3-x}O_4$  nanoparticle synthesis. Reproduced with permission.<sup>[215]</sup> Copyright 2015, RSC.

process through simply tuning the reaction temperatures. Their results indicated that synthesis temperature allow to control the reaction rate. In particular, nanohybrids with rod shape were synthesized at 30 °C, while increase of the temperature to 90 °C significantly changes their shape into spherical nanosystems.

**2.2.1.3. Coaxial Flow Microreactor:** Although capillary tube microreactors are very simple, highly flexible, and facile in operation, these systems still suffer from adhesion to the channel surface, blockage, and broad size distribution of resulted nanoparticles. To overcome these problems in single tubing microfluidic reactor, a microfluidic device was developed by the assembly of coaxial dual tubes (**Figure 13a**).<sup>[221]</sup>

Hassan et al.<sup>[222]</sup> synthesized iron oxide nanoparticles from the reaction of an aqueous solution of iron chloride with a basic solution of NaOH, NH<sub>4</sub>OH, or tetramethyl ammonium hydroxide (TMAOH). They used a coaxial flow microreactor which consists of two tubular reactors coaxially arranged to

contact the two solutions (Figure 13b). A well-defined jet, centered in the channel, is produced by a coaxial injection of iron chloride solution (outer flow) through a silica capillary tube that is introduced inside a millifluidic channel where the basic solution is flowing. Through this approach, nucleation and growth of iron oxide nanoparticles take place far from the channel walls at the border of which the two fluids diffuse in each other. Such a configuration was found to lead to small size distribution. Later, fluorescence confocal laser scanning microscopy<sup>[226]</sup> was used to experimentally map the coaxial flow at different pH values for a better understanding of the influence of pH distribution. To avoid the formation of FeOOH for a better synthesis of monodisperse and high quality iron oxide nanoparticles, a rapid and well defined change in the pH value is required which can be provided by the use of coaxial microflows. The same group has recently reported the production of cobalt ferrite ( $CoFe_2O_4$ ) nanoparticles using two coupled microreactors (**Figure 14a**).<sup>[223]</sup> The first reactor was exploited to induce the

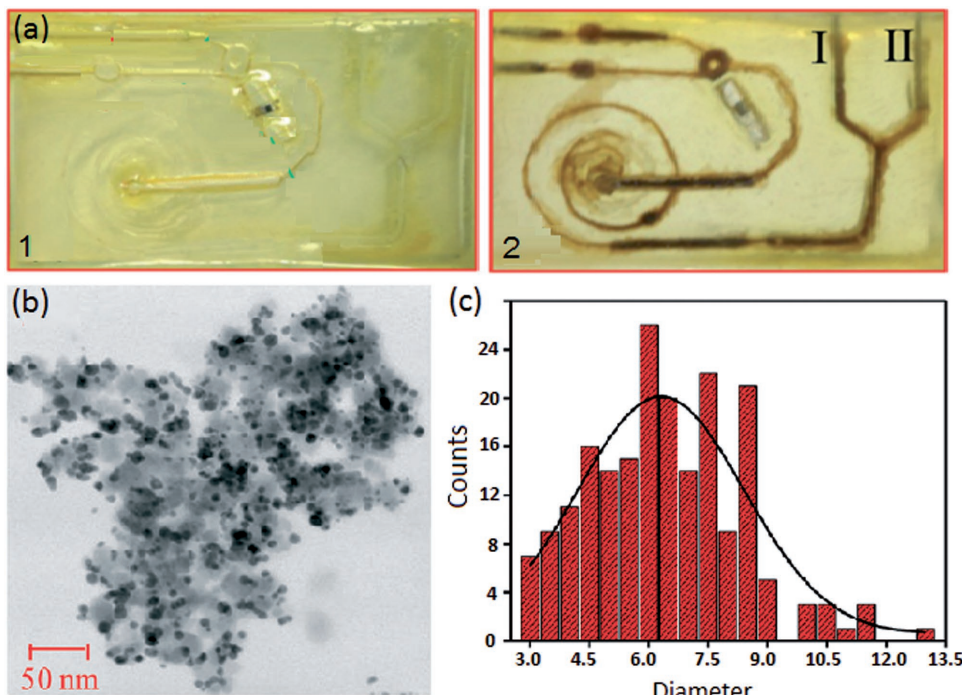


**Figure 12.** a1) An empty natural rubber-based microfluidic device (NRMD) with internal magnetic separation. a2) Flow of MNPs through inlet I to be decorated with Au nanoparticles flowing through inlet II. b) TEM images of  $\text{Fe}_3\text{O}_4$  – Au nanoparticles, and d) and the histogram showing the diameter distribution of Au nanoparticles coating the surface of  $\text{Fe}_3\text{O}_4$  MNPs. Reproduced with permission.<sup>[216]</sup> Copyright 2015, RSC.

fast homogenization of the reagent mixture, while the second reactor accounted for fast aging and the evolution of resultant MNPs into faceted and crystalline  $\text{CoFe}_2\text{O}_4$ . Interestingly, it only took 16 min to yield MNPs of the desired size at 98 °C (Figure 14b). To prove the mixing and time efficiency of the process, simultaneous bulk coprecipitation and hydrothermal synthesis of the same MNPs were performed for 16 min and their products were analyzed by TEM. It was shown that only amorphous hydroxides were obtained by bulk coprecipitation and even by heating the mixture at 98 °C in a hydrothermal bomb, the total transformation of amorphous hydroxides into crystalline and well-defined nanoparticles could not be achieved (Figure 14c,d). However, obtaining the  $\text{CoFe}_2\text{O}_4$  nanoparticles similar in size to those produced by the microfluidic synthesis in 16 min at 98 °C needed a 50 min heating at 200 °C in a hydrothermal bomb and 2 h boiling at 100 °C in normal bulk coprecipitation method.

They have also demonstrated a multistep continuous-flow microsynthesis of magnetic and fluorescent g –  $\text{Fe}_2\text{O}_3@\text{SiO}_2$  core/shell nanoparticles (Figure 15a).<sup>[224]</sup> MNPs with approximately the same shape and dimensions in bulk synthesis were obtained, but the production time was reduced to a few minutes (7 min) compared to several hours in the bulk. The TEM images of the resultant MNPs showed almost spherical core-shell structure with an average overall size of 50 nm (Figure 15b-d). However, since the silica shell was not functionalized to protect the MNPs against aggregation, produced MNPs were very sensitive to aggregation.

In another study performed by Nguyen et al.<sup>[225]</sup> fluorescent magnetic nanoparticles were synthesized in a microchannel

using the La Mer process. This method includes wet chemical coprecipitation of ferrous and ferric ions with ammonia where ammonia is mixed with a stirred solution of ferrous and ferric ions. Three inlets were used to introduce the prepared chemicals into the microchannel as shown in Figure 13c. combination of  $\text{FeCl}_2$  and  $\text{FeCl}_3$  flowing in inlet 1 was mixed with  $\text{NH}_4\text{OH}$  solution that was injected through inlet 3 and resulted in a rapid initiation of the synthesis of magnetic nanoparticles as soon as these two reactants met. Aggregation of nanoparticles on the wall surfaces resulted to channel clogging because of the zero velocity that was imposed on the wall due to non-slip condition and insufficient force of the fluid that was not able to flush the produced magnetic nanoparticles attached to the wall. A Dichloromethane or a non-polar organic solvent was introduced through inlet 2 that led to a formation of a five layered lamination flow in a microchannel. The produced nanoparticles were finally functionalized and became biocompatible coating them with chitosan.

**2.2.1.4. Segmented Flow (Multiphase) Microreactors:** In contrast with continuous flow microreactors which suffer from Taylor dispersion, cross-contamination and relatively long channel lengths along with wide RTD due to the parabolic velocity, segmented flow microreactors can overcome some of the aforementioned drawbacks and provide high quality synthesis of nanoparticles to fulfill the true potential of system miniaturization. In particular, by creating discrete segments in a second immiscible phase within the microchannel, a great enhancement in the mixing of reactants occurs through recirculation within the segments. They also reduce the risk of

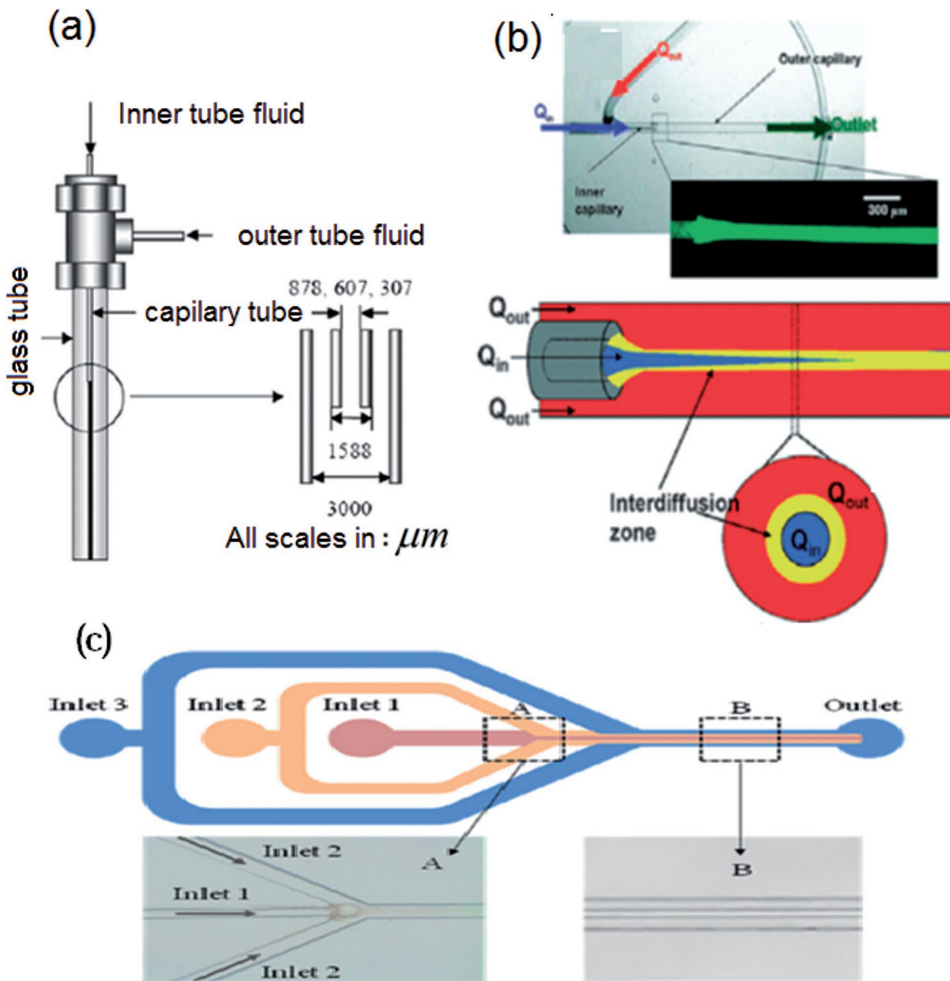


**Figure 13.** Coaxial microfluidic reactors for the synthesis of nanoparticles. a) Schematic of a simple coaxial microfluidic device. b) Photograph, and cartoon of a 3D view and a cross sectional view of the coaxial microfluidic reactor for the synthesis of iron oxide MNPs. c) Five layered laminar flow formed to synthesize the MNPs in the flow-through a coaxial microreactor. a) Reproduced with permission.<sup>[221]</sup> Copyright 2004, Elsevier. b) Reproduced with permission.<sup>[222]</sup> Copyright 2008, RSC. c) Reproduced with permission.<sup>[225]</sup> Copyright 2014, Springer.

fouling by wetting the channel surface and therefore provide a high level of control of the synthesis conditions.<sup>[50,227]</sup> Either liquid–liquid/gas–liquid segmented flow microreactors or droplet-based microreactors can be used for this purpose.<sup>[52]</sup> Reagents can be highly localized by virtue of these immiscible fluids in both commercial and laboratory systems.<sup>[228]</sup>

**2.2.1.5. Gas–Liquid or Liquid–Liquid Microreactors:** Through this approach, mixing process is induced by manipulating two phase flows of gas/liquid or liquid/liquid wherein one liquid phase contains the reactants and the other gas or liquid acts as inert fluid for flow segmentation.<sup>[37]</sup> By this strategy, one can control the initiation of the reaction as well as the whole time of reaction evolution before it is separated or combined with other reactions. Furthermore, axial dispersion within the micro-channel, i.e., wide RTD due to parabolic velocity in continuous flow synthesis, will be eliminated which leads to a narrower size distribution of nanoparticles. However, reactions at high temperature and pressure cannot be performed through gas/liquid flow due to dramatic volume change of gas by temperature. On

the other hand, for liquid/liquid flow, both phases must remain liquid and immiscible during the process.<sup>[37]</sup>

A notable study has been recently conducted by Larrea et al. wherein growth of iron oxide nanoparticles has been highly controlled by exploiting gas slug microfluidics in a two-stage process.<sup>[229]</sup> Firstly, two aqueous solutions (one consists of sulfuric acid and ferrous sulfate, and the other consists of NaOH and KNO<sub>3</sub>) were mixed in a Y-junction and subsequently were irradiated by ultrasound to avoid the formation of micrometric aggregates (**Figure 16**).

In the next stage, different types of gas flows (N<sub>2</sub> (inert), O<sub>2</sub> (oxidizing), CO and H<sub>2</sub> (reducing)) were introduced to the mixture for the formation of gas slugs. Their results showed the potential effect of the gas on phase on the morphology and crystalline structure of the resultant MNPs. In the case of N<sub>2</sub> and H<sub>2</sub> black dispersion of MNPs with their characteristic octahedral shape were produced. While injection of O<sub>2</sub> and CO resulted in orange dispersion of crystalline iron (III) MNPs with a crystalline structure corresponding to feroxyhyte, in the form of nanoflakes and hexagonal nanoplates, respectively.

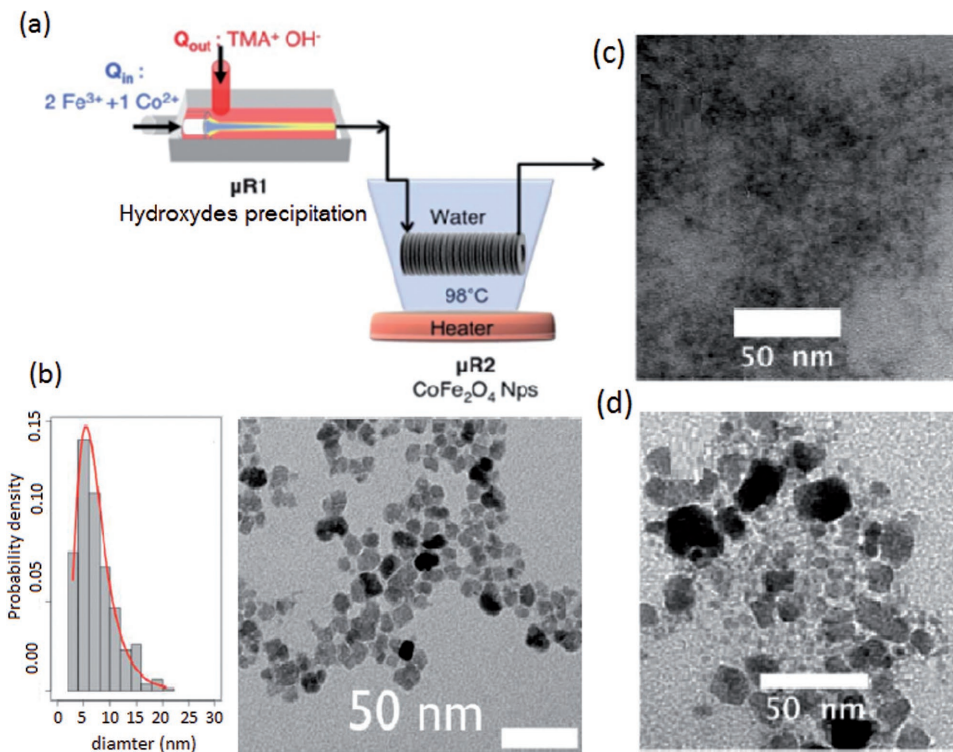


**Figure 14.** The experimental setup designed for the synthesis of cobalt ferrite nanoparticles. TMAOH = tetramethylammonium hydroxide. Tem images of nanoparticles obtained at 98 °C after a 16 min of aging a) in the microreactor synthesis, and its corresponding size histogram, b) in bulk synthesis, c) in bulk, in a hydrothermal bomb. Reproduced with permission.<sup>[223]</sup> Copyright 2012, RSC.

**2.2.1.6. Droplet-Based Microreactors:** One of the most promising strategies in nanomaterial synthesis is performing reactions inside aqueous plugs (droplets large enough to block the channel)<sup>[230]</sup> surrounded by a continuous oil phase (**Figure 17**). In this type of microreactor, reagents are encapsulated in a co-flowing stream just before a droplet is formed and the reaction occurs later inside the droplet. Chaotic advection results in a rapid mixing of reagents encapsulated in droplets as they are carried along the winding channel which eventually leads to a perfect synthesis of monodisperse nanomaterials by eliminating the dispersion problem related to continuous flow microreactors. In addition, channel clogging should be taken into full consideration. The chance of fouling inside the microreactor can be inhibited by isolating solid nanoparticle products to keep them away from inner wall of the channel.<sup>[37,234]</sup>

Frenz et al.<sup>[232]</sup> demonstrated a synchronized production of droplet pairs that are stabilized by surfactant for the synthesis of iron oxide magnetic nanoparticles by coprecipitation ferrous and ferric salts in a presence of a base. The microfluidic device was designed to pair perfect one-by-one droplet by the use of two hydrodynamically coupled nozzles and surface-modified channels (**Figure 18a,b**). Subsequently, a very fast (2 ms) precipitation of iron oxide nanoparticles (**Figure 18c**) were obtained by the fusion of droplets by electrocoalescence which prevented the channel clogging and enabled the increase of the compound concentration compared to previous synthesis of nanoparticles through droplet-based microfluidic approach. The TEM of the iron oxide particles produced showed that compared to bulk mixing, microfluidic compound mixing resulted in particles

with smaller average diameter which are monocrystalline with no visible stacking faults (**Figure 18d**).

Later in 2012, Kumar et al.<sup>[233]</sup> reported a simpler passive methodology for direct synthesis of dextran-coated superparamagnetic iron oxide nanoparticles in a capillary-based droplet reactor where droplets are formed close to the end of a length of silicone tubing at the contact point between two auxiliary capillaries. Compared to Frenz et al. method,<sup>[232]</sup> there was no need for the surface modification of the channel and high voltage power sources. Aqueous reagents were fed into the capillaries by implementing two separate syringe pumps, while a constant flow of immiscible octadecene carrier was maintained through the main capillary by a third syringe pump (**Figure 19a**). A discrete droplet containing reagents subsequently budded off into a polytetrafluoroethylene capillary. Immediately after the confluence of the reagents streams, brown particles of iron oxide particles were observed. As it is illustrated by TEM images of nanoparticles (**Figure 19b**) and its corresponding histogram of particle size (**Figure 19c**), the purified nanoparticles were isotropic in shape with a narrow size distribution (mean diameter of 3.6 nm and standard deviation of  $\sigma_d = 0.8$  nm).

**2.2.1.7. Micromixing-Based Reactors:** Intensifying the mixing in microfluidic reactors is one the most important objectives to obtain nanoparticles with desired properties. Low Reynolds number results in mixing of reagents to be primarily dependent upon molecular diffusion due to absence of turbulence. On the other hand, laminar flow regime leads to a broad distribution of residence time which results in polydisperse

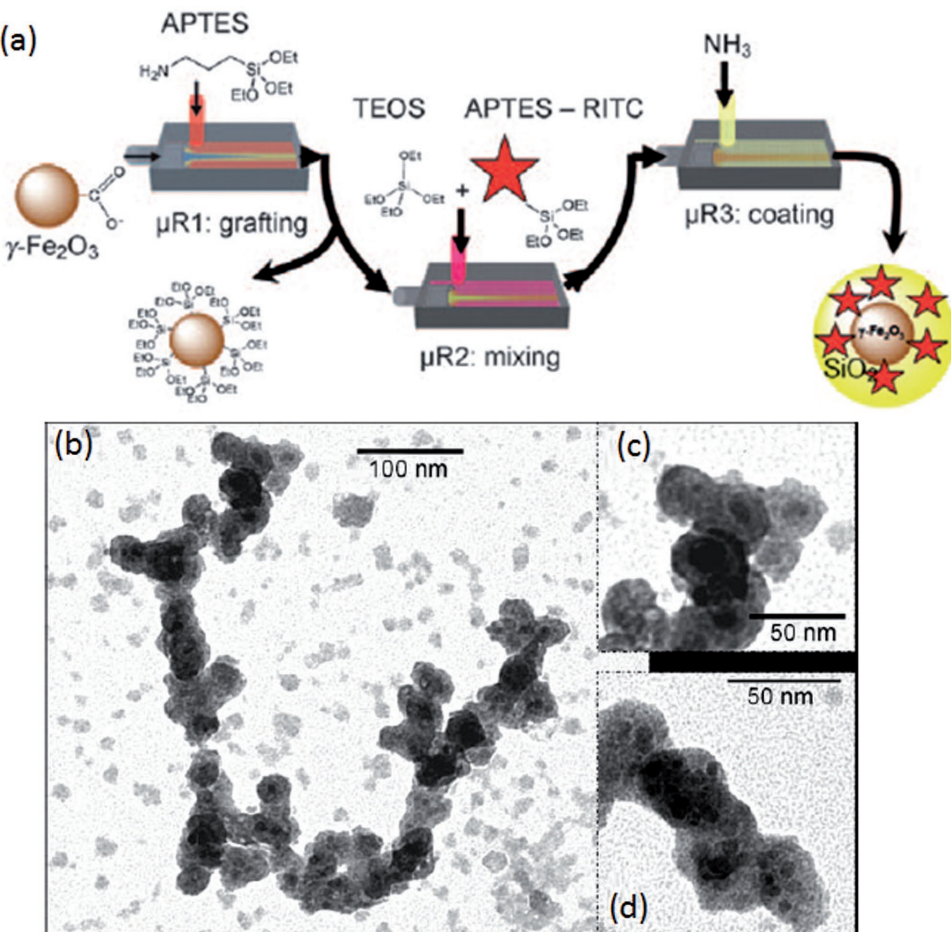


**Figure 15.** a) Schematic illustration of two step microfluidic reactor used for (i) synthesis of iron oxide MNPs (ii) and subsequent coating with silica. b-d) TEM images of showing typical architecture of core/shell MNP@ $\text{SiO}_2$  nanoparticles. Reproduced with permission.<sup>[224]</sup>

nanoparticles.<sup>[50,235]</sup> Micromixers have overcome these limitations by providing a better mixing of the reagents to have more control over the synthesis of nanoparticles with appropriate properties. Exploiting various channel geometries as well as external forces to decrease the mixing path and increasing

the contact surface area inside the channel form the basis of micromixers.

Based on the two different basic principles exploited to induce mixing during the formation of nanomaterials, micro mixers are generally classified as being passive or active. Table 4

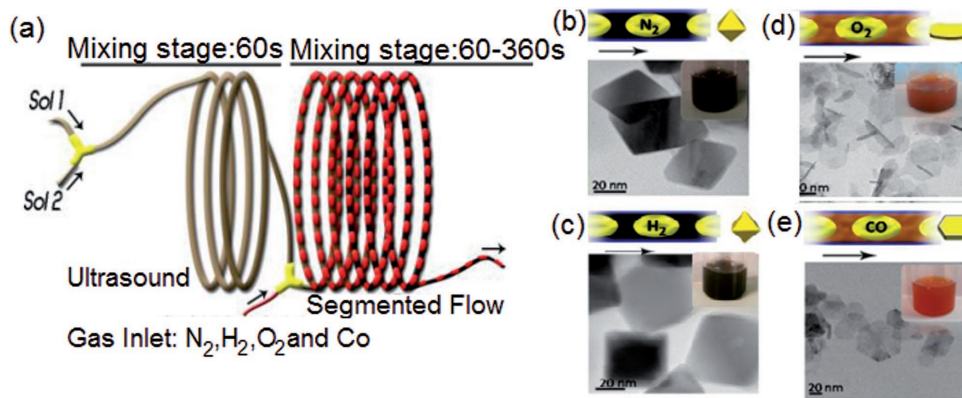


**Figure 16.** a) Microfluidic setup for the production of MNPs in continuous gas–liquid segmented flow and TEM images of MNPs synthesized by the liquid segmentation of reagents with different gas sources: b)  $\text{N}_2$ , 100 °C, and 6 min; c),  $\text{H}_2$  100 °C, and 1 min; d),  $\text{O}_2$  100 °C, and 1 min; e) CO, 80 °C, and 1 min. Reproduced with permission.<sup>[229]</sup> Copyright 2016, ACS.

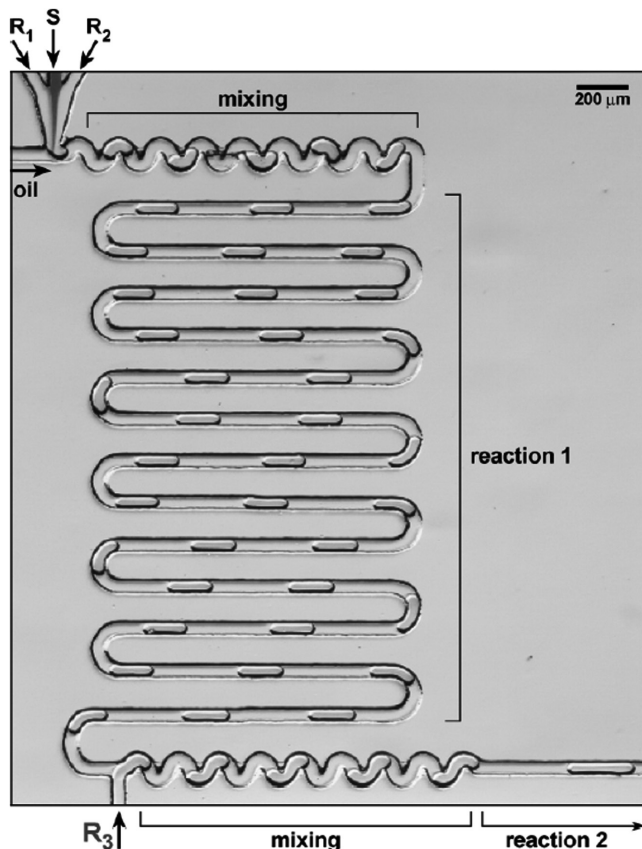


**Figure 17.** Micrograph of a PDMS droplet based microreactor for synthesis of nanoparticles. Reproduced with permission.<sup>[231]</sup> Copyright 2004, RSC.

summarizes different types of passive and active micromixers. Reducing diffusion length and enhancing chaotic advection as well as increasing the surface area form the basis of passive micromixers. In fact, by the use of passive micromixers no external forces are applied to the systems and they all rely on fluid pumping energy.

The surface area between different flows of reagents is increased by particular channel geometry which leads to a decrease in diffusion length of fluid flows. In the case of active micromixers, time-dependent perturbations are introduced to the fluid through both fluid pumping energy and external use of energy input accelerate the mixing process.<sup>[247]</sup> Although higher mixing efficiencies are provided by active micromixers, complex and expensive fabrications process as well as the requirement of the integration of peripheral devices such as external actuators for the external power source into the micro-devices have limited implementation of these kinds of micro-mixers in practical applications. More specifically, when it comes to biological applications, biological fluids can be damaged by the high temperature gradients produced by ultrasonic waves.<sup>[248]</sup>

In a recent comparative study, Larrea et al. analyzed four different approaches to synthesize MNPs.<sup>[249]</sup> Those four approaches were as follows: (a) mixing by internal diffusion. (b) Mixing by liquid segmentation. (c) Mixing by ultrasonic vibration. (d) Mixing with ultrasonic vibration and reaction with a gas segmented flow (Figure 20). In all approaches, solution of  $\text{FeSO}_4$  was precipitated in a basic medium ( $\text{NaOH}$ ) with a mild oxidant ( $\text{KNO}_3$ ). Both solutions were mixed in a PEEK polymer Y-junction. In the case of liquid segmentation, silicone oil was injected after the Y-junction to accelerate the reactants mixing. Their results indicated that MNPs with narrower

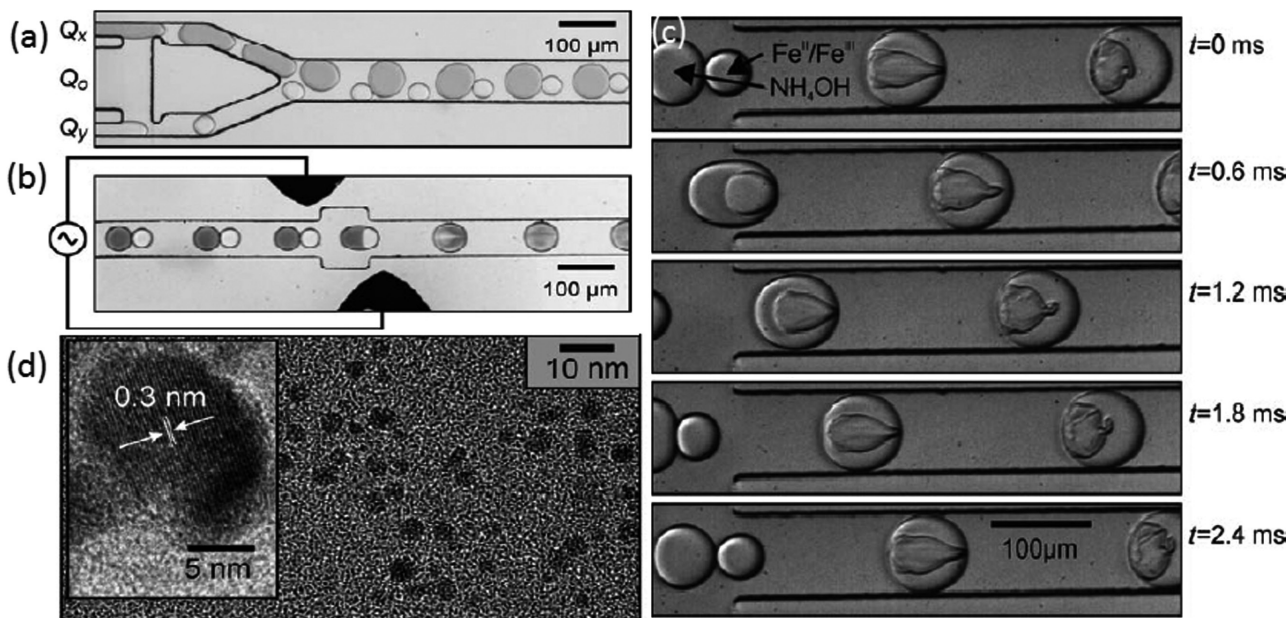


**Figure 18.** a) Pairing module, injection of two aqueous phases by the outer channel and their emulsification by the central oil channel, b) fusion module, coalescence of droplets by applying voltage  $U$  between the two electrodes. c) formation of iron oxide precipitates after coalescence of pairs of droplets. d) TEM image of the nanoparticles. Inset: HRTEM image of a particle showing (220) spinel planes. Reproduced with permission.<sup>[232]</sup>

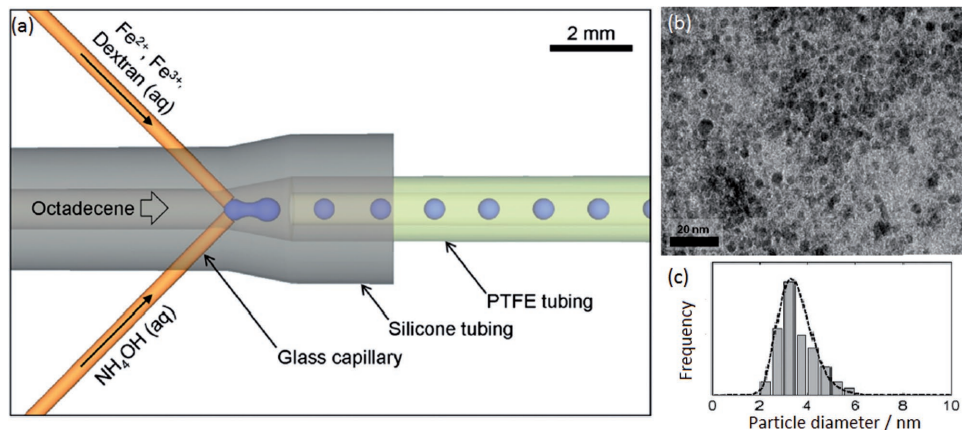


**Figure 19.** a) Scheme of the capillary-based droplet reactor showing the injection of separate precursor streams and  $\text{NH}_4\text{OH}$  into a continuous stream of octadecene carrier fluid; formation of iron oxide nanoparticles take place inside the droplets. b) TEM images of the resultant nanoparticles, and c) its corresponding histogram of particle size. Reproduced with permission.<sup>[233]</sup> Copyright 2012, RSC.

size distribution were produced by using silicone oil for liquid segmentation; however, aggregates were flowing along inside discrete droplets. On the other hand, irradiation of the chemical reagents by ultrasonic waves at the mixing stage avoided of aggregates of micrometric scale. In the case of fourth approach where both ultrasound vibration mixing and  $\text{N}_2$  segments were exploited, the production rate was significantly increased, while MNPs with the same quality compared to mixing by liquid segmentation or ultrasonic vibration were produced.

A complete reactor system can also be made by integrating other units around the micromixer by using micro-electro-mechanical-system (MEMS) technology. A MEMS-based microreactor has been designed for the synthesis of iron oxide magnetic nanoparticles by integrating a double-loop rotary micromixer, two micropumps, and a microvalve on a single chip (**Figure 21**). The synthesis process started by using PDMS-based micropumps and a microvalve for transporting ferrous and ferric ions to be mixed at a predetermined concentration

**Table 4.** Passive and active micromixers to enhance the mixing of reagents.

Passive micromixers	Reduce diffusion length and enhance chaotic advection as well as increasing the surface area between fluids. No external forces are applied	Ref.
T- and Y-shaped	T- and Y-shaped channels guide the two liquids to be mixed in contact. Roughening the channel walls and adding obstacles can enhance the mixing efficiency.	[236]
Parallel lamination	Increase the contact surface area by laminating the inlet main stream into n sub-streams and their subsequent rejoining.	[237]
Sequential lamination	Increase the mixing efficiency by sequentially laminating the inlet main stream to exponentially increase their contact surface area.	[238]
Focusing enhanced	A long microchannel with three inlets and one central outlet is used to constrain the central sample solution by fluids from side channels to achieve a smaller stream and thin lamination width	[239]
Chaotic advection	Use 2D, 3D channel shapes modified by inserting obstacles on the channel to generate a transverse component of flow, termed as chaotic advection, to cause an exponential growth of the interfacial area.	[240]
Active micromixers	Introduce time dependent perturbations to the fluid by the external use of energy input to accelerate the mixing process.	Ref.
Pressure field	Induce a pressure field disturbance by using a micropump which alternatively drives and stops the flow for altering periodically the flow rate in the inlet channel from high to low.	[241]
Electrokinetic	Induce mixing in microfluidic channels or chambers by taking advantage of electrokinetic disturbance. The fluid interfaces with the ability to stir the fluid stream in highly laminar flow are rapidly stretched and folded by the cause of fluctuating electric fields.	[242]
Dielectrophoretic	Use a non-uniform electric field to induce polarization of particles, termed as dielectrophoresis. Mixing of the fluid surrounding the particles is achieved through the chaotic advection produced by the synergistic effect between particles movement toward or away from the electrodes and the channel geometry.	[243]
Electrowetting	Electrowetting on dielectrics (EWOD), control the interfacial tension of droplets formed in multiphase microreactors by means of an electric field to enhance the mixing efficiency inside droplets. Shaking, splitting, and merging of droplets can enhance mixing by creating recirculating patterns.	[244]
Magneto-hydrodynamic	Induce Lorentz body forces in an electrolyte solution by coupling an electric field, produced by deposited electrodes in the channel walls, with a magnetic field. This complex flow field enhances the mixing efficiency by making deformations and stretching the material interface.	[245]
Ultrasound	Ultrasonic waves are introduced into the channel to create acoustic stirring perpendicular to the flow direction by means of integrated piezoelectric ceramic transducers.	[246]

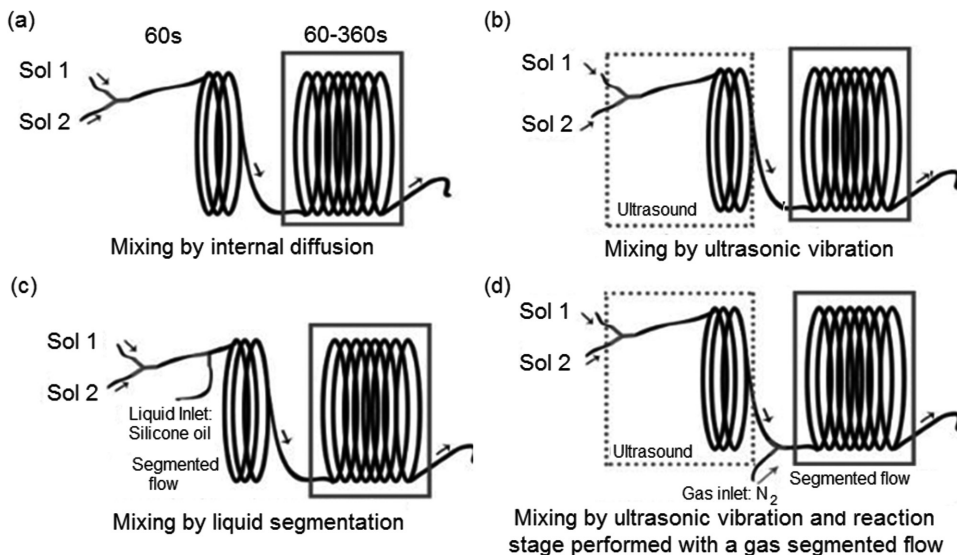


**Figure 20.** Schematic representation of four different micromixing based reactors for synthesis of MNPs via mixing by: a) internal diffusion, b) ultrasonic vibration, c) liquid segmentation, and d) ultrasonic vibration and gas segmented flow. Reproduced with permission.<sup>[249]</sup> Copyright 2015, WASET.

ratio followed by the addition of organic acid as an adherent. Together, they provide a fast and efficiency approach for the synthesis of uniform iron oxide nanoparticles within a shorter period of time (15 min) without requiring any extra additives or heating.<sup>[49]</sup>

### 2.3. Biogenic Synthesis of MNPs

A broad range of hierarchical intricate systems comprising astonishing material properties have been built by the nature to the point that often synthetic materials fail miserably to replicate. Exploiting the state-of-the-art advances in nanotechnology,

it has become possible to understand the natural mechanism and structures for a successful mimicry with less energy and minimum waste generation. In the case of material synthesis, diametrically opposed to the conventional chemical and mechanical synthetic routes which are energy consuming and require the usage of extreme conditions (such as high pressure, temperature, and acidity), biologically inspired synthetic routes take place under mild reaction conditions.<sup>[250]</sup>

The controlled formation of stable and well-ordered solid inorganic compounds by biological systems, referred to as biomimetic mineralization,<sup>[38,251]</sup> has resolved many of the problems related to conventional synthetic routes by providing a strict control over particle size and shape that take part in many

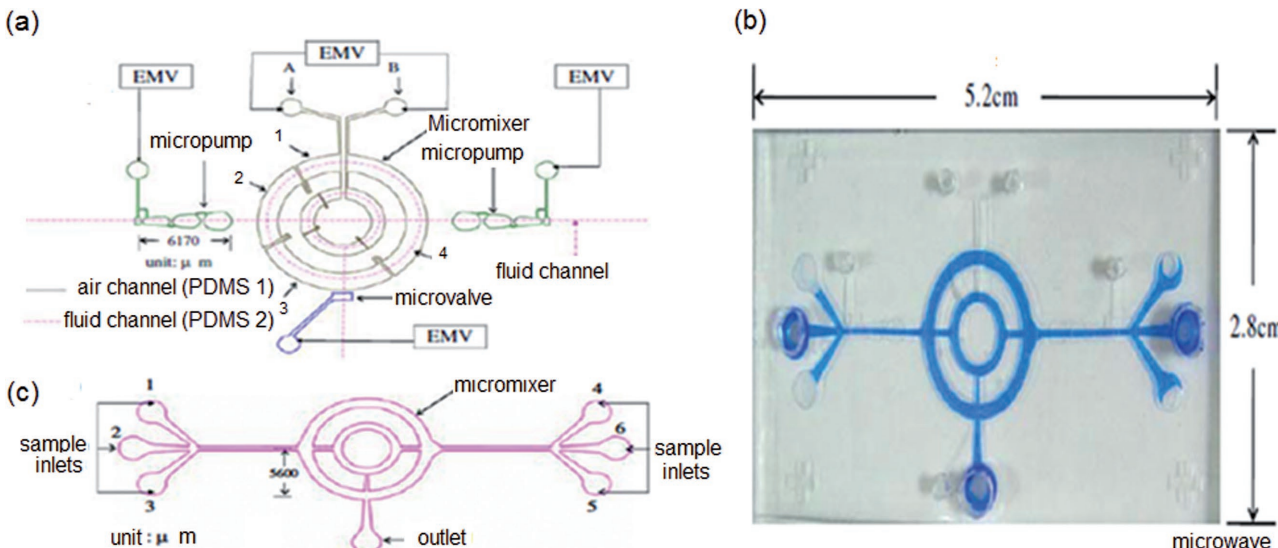


**Figure 21.** Schematic representation of the microfluidic system (top view). a) Automation of sample transportation, mixing and reaction within a PDMS-based microfluidic system consisting of two micropumps, a microvalve and micromixer. b,c) Respectively, a schematic illustration and a photograph of microfluidic system containing three sample inlets on each side of the chip. Reproduced with permission.<sup>[49]</sup> Copyright 2009, Springer.

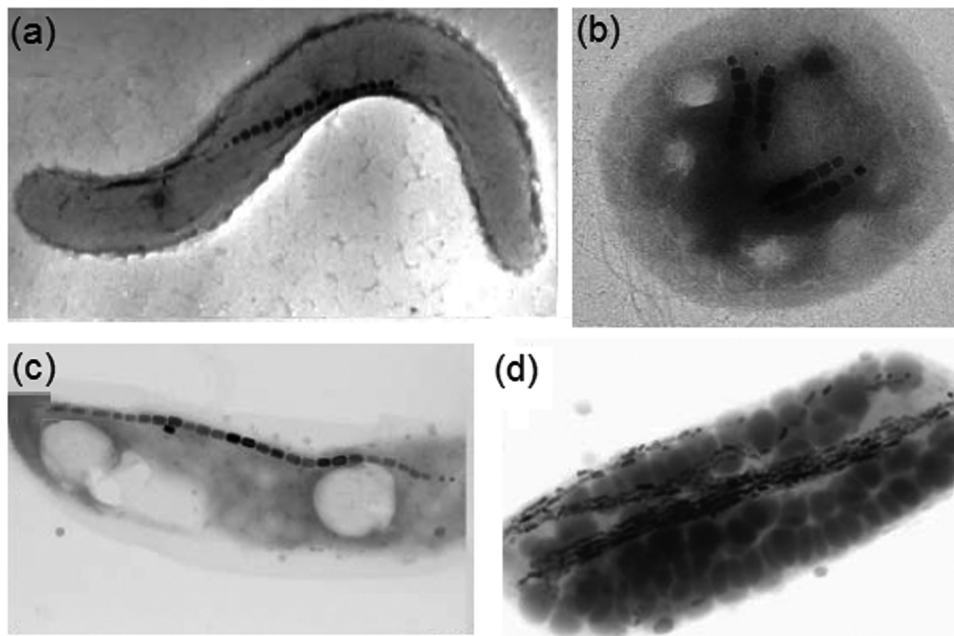


**Figure 22.** TEM images of various magnetotactic bacteria, showing the diversity of cell morphology: a) *Magnetospirillum magneticum* strain AMB-1, b) a coccus with two double chains, c) a rod-shaped bacterium, d) a vibrio with cubooctahedral magnetosomes. a) Reproduced with permission.<sup>[266]</sup> Copyright 2008, RSC. b) Reproduced with permission.<sup>[264]</sup> Copyright 2008, ACS. c) Reproduced with permission.<sup>[267]</sup> Copyright 2007, Mineralogical Society of America.

interesting activities in living organism.<sup>[250,252]</sup> In fact, this involves the uptake of specific elements from the environment by the organism, to form and maintain highly ordered inorganic mineral structures, ranging in size from nanometers to centimeters, under precise biological control.<sup>[253]</sup> A diverse range of organisms, including birds,<sup>[254]</sup> insects,<sup>[255]</sup> algae,<sup>[256]</sup> mollusks,<sup>[257]</sup> or even humans have been reported to biominerlize ferromagnetic materials. As it was mentioned, formation of nanomaterials by biological systems is performed under mild conditions. The required mild condition is provided by a special organelle which mediates the environment for the growth of the nanomaterial. In the case of magnetite nanoparticles, magnetotactic bacteria, a special isolated protein from this bacteria and finally fungi account for mediating the growth conditions.

### 2.3.1. Bacteria Mediated Synthesis of Magnetite Nanoparticles

Bacteria use two mechanistically different methods to biominerlize biogenic magnetite nanoparticles, including biologically induced mineralization (BIM)<sup>[258]</sup> and biologically controlled mineralization (BCM).<sup>[259]</sup> In the case of BIM, magnetite nanocrystals are produced through the metabolic activity of organism, most commonly recognized and studied in the dissimilatory iron-reducing bacteria. On the other hand, the nucleation and growth of the minerals are significantly controlled in BCM through forming them on or within organic matrices or vesicles.<sup>[260]</sup> Magnetotactic bacteria (MTB) are the most ancient and simplest organisms capable of performing BCM of magnetite ( $\text{Fe}_3\text{O}_4$ ) or, less commonly, greigite ( $\text{Fe}_3\text{O}_4$ ) in bacterial magnetosomes.<sup>[261]</sup> A significant breakthrough in biological synthesis of iron oxide nanoparticles has been made

since the first observation of MTB by Bellini in 1963<sup>[262]</sup> and the report of this unprecedented discovery by Blakemore in 1975.<sup>[263]</sup> MTB are ubiquitously distributed in aquatic environments and have been found exclusively in water columns or sediments with no extreme environmental conditions such as acidic mine tailing and thermal springs,<sup>[264]</sup> beside the singular report of MTB from waterlogged soil.<sup>[265]</sup> These bacteria can be easily separated from mud or water samples in the presence of magnetic fields.<sup>[265]</sup> Various morphological types of MTB, including rod-shaped, vibrio-like, coccoid and helicoidal forms have been found in freshwater sediments and coastal environments (Figure 22).<sup>[264]</sup>

Several surveys into the ecology of MTB have been carried out revealing that MTB show a locked-in behavior which directs the bacteria to the bottom of the aquatic body they inhabit, a region that is depleted in oxygen. Actually, MTB are mostly found in aquatic environments wherein oxygen and other redox active compounds are horizontally stratified (Figure 23a).<sup>[268]</sup> Specialized compartments consisting of a lipid membrane and a crystalline magnetic mineral, referred to as magnetosomes, account for this ability to exploit the earth's magnetic field for navigational purposes to efficiently find low oxygen environments.<sup>[270]</sup> The alignment of magnetosomes, which usually measures 50–70 nm in diameter, in chains within the bacteria are postulated to function as biological compass needles by providing the means for alignment with magnetic fields which enable the migration of bacteria along oxygen gradients in aquatic environments (Figure 23b).<sup>[266,268]</sup>

The essential part of magnetosome is the magnetic mineral which yields its superior magnetic property.<sup>[271]</sup> By the help of electron microscopy, closer view of magnetosomes clearly shows these magnetic crystalline minerals enclosed by a faint

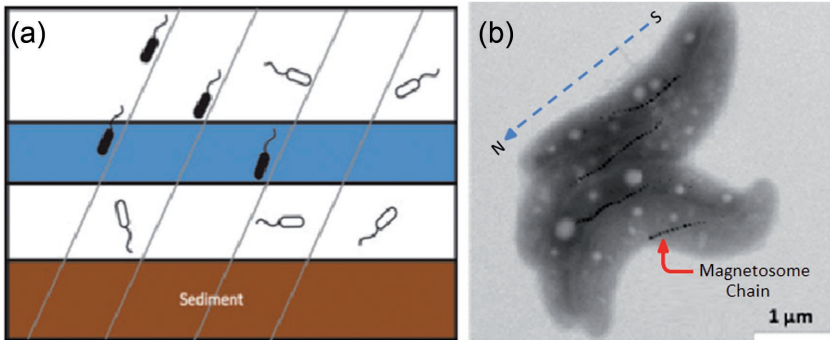


**Figure 23.** a) a schematic model of magnetotactic bacteria (MTB) migration along the earth's magnetic field. MTB (black) exploit the earth's magnetic field (gray lines) as guides to efficiently localize to the oxygen–poor oxic anoxic transition zone, while other organisms (white) must rely on 3D method for finding the same region. b) magnetosomes chains impart magnetic dipole moment which perform as compass needles to align the MTB along the earth's magnetic field. a) Reproduced with permission.<sup>[268]</sup> b) Reproduced with permission.<sup>[269]</sup> Copyright 2014, ACS.

black circle (Figure 24a). This circle is an indicative of an organic membrane<sup>[266]</sup> that mainly consists of phospholipids and proteins.<sup>[272]</sup> Iron oxide<sup>[273]</sup> or/and iron sulfide mineral<sup>[274]</sup> constitute the inorganic core of magnetosomes. Different crystal habits or morphologies of magnetic crystals have been observed in MTB by various forms of electron microscopy.<sup>[275]</sup> Different shapes include: bullet-shaped, elongated prismatic, rectangular, hexagonal, square-like, and cubooctahedral (Figures 24b–d).

Obtaining high yields of MTB cells and magnetosomes is a primarily major challenge to practically utilize these astonishing MNPs for biological applications. Although the molecular biology of the magnetosome and magnetotactic bacteria have not been yet fully elucidated, some great biomimicries have been done to synthesize magnetite nanoparticles in vitro.<sup>[276]</sup>

These high yields of MTB cells and magnetosomes can be produced by either simply scaling up of batch cultures<sup>[277]</sup> or by using a growth method where the oxygen concentration is precisely controlled and yields high level of magnetosomes.<sup>[278]</sup> Surprisingly, there are several species of MTB that can be cultivated in vitro under conditions where growth and magnetite biominerization are optimized to collect their biomineralized magnetosome for biological applications.<sup>[279]</sup> A series of three publications have described the optimization of the growth of the most popular type of MTB, *Magnetospirillum gryphiswaldense* MSR-1, to enable industrial developments required for the large production of magnetosomes.<sup>[280]</sup>

As it was mentioned, MTB exploit the alignment of magnetosomes to migrate into zones where oxygen and other redox active compounds are horizontally stratified. Thus, controlling the level of oxygen to provide microaerobic and anaerobic conditions<sup>[281]</sup> as well as controlling the redox potential<sup>[282]</sup> are of two most important factors which are absolutely required for magnetite biomineralization in MTB. Utilizing an oxygen-controlled fermenter provides a precise control over the culture of MTB, especially the most popular investigated model, *Magnetospirillum* species.<sup>[283]</sup> Sun et al. used a fermenter to control the level of dissolved oxygen and after 60 h of culture incubation obtained magnetite yield of  $16.7 \text{ mg L}^{-1} \text{ d}^{-1}$ .<sup>[284]</sup> In a similar study performed by Liu et al. magnetite yield  $55.49 \text{ mg L}^{-1} \text{ d}^{-1}$  after 36 h of culture was reported in a condition where the amount of carbon and electron source were decreased.<sup>[280]</sup> In a different strategy, Silva et al. used a statistical-based experimental factorial design to

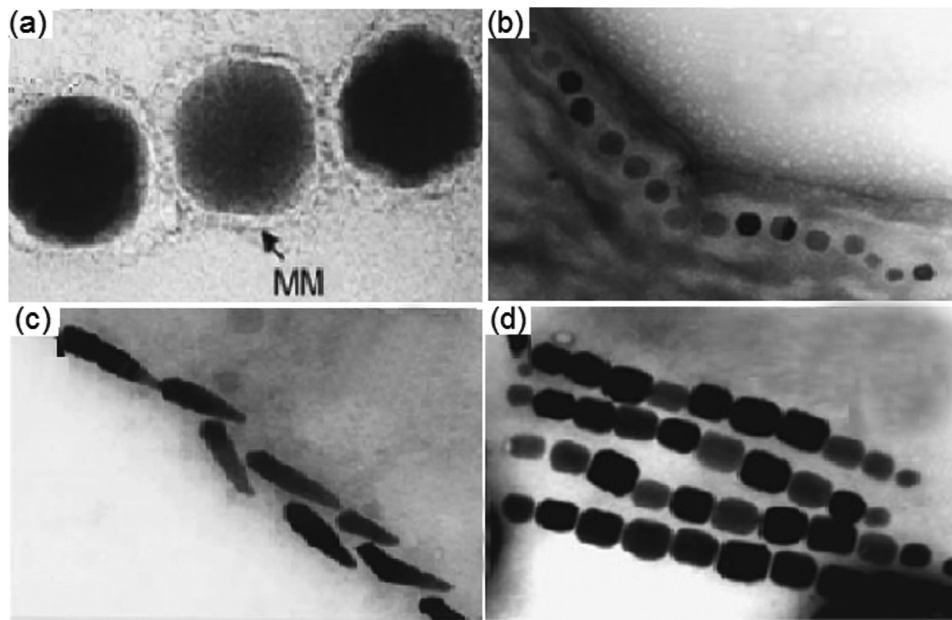


**Figure 24.** TEM images of magnetosome chains. a) a close view of magnetic crystalline shows that minerals are enclosed by a faint black circle. b–d) different shapes of magnetosomes: b) cubo-octahedral; c) bullet-shaped; d) elongated prisms. Reproduced with permission.<sup>[266]</sup> Copyright 2008, RSC.

culture high yields of the marine MTB *M. blakemorei* by determining the key components and amounts in growth medium for maximum yields.<sup>[285]</sup> After cultivation of MTB, mature magnetosomes are extracted from the MTB through methods which use sodium hydroxide (NaOH), sonication, a French press, or a pressure homogenizer to lyse the bacterial cells.<sup>[279]</sup> Subsequently, magnetosomes are purified, most commonly by using a system of magnetic isolation which is followed by low power ultrasonication and a proper treatment with proteins K and electro-elution to remove adsorbed and surface proteins as nucleic acids.<sup>[286]</sup>

### 2.3.2. Protein Mediated Synthesis of Magnetite Nanoparticles

One of the interesting tools for engineering approaches toward material science is taking advantage of various biosystems which are able of templating complex inorganic nanomaterials. Numerous recent molecular studies have been directed toward uncovering the interfaces between proteins and inorganic materials which are directly involved in crystallization mechanisms. Different proteins isolated from biominerals have opened the door for bio-inspired synthesis of nanostructured materials with unique properties. In fact these materials can be synthesized through in vitro use of proteins as mineralization templates.<sup>[287]</sup>

In the previous section, biogenic synthesis of magnetite nanoparticles took place in a mediated growth condition provided by MTB under fairly mild conditions. In a pioneering study carried out by Arakaki et al, Mms6 protein was identified as a protein which is tightly associated with the magnetite formation in *Magnetospirillum magneticum* AMB-1.<sup>[288]</sup> Mms6 is an amphiphilic protein which mainly consists of an N-terminal hydrophobic region responsible for the self-aggregation of the protein,<sup>[289]</sup> and C-terminal hydrophilic region containing multiples of acidic amino acids which is suggested to act as an iron-binding site.<sup>[290]</sup> It was suggested by Arakaki that Mms6 protein is a dominant protein and regulates the biomimeticization and controls the morphology of uniform magnetosomes by acting as a template to guide the shape and size of the magnetite crystals formed.<sup>[291]</sup> Surprisingly, the combination of these biomimetic-associating proteins and their mimic peptides has enabled the biomimicking of inorganic materials, especially magnetite nanoparticles.<sup>[292]</sup> In fact, this protein has been isolated from MTB to facilitate in vitro chemical synthesis of cuboidal magnetite nanoparticles similar to the ones produced in MTB.<sup>[288]</sup>

Two main synthetic methods have been used to elucidate the function of the Mms6 protein for preparing magnetite crystals and use the function for an effective biomimicry.<sup>[290,293]</sup> In the first case, the function of Mms6 during the biomimeticization of magnetosomes in BTM was elucidated through the analysis of the Mms6 deletion during the coprecipitation of ferrous and ferric ions. It was concluded that highly ordered cuboidal magnetite crystals consisting of (1 0 0) and (1 1 1) crystal faces with sizes ranging from 20 to 30 nm were formed in the presence of Mms6, while smaller and irregular-shaped magnetite crystals consisting of mainly (1 1 1) faces were formed in the absence of the protein.<sup>[293]</sup> Some other studies have been also performed to elucidate the function of Mms6 protein during

the biomimeticization of magnetite nanocrystals.<sup>[289,294]</sup> Alternatively, magnetite nanocrystals were prepared with the addition of Mms6 through a method involving partial oxidation of ferrous hydroxide.<sup>[293]</sup> It was concluded that addition of Mms6 results in the production of magnetite crystals of uniform size with narrow size distribution similar to those of magnetosome observed in the *M. magneticum* strain AMB-1. As opposed to the crystals formed in the presence of Mms6, deletion of this protein resulted in larger magnetite crystals with increased size distribution.

Recently, Lenders et al. have presented a design of a bioinspired method for aqueous precipitation of magnetite at room temperature as a mimic of the magnetosome membrane.<sup>[295]</sup> Through this method, the controlled formation of ferrimagnetic magnetite with particle sizes up to 60 nm in the presence of Mms6 protein has closely mimicked the biomimeticization process taken by MTB. It was suggested that Mms6 is a magnetite nucleation protein which binds iron ions specifically to nucleate the formation of magnetite. Galloway et al. have provided a new approach for the synthesis of magnetite nanocrystals on gold surfaces.<sup>[296]</sup> They used micro-contact printing to pattern Mms6 protein onto gold surfaces and subsequently biomimeticized consistent magnetite nanocrystals. Recently, they have also performed a study with some variations of previous approach to pattern engineered Mms6 proteins containing an N-terminal cysteine capable of binding directly onto the surface and biotemplating magnetite nanocrystals.<sup>[297]</sup> This surface based biomimeticization experiment therefore offered a unique in vitro method of studying Mms6 in an environment similar to the native state, anchored in the magnetosome membrane. In their very recent study, they have used a similar biomimetic system to investigate the differences between the Mms6 C-terminal peptide and the intact Mms6 protein in magnetite synthesis.<sup>[298]</sup>

### 2.3.3. Fungi Mediated Synthesis of Magnetite Nanoparticles

Fungi mediated synthesis of nanoparticles is one of the other alternative strategies which is considered as a “green”, environmentally friendly fabrication route. However, the use of fungi in deliberate synthesis of oxide-based nanomaterials was not explored for the first time until the early 2000s.<sup>[299]</sup> During the last decade, there have been several reports on the extracellular biosynthesis of numerous metal oxide nanoparticles by employing fungal microorganisms as efficient biological entities. Capability of fungi to be easily cultured under controlled environments, resistance to mutations as well as their ability to produce abundant amounts of extracellular enzymes and proteins to control and mediate the synthesis process are of important advantages offered by fungi which make them preferable candidates for the synthesis of nanomaterials.<sup>[300]</sup>

In the case of fungi-mediated biosynthesis of magnetite nanoparticles, up to our knowledge, there is only one study performed by Bharde et al.<sup>[301]</sup> Within this elegant study, magnetite nanoparticles with appropriate stoichiometry were produced by challenging *F. oxysporum* and *Verticillium* sp. with an aqueous solution containing a mixture of ferricyanide  $[\text{Fe}(\text{CN})_6]^{3+}$  ions and ferrocyanide  $[\text{Fe}(\text{CN})_6]^{4+}$  ions. TEM images of the resultant

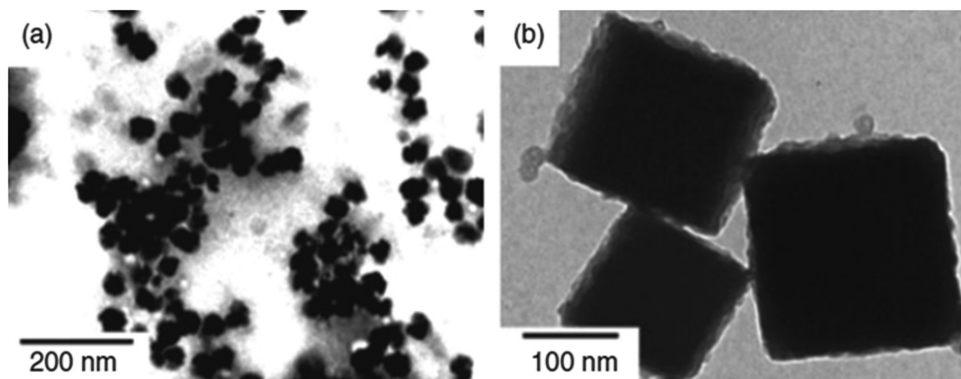


**Figure 25.** Transmission electron micrographs of magnetite nanoparticles synthesized using a) fungus *Fusarium oxysporum*, b) fungus *Verticillium* sp. Reproduced with permission.<sup>[301]</sup>

magnetite nanoparticles revealed that magnetite nanoparticles of quasi-spherical shape in the 20–50 nm size range were synthesized by *F. oxysporum*, while *verticillium* sp. synthesized cubo-octahedral assemblies of magnetite nanoparticles in the 100–400 nm size range (Figure 25). It was found by higher transmission electron microscopy magnification that nanoparticles produced in the latter case are composed of smaller 10–40 nm particles.

### 3. Proper Coating of MNPs

#### 3.1. Exigencies of Coatings MNPs

Proper coatings are needed without a shadow of doubt to translate bare iron oxide magnetic cores into robust MNP systems which come in handy for a wide range of in vivo and in vitro applications. Agglomeration, oxidation, anchoring capability as well as the ability of evading the RES are the obvious motives for developing a various coating chemistry. Diminishing the agglomeration and water-insolubility of MNPs in physiological environment is the first exigency of coating them. Many of the powerful synthetic methods result in nanoparticles covered by hydrophobic surfactants, causing insolubility in water.<sup>[302]</sup> On the other hand, since the size of desired nanoparticles is decreased below 100 nm, they become highly reactive sites due to proportion of surface atoms and hydrophobic interactions between the sub nm size particles (large surface area to volume ration).<sup>[12]</sup> This will lead to less stable nanoparticles as a result of strong tendency to undergo agglomeration. Appropriate surfactant coating can decrease the particle–particle interactions to derive colloidally stable, water soluble MNPs.<sup>[303]</sup>

Bare MNPs are prone to be attacked by oxidative or corrosive environments in a way that their stability in solution and physiological media can be easily compromised due to their high surface-to-volume ratio.<sup>[304]</sup> Furthermore, subsequent formation of reactive oxygen species (ROS) will result in loss of magnetic properties of oxidized MNPs on one hand, in a decrease of their biocompatibility on the other hand.<sup>[305]</sup> Although, magnetite ( $\text{Fe}_3\text{O}_4$ ) nanoparticles are highly magnetizable and resistant to oxidation, a loss in their magnetism properties occur once they are oxidized and convert into hematite nanoparticles.<sup>[306]</sup> Hence, coating is a major determinant of MNPs stability to

protect them from oxidation and corrosion in ambient conditions. It also allows them to retain as single-domain structures for exhibiting better superparamagnetic properties in biological applications.<sup>[81]</sup> However, use of nonmagnetic coating will also decrease the magnetic saturation of MNPs.<sup>[305]</sup> Most importantly, coatings should provide functional groups (e.g., amine, carboxyl groups) for accommodating therapeutics, targeting ligands, and reporter moieties as an important step that assists labeling specificity of MNPs toward different applications.<sup>[302a]</sup> Type of coating is very close to biocompatibility and blood circulation time of MNPs, as it will be described in design considerations section. In fact, a good coating should prolong the half-life of MNPs through limiting undesirable fouling of protein plasma on the surfaces to evade RES.<sup>[307]</sup>

#### 3.2. Coatings Materials

##### 3.2.1. Small Organic Molecules (Carboxylates and Organophosphorus Molecules)

Surfactants such as small organic molecules are mostly frequently used for stabilizing nanoparticles prone to oxidation and aggregations, through forming liposomal or micellar structures. Generally carboxylates, phosphates, and phosphonates are preferred due to their high affinity for iron oxide surfaces.<sup>[308]</sup> Adsorption of carboxylic acid on metal oxide surfaces occurs due to their nucleophilic character through strong anionic and physical interaction with hydroxyl groups present on the electrophilic surfaces.<sup>[309]</sup> Among carboxylic acids, citric and dimercaptosuccinic acids have been used commercially for stabilizing iron oxide MNPs.<sup>[310]</sup> Stable colloidal suspensions are resulted due to adsorption of these polyacids on iron oxide MNPs due to their high coordination on their surfaces via one or two of the carboxylate functionalities.<sup>[311]</sup> Hydrophilic and negatively charged nanoparticles are consequently resulted due to, at least, one carboxylic acid group exposed to the solvent.<sup>[312]</sup> However, this method suffers from labile carboxylic functions which can be easily broken by due to elevation of temperature or presence of carboxylic compounds with higher affinities to the surface.<sup>[308]</sup> Organophosphorus molecules, such as phosphonic acid, alkylphosphoric acid, and their salts, phosphates and phosphonates have been investigated as promising stabilizing

**Table 5.** Advantages offered by different polymers used in coating MNPs.

Polymers	Advantages	Refs.
Polyethylene glycol (PEG)	Easy to functionalize, hydrophilic, improves biocompatibility and blood circulation time as well as internalization efficiency by reducing uptake, non-antigenic, and non-immunogenic properties.	[323]
Polyvinylpyrrolidone (PVP)	Prevents particles' coagulation, gives rise to monodisperse MNPs, improves biocompatibility	[324]
Polyvinyl alcohol (PVA)	Stabilizes the colloid, plays a role in preventing further growth of MNPs followed by the formation of large agglomerates by chemisorption on the surface of particles, excellent emulsifying properties.	[325]
Polyacrylic acids (PAA)	Potential properties to be used for long-term therapy and imaging studies <i>in vivo</i> , increases biocompatibility and helps in bioadhesion.	[326]
Poly (lactic-co-glycolic acid) (PLGA)	Approved by FDA and European Medicine Agency in drug delivery systems, stealth effect for longer blood circulation time and better interaction with biological materials, biodegradability, and biocompatibility, possibility of sustained release and also protecting drugs from degradation.	[327]
Polysaccharides (Dextran)	Enhances blood circulation time, biodegradability, and biocompatibility, constitutes a versatile platform for conjugation to targeting ligands.	[328]
Chitosan	Hydrophilic, biocompatibility, antibacterial property, wound healing activity, and mucoadhesive properties, enhances the contact between drug and ocular mucosa due to its high mucoadhesive properties. Potential use in non-viral gene delivery	[329]
Gelatin	Hydrophilic and biocompatible emulsifier, natural polymer, efficient drug loading properties.	[330]
Starch	Biocompatibility, possibility of being transported in the extracellular spaces as well as being internalized in nerve cells	[331]
poly methyl methacrylate (PMMA)	Biocompatible, having moderate properties, easy handling, and processing, low cost	[332]
Polystyrene	Highly stable, forming uniformly sized particles in suspension	[333]

candidates.<sup>[313]</sup> They provide more stronger bonds compared to carboxylic acid molecules through creating Fe—O—P bond, which equip iron oxide MNPs with coatings having good stability over several weeks at neutral pH.<sup>[314]</sup>

### 3.2.2. Polymer Coating

Generally, polymer coatings on MNPs are infinitely preferable to meet the rigorous design considerations such as oxidation, non-toxicology, overcoming biological barriers along with being appropriate cargos for delivering therapeutics and functionalities.<sup>[315]</sup> An ever-growing number of different polymers both synthetic and natural have been used for coating nanoparticles in different kinds of biological applications demanding biocompatibility and long blood circulation time, ranging from drug delivery to magnetic resonance imaging. Moreover, polymers provide surface functional groups (e.g., carboxylic acids, amines, thiols, etc.) to facilitate the conjugation of therapeutic, diagnostic and optional targeting ligands. **Table 5** summarizes advantages of different types of synthetic and natural polymers which have been used mostly for biological application.

Synthetic polymers are divided into biodegradable and non-biodegradable polymers. The degradation rate of the coating polymer has a direct influence on the drug release rate and needs to be considered for the design of the controlled biodegradable drug releases. Biodegradation of polymers is influenced by factors such as chemical structure and composition, molecular weight distribution, administration route, physical factors (shape, size, defects), and degradation mechanism (enzymatic, hydrolysis, and microbial).<sup>[316]</sup> Compared to natural polymers, synthetic polymers provide longer periods of sustained release with a better drug releasing control. The most widely used synthetic polymer is PEG, which is non-toxic and

prolongs blood circulation time by providing efficient hydrophilicity onto the surface of MNPs.<sup>[317]</sup>

On the other hand, natural polymers, such as dextran, chitosan, gelatin, alginate, and pullulan are advantageous in terms of biocompatibility and having milder formulation processes and can also be used as stabilizing agents, but have limitations in tunability of release for targeting applications. Ferrumoxtran-10 and Feraheme are of commercially available MRI agents coated with natural carbohydrate polymers.<sup>[318]</sup> Due to strong magnetic dipole–dipole attractions between MNPs, there is an innate tendency to aggregate. To overcome this, hydrophilic polymers such as starch and dextran ensure good aqueous dispersion of the MNPs.<sup>[319]</sup> Dextran is also one the most widely used natural polymers for coating MNPs because of its biocompatibility and biodegradability.<sup>[320]</sup> A number of MNPs coated by dextran have been used to enhance the contrast of MR imaging during the past decades.<sup>[321]</sup> Furthermore, chitosan coated iron oxide nanoparticles have been well exploited for targeting photodynamic therapy.<sup>[322]</sup>

### 3.2.3. Copolymers

To take the most advantages of distinct functionalities of different single coating polymers, copolymers as their constituents have been developed to synergize the advantages and overcome disadvantages of each component.<sup>[324]</sup> This method may lead to robust conjugation of payload molecules as well as improving the stability of MNPs and reducing the nonspecific uptake of biomolecule to have longer blood circulation times for biomedical applications.<sup>[325]</sup> SPIONs coated with copolymer of PEG-g-chitosan-g-PEI were developed by Kievit et al.<sup>[326]</sup> for delivering DNA. They reported a good stabilization of SPIONs along with efficient DNA complexation and gene transfection achieved

by three polymers grafted together. Chen et al.<sup>[337]</sup> coated iron oxide nanoparticles obtained from thermal decomposition with a PEGylated amphiphilic triblock copolymer consisting of a polybutylacrylate segment, a polyethylacrylate segment, a polymethacrylic acid segment and a hydrophobic hydrocarbon side chain, to make them water soluble and function-extensible.<sup>[338]</sup> They were also conjugated with peptides and imaging moieties which consequently showed excellent tumor targeting efficiency, relatively long circulation half-life and limited liver macrophage uptake. Chen et al.<sup>[339]</sup> reported the development of an antibiofouling polysiloxane containing amphiphilic diblock copolymer, poly (ethylene oxide)-block-poly(g-methacryloxypropyl trimethoxysilane) (PEO-b-PgMPS), for coating and functionalizing nanoparticles such as iron oxide and quantum dots. This study demonstrated that PEO-b-PgMPS coated nanoparticles, with nearly neutral surface charge, were colloidally stable in biological medium and showed low non-specific binding by macromolecules after incubation with 100% fetal bovine serum. Furthermore, they evaluated the non-specific and RES uptake through both in vitro experiments with macrophages and in vivo biodistribution study in mice. Their results revealed that PEO-b-PgMPS has also an antibiofouling effect which highly reduces the non-specific cell and RES uptake. In a very recent study, Hsiao et al.<sup>[340]</sup> developed hexanoyl-chitosan-PEG (CP6C) copolymer coated iron oxide nanoparticles which were loaded by paclitaxel (PTX) and conjugated by chlorotoxin (CTX) for targeted drug delivery to human glioblastoma (GBM) cells. They reported a successful targeting of GBM cells with therapeutic efficiency greater than that of free PTX which makes copolymer coated iron oxide nanoparticles as potential platform for loading and delivery of many hydrophobic drugs.

### 3.2.4. Silica

Functionalization of magnetic cores through an inorganic approach is most widely done by exploiting silica matrices, which greatly preserves the unique properties of the nanoparticles on one hand,<sup>[341]</sup> and enables transferring the nanoparticles synthesized in organic media to aqueous media on the other hand.<sup>[342]</sup> Silica is in fact, an amorphous material which possesses hydroxyl surface groups that provide intrinsic hydrophilicity and offer versatile choices for grafting the particles with targeting molecules.<sup>[343]</sup> Silica is also a heat-resisting material, with a low specific gravity, high surface area, high stability under aqueous conditions (low pH) and high mechanical strength which specifically makes them suitable for diagnostic applications.<sup>[344]</sup> Moreover, MNPs coated with silica are negatively charged at blood pH which results in avoiding the aggregate formation in body fluids.<sup>[345]</sup> Also, the transparent matrix of silica allows the efficient passage of excitation and emission light for better imaging diagnosis.<sup>[346]</sup>

Modification of magnetite nanoparticles was firstly performed by Philipse et al.<sup>[347]</sup> through a sol-gel approach. They reported a good dispersion of coated magnetite nanoparticles in aqueous suspensions due to intrinsic hydrophilic property of silica. Silica coated MNPs can be exploited for separation of biomolecules through electrostatic interactions due their high capability to be charged above the isoelectric point of silica

(pH  $\approx$  2).<sup>[348]</sup> Successive functionalization can also be easily introduced thanks to the presence of silanol groups ( $-\text{Si}-\text{OH}$ ) on the surface to prevent any direct contact of the magnetic core with additional reagents to avoid unwanted interactions, such as acidic corrosion.

Normally Stöber method,<sup>[349]</sup> reverse microemulsions (water in oil)<sup>[350]</sup> or direct micelle assisted methods<sup>[351]</sup> are used to coat silica on MNPs. The common Stöber process includes the hydrolysis and polycondensation of TEOS under alkaline conditions in ethanol.<sup>[349]</sup> Two major classes of silica coatings are form of solid (dense) and mesoporous, wherein mesoporous silica provides additional drug delivery functionality.<sup>[352]</sup> Shi et al. prepared magnetic nanoparticles coated with a silica shell. They first prepared hematite nanoparticles as the initial cores and covered it with a mesoporous silica layer formed from simultaneous sol-gel polymerization of TEOS and *n*-octadecyltrimethoxysilane (C18TMS) followed by removal of the organic template through calcination. Subsequently  $\text{Fe}_3\text{O}_4/\text{Fe}$  was produced by reducing the hematite cores in a flowing gas mixture of  $\text{H}_2$  and  $\text{N}_2$ .<sup>[353]</sup> In a very recent study, Kuzminská et al.<sup>[354]</sup> reported thin and thick coating of  $\text{Fe}_3\text{O}_4$  MNPs with (3-amino-propyl)triethoxysilane and TEOS to increase their hydrophilicity and their pH stability. Their stability tests showed that coating with silica shell and grafting with organosilanes considerably improve the stability of MNP at pH = 3; the thicker the silica layer the less iron oxide dissolved.

However, recently attentions have been more directed toward multifunctional mesoporous silica nanocomposites for either encapsulating nanoparticles within a silica shell or assembling nanoparticles on mesoporous nanoparticles. A pioneering study conducted by Hyeon group in 2006 reported a novel method which enabled encapsulation of inorganic nanoparticles in mesoporous silica shell.<sup>[355]</sup> CTAB served both as a phase transfer agent and as an organic template for the formation of mesoporous silica spheres. In this method, Transferring the resynthesized iron oxide nanoparticles stabilized with oleic acid from an organic phase to an aqueous phase was performed through capping the with CTAB. Subsequently, mesoporous silica spheres embedded with iron oxides nanoparticles resulted from a sol-gel reaction followed by the removal of surfactants. (Figure 26). Moreover, to enhance physicochemical qualities of mesoporous silica-based nanoparticles, their surface can be further functionalized with camouflage to prolong their blood circulation time.<sup>[356]</sup> Chen et al. developed a novel magnetic drug delivery system in which SPIONs conjugated with doxorubicin were coated with porous silica shell and subsequently functionalized with PEG.<sup>[357]</sup>

However, the large size of such nanoparticles is still a challenge and can lead to their unspecific uptake by the RES. To address this problem, Hyeon et al. the synthesized core-shell mesoporous silica nanoparticles smaller than 100 nm embedded with MNPs and modified with PEG to render them biocompatible by hindering the nonspecific adsorption of proteins on them upon entering the body (Figure 27).<sup>[358]</sup> The same group employed mesoporous silica-coated hollow manganese oxide nanoparticles as contrast agents for  $T_1$  MR imaging. Their results showed that water accessibility to the manganese core was increased due to the feasibility of water exchange across the porous coating, combined with the large surface

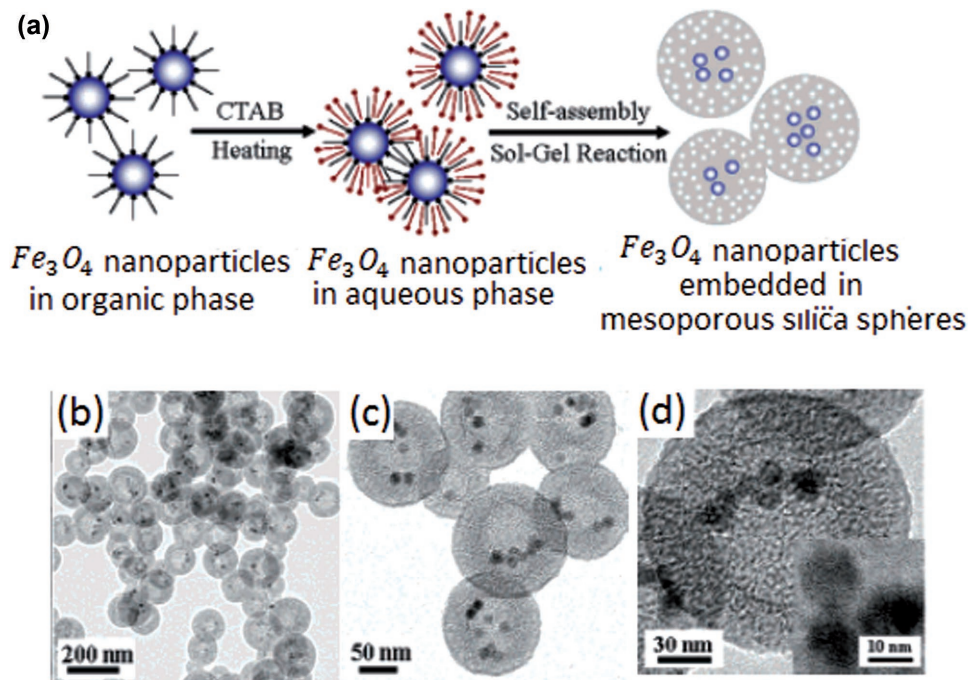


**Figure 26.** a) Schematic representation of monodisperse magnetite nanoparticles embedded in mesoporous silica spheres (M-MSS). b,c) TEM, and d) high resolution TEM images of M-MSS. Reproduced with permission.<sup>[355]</sup> Copyright 2006, ACS.

area to volume ratio of nanoparticles, which led directly to the enhancement of  $T_1$  contrast.<sup>[359]</sup> The unique intrinsic structure of mesoporous nanoparticles impart high capacity for drug loading as well as employing drug control release modules onto such carriers.

In a recent study, ferrite nanoparticle-incorporated mesoporous nanoparticles fabricated by Thomas et al. provided a noninvasive system to remotely control the drug release. In fact, a nanovalve system was perfectly designed by combining controlled drug release ability of mesoporous nanoparticles with hyperthermic effect of MNPs, wherein zinc-doped iron oxide nanoparticles were encapsulated within mesoporous silica shells and subsequently cyclic cucurbituril was used for

capping the pores.<sup>[360]</sup> Interestingly, upon exerting an oscillating magnetic field, the electrostatically bound nanovalve molecules were removed by the induced heat generated by incorporated magnetic nanoparticles, and resulted in cargo release.

Despite all the advantages, silica coatings suffer from the intrinsic instability of the system under basic conditions along with the probability of oxygen and other species to be diffused and reach the magnetic core due to the presence of pores in the amorphous layer. On the other hand, the secondary nucleation of silica particles as well as controlling the thickness of the silica shell is among the problems in using stober process for coating MNPs.<sup>[118]</sup> In addition, although silica is known to be biocompatible, they have are not biodegradable.<sup>[12]</sup>

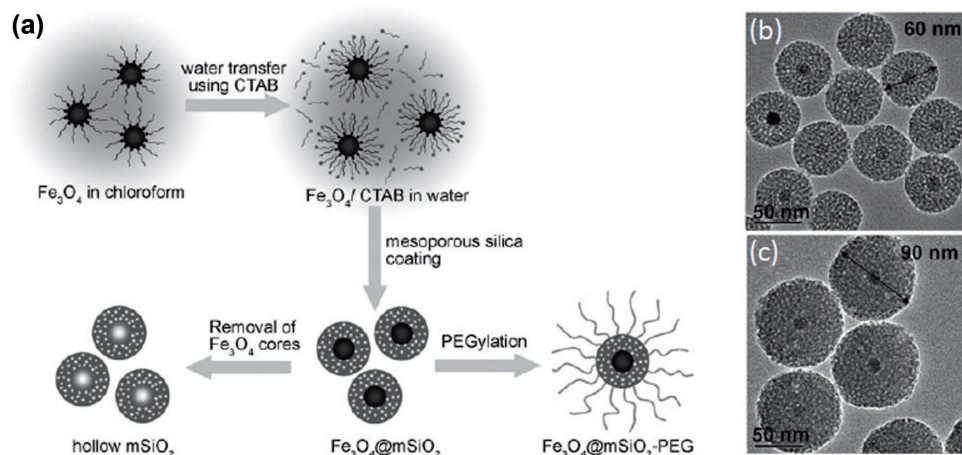


**Figure 27.** a) Schematic illustration of the synthetic procedure for magnetite nanocrystal/mesoporous silica core–shell nanoparticles and TEM images of  $\text{Fe}_3\text{O}_4@\text{mSiO}_2$  with b) 60 nm and c) 90 nm core. Reproduced with permission.<sup>[358]</sup> Copyright 1989, Oxford University Press.

### 3.2.5. Gold Coating

The low reactivity of gold to avoid oxidation on one hand, and its surface chemistry and lack of toxicity on the other hand, have made this precious metal to be a perfect candidate for conjugation with variety of biomolecules.<sup>[361]</sup> Protein purification,<sup>[362]</sup> bioseparation and immunoassay,<sup>[363]</sup> biomolecule immobilization and detection,<sup>[364]</sup> and MRI are to number a few applications where gold-coated MNPs have been utilized. It can be simply functionalized with thiol ( $-SH$ ) organic molecules to form compact and ordered self-assembled monolayers (SAM) on its surface to modify the surface properties. In addition, anchoring of other systems such as molecules, proteins, DNA, and nanoparticles is possible thanks to the presence of the exposed end group ( $-NH_2$ ,  $-COOH$ ,  $-SH$ ,  $-Cl$ ,  $-CH_3$ , ...). Another good advantage of gold coating is that the superparamagnetic nature of magnetic cores is retained with either a decrease<sup>[365]</sup> or an increase<sup>[366]</sup> in the value of saturation magnetization. Furthermore, the near-infrared (NIR) light sensitivity of gold surfaces combined with the intrinsic potential of MNPs for MR imaging render them practical for MR/optical dual imaging applications.<sup>[367]</sup> Currently, there have been considerable number of reports on synthesizing magnetic nanoparticles covered by gold through microemulsion,<sup>[368]</sup> chemical reduction,<sup>[369]</sup> coprecipitation, seed mediated growth,<sup>[370]</sup> self-assembly,<sup>[371]</sup> sonochemical reduction,<sup>[372]</sup> thermal decomposition,<sup>[91]</sup> and laser irradiation<sup>[373]</sup> approaches. Bao et al.<sup>[374]</sup> have also reported synthesis of gold-magnetite composites involving discrete gold nanoparticles on magnetite surface which can be useful for applications such as protein separation, optical imaging, or catalysis, where a full coating is not required. Overlaying of gold can be facilitated by attachment of gold seeds that form a protective layer to increase the particle stability against particle aggregation and make them resistant to chemical attacks.<sup>[375]</sup> Recently, in a very comprehensive study, the effect of gold coatings on the clearance of MNPs has been studied by investigating a long term fate of gold coated MNPs after intravenous injection in mice. The in vivo degradation of magnetic particles and coating shells were shown and compared by two different amphiphilic polymers or glycol coating. It was revealed that the initial surface properties have impact on the degradability and on the kinetics of elimination of magnetic iron and gold from liver and spleen.<sup>[376]</sup>

Overall, although gold offers a lot of advantages for MNP, there are some difficulties that should overcome. The direct coating of iron oxide with gold is hard due the dissimilarity in the nature of the two crystalline surfaces making the coating to be weak which can be overcome by using  $TiO_2$  as a bridging material.<sup>[377]</sup>

## 3.3. Coatings Approaches of MNPs

The coating process of MNPs can be achieved by two major approaches mainly classified as in situ coating and post synthetic coating. Through in situ strategy which is also known as “one-pot synthesis,” the same reaction solution contains both precursors of magnetic cores and coating materials wherein magnetic cores will be first nucleated on the coating materials.

As a matter of fact, simultaneous formation of both magnetic cores and their coating occurs.<sup>[378]</sup> In situ coating process is mainly used in synthesis approaches which lead to surface free nanoparticles in water.<sup>[379]</sup> That would subsequently result in the formation of magnetic cores and the coatings at the same time that uniformly encapsulates the NP core. However, this strategy may have some negative effects on the magnetic susceptibility of MNPs by limiting their crystallinity.<sup>[11a]</sup> On the other hand, the selected coating materials should have good solubility at pH values necessary to precipitate MNPs, i.e., in situ coating of MNPs with chitosan was problematic due to its poor solubility at the desired pH values.<sup>[380]</sup> The precipitating agents are often synthetic polymers such as PEG, PVA, poly (acrylic acid) (PAA), poly (methylacrylic acid) (PMAA), poly (lactic acid) (PLA), polyvinylpyrrolidone (PVP), PEI and biopolymers such as carbohydrates (dextran, chitosan, alginate, arabinogalactan). In contrast to in situ approach, within the post synthesis strategy, bare magnetic cores will be introduced by coating materials onto their surface through ligand exchange,<sup>[140,381]</sup> direct grafting<sup>[382]</sup> or hydrophobic interactions.<sup>[383]</sup> Silica, polymers, gold and other organic dye molecules are of the most commonly used materials through this approach.<sup>[12]</sup>

In order to bind the coating material onto the surface of resultant MNPs, two different strategies have been employed; the first one exploits the weak interactions (van der Waals forces, hydrogen bonds, etc.) for a reversible physisorption of the surfactant, macromolecules, and amphiphilic polymers on the surface of metal oxide nanoparticles and the second one involves the attachment of macromolecular chains onto the nanoparticles surface via chemisorption.<sup>[384]</sup> In the matter of former approach, a so called “ligand addition” process can be performed wherein the physical interaction between the hydrophobic tails of amphiphilic molecules (e.g., phospholipids) and hydrophobic ligands on the surface of MNPs takes place.<sup>[385]</sup> In fact, interaction of the long-chain hydrocarbons with hydrophobic surfactants of the core surface leads to liposomal or micellar structures that can interact with water by either ionic interactions or hydrogen bonding due to the hydrophilic heads of surfactants. Since amphiphilic molecules can be formed around the nanoparticles regardless of their composition, this method can apply to other kinds of nanomaterials such as carbon nanotubes, quantum dots, and noble metal nanocrystals.<sup>[386]</sup> This strategy comes in handy especially in synthesis methods such as thermal decomposition which result in nanoparticles capped with hydrophobic surfactants that are incapable of suspending in polar solvents such as water or PBS solutions.<sup>[141]</sup> Wang et al. presented a surface modification method for increasing the dispersity of MNPs in aqueous phase based on the formation of inclusion complex between surface-bound surfactant molecules and  $\alpha$ -cyclodextrin ( $\alpha$  - CD) (**Figure 28a**).<sup>[387]</sup> They first used a thermal decomposition method for preparing  $Fe_2O_3$  nanoparticles coated with oleate and stored in hexane. Subsequently, an aqueous mixture of  $\alpha$  - CD was created and the phase transfer was conducted by vigorously stirring the two solutions under room temperature. After a 20 h stirring, MNPs’ coating were exchanged from the oleate to the  $\alpha$  - CD coating as the top hexane layer became colorless (Figure 28b). Furthermore, amphiphilic copolymers derived from polysaccharides and PEG can be employed to

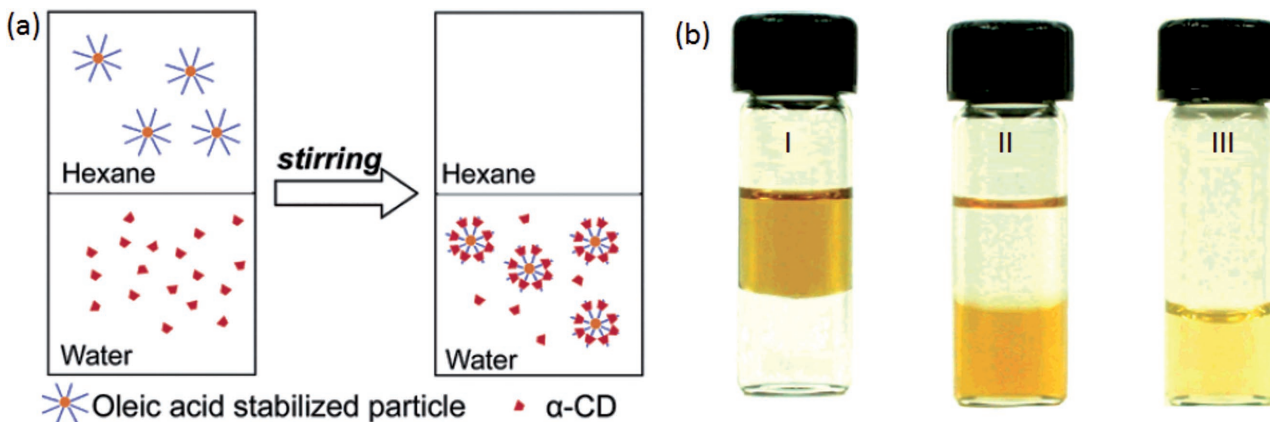


**Figure 28.** a) Schematic illustration of transfer of oleic acid stabilized nanoparticles from organic into aqueous phase by surface modification using  $\alpha$ -cyclodextrin. b) photographs of two phase mixture of 10 nm iron oxide nanoparticles (I) before and (II) after phase transfer, and (III) aqueous suspension after centrifuge. Reproduced with permission.<sup>[387]</sup> Copyright 2003, ACS.

further enhance the aqueous stability of MNP-containing micelles.<sup>[388]</sup> Although large hydrophobic and hydrophilic regions of copolymers wrapped around the magnetic cores lead to great chemical and thermal stability,<sup>[389]</sup> compared to the nanoparticles coated with simple organic molecules the above strategy results in nanoparticles with substantially increased diameters.<sup>[390]</sup> Furthermore, the possibility of the molecules desorption due their weakly bound ligands can lead aggregation, precipitation, and loss of functionality of the nanoparticles.<sup>[391]</sup>

In an alternative strategy, covalent binding of polymeric coating onto the surface of nanoparticles can be performed either by the “grafting to” or “grafting from” methods. In former case, pre-synthesized end-functionalized polymer chain is attached by using the affinity of the polymer end-group and complementary functional groups located on the surface of nanoparticles to form tethered chains.<sup>[392]</sup> However, the overlapping problem of earlier attached chains faces this approach with activation barrier that limits the amount of polymer capable to be tethered onto the nanoparticles. On the contrary, in situ growth of the polymer chains from the substrate surface by attaching initiating groups, mainly by covalent bonds, can overcome the intrinsic problem related to the prior method.<sup>[393]</sup> A wide range of polymerization techniques such as ring-opening metathesis polymerization,<sup>[394]</sup> living cationic,<sup>[395]</sup> living anionic,<sup>[396]</sup> ring-opening polymerization (ROP),<sup>[397]</sup> and controlled/“living” radical polymerization (CRP)<sup>[398]</sup> have been developed during the last decades for coating numerous nanoparticles with polymeric materials. By a study performed by Kang et al. a reversible addition-fragmentation chain transfer (RAFT) process utilizing peroxide and hydroperoxide functionalities was used to functionalize  $\text{Fe}_3\text{O}_4$  MNPs with polystyrene and poly(acrylic acid).<sup>[399]</sup> A flexible methodology was also proposed by Lattuda et al. for the preparation of MNPs coated with poly(lactic acid) end-tethered chains which were grown by surface-initiated ROP and poly(methacrylate) end-grafted chains obtained by atomic transfer radical polymerizations.<sup>[400]</sup>

Overall, some inherent limitations of physical adsorption of coating materials onto nanoparticles can be overcome through applying polymers which are able to bind with more than one chemical group that directly lead to fully encapsulated

nanoparticles which are much more stable under physiological conditions.<sup>[401]</sup> Both linear-/partially branched polymers (such as dextran,<sup>[402]</sup> PAA,<sup>[403]</sup> modified hyaluronic acid,<sup>[404]</sup> and various copolymers)<sup>[405]</sup> and hyperbranched-polymers (such as branched PEI and other types of dendrimers) are used for encapsulation of MNPs. In contrast to the hyper branched and linear branched polymers which encapsulate the nanoparticles, an end-grafting approach can be employed for coating MNPs through connecting the magnetic core and coating material via utilization of surface binding groups such as carboxyl groups,<sup>[378b]</sup> thiol groups,<sup>[406]</sup> hydroxamic acid,<sup>[407]</sup> alkoxysilanes,<sup>[408]</sup> phosphine oxide,<sup>[409]</sup> and catechol-based<sup>[406]</sup> ligands on one end of the coating materials. In an interesting study performed by Jun et al., a cross-linked “mesh” formed by dimercaptosuccinic acid (DMSA) on the surface of ferrites MNPs provided better chemical stability.<sup>[410]</sup> In this case, the surface-capping molecules formed disulfide bridges which not only enhanced the stability, but also left available free thiols for further bioconjugation. Additionally, the highly stable polysiloxane shells formed by alkoxysilanes on the surface of MNPs have also gained extensive attention.<sup>[129,408b,411]</sup> However, availability of functional groups for biocunjugation and the colloidal stability of MNPs can be adversely affected within end-grafting strategy. In fact, the bulky nature of some high affinity capping groups may result in low surface density of end-grafted polymers. In addition, end-grafting coated MNPs are prone to agglomerate due to the probability of linkages break down and coating loss which is caused by the limited amount of binding groups per coating molecules.<sup>[386]</sup>

#### 4. Design Considerations for Entering the Body

Despite the vast perpetual improvements in the quality of MNPs, principal design factors should be taken into full consideration in every step of production process to increase the probability of reaching the target by both prolonging the half-life of nanoparticles and increasing their cellular internalization (**Figure 29**). Potentially, pessimistic insights are given by the inherent properties of MNPs for hyperthermia and MRI,

NPs consideration for entering the body		
Prolonging the half-life		Regulating cellular internalization
<b>Size and Shape</b>	<b>Size and shape</b>	
Materials bigger than 100 nm are readily taken up by RES. Also to avoid vessel embolism and pass through capillary system of organs, particles should be less than 100 nm. Nanoparticles with anisotropical shape and with high length-to-width aspect ratio have better blood circulation time by decreasing the systemic absorption and excretion. Such nanoparticles also showed decreased liver distribution and urinal excretion.	Larger NPs increase the propensity of margination behavior to be migrated near the vascular wall. NPs larger than 60 nm are poorly taken up by tumor cells. NPs with the size of 50 nm have shown optimal cellular uptake. Disk-like NPs exhibit larger lateral drift velocities and lower the hydrodynamic forces due having smaller cross section and larger surface of adhesion compared to spherical NPs. In addition, elongated nanoparticles have shown better cellular uptake compared to spherical nanoparticles.	
<b>Surface charge</b>	<b>Surface charge</b>	
Negatively charged surfaces are less prone to the adsorption of opsonin proteins which will finally reduce the unspecific uptake by phagocytic cells.	Positively charged NPs have better interactions with the anionic cell membranes and increase the chance of endocytosis.	
<b>Hydrophobicity</b>	<b>Toxicity concerns</b>	
The rapid formation of protein corona around the NPs through absorption alters their chemical identity and makes them more visible to phagocytic cells. Protein-repellent coatings such as poly(ethylene glycol) and zwitterionic molecules such as polybetaines or polysaccharides can be used to reduce the hydrophobicity of NPs to inhibit the formation of protein corona. In addition, biomimetic coatings derived from the membranes of erythrocytes, leukocytes, platelets and macrophage cells can disguise NPs.	Some organs may capture and store magnetic NPs, hence a surface modification is needed to prevent their direct contact with cells. Also, iron oxide nanoparticles in concentrations > 100 micro*g/ml demonstrate levels of cytotoxicity and produce mild transient side effects. Magnetic targeting of MNPs also increases their concentration in a localized area which can cause adverse biological effects such as inflammation.	
	<b>Toxicity concerns</b>	
	Targeting ligands are complementary to unique receptors on target cells and increase the affinity and chance of specific cell binding. NPs are decorated with ligands such as antibodies, aptamers, proteins, peptides and small molecules to specifically bind to either pre-existing surface molecules or receptors overexpressed on target organs.	

**Figure 29.** MNPs consideration for entering with prolonged half-life and regulated cellular internalization.

as well as by their high surface to volume ratio which have translated them into potential vehicles capable of carrying an arsenal of therapeutics and imaging modalities. In one special case, incapability of conventional drug formulations to be localized in mass has been one major impetus that a wide range of research efforts have been aimed at exploitation of nanoparticles to overcome the pharmacokinetic limitations associated with such therapeutics leading to substantially prolonged blood circulation times.<sup>[412]</sup> Practically, however, achievement of proper therapeutic and diagnostic outcomes has been severely hindered by a series of biological barriers that nanoparticles encounter during their journey within the highly complex system of the body. Although nanoparticles have dramatically expanded the therapeutic window of drugs, these barriers leave nanoparticles incapable of reaching the target, to the point that in most cases, 5% or less of the injected nanoparticle dose ends up in tumor tissue and the bulk of injected dose still accumulates in healthy tissues which cause adverse effects in other organs.<sup>[413]</sup>

Irrespective of the vehicle and cargo types, unspecific uptake by the cells of mononuclear phagocyte system (MPS) as well as a series of anatomical size restrictions exerted by renal ultrafiltration in kidney, and other organs like spleen and liver are the main physiological barriers for elimination of nanoparticles.<sup>[414]</sup> In addition, nanoparticles are faced with a sequential fashion of cellular barriers (such as the cell membrane, the endosome/lysosome) to go through the cellular gates and deliver their cargoes. In order to overcome these hindrances in the way of transitioning nanoparticles with mere potential to the ideal ones for unprecedented biomedical applications, a vast amount of researches have been carefully invested on better understandings of biophysical interactions at the nano–bio interface for proper negotiation with biological barriers.<sup>[415]</sup> In the light of the extensive researches, it has been concluded the modulation of physicochemical properties of nanoparticles such as size, shape, surface chemistry, and surface charge play important roles in incorporating new design features within conventional nanoparticle constructs. Herein, we highlight profound

implications on directing MNPs to a happy ultimate fate for overcoming these barriers and performing their designated in vivo functions in a clinical field.

#### 4.1. Overcoming Elimination by the Body Immune System

Interaction of MNPs with the immune system of the body and non-targeted cells can be limited or enhanced depending on the physicochemical properties of MNPs. In the first step, the physicochemical properties of nanoparticles should be modulated in a way that prolongs the blood circulation time of nanoparticles through bypassing the MPS (also called reticuloendothelial system or macrophage system) as well as size restrictions in the renal ultrafiltration system (kidney, spleen, and liver).<sup>[10,416]</sup> To this end, along with better understanding between nanoparticles and body system, a series of considerations should be applied on modulating surface chemistry (hydrophobicity and surface charge), size and shape of MNPs to avoid engulfment and filtrations from the bloodstream.

At the core of these considerations is designing MNPs that maintains an appropriate “biological identity” during their journey to the target site, which actually means to protect their primary suitable physicochemical properties against being altered by the adsorption of serum protein on their surfaces.<sup>[417]</sup> This is extremely vital to avoid the immediate sequestration of MNPs by preventing changes in their original identity which may promote MNPs recognition and uptake by MPS.<sup>[418]</sup> In particular, nonspecific uptake of opsonized nanoparticles by MPS, consisting of the phagocytic cells located in reticular connective tissue, mainly limit the delivery of therapeutic cargos at disease sites by depositing a small fraction of the total dose in the tumor.<sup>[419]</sup> Specifically, upon the intravenous injection of MNPs into the body, the sequestration process begins with opsonization by which they are covered with opsonin proteins, including serum albumin, apolipoproteins, and immunoglobulins.<sup>[14a]</sup> This adsorption has significant impacts on biological, biochemical, and cellular behavior of MNPs and transforms the original chemical identity of the surface of MNPs into a biological identity.<sup>[420]</sup> Physicochemical properties of MNPs are dramatically altered by this rapidly forming protein corona to the point that protein corona will be what cells actually see.<sup>[421]</sup> This corona now pinpoints the biological effect on interaction with cells membrane and the uptake mechanism by defining the biological identity of MNPs.<sup>[422]</sup> Following the protein adsorption, MNPs become more visible to macrophages and other phagocytic cells residing in the spleen, lymph nodes, and liver. Subsequently phagocytosis happens by undergoing attachment to specific receptors on the surface of phagocytes.

Although many interactions contribute to the formation of protein corona, it is now understood that hydrophobic interactions and surface charge are mainly in charge of protein adsorption on the surface of nanoparticles (**Figure 30**).<sup>[423]</sup> However, some studies have reported on quantitative<sup>[14b]</sup> and qualitative<sup>[424]</sup> size influence on protein composition. The surface charge which quantitatively is measured as an electrical potential in the interfacial double layer on the nanoparticles in suspension plays a significant role in their colloidal stability, adsorption of proteins and cellular uptake.<sup>[12]</sup> Although many

attempts have been made to investigate the effect of surface charge on the formation of protein corona, there is still a disparity in whether positive or negative surface charged nanoparticle are better suited for biological applications.<sup>[425]</sup> A series of studies have reported that negatively surface charged nanoparticles strongly correlate with reduced protein adsorption, which consequently leads to low phagocytic uptake and longer blood circulation time. Surprisingly, some studies have shown that protein binding affinities are independent of the nanoparticle charge and are not determined by the isoelectric point of the proteins.<sup>[426]</sup> Overall, it may be implied that undesirable clearance by RES can be reduced with slightly negative charged nanoparticle to reach the target cells.<sup>[427]</sup>

It has also been demonstrated that nanoparticles with hydrophobic surfaces are more likely to be covered with proteins compared to hydrophilic ones.<sup>[428]</sup> Furthermore, these hydrophobic interactions lead to a poor dispersion in water and organic solvents and also loss of superparamagnetic properties.<sup>[4]</sup> To inhibit nanoparticles agglomeration and adsorption of plasma protein to the surface of hydrophobic nanoparticles, they have to be equipped with protein-repellent surface to prevent recognition by the RES and extend circulation time in the body.<sup>[429]</sup> This has led to the development of stealth nanoparticles which are a promising tool for avoiding their elimination by the body's defense system.

Avoiding the formation of protein corona, one strategy is modifying the hydrophobic surface of nanoparticles with hydrophilic materials such as PEG as a standard approach to increase the circulation of variety of nanoparticles.<sup>[430]</sup> Tight associations formed between PEG subunits and the water molecules result in generation of a barrier that blocks protein adsorption.<sup>[431]</sup> This steric hydrating layer significantly reduces the recognition of MNPs by MPS and extends the half-life of nanoparticles in circulation. Although PEG reduces the overall protein binding, investigations on PEGylated nanoparticles have represented high amounts of clusterin in the protein corona which was formed on their surfaces.<sup>[432]</sup> In a recent study, the role of clusterin on nanoparticle uptake by phagocytes was evaluated and it was revealed that clusterin has a stealth effect on the cellular uptake of not only PEGylated nanoparticles but also non-PEGylated nanoparticles.<sup>[433]</sup> However, some studies have reported the reduced cellular internalization of nanoparticles through pre-incubation with clusterin proteins.<sup>[432]</sup> Despite all the advantages of PEG, there are some drawbacks such as non-biodegradability, the chance of accumulation in the body, detachment of chains, and the occurrence of accelerated blood clearance (ABC) phenomenon, which necessitates the search for alternatives to PEG.<sup>[434]</sup> Specifically, rapid particle clearance happens within the ABC phenomenon due to formation of antibodies against PEG upon repeated administration of PEGylated nanoparticles.<sup>[435]</sup> In addition, targeting ligands loaded on nanoparticles are prone to be shielded by the outer PEG layer, which will mask their cell-specific recognition and hamper specific targeting.<sup>[431]</sup> Such drawbacks have necessitated search for alternatives to PEG. To this end, poly(phosphoesters)<sup>[432]</sup> and zwitterionic molecules<sup>[436]</sup> such as polybetaines or polysaccharides are also capable of translating hydrophobic surfaces of nanoparticles into hydrophilic ones.

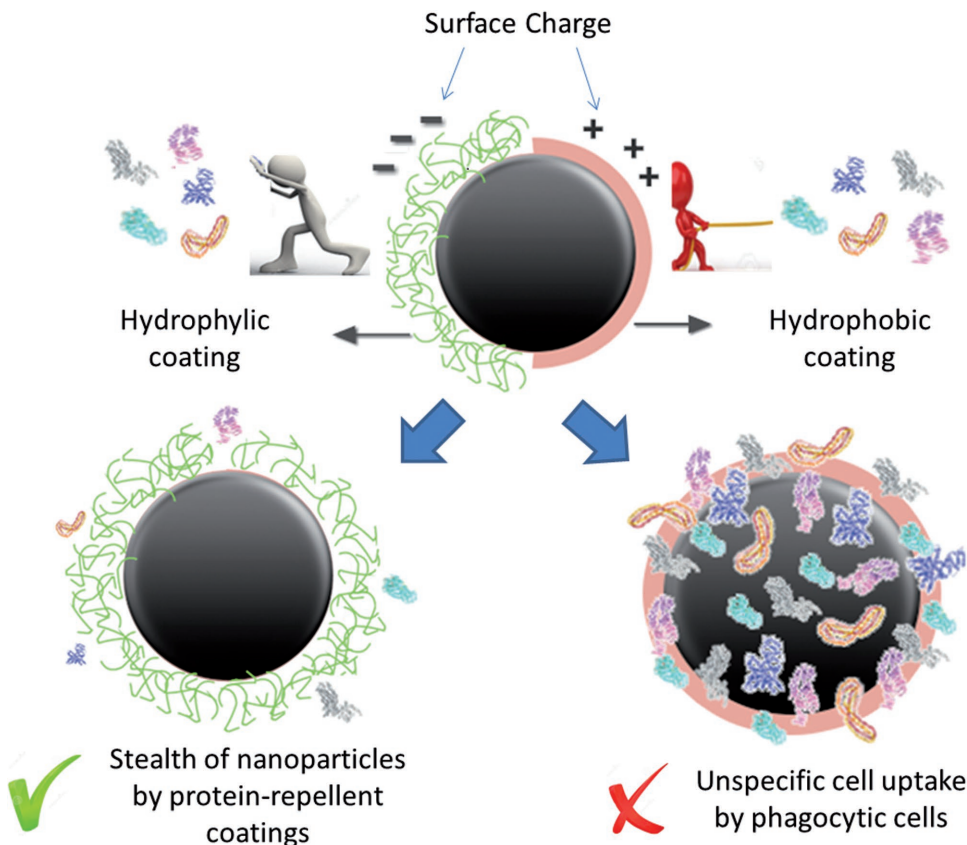


**Figure 30.** Effect of surface charge and hydrophobicity on the adsorption of proteins on the surface of MNPs. Coating the MNPs with protein-repellent material results in stealth of MNPs and prevent their unsepcific uptake while hydrophobic coatings result in formation of protein corona and unspecific uptake by phagocytic cells.

To mimic the whole function of blood cells with synthetic biomaterials cannot be completely performed due to the complexity of living cells and organisms.<sup>[437]</sup> To address this dilemma, biomimetic coatings have emerged as an alternative intriguing strategy to bestow natural characteristic upon nanoparticle surfaces for evading the MPS by “disguising” them with sending “don’t eat-me” signals.<sup>[438]</sup> In fact, derived and purified cellular membrane from a cell source is integrated with the surface of nanoparticles to somehow “camouflage” them. Several reports have proved significant MPS evasion and tumor accumulation of nanoparticles through coating them with the membranes of erythrocytes,<sup>[439]</sup> leukocytes,<sup>[440]</sup> platelets,<sup>[441]</sup> and macrophage cells<sup>[442]</sup> as well as “self” peptides such CD47.<sup>[443]</sup> A simple sonication method can be applied to fully coat nanoparticles by exploiting the asymmetric charge of the cell membranes.<sup>[444]</sup> In a very recent study, for the first time, iron oxide nanoparticles were camouflaged with stem cell membranes within a sonication method.<sup>[445]</sup> They reported significant decreased in the nanoparticles uptake by measuring the intracellular Fe content through *in vitro* analyses.

Hydrodynamic size highly determines MNPs ability to manage biological barriers and escape from the RES and avoid elimination by clearance organs, including liver, kidney, and spleen.<sup>[446]</sup> Furthermore, concentration profile of MNPs in the blood vessel<sup>[447]</sup> and permeability out of the vasculature<sup>[448]</sup>

are also greatly impacted by hydrodynamic size. Materials greater than 100 nm are prone to be taken up by liver, spleen or destroyed by the bone marrow.<sup>[10]</sup> Hence, combined size of the core and coating along with anchored functionalities, such as targeting ligands, imaging modalities, and therapeutics, must be considered at each stage of the designing process to produce an end product with small size (<100 nm). This will make them able to remain in the blood circulation and be capable of passing through capillary systems of organs and tissues avoiding vessel embolism.<sup>[12]</sup> Another physiological barrier encountered by MNPs is kidney, with the basal lamina which consists of pores ≈10 nm sized.<sup>[449]</sup> There have been reported that small sized nanoparticles (<20 nm) are filtered out of the blood through kidney and are consequently excreted renally.<sup>[13]</sup> So, MNPs with hydrodynamic sizes between 10 and 100 nm are too large to undergo renal elimination and as such have greatly reduced liver and kidney uptake.<sup>[450]</sup> This will finally lead to prolonging the half-life of MNPs and therapeutics to enhance the efficacy of designated application through accumulation of MNPs at the tumor sit.<sup>[451]</sup>

A number of comparative studies have investigated the effect of nanoparticles shape on distribution within the body system.<sup>[452]</sup> Typically, the cellular uptake of nanoparticles is better for elongated and cylindrical nanoparticles compared to spherical ones.<sup>[453]</sup> In a very recent study Li et al. reported

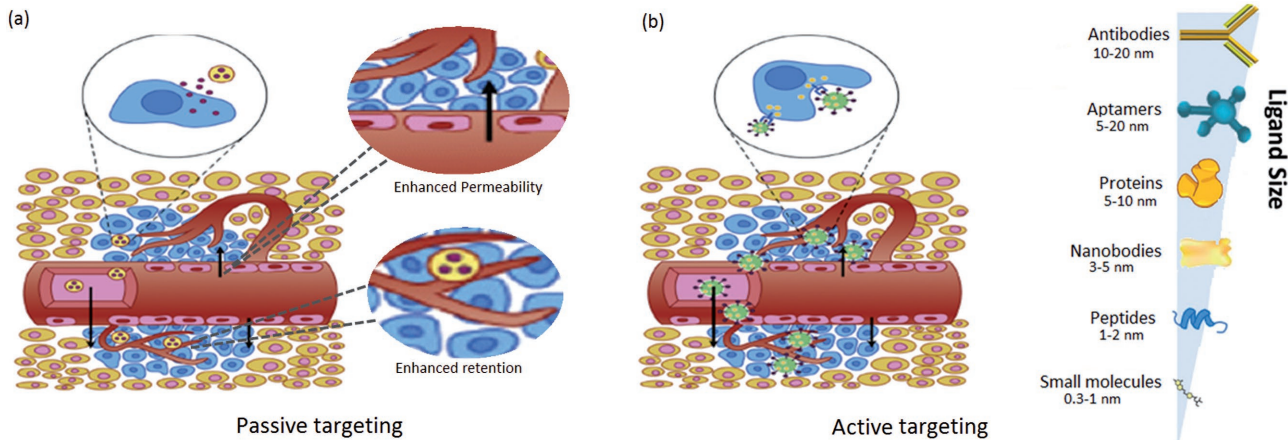


**Figure 31.** Enhancing cell internalization through exploitation of a) enhanced permeability and retention effect in passive targeting, b) and targeting ligands for active targeting. a) Adapted with permission.<sup>[461]</sup> Copyright 2015, Elsevier. b) Adapted with permission.<sup>[462]</sup> Copyright 2014, Elsevier.

nanoparticles with decreased in vivo biodegradation, liver distribution and urinal excretion.<sup>[452a]</sup> Also, some studies have reported that nanoparticles with an anisotropic shape have better blood circulation time and have a greater impact on different aspects of cellular function, including cell proliferation, apoptosis, cytoskeleton formation, adhesion, and migration.<sup>[409,452b]</sup>

#### 4.2. Overcoming the Endocytosis Barrier

##### 4.2.1. Passive Targeting

In addition to all the design considerations for increasing the blood circulation time to approach the surface of tumor cells, these carriers should undergo a so called “endocytosis” process in order to fully internalize the cancerous cells and deliver their cargos. Unique physiological features displayed by tumor along with equipping nanoparticles with targeting ligand form key concepts in passive and active transport oncophysics (Figure 31). Specifically, preferential accumulation of MNPs inside tumor is achieved by exploiting their predetermined physicochemical properties and more importantly the enhanced permeability and retention (EPR) effect, investigated firstly by Maeda and Matsumura in 1986, for targeting metastatic solid tumors.<sup>[454]</sup> The permeation portion of EPR can be denoted by little extravasation resistance encountered by small macromolecules and NPs out of the vasculature upon distributing to the tumor interstitium due to the production of new poorly organized blood vessels having leaky fenestrations.<sup>[455]</sup> In fact, the normal vasculature in the vicinity of tumor tissue is unable to sufficiently supply the increasing oxygen required by the growing tumor, which motivates the budding of new blood vessels.<sup>[456]</sup> Irregular blood vessels produced within this process can have leaky fenestrations from 200 to 2000 nm due to lack of the basal membrane of the normal vascular structure and presenting discontinuous epithelium.<sup>[457]</sup> On the other hand, enhanced retention component of EPR effect is represented by selective accumulation of NPs due to inefficient lymphatic drainage in the tumor tissue which subsequently leads poor clearance

of the extravasated NPs.<sup>[458]</sup> Molecules smaller than 4 nm are readily reabsorbed by diffusing back to the blood circulation.<sup>[459]</sup> Although tumors have defective lymphatic function, larger nanoparticles cannot rely on diffusive and convective forces to return to circulation due to their larger hydrodynamic radii.<sup>[460]</sup> These inherent properties will consequently lead to poor clearance of nanoparticles which have reached the perivascular space and their accumulation in the tumor interstitium.

Since the discovery of EPR effect, it has become the leitmotiv of many scientists to elucidate this effect and the factors affecting that by using dozens of animal models and tumor types.<sup>[457,463]</sup> Proper contact with the endothelial surface has been shown to be the most important prerequisite for increasing the chance of internalization. A wide range of studies have unraveled physicochemical properties of administered nanoparticles, such as surface charge, size, and shape to be among the most important factors affecting margination behavior and interactions with vascular wall.<sup>[462]</sup> Specifically, within the margination effect, white blood cells and platelets migrate to a “cell-free layer” formed near the vascular wall due to accumulation of red blood cells within the center of the blood vessel.<sup>[464]</sup> Engineering the nanoparticles to enter this “cell-free layer” highly increases the likelihood of contacting the vascular wall to have better cellular internalizations.<sup>[425]</sup>

Generally, it has been shown that positively charged nanoparticles will have better interactions with the anionic cell membranes which lead to increased endocytosis.<sup>[465]</sup> Furthermore, the vascular dynamics and cell interaction of nanoparticles is highly affected by the geometry of administered nanoparticles. In the matter of size effect on margination behavior, several studies have been reported on increasing the margination propensity by increasing the diameter of nanoparticles,<sup>[15,466]</sup> however, there is no agreement on the optimal size for margination.<sup>[467]</sup> It has been shown by several studies that nanoparticles of  $\approx 50$  nm in size achieve an optimal cellular uptake.<sup>[468]</sup> Such nanoparticles appear to have the highest internalization and modest exocytosis rates,<sup>[469]</sup> while nanoparticles with hydrodynamic sizes larger than 60 nm are poorly taken up by tumor cells.<sup>[470]</sup> In a recent study, Salva et al. have also reported that manganese oxide nanoparticle with an average

diameter of 25 nm showed high tumor accumulation in an orthotopic lung cancer model.<sup>[46]</sup> In the matter of shape effect on margination behavior, larger lateral drift velocities have been exhibited by disc-like nanoparticles compared to spherical and quasi-hemispherical ones.<sup>[471]</sup> In fact, small cross section and larger surface of adhesion offered by disc-like nanoparticles lead to lower hydrodynamic forces and better adhesive interaction under shear flow.<sup>[472]</sup> In addition, it has been revealed that the endocytic kinetics of nanoparticles upon approaching to the cell surface is highly controlled by the local curvature of their non-spherical shape.<sup>[473]</sup>

#### 4.2.2. Active Targeting

Despite all the advantages offered by passive targeting and exploitation of EPR effect, complex biological processes including vascular permeability, angiogenesis, and heterogeneities in the tumor microenvironment and lymphangiogenesis have somehow hampered the mark of practicality. Furthermore, biological and physicochemical properties of administered NPs affect the distribution and accumulation quality in tumors.<sup>[474]</sup> These reasons coupled with advent personalized medicine fairly bear signs of passive targeting approach to be diminished from the arsenal of vital nanotheranostics by the bloom of active targeting.

Due to limitations of passive targeting, nanoparticles are modified by conjugating targeting species to increase their affinity for specific cell binding to capitalize their full potential benefit.<sup>[475]</sup> Although this approach has been proposed about 40 years ago,<sup>[476]</sup> ligand-decorated nanoparticles have recently paved their way to clinical trials.<sup>[477]</sup> Increase in affinity and its consequent specific cell binding is achieved by NPs equipped with targeting species which are complementary to unique receptors on target cells. Accessibility of the specific antigen on targeted cells for an appropriate binding to ligand-decorated NPs is crucial during this approach. Hence, this strategy displays an increased degree of complexity. In particular, ligands including antibodies, aptamers, proteins, peptides, and small molecules are chosen to specifically bind to either pre-existing surface molecules or receptors overexpressed on targeted organs.<sup>[478]</sup> Lipids, sugars, and proteins can be target molecules to which ligand-mediated nanoparticles will bind.<sup>[479]</sup> Through accommodating extensive copies of the ligands on the surface of NPs, they will gain an extreme avidity for their targets.<sup>[480]</sup> Consequently, upon administration of these novel cargos, interactions with targeted cells are highly increased that leads to enhancing internalization of therapeutic payloads without affecting the overall biodistribution.

However, a major challenge in the way developing active targeting is that recognition of administered NPs would not occur, unless they are in the vicinity of their target antigens.<sup>[481]</sup> Since targeting molecules are usually located in the extravascular space of the tumor,<sup>[462,482]</sup> both passive and active targeting come in handy. In fact, optimal targeting will be achieved by first optimizing the blood circulation time and relying on the EPR effect to reach the target cells, and subsequently exploiting the ligand affinity on the surface of NPs to form efficient bonding with target cells.<sup>[483]</sup>

### 4.3. Targeting Ligands

#### 4.3.1. Antibodies

Antibodies (Ab), also called immunoglobulin (Ig), represent the most commonly used ligands for developing specific targeting due to their high inherent affinities along with the remarkable ability they possess in recognizing a specific part of targets. Typically, Abs are large Y-shaped proteins composed of two large heavy chains and two smaller light chains which are covalently linked through interchain disulfide bonds wherein each chain consists of variable and constant domains (**Figure 32a**).<sup>[484]</sup> Among the five major classes of soluble serum glycoproteins, IgGs which are the major components, contain a variable domain and three constant domains: CH<sub>1</sub>, CH<sub>2</sub>, and CH<sub>3</sub> domains.<sup>[485]</sup> Generally, the small hypervariable dimeric region at the tip of the antibody, called F(ab')<sub>2</sub>, is in charge of forming a wide range of tip structures as bonding sites for recognizing a variety of antigens.<sup>[462]</sup> On the other hand, less variable regions at their bases (CH<sub>2</sub> and CH<sub>3</sub>) constitute the Fc fragment of antibodies, which are responsible for triggering the elimination of antigens.<sup>[486]</sup>

Despite the bulky structure of antibodies, they can equip the nanoparticles to specifically bind to their targets, even if they are conjugated in low densities at the surface of nanoparticles.<sup>[488]</sup> Antibodies were firstly used in 1980s to modify liposome nanoparticle surfaces wherein the antigens on the target cells were recognized.<sup>[489]</sup> Since the first approved antibody in 1986,<sup>[490]</sup> muromonab-CD3, numerous antibody platforms such as chimeric, murine, and humanized antibodies have been developed with more than 30 types of them being approved for clinical uses.<sup>[477]</sup> The inherent antibodies ability to distinguish between healthy and cancerous cells and even among cancer cell types fairly motivates their use for active targeting.<sup>[18]</sup> Anti-HER2 Mab (also called Herceptin or trastuzumab),<sup>[491]</sup> rituximab (Rituxan),<sup>[492]</sup> Anti-CD3 Mab,<sup>[493]</sup> Anti CEA Mab,<sup>[494]</sup> and huA33 mAB<sup>[495]</sup> are of some mostly used antibodies for decorating nanoparticles in treating cancers.

Despite all the advantages offered by antibodies, many limitations and challenges are encountered by antibody conjugated nanoparticles within their use in active targeting applications. One of the major barriers is large hydrodynamic size of antibodies (~150 kDa, 10–15 nm long and 7–9 nm wide),<sup>[496]</sup> which makes it difficult to be effectively conjugated on the surface of nanoparticles and increases the overall sizes up to 30 nm.<sup>[497]</sup> Since fewer antibodies can be conjugated, both targeting efficiency and the potential for multivalent binding effects may be reduced.<sup>[498]</sup> In addition, increased size of nanoparticles results in lack of tumor extravasation, specifically non-uniform uptake into the tumor mass.<sup>[499]</sup> Accumulation of intact antibodies in the liver can also occur due to large hydrodynamic diameter of antibodies.<sup>[500]</sup>

However, since the antigen recognition is not directly attributed to the constant domains of antibodies, this problem has been somehow circumvented by proposing smaller antibody fragments which still retain the antigen-binding activity.<sup>[487]</sup> These smaller antibody fragments, including antigen-binding fragments (Fab), ScFvEGFR, and ScFcCD7, allow a drastic reduction of total molecular weight and immune response.<sup>[501]</sup>

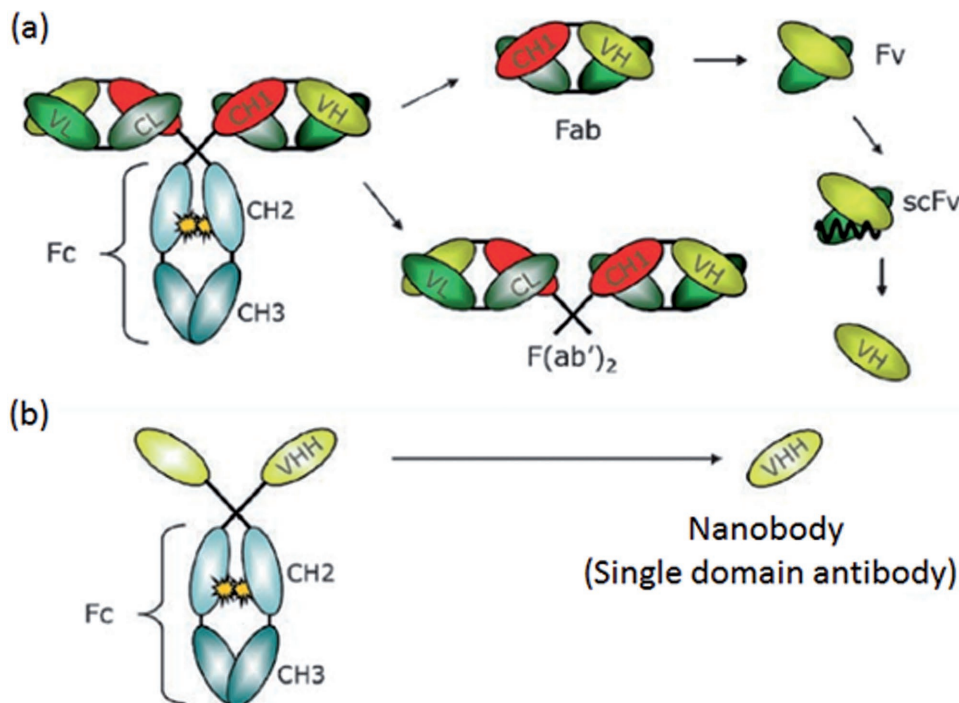


**Figure 32.** Schematic representation of a) conventional antibodies b) and heavy chain antibodies and the antigen-binding fragments thereof. Reproduced with permission from.<sup>[487]</sup> Copyright 2010, Springer.

Such smaller formats of antibodies provide more efficient tumor penetration, faster organ clearance, and better suitability for structural analysis compared with the whole antibody molecules. However, aggregation and low expression yields in heterologous systems within their generation from conventional antibodies as well as decreased affinity and stability are the technical challenges upon their utilization.<sup>[487,502]</sup>

Another limitation of antibody decorated nanoparticles is immunogenicity and purity concerns due to Fc fragment of antibodies which is responsible for the recognition of the protein by the MPS and the immune system.<sup>[462]</sup> In particular, such nanoparticles can be perceived as foreign proteins by the body which nullifies the action of active targeting by their effective clearance from the blood.<sup>[496a,503]</sup> Humanized monoclonal Abs or their production as a chimeric protein have been reported for avoiding unwanted immune responses in patients.<sup>[504]</sup> Slight improvements have also been observed through removing the Fc fragment<sup>[505]</sup> or employing antibody carbohydrates for prospering the orientation of antibodies on the surface of nanoparticles.<sup>[506]</sup> Another limitation encountered by antibodies is that they have fragile structures, which leads to rapid loss in their targeting affinity with slight alterations to their structure by environmental challenges such as temperature and enzyme.<sup>[496a,507]</sup> Hence, technical challenges during synthesis and storage will be created which makes the development and modification of antibodies a complex and expensive process and have direct effects on the cost/efficiency ratio of produced nanoparticles.<sup>[18,462]</sup>

**4.3.1.1. Nanobodies:** An answer to several of concerns mentioned above is provided by a serendipitous discovery of a

special antibody repertoire of camelids by Hamers-Casterman et al. which revolutionized the potential of antibodies for biomedical applications.<sup>[508]</sup> Discovered antibodies consist of only heavy chains and as a result are referred to as heavy-chain antibodies (HCabs, ~95 kDa) (Figure 32b). Although the first constant domain (CH<sub>1</sub>) and the light chain are both absent in the structure of HCabs, extensive antigen recognizing along with sufficient binding affinities similar to those of conventional antibodies have been displayed.<sup>[509]</sup> Surprisingly, only the N-terminal variable domain of the heavy chain of HCabs (VHH) is responsible for the specific binding to the targets.<sup>[510]</sup> The Belgian company Ablynx coined the term “nanobodies” with respect to the nanometer size range of these naturally derived antigen-binding fragments, which are also termed as single domain antibodies.<sup>[511]</sup> Nanobodies, demonstrate essential characteristics such as high specificity and affinity,<sup>[504]</sup> high solubility, stability in aqueous solutions,<sup>[512]</sup> high thermal and chemical resistance,<sup>[513]</sup> capability to be chemically modified, ease of cloning, and ease of gene manipulation<sup>[496b]</sup> which relieves some restrictions related to conventional antibodies. Additionally, low immunogenicity of nanobodies which is both attributed to their high similarity with human VH sequences<sup>[514]</sup> as well as absence of Fc fragment, made nanobodies to pave their way into biomedical applications more easily.<sup>[496b,515]</sup> In particular, compared to conventional antibodies where variable domains of both heavy and light chains are required, nanobodies with much smaller molecular weight (~15 kDa)<sup>[516]</sup> can be highly exploited for preparing more practical targeting ligands.

With respect to all these advantages, multiple nanobodies have been shown promising to effectively and specifically

target the human epidermal growth factor 2 receptor (HER2) and epidermal growth factor receptor 2 (EGFR2) for cancer diagnosis and therapy.<sup>[517]</sup> Specifically, nanobodies have been used as antagonistic drugs<sup>[518]</sup> and targeting agents of effector domains<sup>[519]</sup> in cancer immunotherapy. On the other hand, several molecular imaging modalities of SPECT<sup>[520]</sup> and PET,<sup>[521]</sup> optical imaging,<sup>[522]</sup> and ultrasound imaging<sup>[523]</sup> have been actively directed toward the target by means of nanobodies conjugated to them. Additionally, grafting nanobodies on nanoparticles have shown a considerable potential for increasing their affinity toward the target.<sup>[504]</sup> Conjugation of liposomes,<sup>[524]</sup> micelles,<sup>[525]</sup> albumin,<sup>[526]</sup> gold,<sup>[527]</sup> and magnetic<sup>[528]</sup> nanoparticles with nanobodies has been widely reported for active targeting in drug delivery applications, especially via receptor-mediated internalization.

#### 4.3.2. Aptamers

Another class of efficient ligands for active targeting is nucleic acid-based aptamers (Apts) which have been presented as binding molecules since their development by Szostak, Gold, and Joyce groups.<sup>[529]</sup> Ellington et al. coined the term aptamer in 1990 when they purified RNA molecules through an *in vitro* process by using dye columns with specific binding capabilities.<sup>[530]</sup> In fact, aptamers are artificially selected sequences of short single-stranded nucleic acids such as DNA, RNA or modified oligonucleotides which can fold into numerous unique 3D conformations.<sup>[477,531]</sup> These conformations which originate from intramolecular Watson–Crick interactions,<sup>[462]</sup> have extremely high affinity in binding small and large biochemical targets.<sup>[532]</sup> However, finding the appropriate sequence able to participate in ligand binding is akin to finding a needle in a haystack. To thoroughly comb through vast populations of nucleic acids, a process referred to as systemic evolution of ligands by exponential enrichment (SELEX) was proposed.<sup>[529b]</sup> Through this process aptamers are isolated by successive rounds of *in vitro* screening of random sequence libraries for their binding ability to antigens with high specificity and affinity and subsequently selected and amplified by using polymerase chain reaction.<sup>[462,477]</sup> In recent years, the utility of aptamers has been enhanced through many techniques, in particular the one in which SELEX is performed with complex mixtures of biological materials and cell–SELEX.<sup>[498,533]</sup> By this technique aptamers which recognize specific cell lines are generated within an *in vitro* selection performed with whole live cells.<sup>[498,534]</sup> Finding more efficient aptamers for specific applications, they have also been selected *in vivo* by Mi et al. in 2010.<sup>[535]</sup>

Aptamers have gained a lot interest in numerous cancer diagnostics and therapeutics over the past few years.<sup>[536]</sup> They have been represented as promising candidates of targeting ligands due to their incredible degree of versatility for binding to a wide variety of targets, such as proteins,<sup>[537]</sup> small molecules,<sup>[538]</sup> and carbohydrates.<sup>[539]</sup> Ease of isolation, low cost, simplicity of aptamers chemical derivation, faster and reproducible synthesis,<sup>[462,540]</sup> and high affinity comparable to antibodies are of some advantages offered by aptamers.<sup>[541]</sup> More importantly, aptamers have shown remarkable stability over wide range of pH ( $\approx 4\text{--}9$ ) and temperature, low immunogenicity,

and rapid diffusion through solid tumors due to their small sizes.<sup>[532a,542]</sup> Along with these possibilities, aptamers are suited to be conjugated on the surface of nanoparticles, enabling their active targeting. Aptamers can be found naturally in riboswitches.<sup>[543]</sup> However, when it comes to nanoparticles decorated with aptamers, they are artificially engineered.<sup>[462]</sup> In particular, aptamers can be synthesized to have a specific functional moiety, such as aldehyde, amino or carboxylate, at only one end of them.<sup>[529a]</sup> This will lead to formation of homogeneous mixtures by facilitating the conjugation process.<sup>[544]</sup> In particular, aptamers can be engineered to be effectively bound to iron oxide nanoparticles to ensure their targeting ability especially in imaging applications.<sup>[506b]</sup> Iron oxide magnetic nanoparticles can be decorated with aptamers by employing peptide bond between the carboxylic acid group on the surface of nanoparticles and amine group on the aptamers,<sup>[545]</sup> by modifying the surface with avidine for interaction with biotinylated aptamers.<sup>[546]</sup> In addition, aptamers can be modified to have longer blood circulation times<sup>[547]</sup> while they remain non-toxic.<sup>[548]</sup> Due to small size of aptamers compared to antibodies, aptamers can also bind enzymatic reactive sites and binding sites present on the nanoparticles surface which leads to forming compact structures.<sup>[549]</sup> An important benchmark is the internalization efficacy of ligand-decorated nanoparticles in active targeting. Xiao et al. have recently developed a cell-uptake strategy to discover efficient targeting ligands and exclude non-internalizing ligands.<sup>[550]</sup> Since the report of targeting the prostate-specific membrane antigen (PSMA) by aptamer-decorated nanoparticles in 2004,<sup>[551]</sup> a vast range of *in vivo* and *in vitro* researches have been conducted to prove the effectiveness of aptamers in targeted delivery of multiple types of drugs and imaging applications.<sup>[552]</sup> Dhar et al. synthesized nanoparticles decorated with aptamers having high affinity for PSMA to deliver cisplatin (a platinum-based chemotherapeutic) to prostate cancer cells. Their results demonstrated a drastic increase in therapeutic effectiveness of encapsulated Pt(IV) compared to free cisplatin.

Despite all the advantages offered by aptamers, nucleic acids are easily degraded by their biologically abundant nucleases which remain a concern for stability of ligands on nanoparticles surface in *in vivo* applications. To circumvent this problem, there have been attempts at replacement of the nuclease with other moieties.<sup>[553]</sup> The basic structural modifications to prevent nuclease degradation for improving pharmacokinetics have made reproducible synthesis of aptamers to be an expensive, lengthy process.<sup>[554]</sup> Additionally, the negative charge of aptamers due to their phosphodiester backbone is an obstacle to their deployment as targeting ligands by having direct effects on the blood circulation time and kinetics of the nanoparticles.<sup>[555]</sup>

#### 4.3.3. Peptides

Another class of targeting moieties is linear or cyclic sequences of amino acids, termed as peptides, with high specificity and affinity which have gained a lot of interest in active targeting of tumors as a compromise between large antibodies and small molecules. Peptides have numerous benefits due to their ease

of conjugation, high activity per mass unit, high stability and low cost allowing for long-term storage.<sup>[44,556]</sup> In particular, the physicochemical properties of the nanoparticles decorated with peptides are not likely to be changed due to small sizes of peptides (much smaller than antibodies).<sup>[557]</sup> Besides, simpler structures of peptide which is inherently originated from their shorter chains lead to more environmentally resistant molecules with improved stability.<sup>[462]</sup> In addition, low immunogenicity of peptides reduces the risk of undesirable effects and also allows for longer blood circulation time for *in vivo* applications.<sup>[558]</sup> Furthermore, functional groups can be introduced along with optimizing the biological activity of peptides by modifying their sequences for the preparation of peptide decorated nanoparticles.<sup>[484a]</sup> A phage display is typically used as a screening tool for discovering peptide ligands with high affinities for targets to be selected.<sup>[559]</sup> Through this cyclic selection process, desired peptide ligands, which range from 10–15 amino acids, with affinity for targets are collected and nonspecific binders are washed away. Specifically, peptide ligands for myriad of targets have been synthesized thanks to improved screening techniques and development of highly specific peptide phage libraries and plasmid peptide libraries.<sup>[556]</sup>

Integrins are mostly the targets of peptide decorated nanoparticles for performing their designated *in vivo* function. In fact, integrins act as receptors for molecules of the extracellular matrix (ECM) and also a signaling pathway for communication between the cell and the ECM.<sup>[498,560]</sup> Among the total 24 known integrins,  $\alpha_v\beta_3$  integrin has been mostly exploited as a target for diagnostic and therapeutic applications.  $\alpha_v\beta_3$  integrin receptor is expressed on angiogenic endothelial cells as well as at elevated levels on tumor cancer cell membranes to supply nutrients to the growing tumor.<sup>[561]</sup> A series of studies have demonstrated that peptides with RGD (arginine–glycine–aspartic acid) sequences have great binding affinity for  $\alpha v \beta 3$  integrin.<sup>[562]</sup> In fact, since  $\alpha_v\beta_3$  receptors are widely expressed and directly accessible, the need for nanoparticles to diffuse into the tumor interstitium is reduced.<sup>[563]</sup> Hence, a variety of nanoparticles such as polymeric, metallic, and dendrimers have been decorated with both cyclic and linear RGD peptides for targeted drug delivery and imaging applications in cancerous tissues.<sup>[564]</sup> In the case of SPION decorated with cyclic RGD peptides, strong specific uptakes into tumors have been shown compared to undecorated SPIONs.<sup>[565]</sup> Although RGD peptides offer some advantages, nonspecific adhesion is still a remaining challenge since  $\alpha_v\beta_3$  integrin receptors are also expressed on normal tissue and non-cancerous inflamed tissues.<sup>[477]</sup>

#### 4.3.4. Small Molecules

Small molecules are of other attractive targeting ligands conjugated to nanoparticles for active targeting in therapeutic and diagnostic applications, especially due to their low immunogenicity. Small molecules are technically advantageous in terms of having small size which offers higher ligand densities on the surface of nanoparticles, stability, and ease of handling by being less degradable compared to biomolecular ligands, along with a range of facile coupling chemistries being available for their conjugation and low cost reproducible synthesis.<sup>[477,566]</sup> Also,

thanks to advances in diversity-oriented synthesis, small molecules with functional groups have been available for a wide range of targeting ligands.<sup>[567]</sup> However, the main challenge is that there is no systematic approach for developing small molecule ligands.<sup>[529a]</sup> In fact, since there is a relative lack of utilities for appropriate multiplex screening of small molecules, high throughput screening procedures and serendipity are both noticeable to identify new small molecular weight ligands.<sup>[462]</sup> As a result, most of the small molecule ligands used to decorate nanoparticles for active targeting rely on the ones widely known hitherto.

FA, vitamin B9 has been used extensively as a biologically active small molecule ligand, especially for targeted drug delivery applications.<sup>[568]</sup> Specifically, FA binds to the glycosylphosphatidylinositol-like folate receptor with high affinity ( $K_D \approx 10^{-9}$  M), which is frequently up-regulated and overexpressed at surface of many human cancer cells.<sup>[484a]</sup> In fact, a series of reports have demonstrated the active internalizations of nanoparticles decorated with FA via receptor-mediated endocytosis and their subsequent effective direction to folate receptor cancer cells.<sup>[569]</sup> Hence, numerous delivery vehicles such as liposomes, dendrimers to metal oxide and polymeric NPs have been designed and reached cancer cells to deliver therapeutics and imaging modalities linked to them with no harm to normal cells.<sup>[570]</sup> The inherent limitation toward *in vivo* application of FA decorated nanoparticles is that folate receptors are constitutively expressed in normal tissues and epithelia of many organs.<sup>[462]</sup> Hence, in order to make sure that the “stealth” ability of nanoparticles is not lost, optimal FA density should be taken into full consideration to avoid their rapid sequestration by MPS.<sup>[571]</sup> Additionally, a careful consideration is needed to maximize the binding quality on nanoparticles due to hydrophobic nature of FA ligands.<sup>[572]</sup>

Other vitamins such as biotin (vitamin H), which is a cell growth promoter,<sup>[573]</sup> have been also conjugated on silica, liposome, iron oxides, and polymer based nanoparticles with avidin (strept) functionalities on their surfaces for targeting cancers, oral delivery of insulin and *in vitro* applications.<sup>[574]</sup> However, clinical applications of biotins are somehow limited due to their bacterial origin and consequent immunogenicity.<sup>[529a]</sup> Cobalamin (vitamin B12) has also been used to coat nanoparticles to overcome subcutaneous administration drawbacks for an effective delivery of insulin and protein drugs by the oral route.<sup>[575]</sup>

Other examples of small molecule as targeting ligands are selectin,<sup>[576]</sup> selegiline,<sup>[577]</sup> curcumin,<sup>[578]</sup> triphenylphosphonium (TPP),<sup>[579]</sup> and benzamides (anisamide, in particular).<sup>[580]</sup> But more importantly, carbohydrates have gained more interests for their low molecular weight, inexpensive manufacturing, and efficient modification and characterization by well-known sugar chemistries to serve as nanoparticle small molecule targeting ligands. Lectin receptors, especially asialoglycoprotein receptors (ASGPR),<sup>[581]</sup> which are expressed on the cellular membrane of a number of cells have been the main targets of nanoparticles decorated with carbohydrate moieties such as galactose,<sup>[582]</sup> mannose,<sup>[583]</sup> and glucose.<sup>[584]</sup> A drawback of this targeting method is that multiple interacting carbohydrates are needed to achieve strong bindings with targets.<sup>[529a]</sup> Overall, although it is convenient to employ small molecules as biologically targeting

ligands, they suffer nonspecific interactions, especially in the case of folic acid.<sup>[585]</sup>

#### 4.3.5. Proteins

Compared to antibodies and peptides, some studies have also exploited proteins affinity to actively bind to their endogenous targets, including cell membranes, via receptor-mediated endocytosis.<sup>[586]</sup> However, the bulky nature of protein ligands leads to increase sizes of nanoparticles which may trigger immune responses to be taken up by RES. One of the most abundantly studied protein ligands is the iron transport protein, termed as transferrin (Tf), which has a high affinity for Tf receptors (TfR, also known as CD71) as potential diagnostic targets by enabling endocytosis and internalization into the cellular cytoplasm.<sup>[587]</sup> In fact TfR is a glycoprotein in charge of mediating the uptake of the iron concentration in biological environments.<sup>[498,588]</sup> Since TfR are overexpressed both on the endothelial cells of the blood–brain barriers and in solid tumors, it has been extensively used to decorate nanoparticles for achieving brain delivery and actively targeting cancerous tissues.<sup>[589]</sup> Specifically, TfR over-expression on cancer cells stems from the increasing need of the growing tumor for iron to continue its proliferation.<sup>[587b,590]</sup> Exploiting the high affinity of Tf ligands, numerous chemotherapeutics, including cisplatin, doxorubicin, gemcitabine, mitomycin, and siRNA nanocomplexes have been delivered to their targets either by being encapsulated in nanoparticle vehicles or directly conjugated to Tf ligands.<sup>[591]</sup> Additionally, given the short time of Tf internalization cycle, high turnover rates of Tf molecules per cell per minute is yielded, that comes in handy for stronger MRI signal in the case of internalizing superparamagnetic iron oxide nanoparticles.<sup>[498]</sup>

#### 4.4. Toxicity Concerns of MNPs

In spite of all the valuable biological applications offered by MNPs along with increasing development in fabrication of well-shaped monodisperse magnetic cores, a clear understanding of toxicological profiles of these engineered nanomaterials is necessary to prevent the onset of unexpected adverse health effects.<sup>[592]</sup> Due to direct contact of MNPs with different tissues and organs, the gap between the fast increasing data on production of engineered nanomaterials and that of scarce toxicity data has to be filled in order to understand and overcome the prohibiting prospects of a safe design of nanoparticles. To this end, appropriate animal models have been used to evaluate the toxicity of magnetic cores. Evaluation of toxicity profile of administered nanomaterials is carried out by considering how they interact with the body during the lifetime of performing their designated *in vivo* function and also how they affect the body during biodegradation and liver processing.<sup>[593]</sup> Since MNPs are typically excreted from the body as a construct, it is necessary to use components that can individually be biodegraded by the body. Studies have shown that among all the magnetic materials such as pure metals, bimetallic or magnetic alloys and metal oxides, iron oxide nanoparticles are highly biocompatible nanomaterials with none or low toxicity which do not pose

serious threat to the organism.<sup>[594]</sup> Iron oxide nanoparticles are biodegradable and can be cleared from the body through kidneys or be used for production of red blood cells after they are metabolized in the liver. However, free iron is toxic<sup>[595]</sup> and it is expected to be metabolized and regulated by normal physiological iron homeostatic mechanisms. Iron oxide nanoparticles demonstrate acceptable safety profile and non-cytotoxicity in concentrations  $<100 \mu\text{g mL}^{-1}$ .<sup>[596]</sup> However, some studies indicated that iron oxide nanoparticles demonstrate a slight level of cytotoxicity at doses  $>100 \mu\text{g mL}^{-1}$ <sup>[597]</sup> and produce mild and transient side effects. Note that any aggregated NPs, regardless of material composition, will be toxic to cells and tissues.<sup>[598]</sup> In particular, when iron oxide nanoparticles are magnetically targeted to a tissue/organ to provide their maximum benefit of a diagnostic or therapeutic application, high concentrations in a localized area occurs. Consequently, this iron overload may lead to adverse biological effects such as inflammation, the formation of apoptotic bodies, impaired mitochondrial function (MTT), membrane leakage of lactate dehydrogenase (LDH assay), generation of ROS, increase in micronuclei (indicators of gross chromosomal damage; a measure of genotoxicity), and chromosome condensation.<sup>[599]</sup>

### 5. MNPs as Theranostic Agents in Treating Diseases

Diagnosing disease at its earliest stages, even prior to disease manifestation, and its brisk treatment are of two most important factors within an effective medical procedure, especially for treating cancers. Development of separate approaches in diagnosing and treating of the same target can somewhat miss the mark of practicality. Combination of sensitive and accurate diagnosis with a possibly better efficacy of the treatment on a single nanoscale platform has emerged as a promising technique in biomedical applications and has attracted much attention in the community for adding another piece to mosaic of personalized medicine.<sup>[600]</sup> Exigencies of an accurate diagnosis and better efficacy of the treatment have devoted tremendous efforts in biomedical researches to construct magnetic nanoparticle-based theranostic agents.

These potential magnetic nanotheranostics embrace the aspect of simultaneous diagnosis and treating for real-time tracking which address the shortcomings of conventional techniques.<sup>[601]</sup> Nanotheranostics provide an integrated design capability for imaging, cell targeting, and therapy by using MNPs as their building blocks which render them as ideal MR imaging probes by showing high magnetization in an external magnetic field to locate and report cancerous lesions on one hand, and being appropriate therapeutic cargos with a set of well-developed surface chemistry to deliver therapeutics preferentially to those lesions on the other hand (**Figure 33**).<sup>[602]</sup> Surprisingly, modifications to treatment can be provided by converging imaging, treatment and the data about the evolving course of an illness on this new nanotheranostic trend. To do so, MNPs are engineered as intelligent cargos with large surface to volume ratio which can easily accommodate multiple functionalities to create a library of novel, personalized therapeutics and imaging moieties.

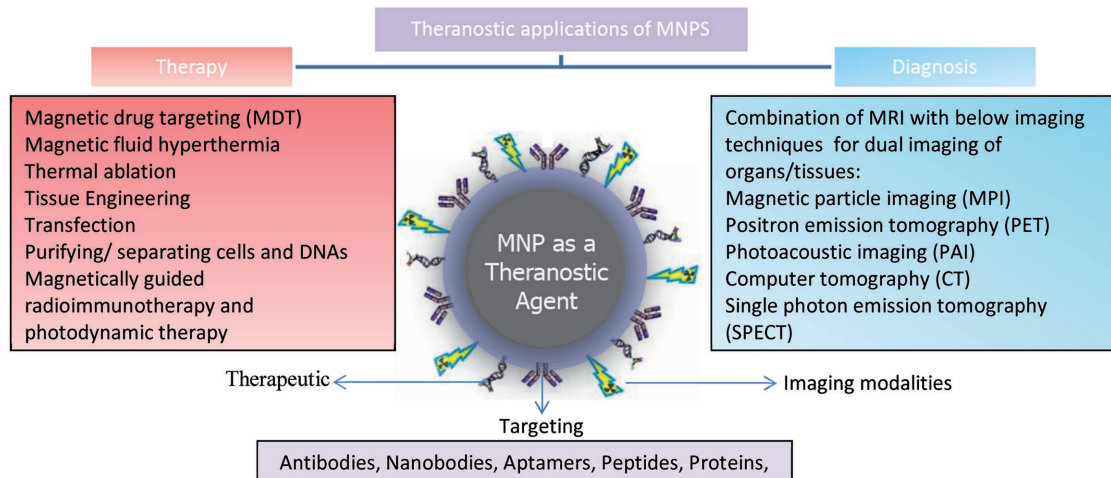


**Figure 33.** Theranostic applications of MNPs. Targeting ligands can also be conjugated for enable active targeting.

## 5.1. Therapeutic Applications of MNPs

### 5.1.1. Magnetic Drug Targeting

In most of the chemotherapeutic approaches, intravenous administration of therapeutic drugs and their subsequent non-specific distribution make drugs unable to accumulate at affected areas in the body.<sup>[17a,304]</sup> This leads to a general systemic distribution of them where normal, healthy cells as well as cancer cells are indiscriminately attacked, exerting a plethora of side effects such as bone marrow depression, inflammation of the lining of the digestive tract (mucositis), reduced immunity, and hair loss (alopecia).<sup>[603]</sup> On the other hand, rapid metabolism and excretion of some drugs cease their effective journey toward the affected areas. Thus, a critical concern is to enhance the effectiveness of drug delivery by increasing the drug concentration and lowering the doses of cytotoxic compounds to ensure that substantial amount of them has reached and accrued at the exact desired area for performing their pharmacological action.<sup>[604]</sup>

In this regard, nanotechnology and drug delivery have merged into so-called “magic bullets,” proposed firstly by Paul Ehrlich, to eliminate these substantial shortcomings by overcoming biological barriers and selectively reaching the cancerous tissues for on-demand release of their cargos in the optimal dosage range.<sup>[345]</sup> These novel drug delivery platforms offer attractive features to significantly improve the pharmacokinetics of conventional drugs by: (1) protecting drugs against harsh environments to increase the half-life of drugs, (2) providing specific targeting to spare healthy cells, (3) capability to ferry multiple types of anticancer drugs as well as imaging modalities, (4) and offering precise control over the drug release thanks to stimuli-responsive coating and material designs.<sup>[605]</sup>

In one special case, there has been an increasing interest in loading the therapeutics on MNPs for magnetic drug targeting (MDT) which provides external means of guiding drug particles within the body.<sup>[11b,606]</sup> Magnetic polarization and magnetophoretic mobility under an external magnetic field (EMF)

along with field gradient form the bases of MDT application. The intrinsic magnetic properties of MNPs and their response to an applied magnetic field render them trackable to literally drag drug molecules to their target (Figure 34). Specifically, significant accumulation of loaded MNPs at the target site is ensured through applying an EMF to create a suitable magnetic field gradient. Hence, drugs will be remaining ultimately localized upon their injection, resulting in a more efficient capture and extravasation into the tumor cells.<sup>[604a]</sup> Tracking particle fate for favoring the cell internalization and allowing a magnetically guided accumulation in tumor tissues are of important advantages of these devices.<sup>[607]</sup> Combined with possibilities offered by EPR effect in passive targeting and high affinities of active targeting, a wide range of therapeutics including biotherapeutics (such as gene, siRNA, peptides, and proteins),<sup>[608]</sup> chemotherapeutics (such as doxorubicin, paclitaxel, and methotrexate)<sup>[609]</sup> and radiotherapeutics<sup>[610]</sup> have been integrated into MNPs to be specifically delivered into their target sites.

SPIONs have been widely used as ideal MNPs because they do not retain any remnant magnetization upon removal of the magnetizing field.<sup>[612]</sup> This property is advantageous in case of reducing the chance of agglomeration to escape the MPS on one hand, and pose no danger of thrombosis or blockage of blood capillaries on the other hand.<sup>[603a,613]</sup> The initial principles for fusion of magnetism and drug delivery can be traced back to the 1960s. It was in 1960 that Freeman et al. introduced the concept of transport of magnetic particles through the vascular system and their increased concentration by means the EMF.<sup>[614]</sup> Senyei et al. discussed also the physical laws underlying the intravascular magnetic guidance of  $\text{Fe}_3\text{O}_4$  microspheres consisting of an albumin matrix and Adriamycin HCl as the prototype drugs. They showed the retention of the microspheres in the area of applied magnetic field by using an in vitro analog of the human circulatory system.<sup>[615]</sup> Since then, a lot of efforts were devoted in this area to improve MDT by designing various magnetic particles with minimized early clearance and more specific targeting to reduce the total dose required by increasing the concentration of drugs in blood vessels, especially in treating cancers.<sup>[603a]</sup> In 1970s,

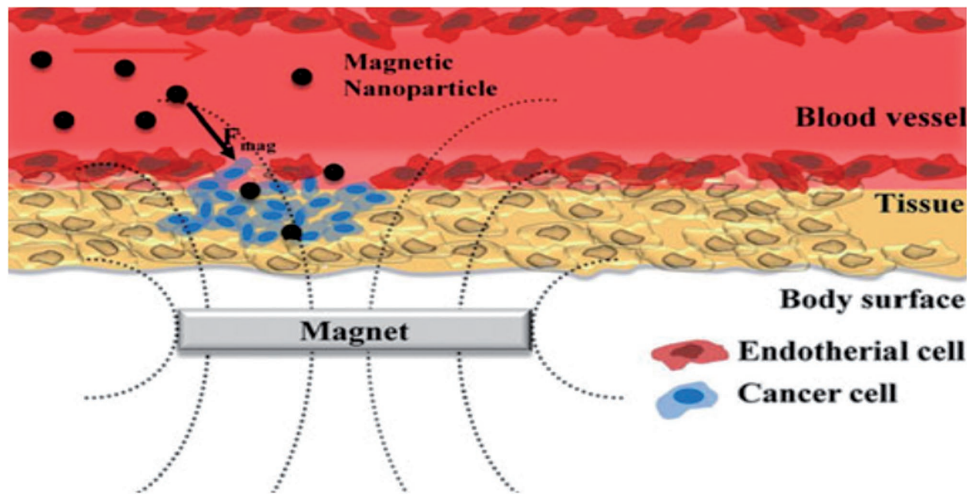


**Figure 34.** Schematic representation of magnetic drug delivery system under the influence of external magnetic field. Reproduced with permission.<sup>[611]</sup> Copyright 2010, Elsevier.

Zimmermann et al. delivered cytotoxic drugs by using magnetic erythrocytes.<sup>[616]</sup> Three years later, Widder et al. reported the delivery of doxorubicin anticancer drugs encapsulated within magnetic albumin microspheres.<sup>[617]</sup> In addition, MDT strategy was developed by several authors in the 1980s to use magnetic microspheres and microcapsules to deliver different drugs.<sup>[618]</sup> There were significant growths in the 1990s when 90Y beta-emitter radiotherapeutics were loaded on poly(lactic acid) coated magnetite microspheres and applied to subcutaneous tumors.<sup>[619]</sup> In addition, Lubbe et al. performed the first clinical trial wherein epirubicine was chemically bounded to magnetic particles coated by starch polymers to be magnetically targeted in human patients.<sup>[620]</sup> A magnetic field strength of 0.8 was provided in tumors located near the body surface by using properly arranged permanent magnets to concentrate the resulting ferrofluid in the target regions.<sup>[621]</sup>

In addition to all these developments, exploiting the stimuli-responsive systems allows for tailored release profiles with excellent spatial, temporal, and dosage control (Figure 35). Specifically, by recognizing their microenvironment, they enable on-demand processes (also termed as “switch on/off”) and react in a dynamic way, which in turn mimic the responsiveness of living organisms.<sup>[622]</sup> It was in the late 1970s that Yatin et al. suggested the concepts of stimuli responsive drug delivery by employing thermosensitive polymers and hyperthermia for the local release of drugs.<sup>[623]</sup> Broadly speaking, temperature changes, light, ultrasound, electric fields, and magnetic fields are of exogenous stimuli exploited for triggering drug release.<sup>[624]</sup> On the other hand, endogenous stimuli-responsive drug delivery systems take advantage of variations in pH, redox potential, or the concentrations of enzymes or specific analytes.<sup>[625]</sup>

Generally, magnetoliposomes,<sup>[626]</sup> core–shell MNPs<sup>[627]</sup> and porous metallic nanoparticles<sup>[628]</sup> are of practical candidates suitable for performing MDT through focusing an extracorporeal magnetic field. Depending on the nature of magnetic response taken by MNPs (whether to be a magnetic guidance or increase in temperature) both magnetically and thermoresponsive modules can be designed for triggering the drug

release. Interestingly, drug delivery can be triggered by using a permanent magnetic field. In this manner, ferrogels consisting of MNPs embedded in polymers gels account for an essential category of stimuli-sensitive hydrogels which are responsive to externally applied magnetic fields.<sup>[629]</sup> Their distinctive magnetoelastic property that makes the ferrogels to be endowed with great magnetically controlled drug-releasing modules has recently gained an extensive attention.<sup>[630]</sup> However, since ferrogels have an intrinsically hydrophilic nature, most of these studies are focused only on water-soluble drug. In this matter, a pioneering study performed by Qin et al.<sup>[631]</sup> addressed the problem of effective incorporation of important hydrophobic drugs in ferrogels by employing Pluronic-F127 micelles encapsulating SPIONs. In fact, in addition to proper biocompatibility, high stability, and low toxicity features,<sup>[632]</sup> Pluronic copolymers could associate into micelles via hydrophobic interactions above a certain critical concentration and temperature. Upon applying

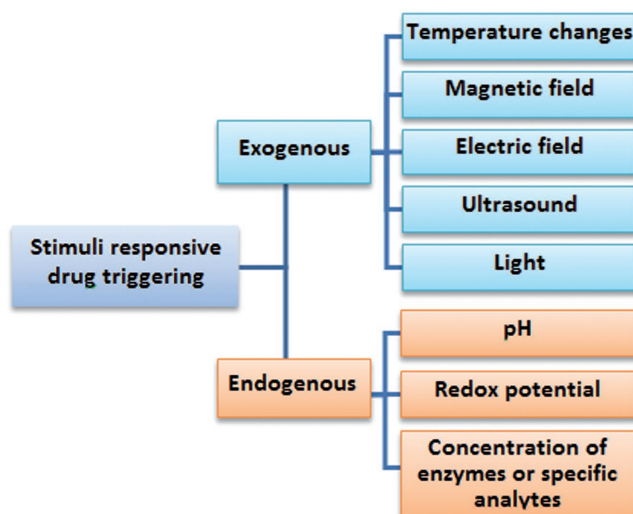


**Figure 35.** Exogenous and endogenous stimuli responsive strategies for triggering drug release.

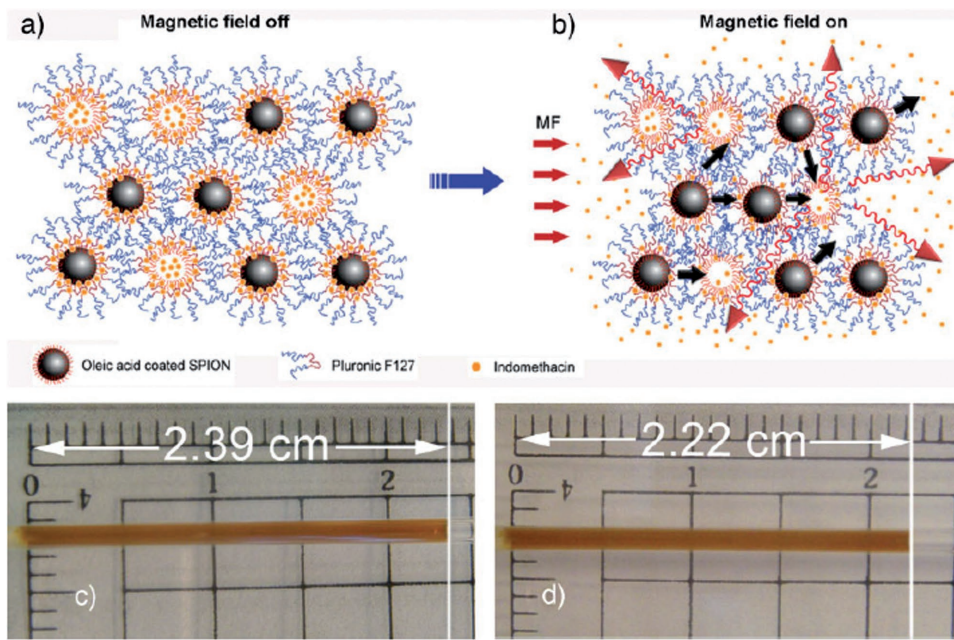


**Figure 36.** Schematic representation of ordered microstructure of superparamagnetic iron oxide nanoparticles and Pluronic F127 copolymers: a) before applying the magnetic field, indomethacin drug molecules are encapsulated in the hydrophobic moiety of micelles; b) upon applying the magnetic field drug releasing is enhanced due to orientation of MNPs and squeezing the micelle. Corresponding photographs of the ferrogel in a capillary c) before and d) after applying a magnetic field. Reproduced with permission.<sup>[631]</sup>

a magnetic field, SPIONs orient and approach each other which squeeze the micelles and lead to the release of drugs (**Figure 36**). In another study, a syringe-like system designed by Cai et al. enabled actively controlled reversible pulsatile release of drugs out of a biodegradable polymeric reservoir. They employed MNPs as switching carriers in a multireservoir device made of poly(D,L-lactic acid) (PDLLA) as the biodegradable substrate for the main body of device, and biodegradable porous polycarbonate as the sealing membrane, which allowed for the complete release of drugs before the device degraded.<sup>[633]</sup>

In the matter of delivering nucleic acids, including siRNA and genes, MNPs have been shown promising for a practical magnetofection through exploiting nanoassemblies integrated with cationic coatings to nucleic acids.<sup>[634]</sup> This approach has especially enhanced the efficiency of siRNA transfection under a permanent magnet in both in vitro and/or in vivo experiments against breast<sup>[635]</sup> and prostate<sup>[636]</sup> cancers. In addition, utilizing MNPs coated with PET has shown a great potential for complexation of plasmid DNA on the surface of nanoparticles for delivering DNA vaccine.<sup>[637]</sup> In an alternative strategy, Tang et al. utilized bacterial magnetic particles (magnetosomes) as a carrier of DNA vaccine for tumor immunotherapy.<sup>[638]</sup> Moreover, MNPs have been employed for delivering antioxidant enzymes to increase resistance to oxidative stress.<sup>[639]</sup>

In contrast to permanent magnets which take advantage of the guidance response taken by MNPs, an oscillating or alternating magnetic field provides a novel on-off fashion for triggering drug release. In fact, by employing thermo-responsive polymers<sup>[640]</sup> and lipids<sup>[641]</sup> onto the surface of MNPs and exploiting the hyperthermia effect the energy transformed into heat through Brownian fluctuations and Neel fluctuations can lead to promising magnetic responsive drug delivery

systems.<sup>[642]</sup> Two main approaches can be postulated for applying hyperthermia-based drug release (**Figure 37**). In the first approach, a thermo-responsive linker is used to attach drug to MNPs. An AMF trigger releasing of drug due to heating of the linker molecule attached to the surface of MNPs, termed as drug delivery through bond breaking (DBB) (**Figure 37a**).<sup>[643]</sup> The second approach takes advantage of AMF and EMF to trigger releasing drugs encapsulated in polymeric matrices (**Figure 37b**).<sup>[644]</sup>

Katagiri et al. prepared magnetoresponsive hybrid liposomes, embedded with thermosensitive polymers and hydrophobized  $\text{Fe}_3\text{O}_4$  nanoparticles.<sup>[640]</sup> MNPs which were synthesized via a hydrothermal process were incorporated into a liposomal micelle using hydrophobic interactions. The release of heat by exerting an AMF induced the transition of the thermosensitive segment of the copolymer for releasing drug (**Figure 38**). They showed a proper control over the release rate of hybrid liposomes through varying the amount of MNPs embedded into the liposomal membrane. In addition, their results showed that varying the design of polymer plays an important role in tuning the magnetoresponsive release rate.

In another study, novel thermosensitive magnetic liposomes containing doxorubicin were equipped with folic acid to combine MDT and hyperthermia effects within a thermo-chemotherapy of cancer. The high sensitivity of liposome to temperature increase, as well as high responsiveness to the localized AC magnetic field led to a simultaneous folate receptor-mediated uptake into tumor cells along with inducing hyperthermia.<sup>[645]</sup> In a very recent study, Al-Jamal et al.<sup>[646]</sup> utilized long-circulating polymeric magnetic nanocarriers, encapsulating increasing amounts of SPIONs in a biocompatible oil carrier, to study the effects of SPION loading and of applied magnetic field strength

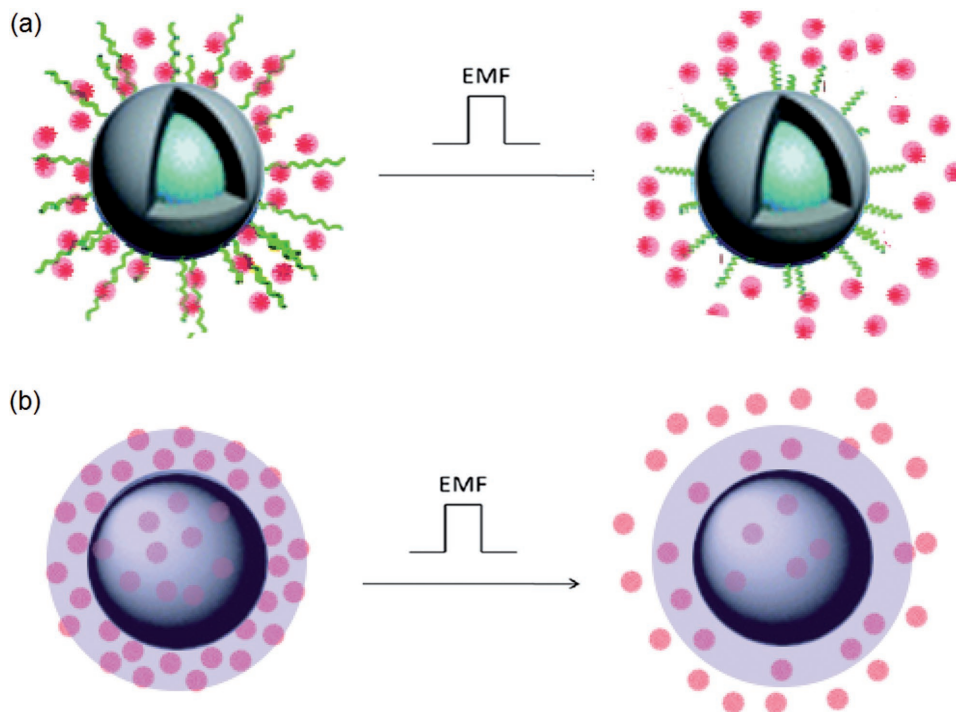


**Figure 37.** Schematic representation of triggering the drug release which are: a) attached to the linker molecules, b) encapsulated in a polymeric matrix.

on magnetic tumor targeting in CT26 tumor-bearing mice (Figures 39a,b). It was shown that uptake in tumors exposed to magnetic field (TU+) is significantly higher compared to that of unexposed (TU-) (Figure 39c). Magnetic targeting was found to offer enhanced therapeutic efficacy (Figure 39d) and improve mice survival compared to passive targeting at drug doses of ca. 5–8 mg of DTX kg<sup>-1</sup>.

Selective controlling of interparticle interactions with the adsorbed molecules can be made due to the small pore size

of silica. In drug delivery systems where silica coated MNPs are used, the drug release rate is slow and can be controlled by tailoring the thickness of the coating as a function of the drug characteristics, which is an advantage compared with polymer-coated MNPs that a faster drug release often take place. Novel drug delivery systems have been synthesized based on mesoporous stimuli responsive silica coatings.<sup>[647]</sup> In this case, therapeutic cargos are capable of releasing their payloads due to the presence of organic or inorganic moieties

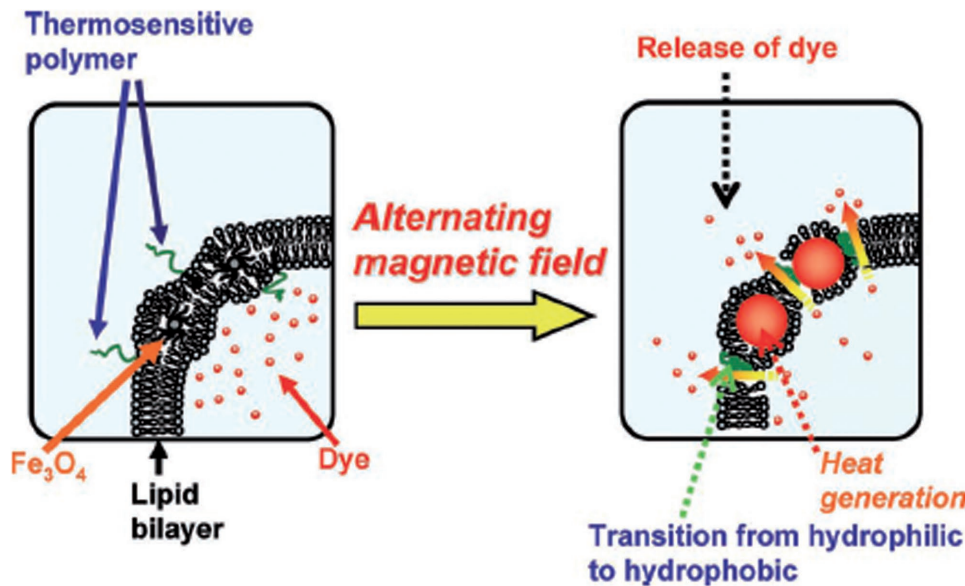


**Figure 38.** Schematic representation of the release mechanism of hybrid liposomes upon alternating magnetic field irradiation. Reproduced with permission.<sup>[640]</sup>

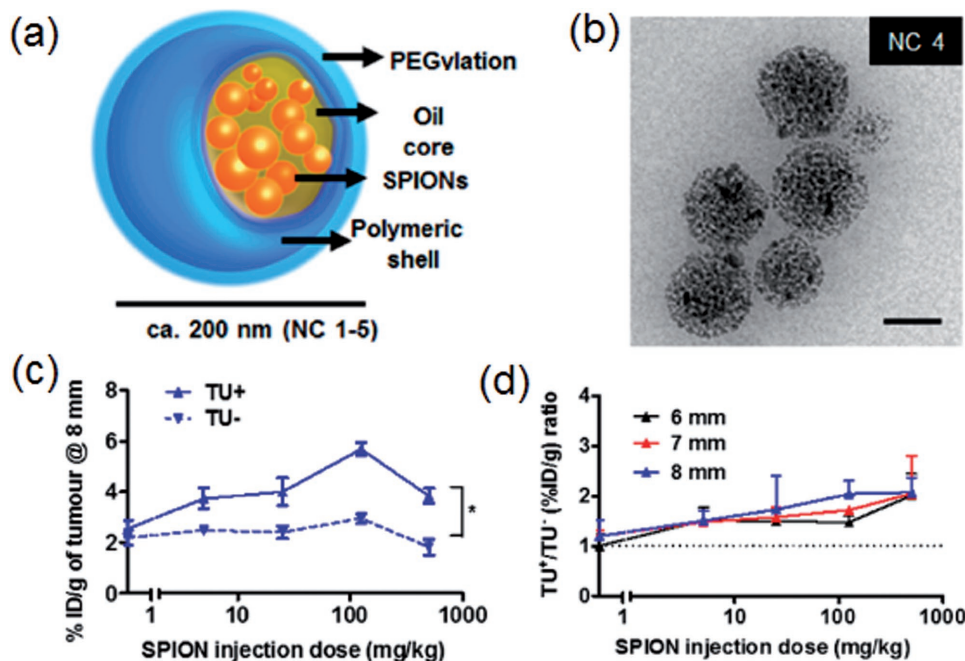


**Figure 39.** a) Schematic illustration of magnetic nanocarriers, comprising a core–shell structure. b) Cryo-TEM image of magnetic nanocarriers. c) Tumor accumulation profiles. d) Magnetic targeting efficacy at different magnet field strengths (dimensions of 8, 7, and 6 diameter). Reproduced with permission.<sup>[646]</sup> Copyright 2016, ACS.

that are responsive to a certain stimuli.<sup>[648]</sup> Special gate keepers such as coumarin molecules,<sup>[649]</sup> azobenzene molecules,<sup>[650]</sup> thymine,<sup>[651]</sup> and polymers<sup>[652]</sup> which are responsive to light source as well as grafting of thermosensitive polymers based on poly-N-isopropylacrylamide (PNIPAM) and its derivatives<sup>[652,653]</sup> have been exploited for a very precise control release of therapeutics in mesoporous silica coated nanoparticles. In a very recent study, Saint-Cricq et al.<sup>[652]</sup> reported design of thermostimuli responsive polymeric cap for magnetic core–shell Fe<sub>3</sub>O<sub>4</sub>@SiO<sub>2</sub> mesoporous nanoparticles by incorporating azo bonds into the backbone of poly(ethylene glycol) (azo-PEG) for a controlled drug release (Figure 40). Since azo-PEG responds to temperature, the drug release was triggered by applying an external magnetic field to produce heat locally with a nonscopic volume. They reported that this approach exhibits no cytotoxicity toward fibroblasts, demonstrating its safety.

Overall, although MDT has been shown promising they suffer from some inherent drawbacks. In the first place, such a strategy is limited to accessible tumor nodules, but not metastasis or disseminated tumors. Another issue is related to the complexity in an EMF set-up. In fact, to ensure the practicality of this approach, the EMF should be adequately focused and needs to be deeply penetrated into the tissues to reach the diseased area with sufficient strength.<sup>[654]</sup> Furthermore, upon being exposed to the heat generated by an AMF, nanocarriers are prone to structural alternation such as deformation of the single-crystal nanoshell lattice,<sup>[655]</sup> disintegration of the core,<sup>[656]</sup> or increase in the porosity of shell.<sup>[657]</sup>

**5.1.1.1. Strategies in Applying Magnetic Field for MDT:** A prerequisite aspect for a good operation of magnetophoretic devices is to generate a strong and localized magnetic field gradient at

different length scales, ranging from a few hundred micrometers to a few centimeters, at the target location in the body.<sup>[658]</sup> In MDT applications, magnetic particles experience a very large hydrodynamic drag in the arteries that has to be overcome for a guided biotransport and aggregation in arterial systems by means of a strong enough magnetic field.<sup>[659]</sup> Generally, external fields including permanent magnets and electromagnets are used for MDT of targets close to the body's surface (Figure 41). However, due to rapid fall off in the magnetic field strength, magnetizable inserts are used as alternatives for MDT of tissues deeper within the body.<sup>[660]</sup>

**5.1.1.2. Permanent Magnets:** Permanent magnets are ferromagnetic materials which retain their magnetization in the absence of magnetic field. These permanent magnets are cheap, widely available, and easy to operate. They are able to generate strong magnetic fields and gradients in a well localized area for a desired volume of material<sup>[661]</sup> and need no auxiliary power supply.<sup>[662]</sup> However, due to the difficulty in mapping the magnetic field distribution around permanent magnet, it is difficult to predict the respond of magnetic particles in the blood stream to these magnets.<sup>[663]</sup> On the other hand, although permanent magnets have large magnetic fields, they produce small gradients and the rapid drops in magnetic field of permanent magnets in space, makes them not strong enough to manipulate particles deep within the body.<sup>[663]</sup> Furthermore, the field of a permanent magnet is more coherent immediately adjacent to the magnet surface which causes them not to be promising for steering particles far from the surface farther from the source.<sup>[664]</sup> And also, due to the constant and not adjustable value of the desired magnetic field and force under different circumstances, one can't change their location to fit carrying

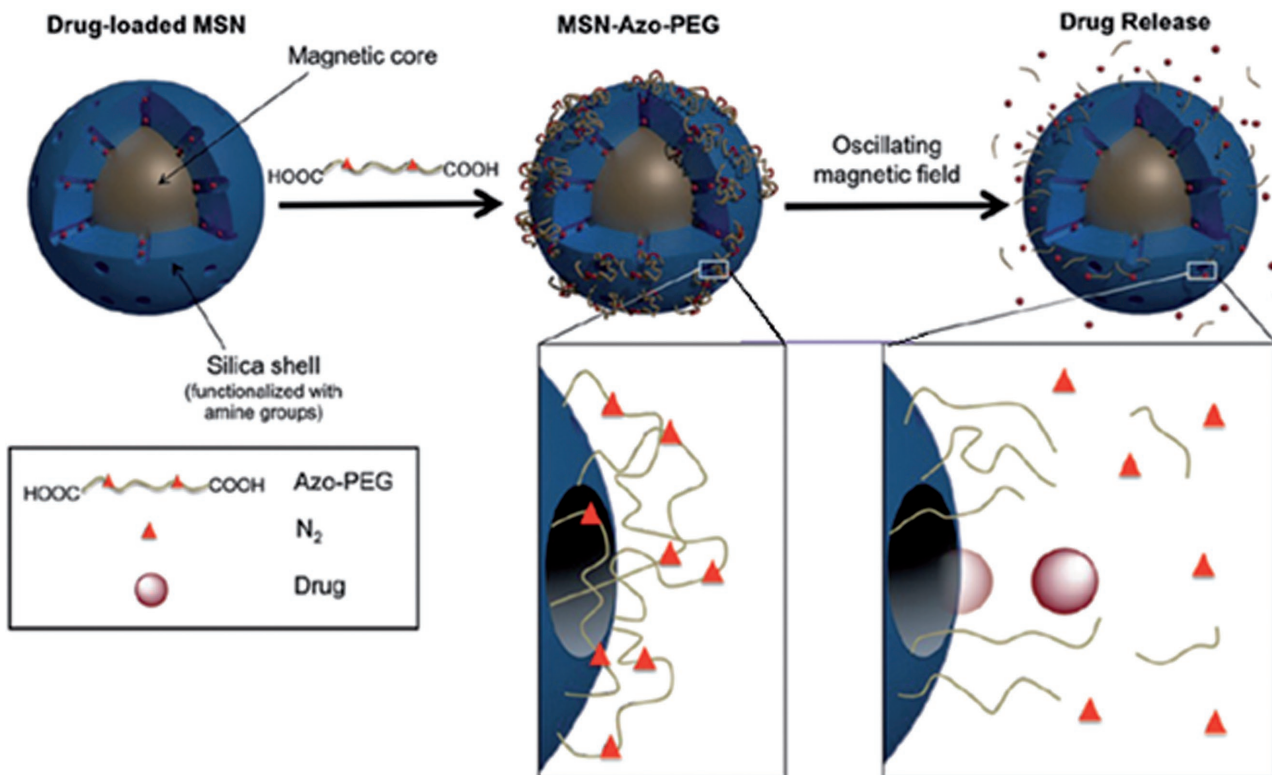


**Figure 40.** Surface modification of amino-modified  $\text{Fe}_3\text{O}_4@\text{SiO}_2$  nanoparticles (MSN) with azo-PEG (MSN-az-PEG), and Drug release after magnetic heating. Reproduced with permission.<sup>[652]</sup>

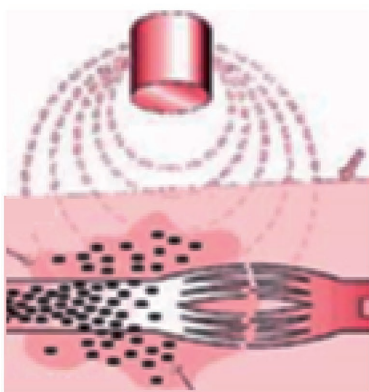
tumor shapes and sizes. Thus, careful design is required to produce the desired magnetic field geometry. In addition, proper orientation of the magnetic field is necessary in order to direct the particles.<sup>[663]</sup>

**5.1.1.3. Electromagnetic Fields:** Electromagnets are able to generate strong magnetic fields farther from the source, i.e., a loop of current-carrying wire generates its most uniform, clinging field along its central axis, which provides a promising particle steering far from the source. They provide an easy change in the location and current for fitting different tumor shapes and sizes.<sup>[664,665]</sup> A dynamic control of magnetic field strength and orientation enable a magnetic manipulator operating on an alternating magnetic field which is useful to target and guide the magnetic particles.<sup>[666]</sup> Electromagnets can produce good magnetic fields, stronger than permanent magnets, but they typically require liquid cooling to produce such fields. Superconducting magnets such as in MRI can produce fields that far exceed those achievable by permanent magnets. However, such magnets are much more complex and costly.<sup>[667]</sup>

**5.1.1.4. Implant Assisted Magnetic Drug Targeting (IA-MDT):** Although MDT is new to the realm of targeted drug delivery,<sup>[668]</sup> the current approach of using permanent magnets and electromagnetic fields in studies is faced by some fundamental issues which hamper the development of MDT past the exploratory stage<sup>[669]</sup> and makes the wide spread acceptance of the technique to be still looming.<sup>[668,670]</sup> One problem is associated with the considerable hydrodynamic force generated by high blood

velocities in the vascular system<sup>[668]</sup> which is the only significant force that should be overcome to prevent adverse hydrodynamic conditions on accumulation of MNPs at the target zone.<sup>[671]</sup> Even in the most favorable situation that the magnetic source is located close to the target zone, which is rarely the case,<sup>[621]</sup> the drag force exerted on the particles by the blood flow may dominate the magnetic force.<sup>[672]</sup> Another important problem is the inherent tendency of magnetic fields to be homogeneous over the target zone, which results in very small magnetic field gradients that makes it difficult to collect appreciable amounts of drugs in that region.<sup>[673]</sup> Typically, the magnetic force exerted on MNPs depends on both magnitude and gradient of the field.<sup>[660b,674]</sup> With the maximal magnetic flux density at the magnet pole face and its short ranged magnetic force, inherently weak forces can be focused at a distance from the magnet.<sup>[675]</sup> As the field intensity decreases abruptly with distance, for targets that are more than a few centimeters deep in the body, the hydrodynamic force of blood flow overwhelms the magnetic force.<sup>[671]</sup> Thus, retention of the magnetic drug carrier particle (MDCPs) becomes quite low to the inherently weak nature of magnetic field,<sup>[7,14]</sup> which in turn, limits the location of this site to be less than a few centimeters deep inside the body.<sup>[660b]</sup> These obstacles in the way of performing external magnetic fields for MDT limit its application to superficial tumors and locations in the body that are very near to the surface of the skin wherein both strong magnetic field and field gradients as well as very low-velocity fields of blood flow are present.

An alternative strategy to circumvent the limitations of traditional MDT is introduced to literature based on high gradient

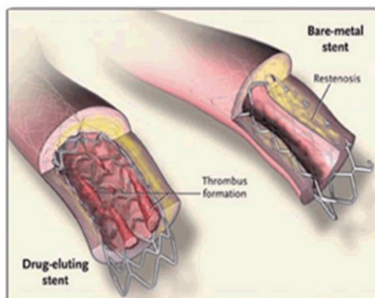
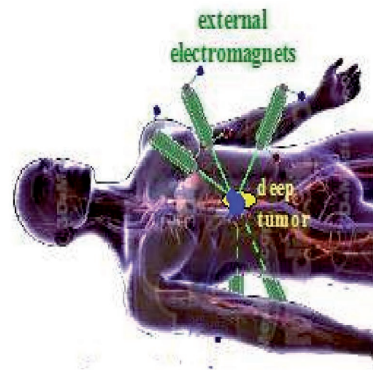


### permanent magnets

- **advantages:** 1. cheap 2. widely available 3. strong magnetic generation for desired volume of material 4. need no auxiliary power supply 5. ease of operation
- **disadvantages :** 1. difficulty in mapping the magnetic field distribution and predicting the MNPs respond 2.having small gradients 3. Not usable for manipulation particle deep in the body 4. Poor particle steering far from the source 5.Constant value of magnetic field

### electromagnetic fields

- **advantages:** 1.strong magnetic field farther from the source. 2. dynamic control of magnetic field strength and orientation due to ease of change in location and current. 3. Good magnetic manipulator operation
- **disadvantages:** 1. Need of prohibitive level of current in generation of strong fields 2.Need of liquid cooling 3.expensive fabrication 4.Complex operation



### Magnetizable inserts

- **advantages:** 1. Ease of strong magnetic field generation by applying weak external magnetic field 2. Localized magnetic field to attract MDCPs. 3. Better and more intense internal magnetic field
- **disadvantages:** 1.risk of surgery 2. Costly

Figure 41. Different strategies in apply magnetic field for magnetic drug targeting.

magnetic separation (HGMS) concept.<sup>[676]</sup> Based on this concept, a wide range of theoretical,<sup>[677]</sup> experimental in vitro<sup>[678]</sup> and ex vivo<sup>[679]</sup> studies have shown that a relatively external magnetic field applied on a ferromagnetic material is capable to create a strong localized magnetic field deep within the body.<sup>[676a,680]</sup> In this new approach referred as Implant assisted (IA) MDT, a ferromagnetic implant placed at the target site combined with an external magnetic field improves the attraction and retention of the MDCPs.<sup>[681]</sup> The implant is magnetically energized by the external magnetic field and generates a short ranged local force to positively affect any MDCP in the vicinity of its surroundings<sup>[682]</sup> due to increase in both magnitude and gradient of the magnetic field.<sup>[672,673b]</sup> These gradients can be produced by magnetizable implants in the form of stents,<sup>[671,683]</sup> wires,<sup>[683,684]</sup> needles or seeds.<sup>[685]</sup> However, despite the promising potential of IA-MDT, its wide clinical application is encumbered by the cost and risk of surgery.<sup>[686]</sup>

#### 5.1.2. Magnetic Fluid Hyperthermia (MFH)

Despite all the progress in medical sciences integrated with materials and nanotechnology to decline adverse effects of diseases, cancer is still a main cause of death in the world.<sup>[687]</sup> The biology of the disease has faced current chemotherapy and radiotherapy treatments with fundamental challenges including difficulty in delivering anticancer drugs into the tumor tissue as well as their collateral damages to the human body.<sup>[688]</sup> In particular, the unregulated growth of cells and chaotic vascularization of tumor hamper the aimed therapeutic dose of cytotoxic drugs to be delivered in radiotherapy-affected regions. Hence, more effective treatment with less aggressive effects is crucial to alleviate the above limitations. As a consequence, hyperthermia has emerged as an alternative thermal treatment to radiotherapy and chemotherapy to cure cancer cancers at elevated temperatures through delivering toxic doses of heat to the tumor.<sup>[689]</sup>

Difference in physical and chemical properties of both tumorous and healthy tissues is the main reason why hyperthermia is useful for treating cancers. In particular, tumorous tissues have a chaotic vasculature and as a result contain hypoxic areas where both pH and oxygen pressure are low, while healthy tissues have an undistributed architecture of vasculature. Hence, healthy tissues that have been normally oxygenated are more resistant compared to the tissues invaded by cancerous cells which deteriorate more easily at elevated temperatures ( $\approx 41\text{--}46^\circ\text{C}$ ). The susceptibility of cancerous cells to heat and the subsequent response of the tissue to the applied heat are of factors which partly depend on the inevitable cancer biology and the mode of heating.<sup>[690]</sup>

Broadly speaking, depending on the location of the disease, hyperthermia therapy can take place as a local hyperthermia, regional hyperthermia and whole-body hyperthermia.<sup>[691]</sup> Generally, in classical hyperthermia, metastatic cancers are treated by directly applying a source of the thermal energy such as hot water or microwave radiation on the whole body of the patient or on a selected part where the tumor is localized.<sup>[692]</sup> In the case of regional hyperthermia, whole tissue or organ are subjected to heat, while in local hyperthermia a smaller area such as tumor is of interest to heat subjection. However, two unsolved challenging tasks regarding with these techniques are poor diffusion of heat through the tissue along with remaining localized heating of a selected area which consequently leads to challenging control of spatial extent of heating in tissues as well as damaging the healthy tissues.<sup>[693]</sup> On the other hand, these traditional treatments suffer from limited penetration of heat into deep tissues, which increase the unavoidable heating and damaging of healthy tissues as well.<sup>[694]</sup>

These substantial shortcomings were eliminated by developing MFH which was first introduced by Gilchrist in 1957 to exploit the inherent capabilities of MNPs for shifting the heating source where it exactly should be, inside the tumor tissue, while preserving the healthy tissues as well.<sup>[695]</sup> This promising tool revolutionized the existing hyperthermia through enabling localized remote heating of bodily tissue by easily placing MNPs in tumors having pore sizes in 380–780 nm range,<sup>[696]</sup> either as a stand-alone intervention for magnetic thermoablation or adjunct to chemotherapy and radiotherapy for “moderate” hyperthermia.<sup>[687,697]</sup> In the case of thermoablation, generated heat rise the temperature between 43 and 55 °C to provoke strong cytotoxic effect causing cells to undergo direct tissue necrosis, coagulation or carbonization.<sup>[698]</sup> While “moderate” hyperthermia involves the rising temperature up to 45–47 °C to make cells more sensitive for conventional chemotherapy or radiotherapy by initiating degradation mechanisms like DNA cross linking, protein folding, and protein denaturation.<sup>[698b,699]</sup> Through these strategies, MNPs are embedded inside or in close vicinity of the tumor and by externally applying an alternating magnetic field, magnetic energy is converted to heat, proportional to the frequency of that field, by loss processes arising due to the changes of the MNP magnetization.<sup>[700]</sup> Four different approaches

can be used to deliver the magnetic fluid carrying MNPs to the tumor, including arterial injection, direct injection, in situ implant formation, and active targeting.<sup>[642c]</sup> As it was mentioned in the section of targeting ligands, the infinity of MNPs to cancerous cells is greatly enhanced by decorating them with targeting ligands to specifically deliver and retain these heat sources inside the tumor tissue. The frequencies of the applied magnetic field also harmlessly pass through the tissues of the body and consequently generate heat only in the region containing MNPs.<sup>[701]</sup> Furthermore, these pioneering heat sources can be potentially used for simultaneous delivery of anticancer drugs and imaging as real theranostics platforms. In a very especial case, MNPs are combined with thermo-responsive cargos for controlled delivery of drugs.<sup>[644b]</sup> Gilchrist et al. were the first to apply MFH for heat lymph nodes in dogs<sup>[695]</sup> and made the initial progress to apply it for humans.<sup>[702]</sup> Since then, numerous animal experiments and studies were carried out to further the potentiate of this technique toward a more practical and safer treating for cancers, especially for the case of gliomas and prostate cancers.<sup>[20,703]</sup>

The heating efficiency of the employed MNPs is of great importance to improve the overall hyperthermia process with lower doses of MNPs.<sup>[704]</sup> SAR or specific loss power (SLP) are the general terms to define transformation of magnetic energy into heat due to an externally applied alternative magnetic field.<sup>[698b]</sup> Generally, three primary mechanisms account for the generation of thermal energy, including hysteresis loss, Brownian relaxation and Neel relaxation wherein domination of each mechanism depends largely on the size of MNPs (Figure 42).<sup>[705]</sup> It has been proven that magnetic particles in the range of nanometer have higher heating efficiencies compared to micrometric particles.<sup>[706]</sup> In addition to size, other effective parameters are shape, crystal structure, magnetic anisotropy of MNPs as well as amplitude and frequency of the applied alternative magnetic field.<sup>[707]</sup>

Hysteresis is the main source of generating heat in large MNPs ( $>100\text{ nm}$ ), which is caused by the coupling of atomic spins to the crystal lattice.<sup>[693a]</sup> Specifically, higher saturation magnetization leads to larger hysteresis loop area which in fact accounts for better heating efficiency and larger amounts of energy loss to generate heat.<sup>[708]</sup> Although the biocompatibility of iron oxide has made it to one of the most desirable MNP used in hyperthermia,<sup>[642c]</sup> larger sizes of such MNPs are more prone to aggregation and have more difficulties in penetrating

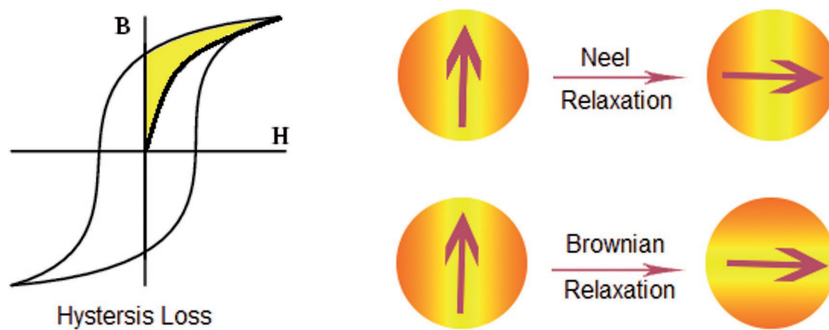


**Figure 42.** Different mechanisms responsible of the generation of heat under an alternative magnetic field.

and dispersing within tumors.<sup>[709]</sup> For smaller sizes of iron oxide nanoparticles, the total heating efficiency regarding with hysteresis loss is reduced as a result of decrease in the saturation magnetization,<sup>[710]</sup> while Brownian and Neel relaxations become the relevant mechanisms to generate heat.<sup>[642c]</sup>

Specifically, the rapid rotation of the particles themselves within a medium account for Brownian relaxation which is hindered by the viscosity of the medium to peter out the movement of particles.<sup>[711]</sup> On the other hand, Neel relaxation is defined by the fluctuations of the spins within the particles which is hindered by inherent tendency of anisotropy energy toward orienting magnetic domain in a given direction relative to crystal lattice.<sup>[698b,712]</sup> It has been reported that movement of MNPs is hindered by intracellular components upon their internalization, which indeed largely leaves the total contribution of heat generation to Neel relaxation.<sup>[713]</sup>

Generally, iron oxide nanoparticles with a size between 5 and 20 nm are superparamagnetic due to the presence of a single magnetic domain. This property enables them to cease their magnetization upon removal of the external magnetic field which indeed allows for rapid relaxations and continuous heat generation by applying an alternative field with higher frequency.<sup>[714]</sup> In particular, higher frequency of the applied magnetic field results in larger specific power loss values. The phase lag of magnetization (M) behind the applied field (H) makes the heat generation to happen through both hysteresis loss and relaxation mechanisms.

To further improve the heating efficiency of MNPs, researchers have proposed different strategies which mainly rely on tuning physical parameters such as effective anisotropy, size, and saturation magnetization.<sup>[688,715]</sup> Compared to other materials such as Fe or Co, iron oxide nanoparticles have lower saturation magnetization which directly leads to lower magnetic response with an external field.<sup>[688]</sup> A class of promising MNPs is based on obtaining ferrites by adding other ions such as Ni<sup>2+</sup>, Mn<sup>2+</sup>, and Co<sup>2+</sup> to Fe<sub>3</sub>O<sub>4</sub> for tuning the magnetic flexibility for more efficient hyperthermia applications.<sup>[716]</sup> Iron oxides doped with Gd, Fe, and Mn also represent a newer class of MNPs in hyperthermia treatments.<sup>[717]</sup> Drake et al.<sup>[718]</sup> performed a study which developed Gd-doped iron oxide nanoparticles with the size of 13 nm for use in magnetic fluid hyperthermia in mouse models. They reported the SAR values of the prepared MNPs to be four times higher than Fe<sub>3</sub>O<sub>4</sub> SAR values. In addition, the models treated with doped iron oxide displayed much slower tumor growth compared to standard iron oxide.

Furthermore, magnetosomes of the magnetotactic bacteria have also showed a great promise in the field of hyperthermia, either in the form of individual magnetosomes or in chains.<sup>[719]</sup> Thanks to their monodomain, ferromagnetic, and cubic-shaped structure, they produce large amount of heat proportional to their large sizes.<sup>[720]</sup> However, it should be mentioned that this superiority is only true for magnetic field strengths larger than 10 mT,<sup>[721]</sup> unless the losses per cycle will be considerably smaller compared to chemically synthesized MNPs.<sup>[722]</sup> Alphandéry et al.<sup>[723]</sup> reported a considerable increase in heating efficiency of magnetosomes by introducing cobalt quinate and chelating agents such as EDTA and rhodamine B<sup>[724]</sup> to increase their size and magnetocrystalline anisotropy.

Magnetic cationic liposomes (MCL) with superparamagnetic iron oxide nanoparticles were developed by Matsuoka et al.<sup>[725]</sup> to investigate the *in vivo* efficacy in hyperthermia application. Resultant MCLs were directly injected into a hamster osteosarcoma. Subsequently an alternating magnetic field was applied to trigger hyperthermia heat generation. They reported a successful diminishing of the average tumor volume by heating that above 42 C.

Considering the difficulty in accumulating enough amounts of MNPs into the cancer cells, as well as the high propensity for them to leak into the surrounding tissue or blood vessels, Xu et al.<sup>[726]</sup> exploited the self-setting ability, biocompatibility, and biodegradation of calcium phosphate cement (CPC) to develop an injectable magnetic media which can confine MNPs and cease their migration out of the targeting tissue to increase their efficacy for hyperthermia application. To do so, Fe<sub>3</sub>O<sub>4</sub> nanoparticles were distributed inside a paste formed by mixing CPC (as the solid phase) and PEG-600 (as the liquid phase) that could prevent the leaking of MNPs out of it. The efficiency of magnetic CPC (MCPC) at an iron/CPC weight ratio of 10% was evaluated for *in vivo* thermal ablation of tumors of mouse model under the guidance of ultrasound imaging. Applying an AMF fields for 180, the thermal images (Figure 43a) and corresponding time-temperature curve (Figure 43b) greatly confirmed the heating efficiency of injected MNPs. Photographs during a two-week thermal ablation showed the high efficiency of injected MNPs in reducing the tumor size to be finally diminished after 15 d (Figure 43c). Comparison of the microscopic structure and size of the ablated and non-ablated tumors respectively in Figure 43d and Figure 43e obviously confirm the practicality of MNPs for hyperthermia.

## 5.2. MNPs in Different Diagnostic Techniques

Numerous imaging techniques have been developed for acquiring *in vivo* images of anatomy and physiology in both animals and humans in the past few decades. They mainly include MRI, PET, SPECT, CT, optical imaging, magnetic particle imaging, and photoacoustic imaging (PAI) (Table 6).<sup>[727]</sup> However, limitations of individual techniques do not allow for a comprehensive characterization of all functional and anatomic information.<sup>[728]</sup> MRI and CT provide acceptable anatomic information, while PET, SPECT, MPI, PAI, and optical imaging are used for acquiring molecular information. To overcome the respective limitations of each individual technique, they have been synergistically combined by applying nanotechnology in the form of imaging probes, enabling multimodal imaging with enhanced sensitivity.<sup>[729]</sup> Reducing the number of separate imaging sessions, this strategy can save time and effort and provide accurate simultaneous imaging of both anatomic and molecular information.<sup>[730]</sup> Superparamagnetic iron oxide nanoparticles have gained a lot interests to serve as workhorses for fusion of MRI with other biomedical imaging modalities due to their high surface to volume and degradability (Figure 44). Specifically, SPIONs have been shown promising to enhance the contrast agents of MR imaging and they have high capability to be loaded with PET, SPECT, PAI, CT, and optical imaging modalities.<sup>[731]</sup>

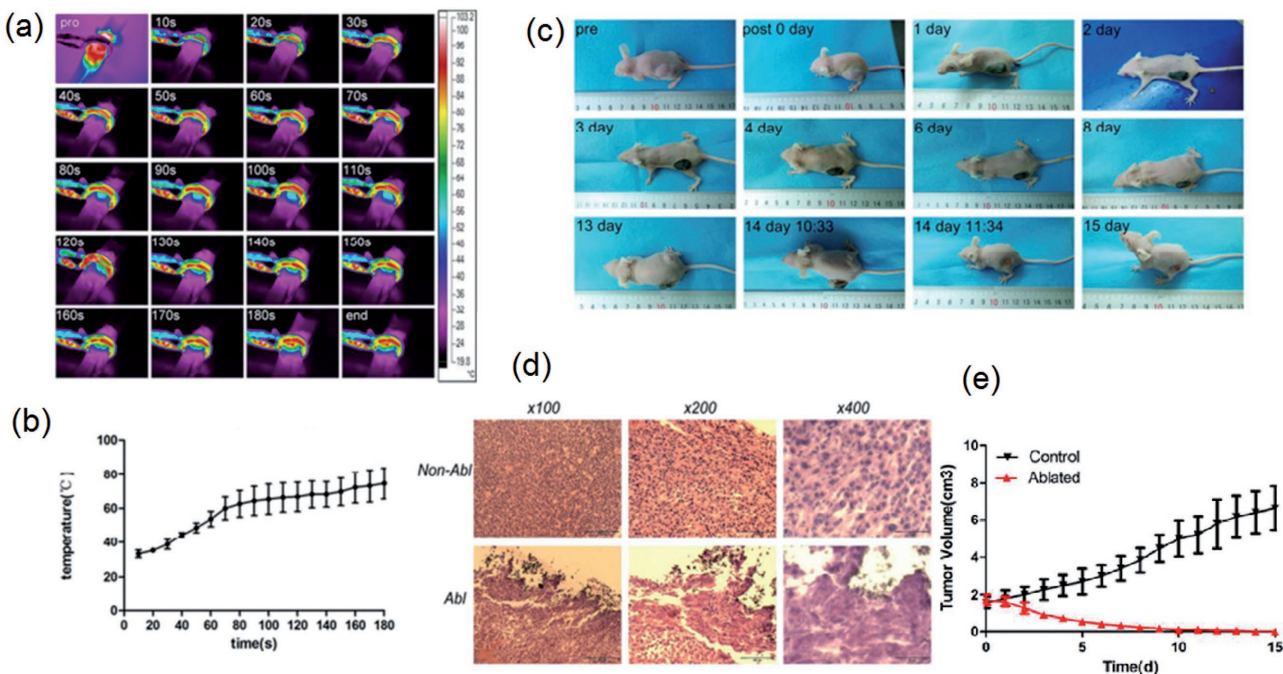


**Figure 43.** Tumor surface temperature monitoring and efficiency of the magnetic hyperthermia ablation: a) Thermal images of tumor containing 0.36 g 10% MCPC which was exposed to an alternating magnetic field for 180 s. b) Corresponding time-temperature curve. c) Size reduction of tumor during a two-week magnetic hyperthermia ablation treatment. d) Microscopic structure of the ablated and non-ablated tumor tissue. e) The time-tumor volume curve. Reproduced with permission.<sup>[726]</sup> Copyright 2015, ACS.

### 5.2.1. MRI

Over the past decade, MRI has been widely used as a powerful noninvasive technique to obtain anatomic and functional information.<sup>[328b]</sup> This technique exploits the nuclear property of hydrogen that originates from water molecules present in our body to offer high spatial and temporal resolution of contrast differences between soft tissues.<sup>[729c,732]</sup> In fact, protons present in the nucleus have an inherent tendency to be excited and aligned parallel to an external applied magnetic field.<sup>[733]</sup> The spins of protons are flipped at a particular frequency, known as the “resonance frequency.”<sup>[11b]</sup> Specifically, when the generated radiofrequency (RF) pulse is in resonance with body’s hydrogen atoms, makes protons in the hydrogen nucleus to be fully aligned parallel to the applied magnetic field direction. By removing the electromagnetic field, an RF signal is produced during a “relaxation” process wherein protons release energy while they realign back to their original states. The variation in realignment speed for protons in different tissues corresponds to precisely delineate the tissues.  $T_1$  and  $T_2$  are respectively the needed time for longitudinal and transverse components of magnetization vectors to return to their original thermal equilibrium state.<sup>[733]</sup> Either  $T_1$  or  $T_2$  relaxation times can be measured by receiver coils to subsequently produce an MR image by a computer algorithm.<sup>[734]</sup>

**5.2.1.1. Contrast Agents:** Developing effective contrast agents is a crucial aspect to enhance and widen the diagnostic utility of imaging techniques, especially for early diagnosis of cancerous tumors. Contrast agents are capable of changing the response of nearby atoms to modify the relaxation rates at  $T_1$  or  $T_2$  through

localized interactions with protons of water molecules that leads to produce distinct signals which can more effectively discriminate and illuminate the tissues.<sup>[735]</sup> In actual practice, due to the small intrinsic differences, better delineation of tissues can be achieved by using exogenous contrast media. Gd-chelates consisted of high-spin paramagnetic Gd<sup>3+</sup> ions, were the first generation of these contrast agents. For about three decades, paramagnetic gadolinium (Gd(III)) have been combined with chelating ligands as  $T_1$  contrast to improve the positive signal quality of  $T_1$ -weighted MR images with brighter tissues where the Gd complex is located.<sup>[736]</sup> The inherent shortcoming of gadolinium chelates is their high levels of toxicity to biological systems which require encapsulation of free gadolinium ions into dendrimers and liposomes.<sup>[737]</sup> In addition, gadolinium chelates suffer from poor cellular uptake and short life span.<sup>[733]</sup>

However, small size tumors cannot be effectively detected due to relatively low sensitivity of traditional techniques. In addition, due to high toxicity of contrast agents such as Gd chelates, it may be risky and difficult to deliver enough of them in cancers.<sup>[738]</sup> Hence, MNPs have aroused the interests as potential alternatives to conventional imaging agents. By modifying the pharmacokinetics of MNPs, they can accumulate in the tissue and enhance the MR contrast through shortening either  $T_1$  or  $T_2$  relaxation of surrounding protons.<sup>[11b]</sup> The ratio of relaxivities (inverse of the relaxation time) is the determinant fact for MNPs to be either used as a positive or negative contrast. Yet, MNPs have shown better capability to reduce the  $T_2$  signal intensity and are more used for providing negative contrast.<sup>[739]</sup> Among the promising MNPs, the next generation was (ultrasmall) superparamagnetic iron oxide (SPIOs and USPIOs) nanoparticles that have been developed for both

**Table 6.** Qualitative comparison of different imaging techniques performed with MNPs and loaded imaging modalities.

Imaging technique	Source	Depth	Spatial resolution	Preclinical use	Clinical use	Advantages		Disadvantages
MRI	Radio-frequency wave	No limit	10–100 μm	Yes	Yes	High 3D spatial resolution	Low sensitivity at cellular/molecular level	
						High contrast differentiation between soft tissues	Magnetic susceptibility artifacts and negative contrast effects during applying T2 contrast agents	
						Long acquisition time		
							Need for expensive equipment	
Optical imaging	Near-IR Light	<10 cm	>0.3 μm	Yes	No	Simultaneous monitoring of several molecular events and multiple markers	Lack of anatomical information	
						Wide applicability and availability of diverse fluorophores	Limited penetration of light and difficulty in imaging of deep tissues	
PET	Positrons gamma ray	No limit	1–2 mm	Yes	Yes	Extremely high sensitivity along with 3D imaging	Exposure to radiation	
						Specificity and fast detection	Lack of anatomical information	
						Capability in monitoring changes in tumor metabolism and biodistribution	Low spatial resolution	
						Offering biochemical information	Need for radiotracer facilities	
SPECT	Positrons gamma ray	No limit	1–2 mm	Yes	Yes	Better quantitative capacity than SPECT	Need for expensive equipment	
						Provides information on molecular process	Lower sensitivity than PET	
						Simultaneous detecting of multiple probes via the energy identification of the gamma photons emitted	Low spatial resolution	
						Specificity and fast detection		
						Less expensive than PET		
CT	X-ray	No limit	50–200 μm	Yes	Yes	More widely available than PET	Use of iodine-based contrast agents which may produce side effects	
						Excellent anatomical information		
						High spatial resolution	Relatively weak in providing functional imaging	
						3D imaging		
MPI	Iron oxide NPs	No limit	<1 mm	Yes	No	High sensitivity, feasibility of real time tracking, high spatial resolution, high temporal resolution, sub-millimeter spatial resolution images, ability of fast volumetric imaging	Lack of anatomical information	
PAI	Photo acoustic waves	<2 cm	<1 mm	Yes	Yes	High spatial resolution	Lack of anatomical information	
						No ionizing radiation	Need for exogenous contrast agents for biological processes with lack of chromophores	
						Feasibility for imaging vasculature tissues by exploiting intrinsic chromophores (melanin and hemoglobin)	Inability for detecting early stage tumors	

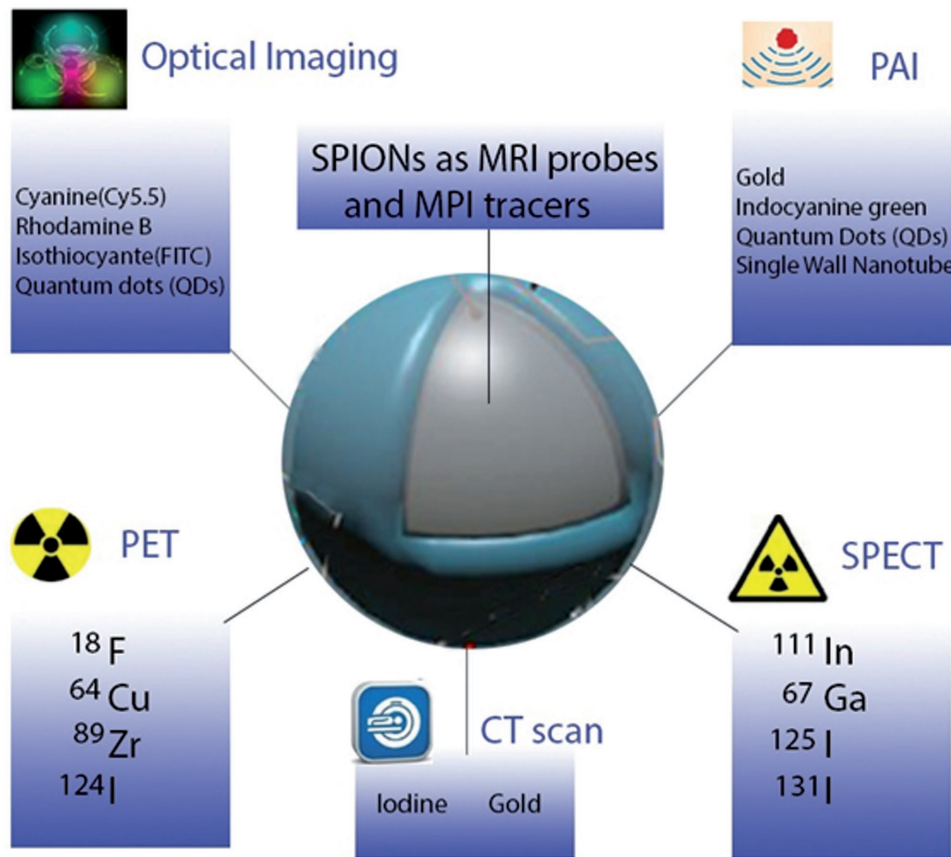


Figure 44. Combination of MRI with other imaging techniques and their specific imaging modalities.

standard and functional MRI by shortening  $T_2$  relaxation time.<sup>[740]</sup> Ferucarbotran, ferumoxtran-10, fetumoxytol (Feraheme), ferumoxides, ferristeneand, and ferumoxsil are of some contrast agents at current clinical trials.<sup>[733]</sup> Feridex and Resovist are approved by food and drug administration (FDA) for liver imaging.

Similar to other paramagnetic substances, SPIOs and USPIOs lose their magnetization by removing the magnetic field. But the substantial higher value of the magnetic moment, due to presence of extensive Fe atoms, can easily increase the relaxation rate of surrounding proton spins more than gadolinium chelates.<sup>[741]</sup> This will lead to precise delineation of tumor margin as well as the vascular blood supply to tumors.<sup>[742]</sup>

Given the higher uptakes by RES, SPIOs can surprisingly distinguish smaller lesions of about 2–3 mm in liver in clinical applications.<sup>[743]</sup> In particular, SPIONs are biocompatible, chemically stable, and also biodegradable. They are metabolized directly by the liver, rather than by the kidney and have been approved for human clinical studies by being much safer than gadoliniums, iodines or other metal alloy based contrast agents.<sup>[744]</sup> However, when it comes to targeting tissues with high initial signal, such as lung, discrimination between the negative contrast induced by nanoparticles and artifacts (e.g., blood flow, motion, and air) is difficult. In addition, relatively long acquisition times are needed to get bright iron signals, which address another shortcoming of these contrast agents.<sup>[745]</sup>

### 5.2.2. Optical Imaging

Optical imaging has been used from diagnosing cancers in its earlier stages<sup>[746]</sup> to immunostainings,<sup>[747]</sup> fluorescence-guided surgery, and endoscopic imaging.<sup>[748]</sup> This technique is based on the detection of light, absorbed and emitted by fluorochrome concentrations as a source of contrast.<sup>[749]</sup> Specifically, fluorescent molecules emit photons with longer wavelengths than that of formerly adsorbed.<sup>[750]</sup> Generally, fluorescent agents that emit photons with wavelengths NIR range (650–900 nm) correspond to optical imaging due to their capability of passing through biological tissues allowing for a whole body tomography in rodents.<sup>[740b,751]</sup> In addition, this shifting to the NIR spectrum has overcome some shortcomings of optical imaging, including photon absorption, scattering, and background from endogenous tissue autofluorescence.<sup>[752]</sup> Overall, optical imaging is advantageous for their cost effectiveness, and use of no ionizing radiation to provide intravital image resolutions on the order of millimeters.<sup>[750,753]</sup> In addition, non-toxicity, sensitivity, and versatility of the optical contrast agents qualify them to be used for *in vivo* applications.<sup>[746,754]</sup> However, optical imaging suffers from limited penetration of light which makes it difficult to image deep tissues.

Given the incapability of MRI to measure molecular events, a vast amount of researches have been dedicated to complement this technique by optical imaging to develop MRI/optical dual imaging techniques.<sup>[755]</sup> Hence, the anatomic information

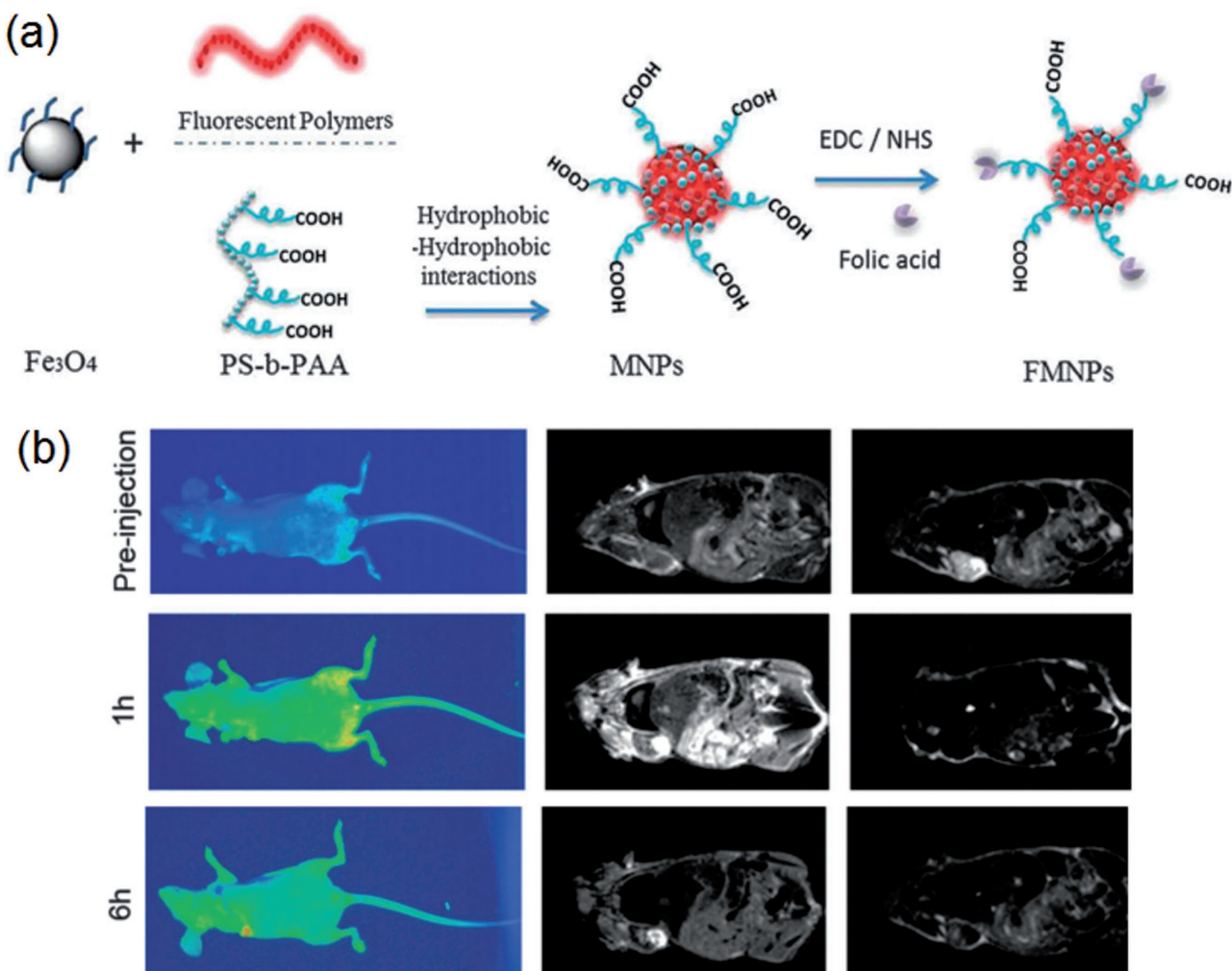


**Figure 45.** a) Schematic representation showing the synthesis of fluorescent magnetic nanoparticles (FMNPs) for targeted imaging. b) In vivo fluorescence images and simultaneous  $T_1$ - and  $T_2$ -weighted MRI of mice injected with FMNPs acquired pre-injection and at 1 and 6 h post-injection. Reproduced with permission.<sup>[763]</sup> Copyright 2015, RSC.

provided by MRI, as well as functional details of a molecular event can be elucidated through manipulation of fluorescent agents either conjugated or doped within nanoparticles to produce pictures with improved quality.<sup>[731b]</sup> These optical imaging agents are commonly combined with magnetic nanoparticles, chemically or physically, to produce an end product which retains as a compact ideal probe through its journey toward the target.<sup>[756]</sup> Iron oxide nanoparticles, mainly with polymer coatings such as dextran, have been widely conjugated with fluorescent agents to provide with dual imaging modality which both enhances the MR contrast and gives functional information.<sup>[129,729b,757]</sup>

Either organic dyes (such as cyanine (Cy5.5), rhodamine B, and isothiocyanate (FITC)) or synthetic/inorganic semiconductor quantum dots (QDs)<sup>[338,758]</sup> have emerged as optical probes. Although these fluorescence units can be directly conjugated on the surface of MNPs, the energy transfer between the MNPs and fluorescent molecules due to low distance between them will lead to fluorescence quenching. As a result, employing thicker coating materials, such as silica, or longer chemical

linkers come in handy to prevent the quenching phenomenon by increasing the distance between MNPs and fluorescent molecules.<sup>[759]</sup> In an effective approach, core-satellite compounds were developed by decorating 30 nm dye-doped silica nanoparticles with 9 nm iron oxide ( $\text{Fe}_3\text{O}_4$ ) nanoparticles.<sup>[760]</sup> They were used for acquiring MRI and optical imaging of polysialic acid (PSA)-positive cells and exhibited increased  $T_2$  MRI and fluorescence signal compared to individual iron oxide nanoparticles conjugated with optical dyes.<sup>[729a]</sup> In another strategy, a silica shell was used to encapsulate both MNPs and fluorescent units<sup>[761]</sup> to enhance the photostability of organic dyes through protecting them against photochemical destruction and photobleaching.<sup>[762]</sup>

In a very recent study performed by Wang et al.<sup>[763]</sup> ultrasmall  $\text{Fe}_3\text{O}_4$  magnetic nanoparticles (2–3 nm) NIR emissive semiconducting polymers (PFBT and PFTBT), and amphiphilic polymers bearing carboxylic acid groups were integrated into one particle by one-step synthesis (Figure 45a). For the first time, such combination was used as MRI/optical imaging agents, providing both NIR fluorescence imaging and

simultaneous  $T_1$  and  $T_2$ -weighted MRI of tumors in a living body (Figure 45b).

### 5.2.3. Positron Emission Tomography

A great enhancement in diagnostic accuracy has been achieved by the fusion of MRI and PET modalities on novel nanoparticles to introduce a cocktail of imaging modalities capable of being simultaneously monitored in body.<sup>[602,728]</sup> In its very first stages of development, different information were obtained by using superparamagnetic iron oxide nanoparticles and <sup>18</sup>F-Fluorodeoxyglucose as separate PET and MRI agents for imaging myocardial infarction in rats.<sup>[764]</sup> Since then, PET/MRI dual imaging strategy have been clinically used for pancreatic and lung cancer<sup>[765]</sup> as well as human brain imaging<sup>[766]</sup> applications. Although MRI offers anatomic information with high spatial resolution, it mainly suffers from inability to provide functional and molecular information. On the other hand, accurate molecular imaging can be achieved by high sensitive PET as a nuclear imaging technique based on radionucleotide emitting positrons to illuminate functional biological process. However, the partial volume effects in PET images which are resulted by limited positron range in tissue, lead to inconclusive anatomic information with low spatial resolution.<sup>[767]</sup> Upon this pioneering integration, both molecular imaging and soft tissue contrast provided respectively by sensitive and quantifiable PET and MRI signals, synergistically compensate for above limitations of each other.<sup>[730b]</sup>

Specifically, by accommodating PET imaging modalities on nanoparticles which enhance the contrast of MRI, the partial volume effects of PET are corrected with MRI spatial resolution. However, sensitivity difference of two imaging techniques must be taken into full consideration to design PET/MRI probes which maintain a relatively low concentration of PET along with a relatively high contrast of MRI. Hence, designed probes should ideally supply sufficient dose of radiotracers to be detected in PET imaging along with MRI agents with sufficiently high MRI contrast ability.<sup>[768]</sup> Since FDA approved iron oxide nanoparticles, they have been served the most popular MRI contrast components to further the utilization of PET/MRI multimodal imaging by influencing the  $T_2$  relaxation time of nearby water protons as well as being biodegradable and nontoxic.<sup>[769]</sup> Furthermore, other metals such as manganese<sup>[770]</sup> and cobalt<sup>[771]</sup> have been added to iron oxide nanoparticles to increase their contrast-enhancing efficiency by gaining superior magnetic anisotropy,<sup>[772]</sup> as well reducing the particle size for longer blood circulation times.<sup>[773]</sup> Simultaneously, PET signals are in charge of resolving the lack of functional information provided by MR images.<sup>[774]</sup> The high sensitivity of PET imaging, down to the pico-molar level deposited in the living subjects,<sup>[775]</sup> combined with its no penetration limit come in handy for numerous in vivo diagnostic applications. Some reports demonstrated the usefulness of radionuclide imaging for noninvasive in vivo imaging of pharmacokinetic, biodistribution, and renal clearance of nanoparticles and drugs.<sup>[409,776]</sup> Within PET imaging technique, a PET scanner is used to acquire the radiation emitted by radioisotopes (also known as radiotracers) to construct tracer concentration dependent images.<sup>[777]</sup> In fact, the radiation involves

pairs of high-energy gamma rays which are produced by either radiohalides or radiometals during their natural decay of emitting positrons, a process called as annihilation. Once the radiotracers are accumulated in a desired organ in the patient's body, their distribution in the body can be provided by detecting the emitted waves by the  $\gamma$  detector. Half-life and maximum positron energy are of two important factors for selecting the accurate PET imaging modality. In general, isotopes with optimal half-lives and lowest maximum positron energy are included as right radionuclides to minimum the loss in spatial resolution by contributing positron emission to the total absorbed dose.<sup>[728,778]</sup> <sup>111</sup>In, <sup>18</sup>F, <sup>64</sup>Cu, <sup>89</sup>Zr or <sup>124</sup>I are commonly used radionuclides for PET imaging.<sup>[779]</sup> Among which, <sup>18</sup>F and <sup>64</sup>Cu have low enough maximum positron energy and optimal half-lives for longer in vivo imaging. Except for (<sup>124</sup>I and <sup>18</sup>F),<sup>[780]</sup> other practical radionuclides require a chelation process to gain enough in vivo stability.<sup>[781]</sup> Commonly, polyazacarboxylate macrocycle such as 1,4,7-triazacyclododecane-*N,N',N''*-triacetic acid (NOTA) and 1,4,7,10-tetraazacyclododecane-*N,N',N'',N'''*-tetraacetic acid (DOTA)<sup>[782]</sup> have been used to complex radionuclides with sufficient stability.

In one notable study performed by Choi et al.,<sup>[783]</sup> <sup>124</sup>I radionuclides were conjugated on Mn-doped ferrite nanoparticles coated by serum albumin (Figure 46a). They were applied as PET/MRI dual imaging agents and precisely delineated small sentinel lymph nodes. In another study,  $\text{Fe}_3\text{O}_4$  contrast agents were coated by polyaspartic acid and applied for in vivo targeting of tumor xenografts to provide both MRI and PET images.<sup>[784]</sup> Subsequent to their surface coating, they were labeled with <sup>64</sup>Cu radionuclides and DOTA stabilizing material. RGD peptides were also employed to specifically target integrin ( $\alpha_v\beta_3$ ). In a recent study oleic acid coated iron oxide nanoparticles were labeled with <sup>68</sup>Ga and DOTA respectively as radionuclide and chelating agents for dual PET/MR imaging of prostate.<sup>[785]</sup> Additionally, they were decorated with glutamate-urea-lysine targeting ligands to increase their affinity for prostate-specific membrane antigen (PSMA) (Figure 46b). The resultant PET/MRI dual images showed a high uptake of the NP by the PSMA-positive tumor with high resolution.

### 5.2.4. Single Photon Emission Computer Tomography

Same as PET, single photon emission computer tomography has also been another representative of the leading nuclear imaging technique for the last few decades.<sup>[786]</sup> Providing important biological information, SPECT directly leads to improved detection of functional processes in living subject with high sensitivity.<sup>[787]</sup> A revolving gamma camera constructs 2D or 3D images via a computer to record data emitted by in vivo distributed radionuclides. The specific radioisotopes used account for the key difference between SPECT and PET imaging from a material point of view. <sup>99m</sup>Tc, <sup>111</sup>In, <sup>67</sup>Ga, <sup>125</sup>I, <sup>131</sup>I, and <sup>201</sup>Ti are of the common radionuclides used for SPECT imaging in researches and biomedical applications.<sup>[788]</sup> Among these, <sup>99m</sup>Tc has been extensively established due to being less expensive and more available than PET.<sup>[789]</sup> A potential advantage toward using SPECT imaging is that parallel biological events can be simultaneously visualized. Specifically, through

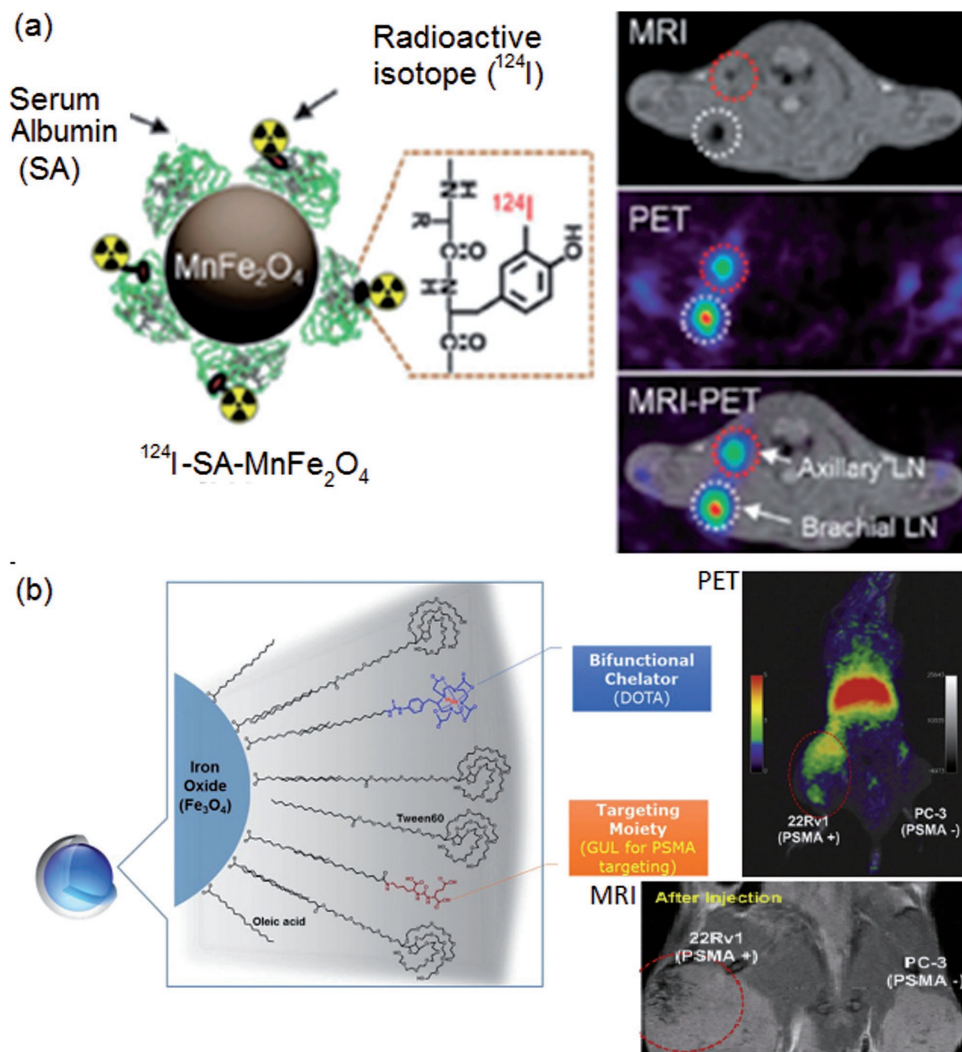


**Figure 46.** a) Mn-doped iron oxide nanocomposites coated with serum albumin (SA) and labeled by radioisotopes ( $^{124}\text{I}$  – SA –  $\text{MnFe}_2\text{O}_4$ ) for delineation of the sentinel lymph nodes (axillary and brachial lymph nodes) with adequate PET signals and the anatomical MR image. b) Iron oxide nanoparticles labeled with radionuclides and equipped with targeting ligands to actively reach the prostate for PET/MRI dual imaging. a) Reproduced with permission.<sup>[783]</sup> b) Reproduced with permission.<sup>[785]</sup> Copyright 2016, the authors, published under CC-BY-NC-ND license.

the energy identification of the emitted photons, simultaneous imaging of different SPECT imaging radionuclides becomes possible.<sup>[790]</sup>

As it was mentioned for PET imaging, SPECT imaging also suffers from incapability to identify anatomic structures. Hence, an imaging technique such as MRI or CT comes in handy to accurately localize an area of increased activity.<sup>[791]</sup> Same as PET radionuclides, SPECT imaging modalities can be used for fusion of SPECT/MRI to synergistically compensate for limitations of single techniques.<sup>[792]</sup> The overall scan time will be also reduced which leads to fewer errors as well as avoiding multiple anesthesia sessions.<sup>[793]</sup> Similar to MRI/PET dual imaging, the morphological and functional metabolic information on molecular process along with anatomical information are provided by SPECT radionuclides conjugated with SPIONs which account for enhancing the contrast of MR images.<sup>[791b,794]</sup> Integrated by targeting ligands, a potential class of radiopharmaceuticals capable of specific localization and

illumination in cancers has emerged. Furthermore, it provides a non-invasive determination of the biodistribution of nanoparticles tagged with radiotracers, even in the pico-molar concentration range.<sup>[729c]</sup>

In a study performed by Sandiford et al.<sup>[23]</sup> iron oxide nanoparticles were loaded by  $^{99\text{m}}\text{Tc}$  radionuclides which were stabilized with bisphosphonate (BP) chelates (Figure 47a). Prepared nanoparticles were applied for MRI/SPECT dual mode imaging of cardiovascular organs such as heart and aorta. In one notable study, Fe<sub>3</sub>O<sub>4</sub> MNPs were respectively coated by Fe and PEG to construct the scaffold for dual MRI/SPECT imaging guided photothermal therapy in vivo (Figure 47b).<sup>[795]</sup> They were conjugated with  $^{125}\text{I}$  and c(RGDyK) respectively as imaging modality and targeting ligands. Their results clearly indicated increased  $T_2$  contrast in MR imaging with simultaneous PET imaging.

However, technological challenges in operating MRI/SPECT dual imaging simultaneously are perhaps the reason why this technique is still in its infancy and has somewhat

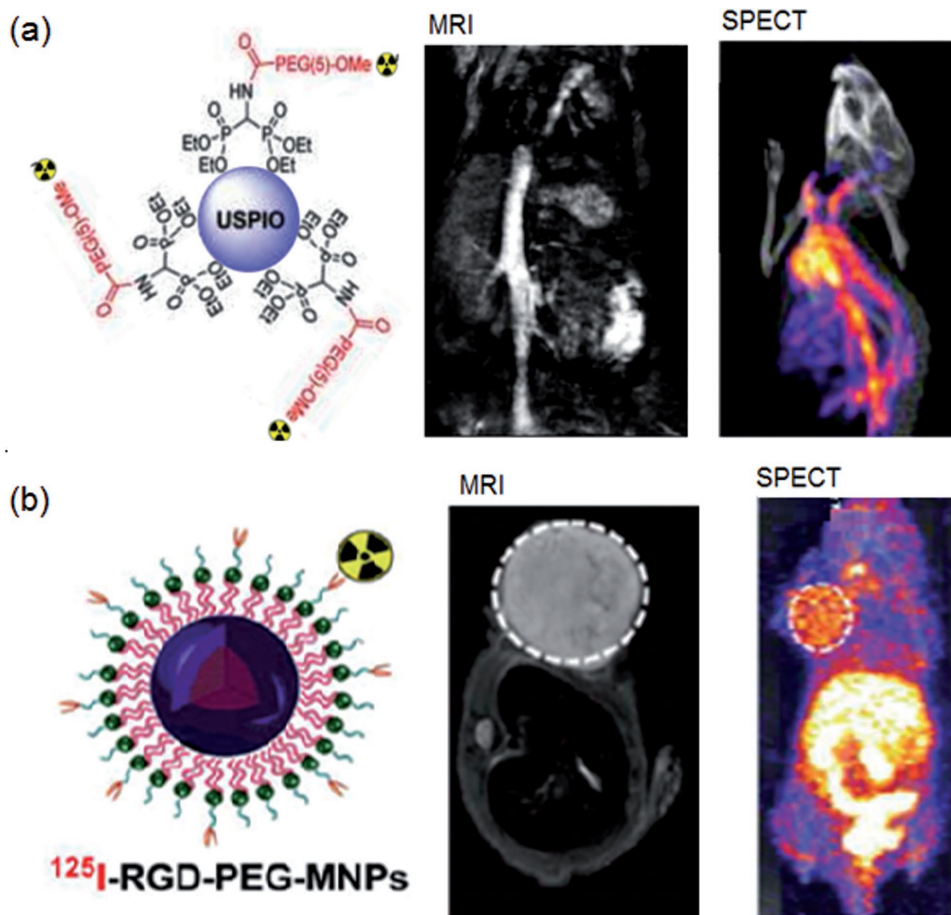


**Figure 47.** a) Superparamagnetic iron oxide (SPIO) nanoparticles labeled with  $^{99m}\text{Tc}$  for MRI–SPECT dual-modal imaging of cardiovascular organs. b) SPIO nanoparticles labeled with  $^{125}\text{I}$  radioisotopes and equipped with c(RGDyK) ligands to actively target tumor of a mice for both MRI and SPECT imaging. a) Reproduced with permission.<sup>[23]</sup> Copyright 2012, ACS. b) Reproduced with permission.<sup>[795]</sup> Copyright 2016, ACS.

lagged behind PET/MRI development.<sup>[793b,796]</sup> Specifically, the revolving gamma camera for detection of a radiotracer creates artifacts in the MR images. On the other hand, designing a SPECT scanner within an MR instrument is problematic due to both limited space inside the magnet and generation of eddy currents which hamper successful realization of SPECT/MRI.<sup>[774]</sup> However, high-performance PET detectors have been fully incorporated within PET/MRI scanners thanks to availability scintillation materials and novel gamma ray detectors based on avalanche photodiodes (APDs) to overcome the above limitations.<sup>[793b,797]</sup>

#### 5.2.5. Computer Tomography

Computer tomography is of anatomic imaging techniques which has aroused considerable interest in clinical applications owing to its low cost, availability, short acquisition time, deep tissue penetration and high hard-tissue imaging contrast and capability to evaluate the hyper vascularization.<sup>[798]</sup> By means of X-rays, images with high spatial resolution are obtained through slices of the body area.<sup>[799]</sup> Iodine and gold-based compounds have been commonly used as CT contrast agents

to block X-rays in a specific part of the body and construct CT images.<sup>[800]</sup> Anatomical structures are hence delimited by differentiations in X-ray attenuation of different tissues.<sup>[801]</sup>

However, subsequent side effects such as anaphylactic shock, itching, and vomiting may occur upon introducing iodine-based contrast agents into the body.<sup>[802]</sup> In addition, their short blood circulation, lack of tissue specificity, and limited vascular permeation provide insufficient short imaging times.<sup>[803]</sup> Hence, developing safer contrast agents based on the intrinsic physical properties of gold has gained a lot of attention in the community to produce strong CT contrast (up to twice that of iodine).<sup>[804]</sup> Specifically, better X-ray attenuation coefficient of gold than that of omnipaque (a conventional iodine-based CT contrast agent)<sup>[805]</sup> has made it to an interesting material in the arsenal of contrast agents, either as single gold nanoparticles or combined with other nanoparticles.<sup>[806]</sup> Thanks to high atomic number of gold and X-ray absorption coefficient, CT images with higher contrast can be obtained for diagnosis various diseases and gaining suitable anatomical information.<sup>[807]</sup>

Although presence of gold layers lower  $T_2$  signal intensity in MRI compared to normal SPION, SPION–dumbbell nanocomposites did not lower the  $T_2$  signal intensity during in vivo MRI study.<sup>[801]</sup> In addition, detectable signals of MRI/CT agents can

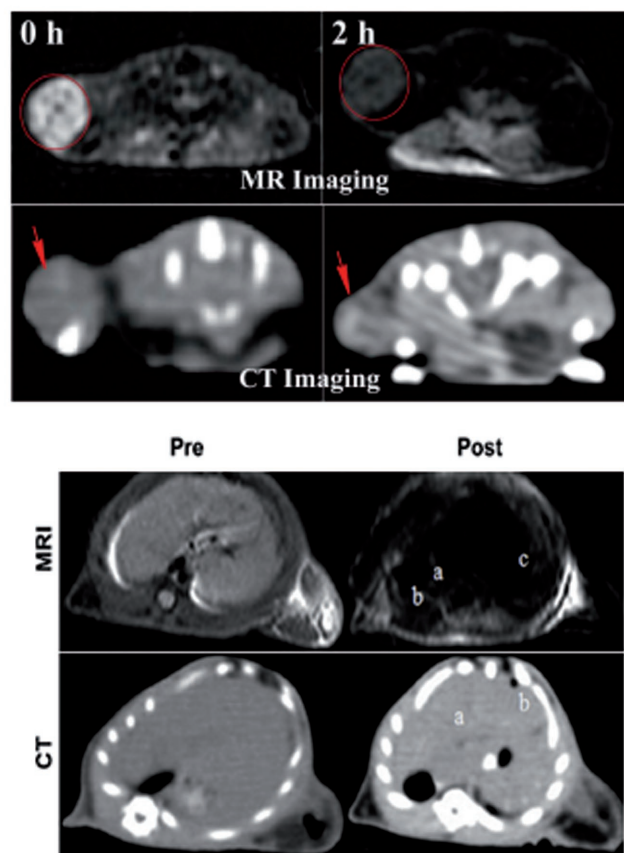
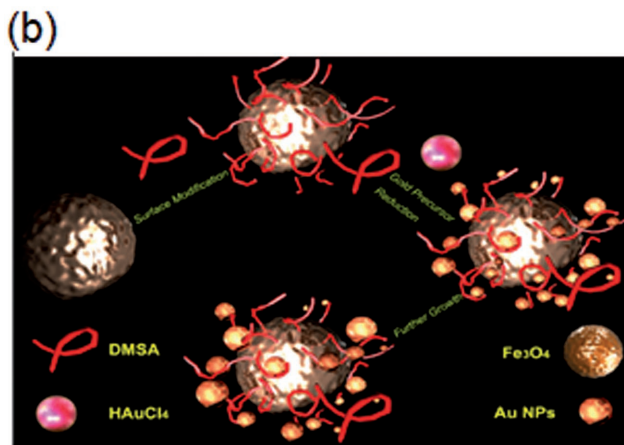
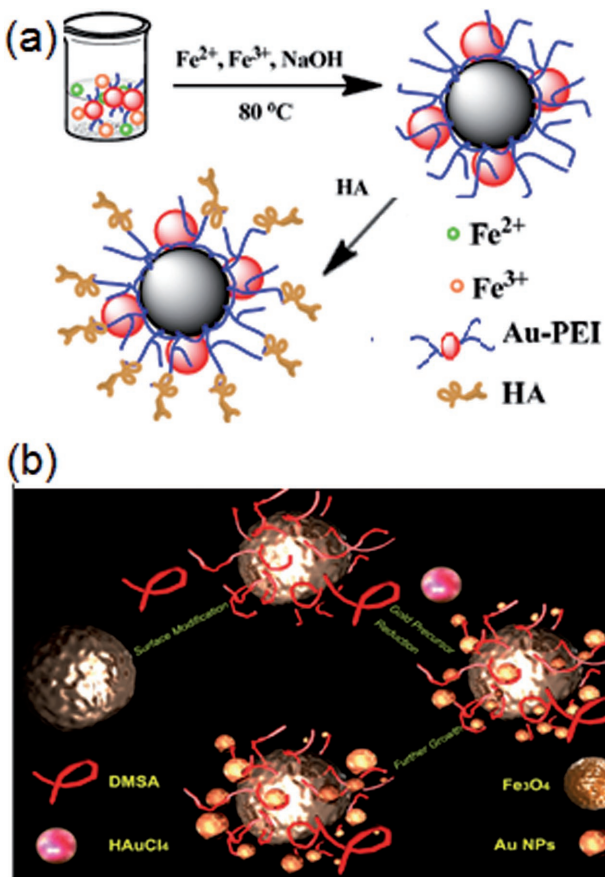


**Figure 48.** a) Schematic representation of the synthesis of hyaluronic acid-modified  $\text{Fe}_3\text{O}_4/\text{Au}$  composite nanoparticles and their application for targeted dual mode MR/CT imaging of tumors. b) Procedure for the preparation of  $\text{Fe}_3\text{O}_4-\text{Au}$  nanoparticles and their application for CT and  $T_2$ -weighted MR imaging of fatty liver bearing rat, pre and 45 min post contrast in transversal view. a) Reproduced with permission.<sup>[810b]</sup> Copyright 2015, RSC. b) Reproduced with permission.<sup>[798b]</sup> Copyright 2015, CRC Press.

accurately delimit tumor margin in a less harmful way which is crucial to preserve other important structures upon using intrasurgical imaging tools.<sup>[24,808]</sup> Performing the imaging procedure in exactly the same area for both techniques via MRI/CT dual imaging agents also leads to better diagnosis. Furthermore, it reduces the total dose of contrast agents administered into the patient's body, which indeed results in less consequent side effects.<sup>[750]</sup>

Despite the advantages offered by CT, the similar X-ray absorption of soft tissues makes it difficult for CT to precisely distinguish between subtle changes in them.<sup>[809]</sup> To produce images with better qualities, extensive experience with use of gold as appropriate shells for iron oxide magnetic nanoparticles along with the capability of these nanoparticles to enhance the contrast of MR images have been extremely exploited to build MRI/CT dual imaging probes.<sup>[810]</sup> Simultaneous combination of the anatomic information provided by both techniques certainly comes in handy for better diagnosis and further decisions to overcome the limitations of each single procedure as a result of higher payload of contrast producing material with longer blood circulation times.<sup>[811]</sup> These hybrid dual imaging agents composed of gold and iron oxide nanoparticles (GION) can be used to provide better CT contrast and relatively higher

$T_2$  relaxivity in MRI even in the form of core shell nanoparticles or SPION–gold dumbbell nanocomposites.<sup>[812]</sup>

Hu et al.<sup>[810b]</sup> prepared  $\text{Fe}_3\text{O}_4/\text{Au}$  composite nanoparticles for targeted dual mode MR/CT imaging of tumor. In the first step, they used PEI as a stabilizer to synthesize PEI–Au nanoparticles. Subsequently, in the presence of resultant nanoparticles coprecipitation of Fe(II) and Fe(III) was applied to form the  $\text{Fe}_3\text{O}_4/\text{Au}$  nanocomposites and eventually modified them with hyaluronic acid (HA) (Figure 48a). The end production showed high  $r_2$  relaxivity in MRI and good X-ray attenuation property to increase the contrast of both imaging approaches. In a very recent study performed by Zhao et al.<sup>[798b]</sup> strawberry-like  $\text{Fe}_3\text{O}_4-\text{Au}$  hybrid nanoparticles were synthesized for performing MRI/CT dual imaging. The  $\text{Fe}_3\text{O}_4$  nanoparticles were synthesized via coprecipitation method and further modified them with in situ reaction of  $\text{HAuCl}_4$  by DMSA at room temperature (Figure 48b). The resultant nanoparticles, after being verified in normal animals, were applied for in vivo CT and MR imaging of three different kinds of liver disease bearing animal models (alcoholic liver, liver cirrhosis, and hepatocellular carcinoma (HCC)). Their results exhibited contrast enhancement for both MR and CT images, especially for fatty liver model.

### 5.2.6. MPI

As it was explained in previous sections, iron oxide core of MNPs can be either exploited for enhancing the contrast of MR images, or they can serve as the workhorses for loading other imaging moieties. In both cases, the iron oxide core itself was not in charge of sending any signal to the imaging systems. In particular, interaction of MNPs with the protons of water molecules modifies the relaxation rates of nearby atoms to produce better MR images. On the other hand, in the cases of SPECT, PET, and optical imaging, radionucleotides, and optical probes are just loaded on MNPs to be carried into the area of particular interest. In 2001, Gleich and Weizenecker conceived of a new imaging technique wherein MNPs are not just supportive contrast agents, but the only source for sending the signals out to the imaging system. This totally clarifies why the used MNPs are referred to as tracers rather than contrast agents.<sup>[813]</sup> In 2005, they unveiled the first completely new imaging technique since the invention of MRI, named as magnetic particle imaging<sup>[814]</sup> which used iron oxide nanoparticles as clinically safe tracers to directly measure the magnetization for quantifying their local concentration.<sup>[815]</sup>

In particular, the non-linear response of these tracers to applied oscillating fields over a broad frequency range allows for a 3D visualization of their distribution in space. The inherently quantitative property of this technique addresses the proportional dependency of the signal strength to the amount of MNPs.<sup>[816]</sup> Since MPI is very dependent on iron oxide tracers, the size, monodispersity, and stability of MNPs are extremely critical parameters to achieving high sensitivity and good spatial resolution of MPI images.<sup>[20,817]</sup> MPI has been shown promising for cancer imaging, stem cell tracking, and angiography,<sup>[818]</sup> and even monitoring the therapeutic effect of magnetic hyperthermia.<sup>[819]</sup>

Compared to other imaging techniques such as CT, MRI and PET, MPI combines high temporal resolution, sub-millimeter spatial resolution images and high sensitivity<sup>[820]</sup> with the ability of fast volumetric imaging.<sup>[821]</sup> Surprisingly, far better resolution of 250  $\mu\text{m}$  and sensitivity of  $20 \times 10^{-9} \text{ M}$  appear feasible in theory.<sup>[821]</sup> Short acquisition time also allows for real time applications, to the point that *in vivo* 3D real-time MPI scans could reveal the details of a beating mouse heart.<sup>[822]</sup> In addition, MPI is free of ionizing radiation and utilizes two static and oscillating magnetic fields to quantitatively map concentrations of iron oxide nanoparticle distributions.<sup>[823]</sup> Within this technique, diamagnetic tissues of the human body<sup>[823]</sup> are transparent and no background signal originates from surrounding tissues, which eliminates problems associated with background signals.<sup>[769b]</sup> As a result, no signal of the anatomical structure of the body interferes with the MPI signals of interest, leading to a superb contrast.<sup>[816]</sup>

Detailed explanations of MPI principles as well as building the scanners and relative applications have been provided in a series of books written by leading innovators of this technology.<sup>[824]</sup> Essentially, the superparamagnetic characteristic of MNPs and the harmonic composition of their response make MPI possible at all.<sup>[813]</sup> In brief, measuring the magnetization change in a tracer material upon applying a time-varying

external magnetic field is exploited to determine the spatial distribution of MNPs with high sensitivity and resolution. Based on Langevin theory,<sup>[825]</sup> there is a nonlinear relation between the external magnetic field and magnetization of MNPs. Such non-linear curve is an indicative of a magnetization response which contains both fundamental frequency of the MPI excitation field and harmonics of this frequency. Image reconstruction specifically takes place by encoding these harmonics. To do so, an additional static gradient field is introduced to locate the origin of the detected signal and spatial encoding. This field is designed through arranging two magnets in a Maxwell configuration, wherein a symmetric point with zero magnetic field, named as field free point is exhibited. The saturated MNPs out of the FFP cannot follow the excitation field, while the ones inside the FFP are free to align and to be magnetized for contributing to MPI signal generation.<sup>[826]</sup> Subsequently, images can be obtained by sweeping the FFP throughout the imaging field of view (FoV). Specifically, a nearby receiver coil detects the induced magnetization reversal upon the FFP movement over an iron oxide nanoparticle. Finally, two MPI image reconstruction techniques can be used for processing the detected signal: the “system matrix” approach, or x-space MPI.<sup>[827]</sup>

In 2009, Weizenecker et al.<sup>[822b]</sup> injected a mouse with commercially available Resovist MNPs and used a cylindrical support with an inner diameter of 29 mm for keeping the mouse in a supine position. Subsequently the animal was inserted into the receiver coil cylinder of the MPI scanner in a way that its heart was within the FoV. They obtained raw data after bolus injection and reconstructed images to 1800 3D volumes. After MPI scanning of the selected mice, reference MR images were also acquired to relate the MPI signal to the mouse anatomy. **Figure 49** shows the results of interpolating the dynamic MPI data to the corresponding static MRI images.

Resultant images with very high spatial and temporal resolutions were obtained while the heart was actually beating. Their results proved the efficiency of MPI to be used for monitoring cardiac activity in real-time. In a very recent study, iron oxide nanoparticles were doped with zinc to perform a MPI-guided hyperthermia.<sup>[20]</sup> Their results showed a twofold enhancement in MPI signal. In addition, fusion of MPI and hyperthermia allowed for focused and selective heating within the FFP. In particular, by the presence of the static gradient field, the zinc-doped cubic MNPs were potentially saturated outside of FFP and did not contribute to heat generation. In another study, Kuboyabu et al.<sup>[828]</sup> investigated the feasibility of visualizing and quantifying the spatial and temporal distribution of MNPs within a tumor to predict the therapeutic effect of a hyperthermia treatment using MPI. Three groups of treated animal were injected with different concentrations of Resovist to perform a hyperthermia treatment by using an alternative magnetic field. A MPI scanner was used to scan the mice immediately before, immediately after, 7 and 14 d after the treatment (**Figure 50**). MPI images which are superimposed on the X-ray CT images show the qualitative evaluation of the temporal change of the MNPs spatial distribution in tumors. Their results showed the feasibility of MPI for predicting the hyperthermia effect.

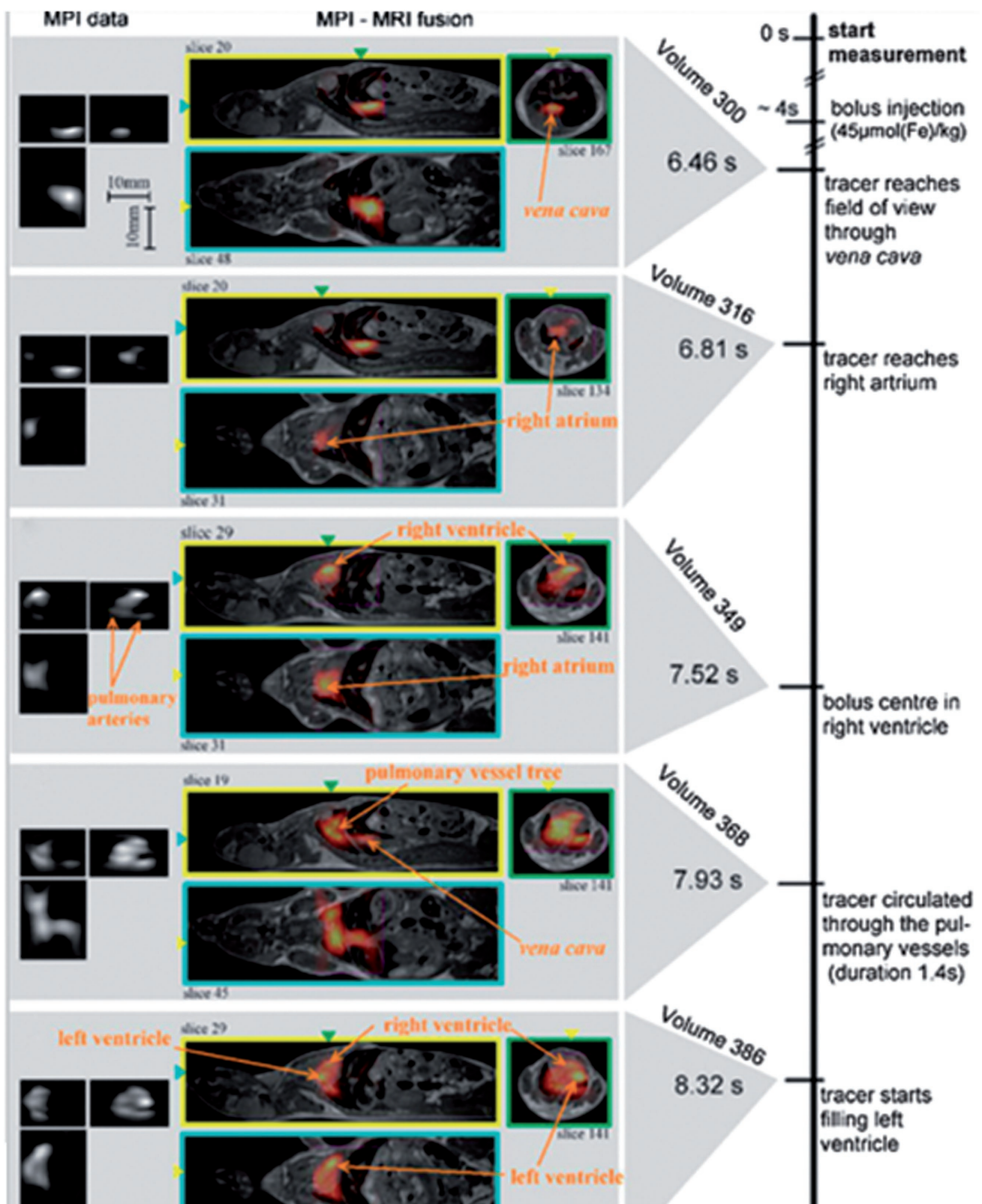


**Figure 49.** Dynamic MPI images of a beating mouse heart (left) and their fusion with corresponding static MR images (right). Reproduced with permission.<sup>[822b]</sup> Copyright 2009, IOP.

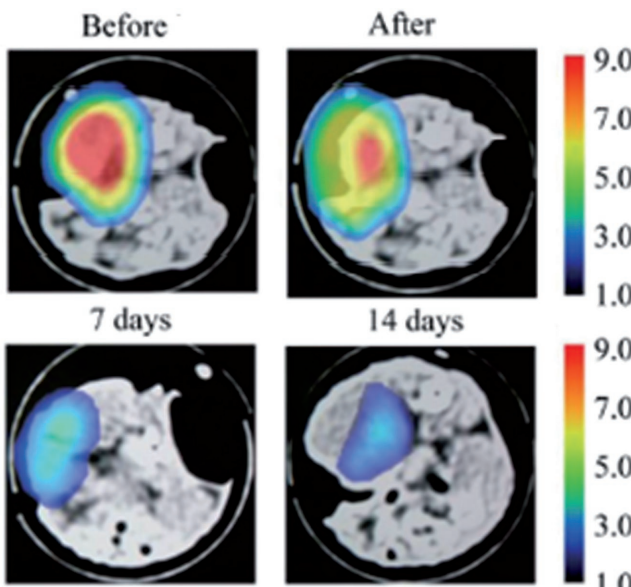


**Figure 50.** MPI superimposed on the X-ray CT images showing the qualitative evaluation of temporal change of MNPs spatial distribution immediately before, immediately after, 7 and 14 d after magnetic hyperthermia. Reproduced with permission.<sup>[828]</sup> Copyright 2016, SCIRP.

#### 5.2.7. PAI

PAI, also called optoacoustic or thermoacoustic, is an interesting hybrid imaging modality based on the photoacoustic effect reported by Alexander Graham Bell in 1880.<sup>[829]</sup> This imaging technique is capable of providing functional imaging based on physiological parameters and thus has gained a widespread acceptance for imaging applications.<sup>[830]</sup> A considerable combination of excellent absorption contrast and high spatial resolution respectively achieved by ultrasound imaging and optical techniques, enables PAI to produce images with high spatial resolution and with sufficient penetration depth simultaneously.<sup>[831]</sup> It relies on detecting the acoustic waves which are produced by the thermoelastic expansion of tissue through the adsorption of electromagnetic energy by chromophores. Specifically, images are produced depending on the absorption magnitude of short pulsed illumination by biological chromophores like melanin and hemoglobin.<sup>[25]</sup> Biological chromophores with strong optical absorbing such as melanin and hemoglobin can be exploited as endogenous contrast agents to provide a non-invasive PAI of these chromophores *in vivo*.<sup>[832]</sup> Although this strategy is practical for visualization of the vasculature tissues, other biological processes with shortage of intrinsic chromophores need additional exogenous contrast for performing PAI. Gold nanoparticles,<sup>[833]</sup> QDs,<sup>[834]</sup> indocyanine green (ICG),<sup>[835]</sup> and single wall nanotubes (SWNTs)<sup>[836]</sup> are of extrinsic contrast agents which enables high optical absorption for better image contrast.<sup>[837]</sup>

Similar to PET, SPECT, and optical imaging, the PAI extrinsic contrast agents can be loaded on iron oxide nanoparticles. In addition to the simultaneous fusion of MRI and PAI to provide better anatomical and functional information, one can make sure that PAI contrast agent has long blood circulation time

and can reach the target thanks to other targeting ligands on the surface of MRI agents. To this end, gold-coated MNPs have been shown as promising agents for MRI/PAI dual imaging applications. In a study performed by Ji et al.<sup>[838]</sup> nanohybrids consisting of iron oxide core and a gold nanoshell were synthesized to investigate their potential for MRI and photothermal therapy. Along with the superparamagnetic behavior, they showed a significant absorbance in the near-infrared region which is essential for PAI. In another study, the feasibility of iron oxide nanoparticle itself to be exploited for dual PAI/MRI imaging was shown.<sup>[25]</sup> The group subcutaneously injected commercial available Endorem MNPs into five Wistar rats and scanned the resected lymph nodes using a tomographic PA setup. PAI detected the iron oxide accumulations in the nodes containing MNPs and the PA response pattern was comparable with the location of MRI signal decrease (**Figure 51**). Their results showed the potential of iron oxide nanoparticles to be used as a PAI contrast agent for lymph node analysis.

## 6. Conclusion

The concept of theranostic applications greatly benefits from the fact that nanobiotechnology has been introducing potential nanoparticles with engineered surfaces to accommodate therapeutics and imaging modalities. Thanks to inherent properties of MNPs such as biodegradability and biocompatibility, along with their high surface to volume ratio, they have been translated into appropriate candidates in theranostic applications. Regarding the implementation of such nanoparticles within the very complex system of the body, it is essential to fulfill a set of design criteria to ensure prolonged blood circulation time as well as efficient cellular internalization for a precise delivery of cargos to the exact area. Since a series of anatomical size

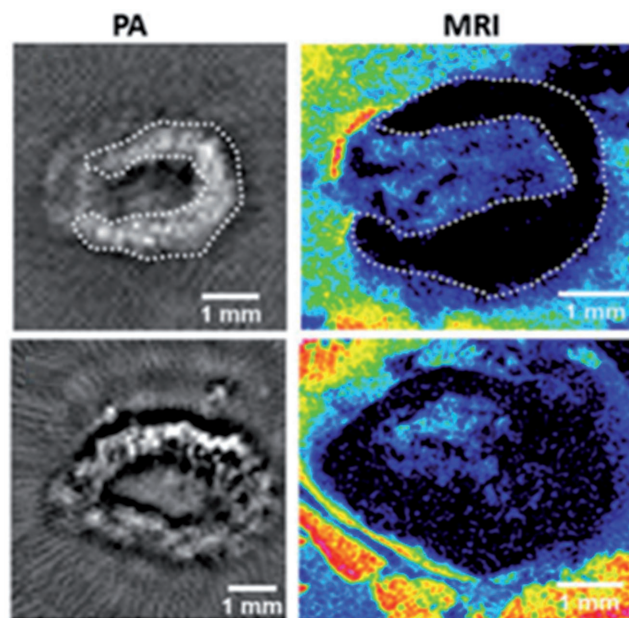


**Figure 51.** Photoacoustic and MR images comparison of lymph nodes. Reproduced with permission.<sup>[25]</sup>

restrictions is exerted by the body, nanoparticles with narrow size distribution range near to the optimum size and shape will be drastically required to prevent their filtration from the bloodstream. On the other hand, surface properties of MNPs such as surface charge and hydrophobicity play an important role in defining their biological identity within the body. To this end, first of all, it is extremely necessary to select an appropriate synthesis and coating strategy which results in MNPs with modulated physicochemical properties, based on optimum design considerations.

Although numerous wet-chemistry routes have been widely used for the batch production of MNPs, they suffer from some of their intrinsic properties, mainly a relative lack of homogeneous reaction environment, ultrafast mixing, high energy-, and time-consuming. Bloom of state-of-the-art microfluidic reactors in the field of chemical synthesis as powerful tools has shrunk the entire chemical and analytical laboratories on a single microchip and provided a precise control over the synthesis of nanoparticles with desired physicochemical properties. The reaction conditions and production of chemicals have been significantly improved thanks to advantages of microfluidic reactors such as small reagent volumes, enhanced heat and mass transfer, automation, continuous synthesis, easy scale out, and most importantly precise control over reaction time which indeed gives a precise control over the shape and size of the resultant nanoparticles. In addition to wet-chemistry routes and microfluidic reactors, biologically inspired synthetic routes have enabled production of MNPs under mild reaction conditions without any need of high pressure, temperature and acidity. Although, magnetosomes exerted from magnetotactic bacteria possess considerable properties for biomedical applications, obtaining high yields of magnetotactic bacteria cells is a primarily major challenge. Overall, poor reproducibility, poor scale up efficiency and poor control over reaction time significantly hinder practical translation of biogenic MNPs into biomedical applications.

Engineering the surface of MNPs, presence of an appropriate coating shell on their surface is significantly important to ensure their stability and also to promote favorable interactions with biological system of the body. Diminishing the agglomeration and water-insolubility of MNPs and protecting them against oxidative or corrosive environments can be reached through appropriate coatings selections. In addition, approaching to more practical theranostic applications requires extensive availability of functional groups to accommodate the imaging, therapeutic and targeting arsenal. Most importantly, a successful limiting of undesirable fouling of protein plasma on the surface of MNPs can be reached by using polymers, copolymers, biomimetic coatings and zwitterionic molecules to practically evade unspecific uptake by RES.

Fundamental principle of theranostic applications is mainly the early diagnostic of disease and its brisk treatment within an effective medical procedure. In the matter of diagnostics, capability of MNPs for multimodal imaging is potentially advantageous for accurate anatomical delineation of cancer tumors simultaneously with precise molecular information. In addition to such a potential imaging capability and drug delivery, the hyperthermia effect of MNPs has also came in handy for tumor ablation and triggering the drug release. Without a

shadow of doubt, successful developments in MNPs biomedical applications will aid a wide range of in vivo and in vitro applications, from cancer imaging, treatment, bioseparation, and immunoassay.

## Conflict of Interest

The authors declare no conflict of interest.

## Keywords

magnetic nanoparticles, microfluidic reactors, multimodal imaging, theranostic applications

Received: March 9, 2017

Revised: June 14, 2017

Published online:

- 
- [1] G. M. Whitesides, *Nat. Biotechnol.* **2003**, *21*, 1161.
  - [2] S. M. Janib, A. S. Moses, J. A. MacKay, *Adv. Drug Delivery Rev.* **2010**, *62*, 1052.
  - [3] D. Yoo, J.-H. Lee, T.-H. Shin, J. Cheon, *Acc. Chem. Res.* **2011**, *44*, 863.
  - [4] A. K. Gupta, M. Gupta, *Biomaterials* **2005**, *26*, 3995.
  - [5] M. Mahmoudi, A. Tachibana, A. B. Goldstone, Y. J. Woo, P. Chakraborty, K. R. Lee, C. S. Foote, S. Piecewicz, J. C. Barrozo, A. Wakeel, *Sci. Rep.* **2016**, *6*, 26960.
  - [6] A. Mendoza-Garcia, S. Sun, *Adv. Funct. Mater.* **2016**, *26*, 3809.
  - [7] E. Fazio, M. Santoro, G. Lentini, D. Franco, S. P. P. Guglielmino, F. Neri, *Colloids Surf., A* **2016**, *490*, 98.
  - [8] M. Lu, A. Ozcelik, C. L. Grigsby, Y. Zhao, F. Guo, K. W. Leong, T. J. Huang, *Nano Today* **2016**, *11*, 778.
  - [9] G. S. Demirer, A. C. Okur, S. Kizilel, *J. Mater. Chem. B* **2015**, *3*, 7831.
  - [10] F. M. Kievit, M. Zhang, *Acc. Chem. Res.* **2011**, *44*, 853.
  - [11] a) O. Veiseh, J. W. Gunn, M. Zhang, *Adv. Drug Delivery Rev.* **2010**, *62*, 284; b) A. Singh, S. K. Sahoo, *Drug Discovery Today* **2014**, *19*, 474; c) J. Gallo, N. J. Long, E. O. Aboagye, *Chem. Soc. Rev.* **2013**, *42*, 7816.
  - [12] M. Mahmoudi, S. Sant, B. Wang, S. Laurent, T. Sen, *Adv. Drug Delivery Rev.* **2011**, *63*, 24.
  - [13] T. Banerjee, S. Mitra, A. K. Singh, R. K. Sharma, A. Maitra, *Int. J. Pharm.* **2002**, *243*, 93.
  - [14] a) S. Tenzer, D. Docter, J. Kuharev, A. Musyanovich, V. Fetz, R. Hecht, F. Schlenk, D. Fischer, K. Kiouptsis, C. Reinhardt, *Nat. Nanotechnol.* **2013**, *8*, 772; b) S. Tenzer, D. Docter, S. Rosfa, A. Włodarski, J. r. Kuharev, A. Rekik, S. K. Knauer, C. Bantz, T. Nawroth, C. Bier, *ACS nano* **2011**, *5*, 7155.
  - [15] P. Charoenphol, R. B. Huang, O. Eniola-Adefeso, *Biomaterials* **2010**, *31*, 1392.
  - [16] R. Savla, O. B. Garbuzenko, S. Chen, L. Rodriguez-Rodriguez, T. Minko, *Pharm. Res.* **2014**, *31*, 3487.
  - [17] a) X. Mou, Z. Ali, S. Li, N. He, *J. Nanosci. Nanotechnol.* **2015**, *15*, 54; b) M. Mahdavi, M. B. Ahmad, M. J. Haron, F. Namvar, B. Nadi, M. Z. A. Rahman, J. Amin, *Molecules* **2013**, *18*, 7533.
  - [18] S. D. Steichen, M. Caldorera-Moore, N. A. Peppas, *Eur. J. Pharm. Sci.* **2013**, *48*, 416.
  - [19] N. D. Thorat, O. Lemine, R. A. Bohara, K. Omri, L. El Mir, S. A. Tofail, *Phys. Chem. Chem. Phys.* **2016**, *18*, 21331.
  - [20] L. M. Bauer, S. F. Situ, M. A. Griswold, A. C. S. Samia, *Nanoscale* **2016**, *8*, 12162.

- [21] A. Lahooti, S. Sarkar, H. S. Rad, A. Gholami, S. Nosrati, R. N. Muller, S. Laurent, C. Grüttner, P. Geramifar, H. Yousefnia, *J. Radioanal. Nucl. Chem.* **2016**, *311*, 769.
- [22] Y. Ma, S. Tong, G. Bao, C. Gao, Z. Dai, *Biomaterials* **2013**, *34*, 7706.
- [23] L. Sandiford, A. Phinikaridou, A. Protti, L. K. Meszaros, X. Cui, Y. Yan, G. Frodsham, P. A. Williamson, N. Gaddum, R. M. Botnar, *ACS Nano* **2012**, *7*, 500.
- [24] J. Zhu, J. Wang, X. Wang, J. Zhu, Y. Yang, J. Tian, W. Cui, C. Ge, Y. Li, Y. Pan, *J. Mater. Chem. B* **2015**, *3*, 6905.
- [25] D. J. Grootendorst, J. Jose, R. M. Fratila, M. Visscher, A. H. Velders, B. Ten Haken, T. G. Van Leeuwen, W. Steenbergen, S. Manohar, T. J. Ruers, *Contrast Media Mol. Imaging* **2013**, *8*, 83.
- [26] A. Espinosa, R. Di Corato, J. Kolosnjaj-Tabi, P. Flaud, T. Pellegrino, C. Wilhelm, *ACS Nano* **2016**.
- [27] S. J. Mattingly, M. G. O'Toole, K. T. James, G. J. Clark, M. H. Nantz, *Langmuir* **2015**, *31*, 3326.
- [28] N. Pramanik, J. De, R. K. Basu, T. Rath, P. P. Kundu, *RSC Adv.* **2016**, *6*, 46116.
- [29] S. Xiao, R. Castro, J. Rodrigues, X. Shi, H. Tomás, *J. Biomed. Nanotechnol.* **2015**, *11*, 1370.
- [30] K. Hola, Z. Markova, G. Zoppellaro, J. Tucek, R. Zboril, *Biotechnol. Adv.* **2015**, *33*, 1162.
- [31] R. Jin, B. Lin, D. Li, H. Ai, *Curr. Opin. Pharmacol.* **2014**, *18*, 18.
- [32] a) T. J. Merkel, K. P. Herlihy, J. Nunes, R. M. Orgel, J. P. Rolland, J. M. DeSimone, *Langmuir* **2009**, *26*, 13086; b) T. Tsuzuki, P. G. McCormick, *J. Mater. Sci.* **2004**, *39*, 5143.
- [33] M. Liong, J. Lu, M. Kovochich, T. Xia, S. G. Ruehm, A. E. Nel, F. Tamanoi, J. I. Zink, *ACS Nano* **2008**, *2*, 889.
- [34] V. Amendola, M. Meneghetti, *Phys. Chem. Chem. Phys.* **2009**, *11*, 3805.
- [35] R. Hudson, Y. Feng, R. S. Varma, A. Moores, *Green Chem.* **2014**, *16*, 4493.
- [36] S. Laurent, D. Forge, M. Port, A. Roch, C. Robic, L. Vander Elst, R. N. Muller, *Chem. Rev.* **2008**, *108*, 2064.
- [37] C.-X. Zhao, A. P. Middelberg, in *Handb. Nanopart.*, (Ed: M. Aliofkhazraei) Springer International Publisher, Cham, **2016**, pp. 455–473.
- [38] D. Faivre, T. U. Godec, *Angew. Chem.* **2015**, *127*, 4810; *Angew. Chem. Int. Ed.* **2015**, *54*, 4728.
- [39] P. M. Valencia, O. C. Farokhzad, R. Karnik, R. Langer, *Nat. Nanotechnol.* **2012**, *7*, 623.
- [40] Y. Song, C. S. Kumar, J. Hormes, *J. Nanosci. Nanotechnol.* **2004**, *4*, 788.
- [41] Y. w. Jun, J. s. Choi, J. Cheon, *Angew. Chem.* **2006**, *37*; *Angew. Chem. Int. Ed.* **2006**, *45*, 3414.
- [42] K. S. Krishna, Y. Li, S. Li, C. S. Kumar, *Adv. Drug Delivery Rev.* **2013**, *65*, 1470.
- [43] J. I. Park, A. Saffari, S. Kumar, A. Günther, E. Kumacheva, *Annu. Rev. Mater. Res.* **2010**, *40*, 415.
- [44] F. X. Gu, R. Karnik, A. Z. Wang, F. Alexis, E. Levy-Nissenbaum, S. Hong, R. S. Langer, O. C. Farokhzad, *Nano Today* **2007**, *2*, 14.
- [45] T. Belin, N. Guique-Millot, T. Caillot, D. Aymes, J. Niepce, *J. Solid State Chem.* **2002**, *163*, 459.
- [46] a) V. F. Puntes, K. Krishnan, A. P. Alivisatos, *Top. Catal.* **2002**, *19*, 145; b) V. F. Puntes, K. M. Krishnan, A. P. Alivisatos, *Science* **2001**, *291*, 2115.
- [47] M. Colombo, S. Carregal-Romero, M. F. Casula, L. Gutierrez, M. P. Morales, I. B. Boehm, J. T. Heverhagen, D. Prosperi, W. J. Parak, *Chem. Soc. Rev.* **2012**, *41*, 4306.
- [48] D. Carta, M. Casula, P. Floris, A. Falqui, G. Mountjoy, A. Boni, C. Sangregorio, A. Corrias, *Phys. Chem. Chem. Phys.* **2010**, *12*, 5074.
- [49] W.-B. Lee, C.-H. Weng, F.-Y. Cheng, C.-S. Yeh, H.-Y. Lei, G.-B. Lee, *Biomed. Microdevices* **2009**, *11*, 161.
- [50] C.-X. Zhao, L. He, S. Z. Qiao, A. P. Middelberg, *Chem. Eng. Sci.* **2011**, *66*, 1463.
- [51] R. Karnik, F. Gu, P. Basto, C. Cannizzaro, L. Dean, W. Kyei-Manu, R. Langer, O. C. Farokhzad, *Nano Lett.* **2008**, *8*, 2906.
- [52] A. Günther, K. F. Jensen, *Lab Chip* **2006**, *6*, 1487.
- [53] L.-H. Hung, K. M. Choi, W.-Y. Tseng, Y.-C. Tan, K. J. Shea, A. P. Lee, *Lab Chip* **2006**, *6*, 174.
- [54] J. H. Bang, K. S. Suslick, *Adv. Mater.* **2010**, *22*, 1039.
- [55] R. Massart, *IEEE Trans. Magn.* **1981**, *17*, 1247.
- [56] N. A. Frey, S. Peng, K. Cheng, S. Sun, *Chem. Soc. Rev.* **2009**, *38*, 2532.
- [57] K. Stojak, H. Srikanth, P. Mukherjee, M.-H. Phan, N. T. K. Thanh, in *Complex-Shaped Metal Nanoparticles*, (Eds: T. K. Sau, A. L. Rogach), Wiley-VCH Verlag GmbH & Co. KGaA, Weinheim, Germany **2012**, pp. 183–214.
- [58] J. Lee, T. Isobe, M. Senna, *J. Colloid Interface Sci.* **1996**, *177*, 490.
- [59] K. M. Krishnan, *IEEE Trans. Magn.* **2010**, *46*, 2523.
- [60] D. Zins, V. Cabuil, R. Massart, *J. Mol. Liq.* **1999**, *83*, 217.
- [61] M.-S. Martina, J.-P. Fortin, C. Ménager, O. Clément, G. Barratt, C. Grabielle-Madelmont, F. Gazeau, V. Cabuil, S. Lesieur, *J. Am. Chem. Soc.* **2005**, *127*, 10676.
- [62] J. Chen, C. Sorensen, K. Klabunde, G. Hadjipanayis, E. Devlin, A. Kostikas, *Phys. Rev. B* **1996**, *54*, 9288.
- [63] Q. Chen, A. J. Rondinone, B. C. Chakoumakos, Z. J. Zhang, *J. Magn. Magn. Mater.* **1999**, *194*, 1.
- [64] Y. S. Kang, S. Risbud, J. F. Rabolt, P. Stroeven, *Chem. Mater.* **1996**, *8*, 2209.
- [65] A. Novakova, V. Y. Lanchinskaya, A. Volkov, T. Gendler, T. Y. Kiseleva, M. Moskvina, S. Zezin, *J. Magn. Magn. Mater.* **2003**, *258*, 354.
- [66] M. Filippousi, M. Angelakeris, M. Katsikini, E. Paloura, I. Efthimiopoulos, Y. Wang, D. Zamboulis, G. Van Tendeloo, *J. Phys. Chem. C* **2014**, *118*, 16209.
- [67] D. Stanicki, S. Boutry, S. Laurent, L. Wacheul, E. Nicolas, D. Crombez, L. Vander Elst, D. L. Lafontaine, R. N. Muller, *J. Mater. Chem. B* **2014**, *2*, 387.
- [68] A. Salunkhe, V. Khot, J. Russo, S. Patil, *RSC Adv.* **2015**, *5*, 18420.
- [69] A. K. Hauser, R. Mathias, K. W. Anderson, J. Z. Hilt, *Mater. Chem. Phys.* **2015**, *160*, 177.
- [70] H.-C. Roth, S. P. Schwaminger, M. Schindler, F. E. Wagner, S. Berensmeier, *J. Magn. Magn. Mater.* **2015**, *377*, 81.
- [71] D. Kumar, H. Singh, S. Jouen, B. Hannoyer, S. Banerjee, *RSC Adv.* **2015**, *5*, 7138.
- [72] S. D. Topel, Ö. Topel, R. B. Bostancioğlu, A. T. Koparal, *Colloids Surf., B* **2015**, *128*, 245.
- [73] R. Bhandari, P. Gupta, T. Dziubla, J. Z. Hilt, *Mater. Sci. Eng., C* **2016**, *67*, 59.
- [74] C. Pereira, A. M. Pereira, C. Fernandes, M. Rocha, R. Mendes, M. P. Fernández-García, A. Guedes, P. B. Tavares, J.-M. Grenèche, J. o. P. Araújo, *Chem. Mater.* **2012**, *24*, 1496.
- [75] J. S. Basuki, A. Jacquemin, L. Esser, Y. Li, C. Boyer, T. P. Davis, *Polym. Chem.* **2014**, *5*, 2611.
- [76] L.-K. Mireles, E. Sacher, L. H. Yahia, S. Laurent, D. Stanicki, *Int. J. Biochem. Cell Biol.* **2015**, *75*, 203.
- [77] L. Shen, Y. Qiao, Y. Guo, S. Meng, G. Yang, M. Wu, J. Zhao, *Ceram. Int.* **2014**, *40*, 1519.
- [78] W. Wu, Q. He, C. Jiang, *ChemInform* **2009**, *40*, i.
- [79] S. Shabestari Khiabani, M. Farshbaf, A. Akbarzadeh, S. Davaran, *Artif. Cells, Nanomed., Biotechnol.* **2016**, *45*, 6.
- [80] H. Hayashi, Y. Hakuta, *Materials* **2010**, *3*, 3794.
- [81] S. R. Dave, X. Gao, *Wiley Interdiscip. Rev.: Nanomed. Nanobiotechnol.* **2009**, *1*, 583.
- [82] J. Liu, Z. Wu, Q. Tian, W. Wu, X. Xiao, *CrystEngComm* **2016**, *18*, 6303.

- [83] a) J. Li, X. Shi, M. Shen, *Part. Part. Syst. Charact.* **2014**, *31*, 1223; b) M. Zhu, Y. Wang, D. Meng, X. Qin, G. Diao, *J. Phys. Chem., C* **2012**, *116*, 16276.
- [84] R. S. Sapieszko, E. Matijević, *J. Colloid Interface Sci.* **1980**, *74*, 405.
- [85] S. Ge, X. Shi, K. Sun, C. Li, C. Uher, J. R. Baker Jr., M. M. Banaszak Holl, B. G. Orr, *J. Phys. Chem., C* **2009**, *113*, 13593.
- [86] W. Cheng, X. Xu, F. Wu, J. Li, *Mater. Lett.* **2016**, *164*, 210.
- [87] a) M. D. de Tercero, M. Bruns, I. G. Martínez, M. Türk, U. Fehrenbacher, S. Jennewein, L. Barner, *Part. Part. Syst. Charact.* **2013**, *30*, 229; b) M.-T. Liang, S.-H. Wang, Y.-L. Chang, H.-I. Hsiang, H.-J. Huang, M.-H. Tsai, W.-C. Juan, S.-F. Lu, *Ceram. Int.* **2010**, *36*, 1131.
- [88] C. Xu, A. S. Teja, *J. Supercrit. Fluids* **2008**, *44*, 85.
- [89] P. Bhavani, C. Rajababu, M. Arif, I. V. S. Reddy, N. R. Reddy, *J. Magn. Magn. Mater.* **2016**.
- [90] S. Gyergyek, D. Makovec, M. Jagodič, M. Drofenik, K. Schenk, O. Jordan, J. Kovač, G. Dražič, H. Hofmann, *J. Alloys Compd.* **2017**, *694*, 261.
- [91] X. Wang, J. Zhuang, Q. Peng, Y. Li, *Nature* **2005**, *437*, 121.
- [92] a) S. Singamaneni, V. N. Bliznyuk, C. Binek, E. Y. Tsymbal, *J. Mater. Chem.* **2011**, *21*, 16819; b) A. H. Lu, E. L. Salabas, F. Schüth, *Angew. Chem.* **2007**, *119*, 1242; *Angew. Chem. Int. Ed.* **2007**, *46*, 1222.
- [93] F. Chen, W. Bu, C. Lu, G. Chen, M. Chen, X. Shen, R. Liu, J. Shi, *J. Nanosci. Nanotechnol.* **2011**, *11*, 10438.
- [94] J. Li, L. Zheng, H. Cai, W. Sun, M. Shen, G. Zhang, X. Shi, *Biomaterials* **2013**, *34*, 8382.
- [95] G. Chatel, D. MacFarlane, *Chem. Soc. Rev.* **2014**, *43*, 8132.
- [96] O. V. Kharissova, B. I. Kharisov, J. J. R. Valdés, U. O. Méndez, *Synth. React. Inorg., Met.-Org., Nano-Met. Chem.* **2011**, *41*, 429.
- [97] D. Dalecki, D. C. Hocking, *Ann. Biomed. Eng.* **2015**, *43*, 747.
- [98] K. S. Suslick, T. Hyeon, M. Fang, *Chem. Mater.* **1996**, *8*, 2172.
- [99] R. Seshadri, in *The Chemistry of Nanomaterials*, (Eds: C. N. R. Rao, A. Müller, A. K. Cheetham), John Wiley & Sons, Weinheim, Germany **2005**, pp. 94–112.
- [100] K. S. Suslick, S.-B. Choe, A. A. Cichowlas, M. W. Grinstaff, *Nature* **1991**, *353*, 414.
- [101] K. S. Suslick, D. A. Hammerton, R. E. Cline, *J. Am. Chem. Soc.* **1986**, *108*, 5641.
- [102] F. Dang, K. Kamada, N. Enomoto, J. Hojo, K. Enpuku, *J. Ceram. Soc. Jpn.* **2007**, *115*, 867.
- [103] E. H. Kim, H. S. Lee, B. K. Kwak, B.-K. Kim, *J. Magn. Magn. Mater.* **2005**, *289*, 328.
- [104] M. N. Islam, J.-R. Jeong, C. Kim, *Thin Solid Films* **2011**, *519*, 8277.
- [105] B. Wang, F. Zhang, J. Qiu, X. Zhang, H. Chen, Y. Du, P. Xu, *Acta Chim. Sinica* **2009**, *67*, 1211.
- [106] M. Abbas, M. Takahashi, C. Kim, *J. Nanopart. Res.* **2013**, *15*, 1.
- [107] J. H. Bang, K. S. Suslick, *J. Am. Chem. Soc.* **2007**, *129*, 2242.
- [108] J. Dai, S. Wu, W. Jiang, P. Li, X. Chen, L. Liu, J. Liu, D. Sun, W. Chen, B. Chen, *J. Magn. Magn. Mater.* **2013**, *331*, 62.
- [109] F. Dang, N. Enomoto, J. Hojo, K. Enpuku, *Ultrasound. Sonochem.* **2010**, *17*, 193.
- [110] a) M. Krieg, M.-P. Pileni, A. Braun, M. Gratzel, *J. Colloid Interface Sci.* **1981**, *83*, 209; b) G. Carrot, J. Valmalette, C. Plummer, S. Scholz, J. Dutta, H. Hofmann, J. Hilborn, *Colloid Polym. Sci.* **1998**, *276*, 853.
- [111] a) J. Lopez-Perez, M. Lopez-Quintela, J. Mira, J. Rivas, *IEEE Trans. Magn.* **1997**, *33*, 4359; b) I. Lisiecki, M. P. Pileni, *J. Am. Chem. Soc.* **1993**, *115*, 3887.
- [112] a) B. Smit, *Phys. Rev. A* **1988**, *37*, 3431; b) M. Telo da Gama, K. Gubbins, *Mol. Phys.* **1986**, *59*, 227.
- [113] P. Luisi, M. Giomini, M. a. Pileni, B. Robinson, *Biochim. Biophys. Acta, Rev. Biomembr.* **1988**, *947*, 209.
- [114] M. Zulauf, H. F. Eicke, *J. Phys. Chem.* **1979**, *83*, 480.
- [115] H.-f. Eicke, J. C. Shepherd, A. Steinemann, *J. Colloid Interface Sci.* **1976**, *56*, 168.
- [116] P. D. Fletcher, B. H. Robinson, *Ber. Bunsenges. Phys. Chem.* **1981**, *85*, 863.
- [117] P. D. Fletcher, A. M. Howe, B. H. Robinson, *J. Chem. Soc. Faraday Trans. Phys. Chem. Condens. Ph.* **1987**, *83*, 985.
- [118] L. Gutiérrez, R. Costo, C. Grüttner, F. Westphal, N. Gehrke, D. Heinke, A. Fornara, Q. Pankhurst, C. Johansson, S. Veintemillas-Verdaguer, *Dalton Trans.* **2015**, *44*, 2943.
- [119] H. F. Eicke, J. Rehak, *Helv. Chim. Acta* **1976**, *59*, 2883.
- [120] M. López-Quintela, J. Rivas, M. Blanco, C. Tojo, in *Nanoscale Materials*, (Eds: L. M. Liz-Marzán, P. V. Kamat), Springer, New York, US **2004**, pp. 135–155.
- [121] B. K. Paul, S. P. Moulik, *Curr. Sci. (Bangalore)* **2001**, *80*, 990.
- [122] a) M. Pileni, *J. Phys. Chem.* **1993**, *97*, 6961; b) C. Petit, P. Lixon, M. P. Pileni, *J. Phys. Chem.* **1993**, *97*, 12974; c) A. Taleb, C. Petit, M. Pileni, *Chem. Mater.* **1997**, *9*, 950; d) M.-P. Pileni, T. Zemb, C. Petit, *Chem. Phys. Lett.* **1985**, *118*, 414; e) C. Petit, M. Pileni, *J. Phys. Chem.* **1988**, *92*, 2282; f) I. Lisiecki, M. Pileni, *J. Phys. Chem.* **1995**, *99*, 5077.
- [123] a) R. Lakshmanan, C. Okoli, M. Boutonnet, S. Järås, G. K. Rajarao, *J. Environ. Chem. Eng.* **2014**, *2*, 185; b) M. T. C. Fernandes, R. B. R. Garcia, C. A. P. Leite, E. Y. Kawachi, *Colloids Surf., A* **2013**, *422*, 136.
- [124] C. Okoli, M. Boutonnet, L. Mariey, S. Järås, G. Rajarao, *J. Chem. Technol. Biotechnol.* **2011**, *86*, 1386.
- [125] T. Lu, J. Wang, J. Yin, A. Wang, X. Wang, T. Zhang, *Colloids Surf., A* **2013**, *436*, 675.
- [126] Y. Zhu, F. Jiang, K. Chen, F. Kang, Z. Tang, *J. Sol-Gel Sci. Technol.* **2013**, *66*, 180.
- [127] B. K. Sodipo, A. A. Aziz, *J. Magn. Magn. Mater.* **2016**, *416*, 275.
- [128] H. Ding, Y. Zhang, S. Wang, J. Xu, S. Xu, G. Li, *Chem. Mater.* **2012**, *24*, 4572.
- [129] O. Veiseh, C. Sun, J. Gunn, N. Kohler, P. Gabikian, D. Lee, N. Bhattachari, R. Ellenbogen, R. Sze, A. Hallahan, *Nano Lett.* **2005**, *5*, 1003.
- [130] R. Hufschmid, H. Arami, R. M. Ferguson, M. Gonzales, E. Teeman, L. N. Brush, N. D. Browning, K. M. Krishnan, *Nanoscale* **2015**, *7*, 11142.
- [131] S. O'Brien, L. Brus, C. B. Murray, *J. Am. Chem. Soc.* **2001**, *123*, 12085.
- [132] C. N. R. Rao, P. J. Thomas, G. U. Kulkarni, *Nanocrystals: Synthesis, Properties and Applications*, Springer Berlin Heidelberg, Germany **2011**, p. 46.
- [133] F. X. Redl, C. T. Black, G. C. Papaefthymiou, R. L. Sandstrom, M. Yin, H. Zeng, C. B. Murray, S. P. O'Brien, *J. Am. Chem. Soc.* **2004**, *126*, 14583.
- [134] N. R. Jana, Y. Chen, X. Peng, *Chem. Mater.* **2004**, *16*, 3931.
- [135] A. C. Samia, K. Hyzer, J. A. Schlueter, C.-J. Qin, J. S. Jiang, S. D. Bader, X.-M. Lin, *J. Am. Chem. Soc.* **2005**, *127*, 4126.
- [136] Y. Li, M. Afzaal, P. O'Brien, *J. Mater. Chem.* **2006**, *16*, 2175.
- [137] W. Y. William, J. C. Falkner, C. T. Yavuz, V. L. Colvin, *Chem. Commun.* **2004**, 2306.
- [138] J. Xie, S. Peng, N. Browne, N. Pourmand, S. X. Wang, S. Sun, *Pure Appl. Chem.* **2006**, *78*, 1003.
- [139] N. T. Thanh, L. A. Green, *Nano Today* **2010**, *5*, 213.
- [140] J. Xie, C. Xu, N. Kohler, Y. Hou, S. Sun, *Adv. Mater.* **2007**, *19*, 3163.
- [141] B. L. Frankamp, N. O. Fischer, R. Hong, S. Srivastava, V. M. Rotello, *Chem. Mater.* **2006**, *18*, 956.
- [142] D. Maity, S. Kale, R. Kaul-Ghanekar, J.-M. Xue, J. Ding, *J. Magn. Magn. Mater.* **2009**, *321*, 3093.
- [143] T. Hyeon, S. S. Lee, J. Park, Y. Chung, H. B. Na, *J. Am. Chem. Soc.* **2001**, *123*, 12798.
- [144] a) J. Van Wonterghem, S. Mørup, S. W. Charles, S. Wells, *J. Colloid Interface Sci.* **1988**, *121*, 558; b) J. Van Wonterghem, S. Mørup,

- S. W. Charles, S. Wells, J. Villadsen, *Hyperfine Interact.* **1986**, 27, 333.
- [145] G. Salazar-Alvarez, J. Qin, V. Sepelak, I. Bergmann, M. Vasilakaki, K. N. Trohidou, J. D. Ardisson, W. A. A. Macedo, M. Mikhaylova, M. Muhammed, M. D. Baró, J. Nogués, *J. Am. Chem. Soc.* **2008**, 130, 13234.
- [146] S. Sun, H. Zeng, D. B. Robinson, S. Raoux, P. M. Rice, S. X. Wang, G. Li, *J. Am. Chem. Soc.* **2004**, 126, 273.
- [147] D. A. Herman, S. Cheong-Tilley, A. J. McGrath, B. F. McVey, M. Lein, R. D. Tilley, *Nanoscale* **2015**, 7, 5951.
- [148] J. Park, K. An, Y. Hwang, J.-G. Park, H.-J. Noh, J.-Y. Kim, J.-H. Park, N.-M. Hwang, T. Hyeon, *Nat. Mater.* **2004**, 3, 891.
- [149] W. Glasgow, B. Fellows, B. Qi, T. Darroudi, C. Kitchens, L. Ye, T. M. Crawford, O. T. Mefford, *Particuology* **2016**, 26, 47.
- [150] a) D. M. P. Mingos, *Chem. Soc. Rev.* **1991**, 20, 1; b) D. R. Baghurst, D. M. P. Mingos, *J. Chem. Soc., Dalton Trans.* **1992**, 1151.
- [151] J. Berlan, *Radiat. Phys. Chem.* **1995**, 45, 581.
- [152] Z. Kozakova, I. Kurikta, N. Kazantseva, V. Babayan, M. Pastorek, M. Machovsky, P. Bazant, P. Saha, *Dalton Trans.* **2015**, 44, 21099.
- [153] S. Riaz, R. Ashraf, A. Akbar, S. Naseem, *IEEE Trans. Magn.* **2014**, 50, 1.
- [154] W.-W. Wang, Y.-J. Zhu, M.-L. Ruan, *J. Nanopart. Res.* **2007**, 9, 419.
- [155] R. Bhavesh, A. V. Lechuga-Vieco, J. Ruiz-Cabello, F. Herranz, *Nanomaterials* **2015**, 5, 1880.
- [156] J.-Y. Hwang, S. Shi, Z. Xu, K. W. Peterson, *Chem. Eng. Commun.* **2006**, 193, 1586.
- [157] L. Gonzalez-Moragas, S.-M. Yu, N. Murillo-Cremaes, A. Laromaine, A. Roig, *Chem. Eng. J.* **2015**, 281, 87.
- [158] B. L. Cushing, V. L. Kolesnichenko, C. J. O'Connor, *Chem. Rev.* **2004**, 104, 3893.
- [159] Q. Guo, X. Teng, S. Rahman, H. Yang, *J. Am. Chem. Soc.* **2003**, 125, 630.
- [160] H. Dai, *Acc. Chem. Res.* **2002**, 35, 1035.
- [161] J. d. Mello, A. d. Mello, *Lab Chip* **2004**, 4, 11N.
- [162] a) S. E. Chung, W. Park, S. Shin, S. A. Lee, S. Kwon, *Nat. Mater.* **2008**, 7, 581; b) J. Wan, W. D. Ristenpart, H. A. Stone, *Proc. Natl. Acad. Sci. USA* **2008**, 105, 16432.
- [163] K. S. Elvira, X. C. i Solvas, R. C. Wootton, *Nat. Chem.* **2013**, 5, 905.
- [164] J. S. L. Philpot, *Trans. Faraday Soc.* **1940**, 35, 38.
- [165] S. C. Terry, *A Gas Chromatography System Fabricated on a Silicon Wafer using Integrated Circuit Technology*, Stanford University, Stanford, USA **1975**.
- [166] A. T. Woolley, R. A. Mathies, *Proc. Natl. Acad. Sci. USA* **1994**, 91, 11348.
- [167] G. M. Whitesides, *Nature* **2006**, 442, 368.
- [168] E. Garcia-Egido, S. Y. Wong, B. H. Warrington, *Lab Chip* **2002**, 2, 31.
- [169] R. Srinivasan, S. Firebaugh, I.-M. Hsing, J. Ryley, M. Harold, K. Jensen, M. Schmidt, Presented at *Int. Conf. Solid State Sens. Actuators, Chemical Performance and High Temperature Characterization of Micromachined Chemical Reactors*, Chicago, June **1997**.
- [170] W. Ehrfeld, K. Golbig, V. Hessel, H. Löwe, T. Richter, *Ind. Eng. Chem. Res.* **1999**, 38, 1075.
- [171] M. C. Mitchell, V. Spikmans, A. Manz, A. J. de Mello, *J. Chem. Soc., Perkin Trans. 1* **2001**, 514.
- [172] J. B. Edel, R. Fortt, *Chem. Commun.* **2002**, 1136.
- [173] T. Thorsen, S. J. Maerkli, S. R. Quake, *Science* **2002**, 298, 580.
- [174] G. H. Seong, R. M. Crooks, *J. Am. Chem. Soc.* **2002**, 124, 13360.
- [175] P. D. Fletcher, S. J. Haswell, E. Pombo-Villar, B. H. Warrington, P. Watts, S. Y. Wong, X. Zhang, *Tetrahedron* **2002**, 58, 4735.
- [176] H. Wang, X. Li, M. Uehara, Y. Yamaguchi, H. Nakamura, M. Miyazaki, H. Shimizu, H. Maeda, *Chem. Commun.* **2004**, 48.
- [177] a) S. Krishnadasan, R. Brown, *Lab Chip* **2007**, 7, 1434; b) L.-H. Hung, A. P. Lee, *J. Med. Biol. Eng.* **2007**, 27, 1.
- [178] V. Sebastián, K. F. Jensen, *Nanoscale* **2016**, 8, 15288.
- [179] J. Hogan, *Nature* **2006**, 442, 351.
- [180] E. M. Chan, A. P. Alivisatos, R. A. Mathies, *J. Am. Chem. Soc.* **2005**, 127, 13854.
- [181] S.-K. Lee, X. Liu, V. S. Cabeza, K. F. Jensen, *Lab Chip* **2012**, 12, 4080.
- [182] S. Gómez-de Pedro, M. Puyol, J. Alonso-Chamarro, *Nanotechnology* **2010**, 21, 415603.
- [183] X. Yao, Y. Zhang, L. Du, J. Liu, J. Yao, *Renew. Sustain. Energy Rev.* **2015**, 47, 519.
- [184] Y. Kikutani, T. Horiuchi, K. Uchiyama, H. Hisamoto, M. Tokeshi, T. Kitamori, *Lab Chip* **2003**, 3, 51.
- [185] K. F. Jensen, *MRS Bull.* **2006**, 31, 101.
- [186] R. Knitter, D. Göhring, P. Risthaus, J. Hausselt, *Microsyst. Technol.* **2001**, 7, 85.
- [187] J. N. Lee, C. Park, G. M. Whitesides, *Anal. Chem.* **2003**, 75, 6544.
- [188] R. L. Hartman, K. F. Jensen, *Lab Chip* **2009**, 9, 2495.
- [189] K. Jähnisch, V. Hessel, H. Löwe, M. Baerns, *Angew. Chem.* **2004**, 116, 410; *Angew. Chem. Int. Ed.* **2004**, 43, 406.
- [190] W. Verboom, *Chem. Eng. Technol.* **2009**, 32, 1695.
- [191] R. Knitter, M. A. Liauw, *Lab Chip* **2004**, 4, 378.
- [192] J. Puigmartí-Luis, *Chem. Soc. Rev.* **2014**, 43, 2253.
- [193] D. Roberge, *Green Process. Synth.* **2012**, 1, 129.
- [194] A. van den Berg, T. Lammerink, in *Microsystem Technology In Chemistry and Life Science*, Springer, Berlin, Germany **1998**, pp. 21–49.
- [195] a) M. Shen, X. Shi, *Nanoscale* **2010**, 2, 1596; b) S. J. Soenen, P. Rivera-Gil, J.-M. Montenegro, W. J. Parak, S. C. De Smedt, K. Braeckmans, *Nano Today* **2011**, 6, 446.
- [196] Y. Song, J. Hormes, C. S. Kumar, *Small* **2008**, 4, 698.
- [197] a) C. B. Murray, C. Kagan, M. Bawendi, *Annu. Rev. Mater. Sci.* **2000**, 30, 545; b) A. Abou-Hassan, O. Sandre, V. Cabuil, *Angew. Chem.* **2010**, 122, 6408; *Angew. Chem. Int. Ed.* **2010**, 49, 6268.
- [198] B. Fadeel, A. E. Garcia-Bennett, *Adv. Drug Delivery Rev.* **2010**, 62, 362.
- [199] M. Tokeshi, T. Minagawa, K. Uchiyama, A. Hibara, K. Sato, H. Hisamoto, T. Kitamori, *Anal. Chem.* **2002**, 74, 1565.
- [200] D. Hönicke, *Stud. Surf. Sci. Catal.* **1999**, 122, 47.
- [201] C.-H. Chang, B. K. Paul, V. T. Remcho, S. Atre, J. E. Hutchison, *J. Nanopart. Res.* **2008**, 10, 965.
- [202] a) A. Mello, *Nature* **2006**, 447, 394; b) P. Yager, T. Edwards, E. Fu, K. Helton, K. Nelson, M. R. Tam, B. H. Weigl, *Nature* **2006**, 442, 412.
- [203] L. Sasias, J. Autebert, L. Malaquin, J.-L. Viovy, *Lab Chip* **2011**, 11, 822.
- [204] B. Pieber, C. O. Kappe, *Green Chem.* **2013**, 15, 320.
- [205] T. Wada, T. Maki, K. Mae, Presented at *Int. Conf. Microreact. Technol. (IMRET), Control of Nuclei Formation and Particle Growth for Nanoparticles by a Multistage Reaction System with Series of Micromixers*, Kyoto, March **2010**.
- [206] K. Geyer, J. D. Codee, P. H. Seeberger, *Chem.-Eur. J.* **2006**, 12, 8434.
- [207] S. J. Haswell, P. Watts, *Green Chem.* **2003**, 5, 240.
- [208] A. Jahn, J. E. Reiner, W. N. Vreeland, D. L. DeVoe, L. E. Locascio, M. Gaitan, *J. Nanopart. Res.* **2008**, 10, 925.
- [209] J. Boleininger, A. Kurz, V. Reuss, C. Sönnichsen, *Phys. Chem. Chem. Phys.* **2006**, 8, 3824.
- [210] Y. Ying, G. Chen, Y. Zhao, S. Li, Q. Yuan, *Chem. Eng. J.* **2008**, 135, 209.
- [211] J. i. Yoshida, in *Flash Chemistry*, Wiley Online Library, London, UK **2008**, pp. 1–225.
- [212] B. K. Yen, A. Günther, M. A. Schmidt, K. F. Jensen, M. G. Bawendi, *Angew. Chem.* **2005**, 117, 5583; *Angew. Chem. Int. Ed.* **2005**, 44, 5447.
- [213] G. Luo, L. Du, Y. Wang, Y. Lu, J. Xu, *Particuology* **2011**, 9, 545.
- [214] H. Nakamura, Y. Yamaguchi, M. Miyazaki, H. Maeda, M. Uehara, P. Mulvaney, *Chem. Commun.* **2002**, 2844.

- [215] M. Simmons, N. Jones, D. Evans, C. Wiles, P. Watts, S. Salamon, M. E. Castillo, H. Wende, D. Lupascu, M. Francesconi, *Lab Chip* **2015**, *15*, 3154.
- [216] F. C. Cabrera, A. F. Melo, J. C. de Souza, A. E. Job, F. N. Crespihlo, *Lab Chip* **2015**, *15*, 1835.
- [217] M. Wen, Q. Li, Y. Li, *J. Electron. Spectrosc. Relat. Phenom.* **2006**, *153*, 65.
- [218] M. Simmons, C. Wiles, V. Rocher, M. G. Francesconi, P. Watts, *J. Flow Chem.* **2013**, *3*, 7.
- [219] V. T. Thu, A. N. Mai, H. Van Trung, P. T. Thu, B. Q. Tien, N. T. Thuat, T. Dai Lam, *J. Electron. Mater.* **2016**, *45*, 2576.
- [220] J. Ma, J. Wang, X. Zhong, G. Li, Y. Song, *RSC Adv.* **2016**, *6*, 84255.
- [221] M. Takagi, T. Maki, M. Miyahara, K. Mae, *Chem. Eng. J.* **2004**, *101*, 269.
- [222] A. A. Hassan, O. Sandre, V. Cabuil, P. Tabeling, *Chem. Commun.* **2008**, *1783*.
- [223] A. Abou-Hassan, S. Neveu, V. Dupuis, V. Cabuil, *RSC Adv.* **2012**, *2*, 11263.
- [224] A. Abou-Hassan, R. Bazzi, V. Cabuil, *Angew. Chem.* **2009**, *101*, 7316; *Angew. Chem. Int. Ed.* **2009**, *48*, 7180.
- [225] T. N. Nguyen, H. J. Joen, B. H. Kwon, H. H. Kim, K. Mortan, J. S. Go, *J. Mater. Sci.* **2014**, *49*, 4583.
- [226] A. Abou-Hassan, J.-F. Dufrêche, O. Sandre, G. Mériguet, O. Bernard, V. Cabuil, *J. Phys. Chem., C* **2009**, *113*, 18097.
- [227] H. Song, D. L. Chen, R. F. Ismagilov, *Angew. Chem.* **2006**, *118*, 7494; *Angew. Chem. Int. Ed.* **2006**, *45*, 7336.
- [228] K. Handique, D. Burke, C. Mastrangelo, M. Burns, *Anal. Chem.* **2001**, *73*, 1831.
- [229] A. Larrea, V. Sebastian, A. Ibarra, M. Arruebo, J. Santamaria, *Chem. Mater.* **2015**, *27*, 4254.
- [230] H. Song, J. D. Tice, R. F. Ismagilov, *Angew. Chem.* **2003**, *115*, 792; *Angew. Chem. Int. Ed.* **2003**, *42*, 768.
- [231] I. Shestopalov, J. D. Tice, R. F. Ismagilov, *Lab Chip* **2004**, *4*, 316.
- [232] L. Frenz, A. El Harrak, M. Pauly, S. Bégin-Colin, A. D. Griffiths, J. C. Baret, *Angew. Chem.* **2008**, *120*, 6923; *Angew. Chem. Int. Ed.* **2008**, *47*, 6817.
- [233] K. Kumar, A. M. Nightingale, S. H. Krishnadasan, N. Kamaly, M. Wylenzinska-Arridge, K. Zeissler, W. R. Branford, E. Ware, *J. Mater. Chem.* **2012**, *22*, 4704.
- [234] R. K. Shah, H. C. Shum, A. C. Rowat, D. Lee, J. J. Agresti, A. S. Utada, L.-Y. Chu, J.-W. Kim, A. Fernandez-Nieves, C. J. Martinez, *Mater. Today* **2008**, *11*, 18.
- [235] V. Hessel, S. Hardt, H. Löwe, F. Schönfeld, *AIChE J.* **2003**, *49*, 566.
- [236] a) D. Gobby, P. Angeli, A. Gavrilidis, *J. Micromech. Microeng.* **2001**, *11*, 126; b) A. Soleymani, E. Kolehmainen, I. Turunen, *Chem. Eng. J.* **2008**, *135*, S219.
- [237] a) F. G. Bessoth, A. Manz, *Anal. Commun.* **1999**, *36*, 213; b) T. M. Floyd, M. A. Schmidt, K. F. Jensen, *Ind. Eng. Chem. Res.* **2005**, *44*, 2351.
- [238] a) S. W. Lee, D. S. Kim, S. S. Lee, T. H. Kwon, *J. Micromech. Microeng.* **2006**, *16*, 1067; b) A. D. Radadia, L. Cao, H.-K. Jeong, M. A. Shannon, R. I. Masel, presented at *Micro Electro Mechanical Systems, 2007. MEMS. IEEE 20th International Conf. on, A 3D Micro-mixer Fabricated With Dry Film Resist*, Hyogo, Japan, January **2007**.
- [239] J. B. Knight, A. Vishwanath, J. P. Brody, R. H. Austin, *Phys. Rev. Lett.* **1998**, *80*, 3863.
- [240] a) C. Leong, J. Ottino, *J. Fluid Mech.* **1989**, *209*, 463; b) H. Chen, J.-C. Meiners, *Appl. Phys. Lett.* **2004**, *84*, 2193.
- [241] a) I. Glasgow, N. Aubry, *Lab Chip* **2003**, *3*, 114; b) C. Y. Lim, Y. C. Lam, C. Yang, *Biomicrofluidics* **2010**, *4*, 014101.
- [242] a) R.-J. Yang, C.-H. Wu, T.-I. Tseng, S.-B. Huang, G.-B. Lee, *Jpn. J. Appl. Phys.* **2005**, *44*, 7634; b) J. D. Posner, J. G. Santiago, *J. Fluid Mech.* **2006**, *555*, 1.
- [243] a) H.-Y. Lee, J. Voldman, *Anal. Chem.* **2007**, *79*, 1833; b) G. Goet, T. Baier, S. Hardt, *Lab Chip* **2009**, *9*, 3586.
- [244] a) P. Paik, V. K. Pamula, M. G. Pollack, R. B. Fair, *Lab Chip* **2003**, *3*, 28; b) J. Fowler, H. Moon, C. K. Chang-Jin, Presented at *Proceedings, IEEE Micro Electro Mechanical Systems, Enhancement of Mixing by Droplet-Based Microfluidics*, Las Vegas, USA, January **2002**.
- [245] a) J. West, B. Karamata, B. Lillis, J. P. Gleeson, J. Alderman, J. K. Collins, W. Lane, A. Mathewson, H. Berney, *Lab Chip* **2002**, *2*, 224; b) D.-W. Oh, J. S. Jin, J. H. Choi, H.-Y. Kim, J. S. Lee, *J. Micromech. Microeng.* **2007**, *17*, 2077.
- [246] a) Z. Yang, S. Matsumoto, H. Goto, M. Matsumoto, R. Maeda, *Sens. Actuators, A* **2001**, *93*, 266; b) L.-S. Jang, S.-H. Chao, M. R. Holl, D. R. Meldrum, *Sens. Actuators, A* **2007**, *138*, 179.
- [247] G. G. Yaralioglu, I. O. Wygant, T. C. Marentis, B. T. Khuri-Yakub, *Anal. Chem.* **2004**, *76*, 3694.
- [248] N.-T. Nguyen, Z. Wu, *J. Micromech. Microeng.* **2004**, *15*, R1.
- [249] A. Larrea, V. Sebastian, M. Arruebo, J. Santamaria, *Int. J. Chem. Mol. Nucl. Mater. Metall.* **2015**, *9*, 780.
- [250] F. Kök, in *Low-Dimensional and Nanostructured Materials and Devices*, Springer, Cham, Switzerland **2016**, pp. 535–553.
- [251] C. Moisescu, I. I. Ardelean, L. G. Benning, *Intracell. Biominer. Bact.* **2014**, *5*, 49.
- [252] S. S. Staniand, in *Nanotechnol. Life Sci.*, Vol. 4 (Ed: Challa S. S. R. Kumar), Wiley-VCH Verlag GmbH & Co. KGaA, Weinheim **2007**, pp. 399–431.
- [253] K. Zeth, E. Hoiczyk, M. Okuda, *Trends Biochem. Sci.* **2016**, *41*, 190.
- [254] R. Wiltschko, *Magnetic Orientation in Animals*, Springer Berlin Heidelberg, Germany **2012**, p. 17.
- [255] B. A. Maher, *Proc. R. Soc. Lond., Ser. B* **1998**, *265*, 733.
- [256] F. T. De Araujo, M. Pires, R. B. Frankel, C. Bicudo, *Biophys. J.* **1986**, *50*, 375.
- [257] H. A. Lowenstam, *Science* **1981**, *211*, 1126.
- [258] H. A. Lowenstam, S. Weiner, *Biomineralization*, Oxford University Press, **1989**.
- [259] R. B. Frankel, D. A. Bazylinski, *Rev. Mineral. Geochem.* **2003**, *54*, 95.
- [260] C. Jimenez-Lopez, C. S. Romanek, D. A. Bazylinski, *J. Geophys. Res.: Biogeosci.* **2010**, *115*.
- [261] J. Xie, K. Chen, X. Chen, *Nano Res.* **2009**, *2*, 261.
- [262] S. Bellini, *Su di un Particolare Comportamento di Batteri d'acqua dolce*, Instituto di Microbiologia dell'Università di Pavia Pavia, Italy **1963**.
- [263] R. Blakemore, *Science* **1975**, *190*, 377.
- [264] D. Faivre, D. Schuler, *Chem. Rev.* **2008**, *108*, 4875.
- [265] J. W. Fassbinder, H. Stanjek, H. Vali, *Nature* **1990**, *343*, 161.
- [266] A. Arakaki, H. Nakazawa, M. Nemoto, T. Mori, T. Matsunaga, *J. R. Soc., Interface* **2008**, *5*, 977.
- [267] A. Isambert, N. Menguy, E. Larquet, F. Guyot, J.-P. Valet, *Am. Mineral.* **2007**, *92*, 621.
- [268] A. Komeili, *FEMS Microbiol. Rev.* **2012**, *36*, 232.
- [269] A. Körnig, J. Dong, M. Bennet, M. Widdrat, J. Andert, F. D. Müller, D. Schüler, S. Klumpp, D. Faivre, *Nano Lett.* **2014**, *14*, 4653.
- [270] Y. A. Gorby, T. J. Beveridge, R. P. Blakemore, *J. Bacteriol.* **1988**, *170*, 834.
- [271] D. A. Bazylinski, A. J. Garratt-Reed, R. B. Frankel, *Microsc. Res. Tech.* **1994**, *27*, 389.
- [272] K. Grünberg, E.-C. Müller, A. Otto, R. Reszka, D. Linder, M. Kube, R. Reinhardt, D. Schüler, *Appl. Environ. Microbiol.* **2004**, *70*, 1040.
- [273] R. B. Frankel, R. P. Blakemore, R. S. Wolfe, *Science* **1979**, *203*, 1355.
- [274] S. Mann, N. C. Sparks, R. B. Frankel, D. A. Bazylinski, H. W. Jannasch, *Nature* **1990**, *343*, 258.
- [275] C. T. Lefevre, F. Abreu, U. Lins, D. A. Bazylinski, in *Metal Nanoparticles in Microbiology*, Springer, Heidelberg, Germany **2011**, pp. 75–102.
- [276] K. Iwahori, I. Yamashita, *J. Cluster Sci.* **2007**, *18*, 358.
- [277] T. Matsunaga, P. Tadokoro, N. Nakamura, *IEEE Trans. Magn.* **1990**, *26*, 1557.

- [278] Y. Zhang, X. Zhang, W. Jiang, Y. Li, J. Li, *Appl. Environ. Microbiol.* **2011**, *77*, 5851.
- [279] E. Alphandéry, I. Chebbi, F. Guyot, M. Durand-Dubief, *Int. J. Hyperthermia* **2013**, *29*, 801.
- [280] Y. Liu, G. R. Li, F. F. Guo, W. Jiang, Y. Li, L. J. Li, *Microb. Cell Fact.* **2010**, *9*, 1.
- [281] C. T. Lefèvre, D. A. Bazylinski, *Microbiol. Mol. Biol. Rev.* **2013**, *77*, 497.
- [282] Y. Li, S. Bali, S. Borg, E. Katzmann, S. J. Ferguson, D. Schüler, *J. Bacteriol.* **2013**, *195*, 4297.
- [283] U. Heyen, D. Schüler, *Appl. Microbiol. Biotechnol.* **2003**, *61*, 536.
- [284] J.-B. Sun, F. Zhao, T. Tang, W. Jiang, J.-s. Tian, Y. Li, J.-L. Li, *Appl. Microbiol. Biotechnol.* **2008**, *79*, 389.
- [285] K. T. Silva, P. E. Leão, F. Abreu, J. A. López, M. L. Gutarra, M. Farina, D. A. Bazylinski, D. M. Freire, U. Lins, *Appl. Environ. Microbiol.* **2013**, *79*, 2823.
- [286] F. Guo, Y. Liu, Y. Chen, T. Tang, W. Jiang, Y. Li, J. Li, *Appl. Microbiol. Biotechnol.* **2011**, *90*, 1277.
- [287] R. J. Usselman, M. Klem, M. Allen, E. D. Walter, K. Gilmore, T. Douglas, M. Young, Y. Idzerda, D. Singel, *J. Appl. Phys.* **2005**, *97*, 10M523.
- [288] A. Arakaki, J. Webb, T. Matsunaga, *J. Biol. Chem.* **2003**, *278*, 8745.
- [289] L. Wang, T. Prozorov, P. E. Palo, X. Liu, D. Vaknin, R. Prozorov, S. Mallapragada, M. Nilsen-Hamilton, *Biomacromolecules* **2011**, *13*, 98.
- [290] A. Arakaki, F. Masuda, Y. Amemiya, T. Tanaka, T. Matsunaga, *J. Colloid Interface Sci.* **2010**, *343*, 65.
- [291] L. Wang, M. Nilsen-Hamilton, *Front. Biol.* **2013**, *8*, 234.
- [292] P. K. Ajikumar, S. Vivekanandan, R. Lakshminarayanan, S. D. Jois, R. M. Kini, S. Valiyaveettil, *Angew.* **2005**, *117*, 5612; *Angew. Chem. Int. Ed.* **2005**, *44*, 5476.
- [293] Y. Amemiya, A. Arakaki, S. S. Staniland, T. Tanaka, T. Matsunaga, *Biomaterials* **2007**, *28*, 5381.
- [294] H. Zhang, X. Liu, S. Feng, W. Wang, K. Schmidt-Rohr, M. Akinc, M. Nilsen-Hamilton, D. Vaknin, S. Mallapragada, *Langmuir* **2015**, *31*, 2818.
- [295] J. J. Lenders, C. L. Altan, P. H. Bornans, A. Arakaki, S. Bucak, G. de With, N. A. Sommerdijk, *Cryst. Growth Des.* **2014**, *14*, 5561.
- [296] J. M. Galloway, J. P. Bramble, A. E. Rawlings, G. Burnell, S. D. Evans, S. S. Staniland, *Nano Res.* **2012**, *17*, 127.
- [297] S. M. Bird, J. M. Galloway, A. E. Rawlings, J. P. Bramble, S. S. Staniland, *Nanoscale* **2015**, *7*, 7340.
- [298] S. M. Bird, A. E. Rawlings, J. M. Galloway, S. S. Staniland, *RSC Adv.* **2016**, *6*, 7356.
- [299] V. Bansal, D. Rautaray, A. Ahmad, M. Sastry, *J. Mater. Chem.* **2004**, *14*, 3303.
- [300] a) R. Ramanathan, V. Bansal, in *Bio-Nanoparticles*, John Wiley & Sons, Inc. **2015**, pp. 31–51; b) V. Bansal, R. Ramanathan, S. K. Bhargava, *Aust. J. Chem.* **2011**, *64*, 279.
- [301] A. Bhardwaj, D. Rautaray, V. Bansal, A. Ahmad, I. Sarkar, S. M. Yusuf, M. Sanyal, M. Sastry, *Small* **2006**, *2*, 135.
- [302] a) S. Basiruddin, A. Saha, N. Pradhan, N. R. Jana, *J. Phys. Chem., C* **2010**, *114*, 11009; b) N. Erathodiyil, J. Y. Ying, *Acc. Chem. Res.* **2011**, *44*, 925.
- [303] A. Agarwala, N. Kaynan, S. Zaidiner, R. Yerushalmi, *Chem. Commun.* **2014**, *50*, 5397.
- [304] C. Sun, J. S. Lee, M. Zhang, *Adv. Drug Delivery Rev.* **2008**, *60*, 1252.
- [305] S. Gomez-Lopera, R. Plaza, A. Delgado, *J. Colloid Interface Sci.* **2001**, *240*, 40.
- [306] Z. Karimi, L. Karimi, H. Shokrollahi, *Mater. Sci. Eng., C* **2013**, *33*, 2465.
- [307] R. Toy, K. Roy, *Bioeng. Transl. Med.* **2016**.
- [308] S. Laurent, A. A. Saei, S. Behzadi, A. Panahifar, M. Mahmoudi, *Expert Opin. Drug Delivery* **2014**, *11*, 1449.
- [309] N. J. Turro, P. Lakshminarasimhan, S. Jockusch, S. P. O'Brien, S. G. Grancharov, F. X. Redl, *Nano Lett.* **2002**, *2*, 325.
- [310] K. Turcheniuk, A. V. Tarasevych, V. P. Kukhar, R. Boukherroub, S. Szunerits, *Nanoscale* **2013**, *5*, 10729.
- [311] A. Bee, R. Massart, S. Neveu, *J. Magn. Magn. Mater.* **1995**, *149*, 6.
- [312] C. Liu, P. Huang, *Soil Sci. Soc. Am. J.* **1999**, *63*, 65.
- [313] S. Mallakpour, M. Madani, *Prog. Org. Coat.* **2015**, *86*, 194.
- [314] Y. Sahoo, H. Pizem, T. Fried, D. Golodnitsky, L. Burstein, C. N. Sukenik, G. Markovich, *Langmuir* **2001**, *17*, 7907.
- [315] a) M. Muthiah, I.-K. Park, C.-S. Cho, *Expert Opin. Drug Delivery* **2013**, *10*, 1259; b) L. M. Bronstein, Z. B. Shifrina, *Chem. Rev.* **2011**, *111*, 5301.
- [316] H. Tian, Z. Tang, X. Zhuang, X. Chen, X. Jing, *Prog. Polym. Sci.* **2012**, *37*, 237.
- [317] a) M. Anbarasu, M. Anandan, E. Chinnasamy, V. Gopinath, K. Balamurugan, *Spectrochim. Acta, Part A* **2015**, *135*, 536; b) T. Blin, A. Kakinen, E. H. Pilkington, A. Ivask, F. Ding, J. F. Quinn, M. R. Whittaker, P. C. Ke, T. P. Davis, *Polym. Chem.* **2016**, *7*, 1931.
- [318] H. Cho, D. Alcantara, H. Yuan, R. A. Sheth, H. H. Chen, P. Huang, S. B. Andersson, D. E. Sosnovik, U. Mahmood, L. Josephson, *ACS Nano* **2013**, *7*, 2032.
- [319] S. R. Bhattarai, R. B. Kc, S. Aryal, M. S. Khil, H. Y. Kim, *Carbohydr. Polym.* **2007**, *69*, 467.
- [320] T.-H. Chung, C.-C. Hsieh, J.-K. Hsiao, S.-C. Hsu, M. Yao, D.-M. Huang, *RSC Adv.* **2016**, *6*, 45553.
- [321] P. C. Naha, A. Al Zaki, E. Hecht, M. Chorny, P. Chhour, E. Blankemeyer, D. M. Yates, W. R. Witschey, H. I. Litt, A. Tsourkas, *J. Mater. Chem. B* **2014**, *2*, 8239.
- [322] Y. Sun, Z.-I. Chen, X.-x. Yang, P. Huang, X.-p. Zhou, X.-x. Du, *Nanotechnology* **2009**, *20*, 135102.
- [323] a) B. Pelaz, P. del Pino, P. Maffre, R. Hartmann, M. Gallego, S. Rivera-Fernández, J. M. de la Fuente, G. U. Nienhaus, W. J. Parak, *ACS Nano* **2015**, *9*, 6996; b) A. Ruiz, G. Salas, M. Calero, Y. Hernández, A. Villanueva, F. Herranz, S. Veintemillas-Verdaguer, E. Martínez, D. Barber, M. Morales, *Acta Biomater.* **2013**, *9*, 6421.
- [324] a) H. Y. Lee, N. H. Lim, J. A. Seo, S. H. Yuk, B. K. Kwak, G. Khang, H. B. Lee, S. H. Cho, *J. Biomed. Mater. Res., Part B* **2006**, *79*, 142; b) J. Huang, L. Bu, J. Xie, K. Chen, Z. Cheng, X. Li, X. Chen, *ACS Nano* **2010**, *4*, 7151.
- [325] a) M. Mahmoudi, A. Simchi, M. Imani, A. S. Milani, P. Stroeve, *J. Phys. Chem., B* **2008**, *112*, 14470; b) L. E. Udrea, D. Hritcu, M. I. Popa, O. Rotariu, *J. Magn. Magn. Mater.* **2011**, *323*, 7.
- [326] L. Xiong, T. Yang, Y. Yang, C. Xu, F. Li, *Biomaterials* **2010**, *31*, 7078.
- [327] a) F. Danhier, E. Ansorena, J. M. Silva, R. Coco, A. Le Breton, V. Préat, *J. Controlled Release* **2012**, *161*, 505; b) E. A. Sander, A. M. Alb, E. A. Nauman, W. F. Reed, K. C. Dee, *J. Biomed. Mater. Res., Part A* **2004**, *70*, 506.
- [328] a) C. Tassa, S. Y. Shaw, R. Weissleder, *Acc. Chem. Res.* **2011**, *44*, 842; b) M. G. Harisinghani, J. Barentsz, P. F. Hahn, W. M. Deserno, S. Tabatabaei, C. H. van de Kaa, J. de la Rosette, R. Weissleder, *N. Engl. J. Med.* **2003**, *348*, 2491.
- [329] a) J.-P. Chen, P.-C. Yang, Y.-H. Ma, T. Wu, *Carbohydr. Polym.* **2011**, *84*, 364; b) M. Mahmoudi, A. Simchi, M. Imani, *J. Iran. Chem. Soc.* **2010**, *7*, S1.
- [330] a) B. Gaihre, M. S. Khil, D. R. Lee, H. Y. Kim, *Int. J. Pharm.* **2009**, *365*, 180; b) B. Gaihre, M. S. Khil, H. K. Kang, H. Y. Kim, *J. Mater. Sci.: Mater. Med.* **2009**, *20*, 573.
- [331] a) D. K. Kim, M. Mikhaylova, F. H. Wang, J. Kehr, B. Bjelke, Y. Zhang, T. Tsakalatos, M. Muhammed, *Chem. Mater.* **2003**, *15*, 4343; b) A. J. Cole, A. E. David, J. Wang, C. J. Galbán, H. L. Hill, V. C. Yang, *Biomaterials* **2011**, *32*, 2183.

- [332] a) L. G. Bach, M. R. Islam, J. T. Kim, S. Seo, K. T. Lim, *Appl. Surf. Sci.* **2012**, 258, 2959; b) Z. Guo, L. L. Henry, V. Palshin, E. J. Podlaha, *J. Mater. Chem.* **2006**, 16, 1772.
- [333] a) Z. Huang, F. Tang, *J. Colloid Interface Sci.* **2004**, 275, 142; b) Y. Xie, R. Sougrat, S. P. Nunes, *J. Appl. Polym. Sci.* **2015**, 132, <http://onlinelibrary.wiley.com/wol1/doi/10.1002/app.41368/abstract>.
- [334] a) E. Ebrahimi, A. Akbarzadeh, E. Abbasi, A. A. Khandaghi, F. Abasalizadeh, S. Davaran, *Artif. Cells, Nanomed., Biotechnol.* **2016**, 44, 290; b) O. Veiseh, F. M. Kievit, J. W. Gunn, B. D. Ratner, M. Zhang, *Biomaterials* **2009**, 30, 649.
- [335] a) C. Prashant, M. Dipak, C.-T. Yang, K.-H. Chuang, D. Jun, S.-S. Feng, *Biomaterials* **2010**, 31, 5588; b) N. Bhattacharai, F. A. Matsen, M. Zhang, *Macromol. Biosci.* **2005**, 5, 107.
- [336] F. M. Kievit, O. Veiseh, N. Bhattacharai, C. Fang, J. W. Gunn, D. Lee, R. G. Ellenbogen, J. M. Olson, M. Zhang, *Adv. Funct. Mater.* **2009**, 19, 2244.
- [337] K. Chen, J. Xie, H. Xu, D. Behera, M. H. Michalski, S. Biswal, A. Wang, X. Chen, *Biomaterials* **2009**, 30, 6912.
- [338] X. Gao, Y. Cui, R. M. Levenson, L. W. Chung, S. Nie, *Nat. Biotechnol.* **2004**, 22, 969.
- [339] H. Chen, L. Wang, J. Yeh, X. Wu, Z. Cao, Y. A. Wang, M. Zhang, L. Yang, H. Mao, *Biomaterials* **2010**, 31, 5397.
- [340] M.-H. Hsiao, Q. Mu, Z. R. Stephen, C. Fang, M. Zhang, *ACS Macro Lett.* **2015**, 4, 403.
- [341] A. Guerrero-Martínez, J. Pérez-Juste, L. M. Liz-Marzáñ, *Adv. Mater.* **2010**, 22, 1182.
- [342] a) G. Kılıç, C. Costa, N. Fernández-Bertólez, E. Pásaro, J. P. Teixeira, B. Laffon, V. Valdignesias, *Toxicol. Res.* **2016**, 5, 235; b) Y. Zhu, C. Tao, *RSC Adv.* **2015**, 5, 22365; c) J. Park, J. Joo, S. G. Kwon, Y. Jang, T. Hyeon, *Angew. Chem. Int. Ed.* **2007**, 46, 4630.
- [343] P. Ashtari, X. He, K. Wang, P. Gong, *Talanta* **2005**, 67, 548.
- [344] a) S. L. Pinho, G. A. Pereira, P. Voisin, J. Kassem, V. Bouchaud, L. Etienne, J. A. Peters, L. Carlos, S. Mornet, C. F. Geraldes, *ACS Nano* **2010**, 4, 5339; b) M. Z. Iqbal, X. Ma, T. Chen, L. e. Zhang, W. Ren, L. Xiang, A. Wu, *J. Mater. Chem. B* **2015**, 3, 5172.
- [345] M. Arruebo, R. Fernández-Pacheco, M. R. Ibarra, J. Santamaría, *Nano Today* **2007**, 2, 22.
- [346] R. Alwi, S. Telenkov, A. Mandelis, T. Leshuk, F. Gu, S. Oladepo, K. Michaelian, *Biomed. Opt. Express* **2012**, 3, 2500.
- [347] A. P. Philipse, M. P. Van Bruggen, C. Pathmamanoharan, *Langmuir* **1994**, 10, 92.
- [348] S. Kyeong, C. Jeong, H. Kang, H.-J. Cho, S.-J. Park, J.-K. Yang, S. Kim, H.-M. Kim, B.-H. Jun, Y.-S. Lee, *PloS One* **2015**, 10, e0143727.
- [349] W. Stöber, A. Fink, E. Bohn, *J. Colloid Interface Sci.* **1968**, 26, 62.
- [350] R. P. Bagwe, C. Yang, L. R. Hilliard, W. Tan, *Langmuir* **2004**, 20, 8336.
- [351] Q. Huo, J. Liu, L.-Q. Wang, Y. Jiang, T. N. Lambert, E. Fang, *J. Am. Chem. Soc.* **2006**, 128, 6447.
- [352] J. E. Lee, N. Lee, T. Kim, J. Kim, T. Hyeon, *Acc. Chem. Res.* **2011**, 44, 893.
- [353] W. Zhao, J. Gu, L. Zhang, H. Chen, J. Shi, *J. Am. Chem. Soc.* **2005**, 127, 8916.
- [354] M. Kuzminská, N. Carlier, R. Backov, E. M. Gaigneaux, *Appl. Catal., A* **2015**, 505, 200.
- [355] J. Kim, J. E. Lee, J. Lee, J. H. Yu, B. C. Kim, K. An, Y. Hwang, C.-H. Shin, J.-G. Park, J. Kim, *J. Am. Chem. Soc.* **2006**, 128, 688.
- [356] J.-H. Jeong, S. W. Hong, S. Hong, S. Yook, Y. Jung, J.-B. Park, C. D. Khue, B.-H. Im, J. Seo, H. Lee, *Biomaterials* **2011**, 32, 7961.
- [357] F.-H. Chen, L.-M. Zhang, Q.-T. Chen, Y. Zhang, Z.-J. Zhang, *Chem. Commun.* **2010**, 46, 8633.
- [358] J. Kim, H. S. Kim, N. Lee, T. Kim, H. Kim, T. Yu, I. C. Song, W. K. Moon, T. Hyeon, *Angew. Chem. Int. Ed.* **2008**, 47, 8438.
- [359] T. Kim, E. Momin, J. Choi, K. Yuan, H. Zaidi, J. Kim, M. Park, N. Lee, M. T. McMahon, A. Quinones-Hinojosa, *J. Am. Chem. Soc.* **2011**, 133, 2955.
- [360] C. R. Thomas, D. P. Ferris, J.-H. Lee, E. Choi, M. H. Cho, E. S. Kim, J. F. Stoddart, J.-S. Shin, J. Cheon, J. I. Zink, *J. Am. Chem. Soc.* **2010**, 132, 10623.
- [361] L. Lou, K. Yu, Z. Zhang, R. Huang, J. Zhu, Y. Wang, Z. Zhu, *Nano Res.* **2012**, 5, 272.
- [362] Y. Okada, T. Y. Takano, N. Kobayashi, A. Hayashi, M. Yonekura, Y. Nishiyama, T. Abe, T. Yoshida, T. A. Yamamoto, S. Seino, *Bioconjugate Chem.* **2011**, 22, 887.
- [363] G. K. Kouassi, P. Wang, S. Sreevatan, J. Irudayaraj, *Biotechnol. Prog.* **2007**, 23, 1239.
- [364] U. Turner, Y. Gündoğdu, İ. H. Boyaci, K. Pekmez, *J. Nanopart. Res.* **2010**, 12, 1187.
- [365] H.-Y. Xie, R. Zhen, B. Wang, Y.-J. Feng, P. Chen, J. Hao, *J. Phys. Chem. C* **2010**, 114, 4825.
- [366] S. Banerjee, S. Raja, M. Sardar, N. Gayathri, B. Ghosh, A. Dasgupta, *J. Appl. Phys.* **2011**, 109, 123902.
- [367] D. M. Fouad, W. A. El-Said, M. B. Mohamed, *Spectrochim. Acta, Part A* **2015**, 140, 392.
- [368] S.-J. Cho, J.-C. Idrobo, J. Olamit, K. Liu, N. D. Browning, S. M. Kauzlarich, *Chem. Mater.* **2005**, 17, 3181.
- [369] a) V. Arora, A. Sood, J. Shah, R. Kotnala, T. K. Jain, *Mater. Chem. Phys.* **2016**, 173, 161; b) B. K. Sodipo, A. A. Aziz, M. Mustapa, *Int. J. Nanoelectron. Mater.* **2015**, 8, 1.
- [370] T. Liu, D. Li, D. Yang, M. Jiang, *Colloids Surf., A* **2011**, 387, 17.
- [371] T. Pham, J. B. Jackson, N. J. Halas, T. R. Lee, *Langmuir* **2002**, 18, 4915.
- [372] J. L. Lyon, D. A. Fleming, M. B. Stone, P. Schiffer, M. E. Williams, *Nano Lett.* **2004**, 4, 719.
- [373] J. Zhang, M. Post, T. Veres, Z. J. Jakubek, J. Guan, D. Wang, F. Normandin, Y. Deslandes, B. Simard, *J. Phys. Chem., B* **2006**, 110, 7122.
- [374] J. Bao, W. Chen, T. Liu, Y. Zhu, P. Jin, L. Wang, J. Liu, Y. Wei, Y. Li, *Acs Nano* **2007**, 1, 293.
- [375] I. Y. Goon, L. M. Lai, X. Wang, M. Lim, D. Leech, R. Amal, J. J. Gooding, presented at *Int. Conf. Nanosci. Nanotechnol. (ICNN)*. *Thiol Functionalisation of Gold-Coated Magnetic Nanoparticles: Enabling the Controlled Attachment of Functional Molecules*, Thessaloniki, Greece, September **2010**.
- [376] J. Kolosnjai-Tabi, Y. Javed, L. Lartigue, J. Volatron, D. Elgrabli, I. Marangon, G. Pugliese, B. Caron, A. Figuerola, N. Luciani, *ACS Nano* **2015**, 9, 7925.
- [377] B. L. Oliva, A. Pradhan, D. Caruntu, C. J. O'Connor, M. A. Tarr, *J. Mater. Res.* **2006**, 21, 1312.
- [378] a) F. Evanics, P. Diamente, F. Van Veggel, G. Stanisz, R. Prosser, *Chem. Mater.* **2006**, 18, 2499; b) F. Hu, L. Wei, Z. Zhou, Y. Ran, Z. Li, M. Gao, *Adv. Mater.* **2006**, 18, 2553.
- [379] R. Qiao, C. Yang, M. Gao, *J. Mater. Chem.* **2009**, 19, 6274.
- [380] M. R. Kumar, R. A. Muzzarelli, C. Muzzarelli, H. Sashiwa, A. Domb, *Chem. Rev.* **2004**, 104, 6017.
- [381] K. J. Landmark, S. DiMaggio, J. Ward, C. Kelly, S. Vogt, S. Hong, A. Kotlyar, A. Myc, T. P. Thomas, J. E. Penner-Hahn, *ACS Nano* **2008**, 2, 773.
- [382] a) J.-L. Bridot, A.-C. Faure, S. Laurent, C. Rivière, C. Billotey, B. Hiba, M. Janier, V. Josserand, J.-L. Coll, L. Vander Elst, *J. Am. Chem. Soc.* **2007**, 129, 5076; b) Y. Zhang, C. Sun, N. Kohler, M. Zhang, *Biomed. Microdevices* **2004**, 6, 33.
- [383] a) W. W. Yu, E. Chang, J. C. Falkner, J. Zhang, A. M. Al-Somali, C. M. Sayes, J. Johns, R. Drezek, V. L. Colvin, *J. Am. Chem. Soc.* **2007**, 129, 2871; b) C. Barcena, A. K. Sra, G. S. Chaubey, C. Khemtong, J. P. Liu, J. Gao, *Chem. Commun.* **2008**, 2224.
- [384] D. S. Achilleos, M. Vamvakaki, *Materials* **2010**, 3, 1981.
- [385] N. Tomczak, R. Liu, J. G. Vancso, *Nanoscale* **2013**, 5, 12018.

- [386] C. Fang, M. Zhang, *J. Mater. Chem.* **2009**, *19*, 6258.
- [387] Y. Wang, J. F. Wong, X. Teng, X. Z. Lin, H. Yang, *Nano Lett.* **2003**, *3*, 1555.
- [388] a) A. P. Goodwin, S. M. Tabakman, K. Welsher, S. P. Sherlock, G. Prencipe, H. Dai, *J. Am. Chem. Soc.* **2008**, *131*, 289; b) S.-H. Choi, H. B. Na, Y. I. Park, K. An, S. G. Kwon, Y. Jang, M.-h. Park, J. Moon, J. S. Son, I. C. Song, *J. Am. Chem. Soc.* **2008**, *130*, 15573.
- [389] C. A. J. Lin, R. A. Sperling, J. K. Li, T. Y. Yang, P. Y. Li, M. Zanella, W. H. Chang, W. J. Parak, *Small* **2008**, *4*, 334.
- [390] a) A. M. Smith, H. Duan, M. N. Rhyner, G. Ruan, S. Nie, *Phys. Chem. Chem. Phys.* **2006**, *8*, 3895; b) T. Pons, H. T. Uyeda, I. L. Medintz, H. Mattoissi, *J. Phys. Chem., B* **2006**, *110*, 20308.
- [391] a) J. Aldana, N. Lavelle, Y. Wang, X. Peng, *J. Am. Chem. Soc.* **2005**, *127*, 2496; b) J. Aldana, Y. A. Wang, X. Peng, *J. Am. Chem. Soc.* **2001**, *123*, 8844.
- [392] S. Minko, in *Polymer Surfaces and Interfaces*, (Ed: M. Stamm), Springer, Heidelberg, Germany **2008**, pp. 215–234.
- [393] a) S. T. Milner, T. Witten, M. Cates, *Macromolecules* **1988**, *21*, 2610; b) P. Akcora, H. Liu, S. K. Kumar, J. Moll, Y. Li, B. C. Benicewicz, L. S. Schadler, D. Acehan, A. Z. Panagiotopoulos, V. Pryamitsyn, *Nat. Mater.* **2009**, *8*, 354.
- [394] a) M. E. Piotti, *Curr. Opin. Solid State Mater. Sci.* **1999**, *4*, 539; b) C. W. Bielawski, R. H. Grubbs, *Prog. Polym. Sci.* **2007**, *32*, 1.
- [395] a) R. Jordan, A. Ulman, *J. Am. Chem. Soc.* **1998**, *120*, 243; b) R. Jordan, N. West, A. Ulman, Y.-M. Chou, O. Nuyken, *Macromolecules* **2001**, *34*, 1606.
- [396] a) K. Hong, D. Uhrig, J. W. Mays, *Curr. Opin. Solid State Mater. Sci.* **1999**, *4*, 531; b) N. Hadjichristidis, M. Pitsikalis, S. Pispas, H. Iatrou, *Chem. Rev.* **2001**, *101*, 3747.
- [397] a) T. Saegusa, E. Goethals, *Ring-Opening Polymerization*, ACS Publications, **1977**; p; b) D. A. Foucher, B. Z. Tang, I. Manners, *J. Am. Chem. Soc.* **1992**, *114*, 6246; c) M. Save, M. Schappacher, A. Soum, *Macromol. Chem. Phys.* **2002**, *203*, 889.
- [398] a) S. Gaynor, D. Greszta, D. Mardare, M. Teodorescu, K. Matyjaszewski, *J. Macromol. Sci., Part A* **1994**, *31*, 1561; b) D. Bertin, B. Boutevin, *Polym. Bull.* **1996**, *37*, 337; c) K. Matyjaszewski, *Curr. Opin. Solid State Mater. Sci.* **1996**, *1*, 769.
- [399] W. C. Wang, K. G. Neoh, E. T. Kang, *Macromol. Rapid Commun.* **2006**, *27*, 1665.
- [400] M. Lattuada, T. A. Hatton, *Langmuir* **2007**, *23*, 2158.
- [401] E. Giovanelli, E. Muro, G. Sitbon, M. Hanafi, T. Pons, B. Dubertret, N. Lequeux, *Langmuir* **2012**, *28*, 15177.
- [402] T. Shen, R. Weissleder, M. Papisov, A. Bogdanov, T. J. Brady, *Magn. Reson. Med.* **1993**, *29*, 599.
- [403] T. Zhang, J. Ge, Y. Hu, Y. Yin, *Nano Lett.* **2007**, *7*, 3203.
- [404] Y. Lee, H. Lee, Y. B. Kim, J. Kim, T. Hyeon, H. Park, P. B. Messersmith, T. G. Park, *Adv. Mater.* **2008**, *20*, 4154.
- [405] J.-F. Lutz, S. Stiller, A. Hoth, L. Kaufner, U. Pison, R. Cartier, *Biomacromolecules* **2006**, *7*, 3132.
- [406] C. Xu, J. Xie, D. Ho, C. Wang, N. Kohler, E. G. Walsh, J. R. Morgan, Y. E. Chin, S. Sun, *Angew. Chem.* **2008**, *120*, 179; *Angew. Chem. Int. Ed.* **2008**, *47*, 173.
- [407] M. Kim, Y. Chen, Y. Liu, X. Peng, *Adv. Mater.* **2005**, *17*, 1429.
- [408] a) N. R. Jana, C. Earhart, J. Y. Ying, *Chem. Mater.* **2007**, *19*, 5074; b) R. De Palma, S. Peeters, M. J. Van Bael, H. Van den Rul, K. Bonroy, W. Laureyn, J. Mullens, G. Borghs, G. Maes, *Chem. Mater.* **2007**, *19*, 1821.
- [409] Z. Liu, W. Cai, L. He, N. Nakayama, K. Chen, X. Sun, X. Chen, H. Dai, *Nat. Nanotechnol.* **2007**, *2*, 47.
- [410] Y.-w. Jun, Y.-M. Huh, J.-s. Choi, J.-H. Lee, H.-T. Song, S. Kim, S. Kim, S. Yoon, K.-S. Kim, J.-S. Shin, *J. Am. Chem. Soc.* **2005**, *127*, 5732.
- [411] Y. Zhang, N. Kohler, M. Zhang, *Biomaterials* **2002**, *23*, 1553.
- [412] V. P. Torchilin, *Nat. Rev. Drug Discovery* **2005**, *4*, 145.
- [413] A. Khalid, S. Persano, H. Shen, Y. Zhao, E. Blanco, M. Ferrari, J. Wolfram, *Expert Opin. Drug Delivery* **2016**, *14*, 865.
- [414] M. Longmire, P. L. Choyke, H. Kobayashi, **2008**.
- [415] a) V. J. Venditto, F. C. Szoka, *Adv. Drug Delivery Rev.* **2013**, *65*, 80; b) K. Park, *ACS Nano* **2013**, *7*, 7442.
- [416] L. A. Lane, X. Qian, A. M. Smith, S. Nie, *Annu. Rev. Phys. Chem.* **2015**, *66*, 521.
- [417] H. H. Gustafson, D. Holt-Casper, D. W. Grainger, H. Chandehari, *Nano Today* **2015**, *10*, 487.
- [418] D. E. Owens, N. A. Peppas, *Int. J. Pharm.* **2006**, *307*, 93.
- [419] E. Blanco, H. Shen, M. Ferrari, *Nat. Biotechnol.* **2015**, *33*, 941.
- [420] S. Schöttler, K. Landfester, V. Mailänder, *Angew. Chem.* **2016**, *128*, 8950; *Angew. Chem. Int. Ed.* **2016**, *55*, 8806.
- [421] G. Caracciolo, O. C. Farokhzad, M. Mahmoudi, *Trends Biotechnol.* **2016**, *35*, 257.
- [422] C. D. Walkey, W. C. Chan, *Chem. Soc. Rev.* **2012**, *41*, 2780.
- [423] a) M. Mahmoudi, N. Bertrand, H. Zope, O. C. Farokhzad, *Nano Today* **2016**, *11*, 817; b) M. S. Ehrenberg, A. E. Friedman, J. N. Finkelstein, G. Oberdörster, J. L. McGrath, *Biomaterials* **2009**, *30*, 603.
- [424] M. Schäffler, M. Semmler-Behnke, H. Sarioglu, S. Takenaka, A. Wenk, C. Schlehe, S. M. Hauck, B. D. Johnston, W. G. Kreyling, *Nanotechnology* **2013**, *24*, 265103.
- [425] X. Duan, Y. Li, *Small* **2013**, *9*, 1521.
- [426] a) K. Thode, M. Lück, W. Semmler, R. H. Müller, M. Kresse, *Pharm. Res.* **1997**, *14*, 905; b) T. Cedervall, I. Lynch, M. Foy, T. Berggård, S. C. Donnelly, G. Cagney, S. Linse, K. A. Dawson, *Angew. Chem.* **2007**, *119*, 5856; *Angew. Chem. Int. Ed.* **2007**, *46*, 5754.
- [427] a) M. Roser, D. Fischer, T. Kissel, *Eur. J. Pharm. Biopharm.* **1998**, *46*, 255; b) Y. Yamamoto, Y. Nagasaki, Y. Kato, Y. Sugiyama, K. Kataoka, *J. Controlled Release* **2001**, *77*, 27; c) K. Xiao, Y. Li, J. Luo, J. S. Lee, W. Xiao, A. M. Gonik, R. G. Agarwal, K. S. Lam, *Biomaterials* **2011**, *32*, 3435.
- [428] M. Rahman, S. Laurent, N. Tawil, L. Yahia, M. Mahmoudi, *Protein-Nanoparticle Interactions*, Springer, Heidelberg, Germany **2013**, *p*. 31.
- [429] C. Chouly, D. Pouliquen, I. Lucet, J. Jeune, P. Jallet, *J. Microencapsul.* **1996**, *13*, 245.
- [430] a) J. S. Suk, Q. Xu, N. Kim, J. Hanes, L. M. Ensign, *Adv. Drug Delivery Rev.* **2016**, *99*, 28; b) T. Ishii, K. Miyata, Y. Anraku, M. Naito, Y. Yi, T. Jinbo, S. Takae, Y. Fukusato, M. Hori, K. Osada, *Chem. Commun.* **2016**, *52*, 1517.
- [431] C. von Roemeling, W. Jiang, C. K. Chan, I. L. Weissman, B. Y. Kim, *Trends Biotechnol.* **2016**, *35*, 159.
- [432] S. Schöttler, G. Becker, S. Winzen, T. Steinbach, K. Mohr, K. Landfester, V. Mailänder, F. R. Wurm, *Nat. Nanotechnol.* **2016**, *11*, 372.
- [433] M. Aoyama, K. Hata, K. Higashisaka, K. Nagano, Y. Yoshioka, Y. Tsutsumi, *Biochem. Biophys. Res. Commun.* **2016**, *480*, 690.
- [434] Q. Hu, Z. Gu, in *Nanotechnology: Delivering on the Promise*, Vol. 2, (Eds: H. N. Cheng, L. Doemeny, C. L. Geraci, D. G. Schmidt), ACS Publications, US **2016**, pp. 197–211.
- [435] A. S. A. Lila, H. Kiwada, T. Ishida, *J. Controlled Release* **2013**, *172*, 38.
- [436] D. F. Moyano, K. Saha, G. Prakash, B. Yan, H. Kong, M. Yazdani, V. M. Rotello, *ACS Nano* **2014**, *8*, 6748.
- [437] W. Gao, L. Zhang, *J. Drug Targeting* **2015**, *23*, 619.
- [438] A. Kroll, R. H. Fang, L. Zhang, *Bioconjugate Chem.* **2016**, *28*, 23.
- [439] a) X. Ren, R. Zheng, X. Fang, X. Wang, X. Zhang, W. Yang, X. Sha, *Biomaterials* **2016**, *92*, 13; b) M. Bhateria, R. Rachumallu, R. Singh, R. S. Bhatta, *Expert Opin. Drug Delivery* **2014**, *11*, 1219.
- [440] a) R. Palomba, A. Parodi, M. Evangelopoulos, S. Acciardo, C. Corbo, E. De Rosa, I. Yazdi, S. Scaria, R. Molinaro, N. T. Furman, *Sci. Rep.* **2016**, *6*, 34422; b) A. Parodi, N. Quattrochi, A. L. Van De Ven,

- C. Chiappini, M. Evangelopoulos, J. O. Martinez, B. S. Brown, S. Z. Khaled, I. K. Yazdi, M. V. Enzo, *Nat. Nanotechnol.* **2013**, *8*, 61.
- [441] a) Q. Hu, W. Sun, C. Qian, C. Wang, H. N. Bomba, Z. Gu, *Adv. Mater.* **2015**, *27*, 7014; b) C.-M. J. Hu, R. H. Fang, K.-C. Wang, B. T. Luk, S. Thamphiwatana, D. Dehainai, P. Nguyen, P. Angsanikul, C. H. Wen, A. V. Kroll, *Nature* **2015**, *526*, 118.
- [442] M. Xuan, J. Shao, L. Dai, J. Li, Q. He, *ACS Appl. Mater. Interfaces* **2016**, *8*, 9610.
- [443] a) P. L. Rodriguez, T. Harada, D. A. Christian, D. A. Pantano, R. K. Tsai, D. E. Discher, *Science* **2013**, *339*, 971; b) J. E. Tengood, R. J. Levy, S. J. Stachelek, *Exp. Biol. Med.* **2016**, *241*, 1033.
- [444] Z. Pang, C.-M. J. Hu, R. H. Fang, B. T. Luk, W. Gao, F. Wang, E. Chuluun, P. Angsanikul, S. Thamphiwatana, W. Lu, *ACS Nano* **2015**, *9*, 6450.
- [445] P.-Y. Lai, R.-Y. Huang, S.-Y. Lin, Y.-H. Lin, C.-W. Chang, *RSC Adv.* **2015**, *5*, 98222.
- [446] a) N. Hoshyar, S. Gray, H. Han, G. Bao, *Nanomedicine* **2016**, *11*, 673; b) Y. Yoshioka, K. Higashisaka, Y. Tsutsumi, in *Nanomater. Pharmacol.*, (Eds: Z.-R. Lu, S. Sakuma), Springer New York, New York, NY **2016**, pp. 185–199.
- [447] P. Decuzzi, M. Ferrari, *Biomaterials* **2006**, *27*, 5307.
- [448] M. D. Chavanpatil, A. Khadair, J. Panyam, *J. Nanosci. Nanotechnol.* **2006**, *6*, 2651.
- [449] J. V. Jokerst, T. Lobovkina, R. N. Zare, S. S. Gambhir, *Nanomedicine* **2011**, *6*, 715.
- [450] I. Posadas, S. Monteagudo, V. Ceña, *Nanomedicine* **2016**, *11*, 833.
- [451] S.-D. Li, L. Huang, *Mol. Pharmaceutics* **2008**, *5*, 496.
- [452] a) L. Li, T. Liu, C. Fu, L. Tan, X. Meng, H. Liu, *Nanomed.: Nanotechnol., Biol. Med.* **2015**, *11*, 1915; b) X. Lin, N. Zhao, P. Yan, H. Hu, F.-J. Xu, *Acta Biomater.* **2015**, *11*, 381.
- [453] a) A. A. Chen, A. M. Derfus, S. R. Khetani, S. N. Bhatia, *Nucleic Acids Res.* **2005**, *33*, e190; b) Y. Geng, P. Dalhaimer, S. Cai, R. Tsai, M. Tewari, T. Minko, D. E. Discher, *Nat. Nanotechnol.* **2007**, *2*, 249.
- [454] a) Y. Matsumura, H. Maeda, *Cancer Res.* **1986**, *46*, 6387; b) H. Maeda, *Adv. Drug Delivery Rev.* **2001**, *46*, 169.
- [455] a) R. K. Jain, *J. Controlled Release* **2001**, *74*, 7; b) R. K. Jain, *Annu. Rev. Biomed. Eng.* **1999**, *1*, 241.
- [456] D. Bates, N. Hillman, B. Williams, C. Neal, T. Pocock, *J. Anat.* **2002**, *200*, 581.
- [457] R. K. Jain, T. Stylianopoulos, *Nat. Rev. Clin. Oncol.* **2010**, *7*, 653.
- [458] S. E. McNeil, *J. Leukocyte Biol.* **2005**, *78*, 585.
- [459] M. A. Swartz, *Adv. Drug Delivery Rev.* **2001**, *50*, 3.
- [460] T. P. Padera, B. R. Stoll, J. B. Tooredman, D. Capen, E. di Tomaso, R. K. Jain, *Nature* **2004**, *427*, 695.
- [461] X. Xu, W. Ho, X. Zhang, N. Bertrand, O. Farokhzad, *Trends Mol. Med.* **2015**, *21*, 223.
- [462] N. Bertrand, J. Wu, X. Xu, N. Kamaly, O. C. Farokhzad, *Adv. Drug Delivery Rev.* **2014**, *66*, 2.
- [463] J. M Rabanel, V. Aoun, I. Elkin, M. Mokhtar, P. Hildgen, *Curr. Med. Chem.* **2012**, *19*, 3070.
- [464] J. C. Firrell, H. H. Lipowsky, *Am. J. Physiol.: Heart Circ. Physiol.* **1989**, *256*, H1667.
- [465] a) L. Chen, J. M. McCrate, J. C. Lee, H. Li, *Nanotechnology* **2011**, *22*, 105708; b) R. R. Arvizu, O. R. Miranda, M. A. Thompson, C. M. Pabelick, R. Bhattacharya, J. D. Robertson, V. M. Rotello, Y. Prakash, P. Mukherjee, *Nano Lett.* **2010**, *10*, 2543.
- [466] T.-R. Lee, M. Choi, A. M. Kopacz, S.-H. Yun, W. K. Liu, P. Decuzzi, *Sci. Rep.* **2013**, *3*.
- [467] a) R. Toy, E. Hayden, C. Shoup, H. Baskaran, E. Karathanasis, *Nanotechnology* **2011**, *22*, 115101; b) J. Tan, A. Thomas, Y. Liu, *Soft matter* **2012**, *8*, 1934.
- [468] a) B. D. Chithrani, A. A. Ghazani, W. C. Chan, *Nano Lett.* **2006**, *6*, 662; b) H. Margus, P. Arukuusk, U. I. Langel, M. Pooga, *Mol. Pharmaceutics* **2015**, *13*, 172; c) S.-H. Wang, C.-W. Lee, A. Chiou, P.-K. Wei, *J. Nanobiotechnol.* **2010**, *8*, 1; d) F. Lu, S. H. Wu, Y. Hung, C. Y. Mou, *Small* **2009**, *5*, 1408.
- [469] R. Savla, T. Minko, *Adv. Drug Delivery Rev.* **2017**, *113*, 122.
- [470] Z. Popović, W. Liu, V. P. Chauhan, J. Lee, C. Wong, A. B. Greystak, N. Insin, D. G. Nocera, D. Fukumura, R. K. Jain, *Angew. Chem.* **2010**, *122*, 8831; *Angew. Chem. Int. Ed.* **2010**, *49*, 8649.
- [471] a) F. Gentile, C. Chiappini, D. Fine, R. Bhavane, M. Peluccio, M. M.-C. Cheng, X. Liu, M. Ferrari, P. Decuzzi, *J. Biomech.* **2008**, *41*, 2312; b) S.-Y. Lee, M. Ferrari, P. Decuzzi, *Nanotechnology* **2009**, *20*, 495101.
- [472] a) P. Decuzzi, R. Pasqualini, W. Arap, M. Ferrari, *Pharm. Res.* **2009**, *26*, 235; b) Y. Li, Y. Lian, L. T. Zhang, S. M. Aldousari, H. S. Hedia, S. A. Asiri, W. K. Liu, *Interface Focus* **2016**, *6*, 20150086.
- [473] a) J. A. Champion, S. Mitragotri, *Proc. Natl. Acad. Sci. USA* **2006**, *103*, 4930; b) S. E. Gratton, P. A. Ropp, P. D. Pohlhaus, J. C. Luft, V. J. Madden, M. E. Napier, J. M. DeSimone, *Proc. Natl. Acad. Sci. USA* **2008**, *105*, 11613.
- [474] U. Prabhakar, H. Maeda, R. K. Jain, E. M. Sevick-Muraca, W. Zamboni, O. C. Farokhzad, S. T. Barry, A. Gabizon, P. Grodzinski, D. C. Blakey, *Cancer Res.* **2013**, *73*, 2412.
- [475] R. Sinha, G. J. Kim, S. Nie, D. M. Shin, *Mol. Cancer Ther.* **2006**, *5*, 1909.
- [476] L. D. Leserman, J. N. Weinstein, R. Blumenthal, W. D. Terry, *Proc. Natl. Acad. Sci. USA* **1980**, *77*, 4089.
- [477] N. Kamaly, Z. Xiao, P. M. Valencia, A. F. Radovic-Moreno, O. C. Farokhzad, *Chem. Soc. Rev.* **2012**, *41*, 2971.
- [478] a) A. Koshkaryev, R. Sawant, M. Deshpande, V. Torchilin, *Adv. Drug Delivery Rev.* **2013**, *65*, 24; b) Z. Cheng, A. Al Zaki, J. Z. Hui, V. R. Muzykantov, A. Tsourkas, *Science* **2012**, *338*, 903.
- [479] a) A. des Rieux, V. Pourcelle, P. D. Cani, J. Marchand-Brynaert, V. Préat, *Adv. Drug Delivery Rev.* **2013**, *65*, 833; b) B. Yu, H. C. Tai, W. Xue, L. J. Lee, R. J. Lee, *Mol. Membr. Biol.* **2010**, *27*, 286.
- [480] J. Wang, S. Tian, R. A. Petros, M. E. Napier, J. M. DeSimone, *J. Am. Chem. Soc.* **2010**, *132*, 11306.
- [481] A. T. Florence, *J. Controlled Release* **2012**, *164*, 115.
- [482] S. Taurin, H. Nehoff, K. Greish, *J. Controlled Release* **2012**, *164*, 265.
- [483] a) O. C. Farokhzad, R. Langer, *ACS Nano* **2009**, *3*, 16; b) J. Hrkach, D. Von Hoff, M. M. Ali, E. Andrianova, J. Auer, T. Campbell, D. De Witt, M. Figa, M. Figueiredo, A. Horhota, *Sci. Transl. Med.* **2012**, *4*, 128ra39.
- [484] a) J. Nicolas, S. Mura, D. Brambilla, N. Mackiewicz, P. Couvreur, *Chem. Soc. Rev.* **2013**, *42*, 1147; b) E. A. Padlan, *Mol. Immunol.* **1994**, *31*, 169.
- [485] T. S. Raju, in *Current Trends in Monoclonal Antibody Development and Manufacturing*, Springer, New York, US **2010**, pp. 249–269.
- [486] R. A. Dwek, B. J. Sutton, S. J. Perkins, T. W. Rademacher, *Biochem. Soc. Symp.*, **1984**, *49*, 123.
- [487] G. H. Ghassabeh, S. Muyldermans, D. Saerens, in *Current Trends in Monoclonal Antibody Development and Manufacturing*, Springer, New York, US **2010**, pp. 29–48.
- [488] D. Sutton, N. Nasongkla, E. Blanco, J. Gao, *Pharm. Res.* **2007**, *24*, 1029.
- [489] T. D. Heath, R. T. Fraley, D. Papahdopoulos, *Science* **1980**, *210*, 539.
- [490] M. A. Hooks, C. S. Wade, W. J. Millikan, *Pharmacotherapy* **1991**, *11*, 26.
- [491] a) J. Albanell, J. Baselga, *Drugs Today (Barc)* **1999**, *35*, 931; b) R. Nahta, F. J. Esteva, *Cancer Lett.* **2006**, *232*, 123.
- [492] a) J. James, G. Dubs, *AIDS. Treat. News* **1997**, *2*; b) J. Boye, T. Elter, A. Engert, *Ann. Oncol.* **2003**, *14*, 520.
- [493] M. Buschle, M. Cotten, H. Kirlappos, K. Mechtler, G. Schaffner, W. Zauner, M. L. Birnstiel, E. Wagner, *Hum. Gene Ther.* **1995**, *6*, 753.

- [494] F. Ona, N. Zamcheck, P. Dhar, T. Moore, H. Kupchik, *Cancer* **1973**, 31, 324.
- [495] A. P. Johnston, M. M. Kamphuis, G. K. Such, A. M. Scott, E. C. Nice, J. K. Heath, F. Caruso, *Acs Nano* **2012**, 6, 6667.
- [496] a) W. C. Weinberg, M. R. Frazier-Jessen, W. J. Wu, A. Weir, M. Hartsough, P. Keegan, C. Fuchs, *Cancer Metastasis Rev.* **2005**, 24, 569; b) I. Van Audenhove, J. Gettemans, *EBioMedicine* **2016**.
- [497] a) D. W. Bartlett, H. Su, I. J. Hildebrandt, W. A. Weber, M. E. Davis, *Proc. Natl. Acad. Sci. U. S. A.* **2007**, 104, 15549; b) D. B. Kirpotin, D. C. Drummond, Y. Shao, M. R. Shalaby, K. Hong, U. B. Nielsen, J. D. Marks, C. C. Benz, J. W. Park, *Cancer Res.* **2006**, 66, 6732.
- [498] J. E. Rosen, L. Chan, D.-B. Shieh, F. X. Gu, *Nanomed.: Nanotechnol., Biol. Med.* **2012**, 8, 275.
- [499] K. A. Chester, R. E. Hawkins, *Trends Biotechnol.* **1995**, 13, 294.
- [500] P. Driel, J. Vorst, F. Verbeek, S. Oliveira, T. Snoeks, S. Keereweer, B. Chan, M. Boonstra, J. Frangioni, P. Bergen en Henegouwen, *Int. J. Cancer* **2014**, 134, 2663.
- [501] E. Horak, T. Heitner, M. K. Robinson, H. H. Simmons, J. Garrison, M. Russeva, P. Furmanova, J. Lou, Y. Zhou, Q.-A. Yuan, *Cancer Biother. Radiopharm.* **2005**, 20, 603.
- [502] M. Kijanka, B. Dorresteijn, S. Oliveira, P. M. v. B. en Henegouwen, *Nanomedicine* **2015**, 10, 161.
- [503] F. R. Brennan, L. Shaw, M. G. Wing, C. Robinson, *Mol. Biotechnol.* **2004**, 27, 59.
- [504] S. Oliveira, R. Heukers, J. Sornkorn, R. J. Kok, P. M. v. B. en Henegouwen, *J. Controlled Release* **2013**, 172, 607.
- [505] P. Simard, J.-C. Leroux, *Mol. Pharmaceutics* **2010**, 7, 1098.
- [506] a) S. M. Ansell, P. G. Tardi, S. S. Buchkowsky, *Bioconjugate Chem.* **1996**, 7, 490; b) M. Fuentes, C. Mateo, J. Guisán, R. Fernández-Lafuente, *Biosens. Bioelectron.* **2005**, 20, 1380.
- [507] L. X. Tiefenauer, G. Kuehne, R. Y. Andres, *Bioconjugate Chem.* **1993**, 4, 347.
- [508] C. Hamers-Casterman, T. Atarhouch, S. Muyldermans, G. Robinson, C. Hammers, E. B. Songa, N. Bendahman, R. Hammers, *Nature* **1993**, 363, 446.
- [509] K. Conrath, U. Wernery, S. Muyldermans, V. Nguyen, *Dev. Comp. Immunol.* **2003**, 27, 87.
- [510] G. Hassanzadeh-Ghassabeh, N. Devoogdt, P. De Pauw, C. Vincke, S. Muyldermans, *Nanomedicine* **2013**, 8, 1013.
- [511] S. Muyldermans, *Annu. Rev. Biochem* **2013**, 82, 775.
- [512] H. Revets, P. De Baetselier, S. Muyldermans, *Expert Opin. Biol. Ther.* **2005**, 5, 111.
- [513] P. B. Van Driel, M. C. Boonstra, M. D. Slooter, R. Heukers, M. A. Stammes, T. J. Snoeks, H. S. De Bruijn, P. J. van Diest, A. L. Vahrmeijer, P. M. v. B. en Henegouwen, *J. Controlled Release* **2016**, 229, 93.
- [514] V. Cortez-Retamozo, M. Lauwereys, M. Gobert, K. Conrath, S. Muyldermans, P. De Baetselier, H. Revets, *Int. J. Cancer* **2002**, 98, 456.
- [515] R. Chakravarty, S. Goel, W. Cai, *Theranostics* **2014**, 4, 386.
- [516] S. Muyldermans, T. Atarhouch, J. Saldanha, J. Barbosa, R. Hamers, *Protein Eng.* **1994**, 7, 1129.
- [517] I. Vaneycken, N. Devoogdt, N. Van Gassen, C. Vincke, C. Xavier, U. Wernery, S. Muyldermans, T. Lahoutte, V. Caveliers, *FASEB J.* **2011**, 25, 2433.
- [518] R. C. Roovers, M. J. Vosjan, T. Laeremans, R. el Khoulati, R. C. de Bruin, K. M. Ferguson, A. J. Verkleij, G. A. van Dongen, P. M. van Bergen en Henegouwen, *Int. J. Cancer* **2011**, 129, 2013.
- [519] a) V. Cortez-Retamozo, N. Backmann, P. D. Senter, U. Wernery, P. De Baetselier, S. Muyldermans, H. Revets, *Cancer Res.* **2004**, 64, 2853; b) M. Behdani, S. Zeinali, M. Karimipour, H. Khanahmad, S. Schoonooghe, A. Aslemarz, N. Seyed, R. Moazami-Godarzi, F. Baniahamad, M. Habibi-Arbouhi, *New biotechnology* **2013**, 30, 205.
- [520] L. Huang, L. O. T. Gainkam, V. Caveliers, C. Vanhove, M. Keyaerts, P. De Baetselier, A. Bossuyt, H. Revets, T. Lahoutte, *Mol. Imaging Biol.* **2008**, 10, 167.
- [521] M. J. Vosjan, L. R. Perk, R. C. Roovers, G. W. Visser, M. Stigter-van Walsum, P. M. v. B. en Henegouwen, G. A. van Dongen, *Eur. J. Nucl. Med. Mol. Imaging* **2011**, 38, 753.
- [522] S. Oliveira, G. A. van Dongen, M. S.-v. Walsum, R. C. Roovers, J. C. Stam, W. Mali, P. J. van Diest, Vieweg+Teubner Verlag van Bergen en Henegouwen, *Mol. Imaging* **2012**, 11.
- [523] S. Hernot, S. Unnikrishnan, Z. Du, T. Shevchenko, B. Cosyns, A. Broisat, J. Toczek, V. Caveliers, S. Muyldermans, T. Lahoutte, *J. Controlled Release* **2012**, 158, 346.
- [524] R. van der Meel, S. Oliveira, I. Altintas, R. Haselberg, J. van der Veeken, R. C. Roovers, P. M. v. B. en Henegouwen, G. Storm, W. E. Hennink, R. M. Schiffelers, *J. Controlled Release* **2012**, 159, 281.
- [525] M. Talelli, C. J. Rijcken, S. Oliveira, R. van der Meel, P. M. v. B. en Henegouwen, T. Lammers, C. F. van Nostrum, G. Storm, W. E. Hennink, *J. Controlled Release* **2011**, 153, 93.
- [526] I. Altintas, R. Heukers, R. van der Meel, M. Lacombe, M. Amidi, P. M. v. B. en Henegouwen, W. E. Hennink, R. M. Schiffelers, R. J. Kok, *J. Controlled Release* **2013**, 165, 110.
- [527] a) A. D'Hollander, H. Jans, G. V. Velde, C. Verstraete, S. Massa, N. Devoogdt, T. Stakenborg, S. Muyldermans, L. Lagae, U. Himmelreich, *Biomaterials*. <https://doi.org/10.1016/j.biomaterials.2017.01.007>; b) B. Van de Broek, N. Devoogdt, A. D'Hollander, H.-L. Gijs, K. Jans, L. Lagae, S. Muyldermans, G. Maes, G. Borghs, *ACS nano* **2011**, 5, 4319.
- [528] M. Zhu, Y. Hu, G. Li, W. Ou, P. Mao, S. Xin, Y. Wan, *Nanoscale Res. Lett.* **2014**, 9, 1.
- [529] a) A. D. Friedman, S. E. Claypool, R. Liu, *Curr. Pharm. Des.* **2013**, 19, 6315; b) D. S. Wilson, J. W. Szostak, *Annu. Rev. Biochem* **1999**, 68, 611.
- [530] A. D. Ellington, J. W. Szostak, *nature* **1990**, 346, 818.
- [531] V. B. Pinheiro, A. I. Taylor, C. Cozens, M. Abramov, M. Renders, S. Zhang, J. C. Chaput, J. Wengel, S.-Y. Peak-Chew, S. H. McLaughlin, *Science* **2012**, 336, 341.
- [532] a) S. Sultana, M. R. Khan, M. Kumar, S. Kumar, M. Ali, *J. Drug Targeting* **2013**, 21, 107; b) C.-H. Wang, S.-T. Kang, Y.-H. Lee, Y.-L. Luo, Y.-F. Huang, C.-K. Yeh, *Biomaterials* **2012**, 33, 1939.
- [533] K. N. Morris, K. B. Jensen, C. M. Julin, M. Weil, L. Gold, *Proc. Natl. Acad. Sci. U. S. A.* **1998**, 95, 2902.
- [534] D. Shangguan, Y. Li, Z. Tang, Z. C. Cao, H. W. Chen, P. Mallikaratchy, K. Sefah, C. J. Yang, W. Tan, *Proc. Natl. Acad. Sci. U. S. A.* **2006**, 103, 11838.
- [535] J. Mi, Y. Liu, Z. N. Rabbani, Z. Yang, J. H. Urban, B. A. Sullenger, B. M. Clary, *Nat. Chem. Biol.* **2010**, 6, 22.
- [536] L. Zhang, A. F. Radovic-Moreno, F. Alexis, F. X. Gu, P. A. Basto, V. Bagalkot, S. Jon, R. S. Langer, O. C. Farokhzad, *ChemMedChem* **2007**, 2, 1268.
- [537] J. Lapointe, T. Q. Truong, L. Falstrault, L. Brissette, *Biochem. Cell Biol.* **2006**, 84, 250.
- [538] C.-L. Zhu, C.-H. Lu, X.-Y. Song, H.-H. Yang, X.-R. Wang, *J. Am. Chem. Soc.* **2011**, 133, 1278.
- [539] D. Peer, J. M. Karp, S. Hong, O. C. Farokhzad, R. Margalit, R. Langer, *Nat. Nanotechnol.* **2007**, 2, 751.
- [540] Z. Xiao, O. C. Farokhzad, *ACS nano* **2012**, 6, 3670.
- [541] B. J. Hicke, A. W. Stephens, T. Gould, Y.-F. Chang, C. K. Lynott, J. Heil, S. Borkowski, C.-S. Hilger, G. Cook, S. Warren, *J. Nucl. Med.* **2006**, 47, 668.
- [542] P. R. Mallikaratchy, A. Ruggiero, J. R. Gardner, V. Kuryavyi, W. F. Maguire, M. L. Heaney, M. R. McDevitt, D. J. Patel, D. A. Scheinberg, *Nucleic Acids Res.* **2011**, 39, 2458.
- [543] W. Winkler, A. Nahvi, R. R. Breaker, *Nature* **2002**, 419, 952.
- [544] W. R. L. de Campos, D. Coopusamy, L. Morris, B. M. Mayosi, M. Khati, *Antimicrob. Agents Chemother.* **2009**, 53, 3056.

- [545] A. Wang, V. Bagalkot, F. Gu, F. Alexis, C. Vasiliou, M. Cima, S. Jon, O. Farokhzad, *International Journal of Radiation Oncology\* Biology\* Physics* **2007**, 69, S110.
- [546] a) J. K. Herr, J. E. Smith, C. D. Medley, D. Shangguan, W. Tan, *Anal. Chem.* **2006**, 78, 2918; b) J. E. Smith, C. D. Medley, Z. Tang, D. Shangguan, C. Lofton, W. Tan, *Anal. Chem.* **2007**, 79, 3075.
- [547] N. C. Pagratis, C. Bell, Y.-F. Chang, S. Jennings, T. Fitzwater, D. Jellinek, C. Dang, *Nat. Biotechnol.* **1997**, 15, 68.
- [548] a) E. S. Group, *Retina* **2002**, 22, 143; b) E. S. Group, *Ophthalmology* **2003**, 110, 979.
- [549] M. Khati, *J. Clin. Pathol.* **2010**, 63, 480.
- [550] Z. Xiao, E. Levy-Nissenbaum, F. Alexis, A. Lupták, B. A. Teply, J. M. Chan, J. Shi, E. Digga, J. Cheng, R. Langer, *ACS nano* **2012**, 6, 696.
- [551] O. C. Farokhzad, S. Jon, A. Khademhosseini, T.-N. T. Tran, D. A. LaVan, R. Langer, *Cancer Res.* **2004**, 64, 7668.
- [552] a) Z. Xiao, C. Ji, J. Shi, E. M. Pridgen, J. Frieder, J. Wu, O. C. Farokhzad, *Angew. Chem.* **2012**, 124, 12023; *Angew. Chem. Int. Ed.* **2012**, 51, 11853; b) D. Ahmadvand, F. Rahbarizadeh, S. M. Moghimi, *Curr. Opin. Biotechnol.* **2011**, 22, 832.
- [553] a) W. A. Pieken, D. B. Olsen, F. Benseler, H. Aurup, F. Eckstein, *Science* **1991**, 253, 314; b) R. R. White, S. Shan, C. P. Rusconi, G. Shetty, M. W. Dewhirst, C. D. Kontos, B. A. Sullenger, *Proc. Natl. Acad. Sci. U. S. A.* **2003**, 100, 5028.
- [554] C. S. Ferreira, S. Missailidis, *Braz. Arch. Biol. Technol.* **2007**, 50, 63.
- [555] N. Bertrand, J.-C. Leroux, *J. Controlled Release* **2012**, 161, 152.
- [556] R. Brissette, J. Prendergast, N. I. Goldstein, *Curr. Opin. Drug Discovery Dev.* **2006**, 9, 363.
- [557] R. C. Ladner, A. K. Sato, J. Gorzelany, M. de Souza, *Drug Discovery Today* **2004**, 9, 525.
- [558] H. Koo, M. S. Huh, I.-C. Sun, S. H. Yuk, K. Choi, K. Kim, I. C. Kwon, *Acc. Chem. Res.* **2011**, 44, 1018.
- [559] S. L. Deutscher, *Chem. Rev.* **2010**, 110, 3196.
- [560] R. O. Hynes, *Cell* **2002**, 110, 673.
- [561] a) M. Schottelius, B. Laufer, H. Kessler, H.-J. r. Wester, *Acc. Chem. Res.* **2009**, 42, 969; b) P. C. Brooks, A. M. Montgomery, M. Rosenfeld, R. A. Reisfeld, T. Hu, G. Klier, D. A. Cheresh, *Cell* **1994**, 79, 1157.
- [562] a) A. S. Wadajkar, Z. Bhavsar, C.-Y. Ko, B. Koppolu, W. Cui, L. Tang, K. T. Nguyen, *Acta biomaterialia* **2012**, 8, 2996; b) X. Ming, L. Feng, *Mol. Pharmaceutics* **2012**, 9, 1502.
- [563] R. Pasqualini, E. Koivunen, E. Ruoslahti, *Nat. Biotechnol.* **1997**, 15, 542.
- [564] a) P.-P. Lv, Y.-F. Ma, R. Yu, H. Yue, D.-Z. Ni, W. Wei, G.-H. Ma, *Mol. Pharmaceutics* **2012**, 9, 1736; b) F. Zhang, X. Huang, L. Zhu, N. Guo, G. Niu, M. Swierczewska, S. Lee, H. Xu, A. Y. Wang, K. A. Mohamedali, *Biomaterials* **2012**, 33, 5414.
- [565] a) J. Xie, K. Chen, H.-Y. Lee, C. Xu, A. R. Hsu, S. Peng, X. Chen, S. Sun, *J. Am. Chem. Soc.* **2008**, 130, 7542; b) C. Zhang, M. Jugold, E. C. Woenne, T. Lammers, B. Morgenstern, M. M. Mueller, H. Zentgraf, M. Bock, M. Eisenhut, W. Semmler, *Cancer Res.* **2007**, 67, 1555.
- [566] M. Talekar, J. Kendall, W. Denny, S. Garg, *Anti-Cancer Drugs* **2011**, 22, 949.
- [567] A. P. Drabovich, M. V. Berezovski, M. U. Musheev, S. N. Krylov, *Anal. Chem.* **2008**, 81, 490.
- [568] a) P. S. Low, W. A. Henne, D. D. Doorneweerd, *Acc. Chem. Res.* **2007**, 41, 120; b) B. Haley, E. Frenkel, *Urol. Oncol.: Semin. orig. invest.* **2008**, 26, 57.
- [569] a) X. Zhao, H. Li, R. J. Lee, *Expert Opin. Drug Delivery* **2008**, 5, 309; b) G. M. Van Dam, G. Themelis, L. M. Crane, N. J. Harlaar, R. G. Pleijhuis, W. Kelder, A. Sarantopoulos, J. S. De Jong, H. J. Arts, A. G. Van Der Zee, *Nat. Med.* **2011**, 17, 1315.
- [570] a) W. Xia, P. S. Low, *J. Med. Chem.* **2010**, 53, 6811; b) M. E. Werner, S. Karve, R. Sukumar, N. D. Cummings, J. A. Copp, R. C. Chen, T. Zhang, A. Z. Wang, *Biomaterials* **2011**, 32, 8548.
- [571] a) F. Gu, L. Zhang, B. A. Teply, N. Mann, A. Wang, A. F. Radovic-Moreno, R. Langer, O. C. Farokhzad, *Proc. Natl. Acad. Sci. U. S. A.* **2008**, 105, 2586; b) N. Kamaly, T. Kalber, M. Thanou, J. D. Bell, A. D. Miller, *Bioconjugate Chem.* **2009**, 20, 648.
- [572] P. M. Valencia, M. H. Hanewich-Hollatz, W. Gao, F. Karim, R. Langer, R. Karnik, O. C. Farokhzad, *Biomaterials* **2011**, 32, 6226.
- [573] W. Yang, Y. Cheng, T. Xu, X. Wang, L.-p. Wen, *Eur. J. Med. Chem.* **2009**, 44, 862.
- [574] X. Zhang, J. Qi, Y. Lu, W. He, X. Li, W. Wu, *Nanomed.: Nanotechnol., Biol. Med.* **2014**, 10, 167.
- [575] a) H. H. Salman, C. Gamazo, P. C. de Smidt, G. Russell-Jones, J. M. Irache, *Pharm. Res.* **2008**, 25, 2859; b) G. J. Russell-Jones, *Crit. Rev. Ther. Drug Carrier Syst.* **1998**, 15.
- [576] a) C. Ehrhardt, C. Kneuer, U. Bakowsky, *Adv. Drug Delivery Rev.* **2004**, 56, 527; b) E. E. Simanek, G. J. McGarvey, J. A. Jablonowski, C.-H. Wong, *Chem. Rev.* **1998**, 98, 833.
- [577] a) D. Singh, M. Rashid, S. S. Hallan, N. K. Mehra, A. Prakash, N. Mishra, *Artif. Cells, Nanomed., Biotechnol.* **2016**, 44, 865; b) L. Goswami, N. S. Madhav, K. Upadhyaya, *Int. Curr. Pharm. J.* **2016**, 5, 33.
- [578] a) F. Yang, G. P. Lim, A. N. Begum, O. J. Ubeda, M. R. Simmons, S. S. Ambegaokar, P. P. Chen, R. Kayed, C. G. Glabe, S. A. Frautschy, *J. Biol. Chem.* **2005**, 280, 5892; b) Y. Porat, A. Abramowitz, E. Gazit, *Chem. Biol. Drug Des.* **2006**, 67, 27.
- [579] a) S. Marrache, S. Dhar, *Proc. Natl. Acad. Sci. U. S. A.* **2012**, 109, 16288; b) R. A. Smith, C. M. Porteous, A. M. Gane, M. P. Murphy, *Proc. Natl. Acad. Sci. U. S. A.* **2003**, 100, 5407.
- [580] a) R. H. Mach, Y. Huang, R. A. Freeman, L. Wu, S. Vangveravong, R. R. Luedtke, *Bioorg. Med. Chem. Lett.* **2004**, 14, 195; b) R. Banerjee, P. Tyagi, S. Li, L. Huang, *Int. J. Cancer* **2004**, 112, 693.
- [581] M. Goto, H. Yura, C.-W. CHANG, A. Kobayashi, T. Shinoda, A. Maeda, S. Kojima, K. Kobayashi, T. Akaike, *J. Controlled Release* **1994**, 28, 223.
- [582] a) S. Basiruddin, A. R. Maity, N. R. Jana, *RSC Advances* **2012**, 2, 11915; b) A. Jain, P. Kesharwani, N. K. Garg, A. Jain, S. A. Jain, A. K. Jain, P. Nirbhavane, R. Ghaghoria, R. K. Tyagi, O. P. Katare, *Colloids Surf., B* **2015**, 134, 47.
- [583] a) S. Zhu, M. Niu, H. O'Mary, Z. Cui, *Mol. Pharmaceutics* **2013**, 10, 3525; b) J. M. Irache, H. H. Salman, C. Gamazo, S. Espuelas, *Expert Opin. Drug Delivery* **2008**, 5, 703.
- [584] a) R. Gromnicova, H. A. Davies, P. Sreekanthreddy, I. A. Romero, T. Lund, I. M. Roitt, J. B. Phillips, D. K. Male, *PLoS One* **2013**, 8, e81043; b) C. Chen, X. Jiang, Y. V. Kaneti, A. Yu, *Powder Technol.* **2013**, 236, 157.
- [585] T. M. Allen, *Nat. Rev. Cancer* **2002**, 2, 750.
- [586] L. Y. Chou, K. Ming, W. C. Chan, *Chem. Soc. Rev.* **2011**, 40, 233.
- [587] a) T. R. Daniels, T. Delgado, J. A. Rodriguez, G. Helguera, M. L. Penichet, *Clin. Immunol.* **2006**, 121, 144; b) T. R. Daniels, T. Delgado, G. Helguera, M. L. Penichet, *Clin. Immunol.* **2006**, 121, 159.
- [588] S. K. Sahoo, W. Ma, V. Labhasetwar, *Int. J. Cancer* **2004**, 112, 335.
- [589] a) K. Ulbrich, T. Hekmatara, E. Herbert, J. Kreuter, *Eur. J. Pharm. Biopharm.* **2009**, 71, 251; b) Y. Gupta, A. Jain, S. K. Jain, *J. Pharm. Pharmacol.* **2007**, 59, 935.
- [590] T. Islam, L. Josephson, *Cancer Biomarkers* **2009**, 5, 99.
- [591] Y. Cui, Q. Xu, P. K.-H. Chow, D. Wang, C.-H. Wang, *Biomaterials* **2013**, 34, 8511.
- [592] V. Valdighesias, N. Fernández-Bertólez, G. Kılıç, C. Costa, S. Costa, S. Fraga, M. J. Bessa, E. Pásaro, J. P. Teixeira, B. Laffon, *J. Trace Elem. Med. Biol.* **2016**.

- [593] N. Lewinski, V. Colvin, R. Drezek, *small* **2008**, *4*, 26.
- [594] M. Mahmoudi, A. Simchi, M. Imani, M. A. Shokrgozar, A. S. Milani, U. O. Häfeli, P. Stroeve, *Colloids Surf., B* **2010**, *75*, 300.
- [595] J. A. Gaasch, P. R. Lockman, W. J. Geldenhuys, D. D. Allen, C. J. Van der Schyf, *Neurochem. Res.* **2007**, *32*, 1196.
- [596] H. L. Karlsson, P. Cronholm, J. Gustafsson, L. Moller, *Chem. Res. Toxicol.* **2008**, *21*, 1726.
- [597] B. Ankanwar, T. Lai, J. Huang, R. Liu, M. Hsiao, C. Chen, Y. Hwu, *Nanotechnology* **2010**, *21*, 075102.
- [598] R. A. Revia, M. Zhang, *Mater. Today* **2016**, *19*, 157.
- [599] N. Singh, G. J. Jenkins, R. Asadi, S. H. Doak, *Nano Rev. Exp.* **2010**, *1*.
- [600] a) Z. Ding, P. Liu, H. Yi, Y. Wu, P. Zhang, L. Cai, *Nanomed.: Nanotechnol., Biol. Med.* **2016**, *12*, 527; b) H. Zhou, X. Hou, Y. Liu, T. Zhao, Q. Shang, J. Tang, J. Liu, Y. Wang, Q. Wu, Z. Luo, *ACS Appl. Mater. Interfaces* **2016**, *8*, 4424.
- [601] a) B. Sumer, J. Gao, *Nanomedicine* **2008**, *3*, 137; b) E. Blanco, C. W. Kessinger, B. D. Sumer, J. Gao, *Exp. Biol. Med.* **2009**, *234*, 123.
- [602] J. Xie, G. Liu, H. S. Eden, H. Ai, X. Chen, *Acc. Chem. Res.* **2011**, *44*, 883.
- [603] a) S. A. Wahajuddin, *Int. J. Nanomed.* **2012**, *7*, 3445; b) J.-E. Kim, J.-Y. Shin, M.-H. Cho, *Arch. Toxicol.* **2012**, *86*, 685.
- [604] a) S. Mura, J. Nicolas, P. Couvreur, *Nat. Mater.* **2013**, *12*, 991; b) M. Ahmad, M. U. Minhas, M. Sohail, M. Faisal, H. Rashid, *J. Pharm. Altern. Med.* **2013**, *2*, 13.
- [605] a) P. Couvreur, *Adv. Drug Delivery Rev.* **2013**, *65*, 21; b) G. Bao, S. Mitragotri, S. Tong, *Annu. Rev. Biomed. Eng.* **2013**, *15*, 253.
- [606] C. Sanson, O. Diou, J. Thevenot, E. Ibarboure, A. Soum, A. Brûlet, S. Miraux, E. Thiaudière, S. Tan, A. Brisson, *ACS nano* **2011**, *5*, 1122.
- [607] A. Baeza, M. Colilla, M. Vallet-Regí, *Expert Opin. Drug Delivery* **2015**, *12*, 319.
- [608] D. Kami, S. Takeda, Y. Itakura, S. Gojo, M. Watanabe, M. Toyoda, *Int. J. Mol. Sci.* **2011**, *12*, 3705.
- [609] a) M. Chorny, I. Fishbein, B. B. Yellen, I. S. Alferiev, M. Bakay, S. Ganta, R. Adarno, M. Arnjii, G. Friedman, R. J. Levy, *Proc Natl Acad Sci U S A* **2010**, *107*, 8346; b) P. Pouponneau, J.-C. Leroux, G. Soulez, L. Gaboury, S. Martel, *Biomaterials* **2011**, *32*, 3481.
- [610] a) J. M. Jeong, J.-K. Chung, *Cancer Biother. Radiopharm.* **2003**, *18*, 707; b) R. Torres Martin de Rosales, R. Tavaré, A. Glaria, G. Varma, A. Protti, P. J. Blower, *Bioconjugate Chem.* **2011**, *22*, 455.
- [611] J. H. Park, G. Saravanakumar, K. Kim, I. C. Kwon, *Adv. Drug Delivery Rev.* **2010**, *62*, 28.
- [612] V. V. Mody, A. Cox, S. Shah, A. Singh, W. Bevins, H. Parihar, *Appl. Nanosci.* **2014**, *4*, 385.
- [613] M. Bietenbeck, A. Florian, C. Faber, U. Sechtem, A. Yilmaz, *Int. J. Nanomed.* **2016**, *11*, 3191.
- [614] M. Freeman, A. Arrott, J. Watson, *J. Appl. Phys.* **1960**, *31*, S404.
- [615] A. Senyei, K. Widder, G. Czerlinski, *J. Appl. Phys.* **1978**, *49*, 3578.
- [616] U. Zimmermann, G. Pilwat, *Zeitschrift für Naturforschung. Section C: Biosciences* **1975**, *31*, 732.
- [617] K. J. Widder, A. E. Senyei, D. G. Scarpelli, *Exp. Biol. Med.* **1978**, *158*, 141.
- [618] a) Y. Morimoto, K. Sugibayashi, M. Okumura, Y. Kato, *J. Pharmacobi-Dyn.* **1980**, *3*, 264; b) K. J. Widder, R. M. Morris, G. Poore, D. P. Howard, A. E. Senyei, *Proc. Natl. Acad. Sci. U. S. A.* **1981**, *78*, 579; c) T. Kato, R. Nemoto, H. Mori, R. Abe, K. Unno, A. Goto, H. Murota, M. Harada, M. Homma, in *Microencapsulation and Artificial Cells*, Springer, **1984**, pp. 199–211; d) P. K. Gupta, C. T. Hung, N. S. Rao, *J. Pharm. Sci.* **1989**, *78*, 290.
- [619] a) U. O. Häfeli, S. M. Sweeney, B. A. Beresford, E. H. Sim, R. M. Macklis, *J. Biomed. Mater. Res.* **1994**, *28*, 901; b) U. O. Häfeli, S. M. Sweeney, B. A. Beresford, J. L. Humm, R. M. Macklis, *Nucl. Med. Biol.* **1995**, *22*, 147.
- [620] a) G. Bonadonna, L. Gianni, A. Santoro, V. Bonfante, P. Bidoli, P. Casali, R. Demicheli, P. Valagussa, *Ann. Oncol.* **1993**, *4*, 359; b) A. S. Lübbe, C. Bergemann, W. Huhnt, T. Fricke, H. Riess, J. W. Brock, D. Huhn, *Cancer Res.* **1996**, *56*, 4694.
- [621] A. S. Lübbe, C. Alexiou, C. Bergemann, *J. Surg. Res.* **2001**, *95*, 200.
- [622] a) R. Cheng, F. Meng, C. Deng, H.-A. Klok, Z. Zhong, *Biomaterials* **2013**, *34*, 3647; b) E. Fleige, M. A. Quadir, R. Haag, *Adv. Drug Delivery Rev.* **2012**, *64*, 866.
- [623] M. B. Yatvin, J. N. Weinstein, W. H. Dennis, R. Blumenthal, *Science* **1978**, *202*, 1290.
- [624] a) S. D. Kong, M. Sartor, C.-M. J. Hu, W. Zhang, L. Zhang, S. Jin, *Acta biomaterialia* **2013**, *9*, 5447; b) F. Ding, X. Shi, Z. Jiang, L. Liu, J. Cai, Z. Li, S. Chen, Y. Du, *J. Mater. Chem. B* **2013**, *1*, 1729.
- [625] a) Y.-J. Pan, Y.-Y. Chen, D.-R. Wang, C. Wei, J. Guo, D.-R. Lu, C.-C. Chu, C.-C. Wang, *Biomaterials* **2012**, *33*, 6570; b) R. De La Rica, D. Aili, M. M. Stevens, *Adv. Drug Delivery Rev.* **2012**, *64*, 967.
- [626] V. Plassat, C. Wilhelm, V. Marsaud, C. Ménager, F. Gazeau, J. M. Renoir, S. Lesieur, *Adv. Funct. Mater.* **2011**, *21*, 83.
- [627] L. Zhang, T. Wang, L. Yang, C. Liu, C. Wang, H. Liu, Y. A. Wang, Z. Su, *Chem. – Eur. J.* **2012**, *18*, 12512.
- [628] F. Zhang, G. B. Braun, A. Pallaoro, Y. Zhang, Y. Shi, D. Cui, M. Moskovits, D. Zhao, G. D. Stucky, *Nano Lett.* **2011**, *12*, 61.
- [629] a) G. Lattermann, M. Krekhova, *Macromol. Rapid Commun.* **2006**, *27*, 1373; b) A. V. Teixeira, I. Morfin, F. Ehrburger-Dolle, C. Rochas, P. Panine, P. Licinio, E. Geissler, *Compos. Sci. Technol.* **2003**, *63*, 1105; c) P. M. Xulu, G. Filipcsei, M. Zrínyi, *Macromolecules* **2000**, *33*, 1716.
- [630] a) T.-Y. Liu, S.-H. Hu, T.-Y. Liu, D.-M. Liu, S.-Y. Chen, *Langmuir* **2006**, *22*, 5974; b) N. J. Francois, S. Allo, S. E. Jacobo, M. E. Daraio, *J. Appl. Polym. Sci.* **2007**, *105*, 647; c) T.-Y. Liu, S.-H. Hu, K.-H. Liu, D.-M. Liu, S.-Y. Chen, *J. Controlled Release* **2008**, *126*, 228.
- [631] J. Qin, I. Asemah, S. Laurent, A. Fornara, R. N. Muller, M. Muhammed, *Adv. Mater.* **2009**, *21*, 1354.
- [632] a) J. M. Blonder, L. Baird, J. C. Fulfs, G. J. Rosenthal, *Life Sci.* **1999**, *65*, PL261; b) J. M. Barichello, M. Morishita, K. Takayama, T. Nagai, *Int. J. Pharm.* **1999**, *184*, 189.
- [633] K. Cai, Z. Luo, Y. Hu, X. Chen, Y. Liao, L. Yang, *Adv. Mater.* **2009**, *21*, 4045.
- [634] a) S. Zheng, G. Liu, R. Hong, H. Li, Y. Li, D. Wei, *Appl. Surf. Sci.* **2012**, *259*, 201; b) S. McBain, U. Griesenbach, S. Xenariou, A. Keramane, C. Batich, E. Alton, J. Dobson, *Nanotechnology* **2008**, *19*, 405102; c) C. Plank, M. Anton, C. Rudolph, J. Rosenzweig, F. Krötz, *Expert Opin. Biol. Ther.* **2003**, *3*, 745; d) O. Mykhaylyk, Y. S. Antequera, D. Vlaskou, C. Plank, *Nat. Protocols* **2007**, *2*, 2391.
- [635] S. Prijic, L. Prosen, M. Cemazar, J. Scancar, J. Lavrencak, V. B. Bregar, A. Coer, M. Krzan, A. Znidarsic, G. Sersa, *Biomaterials* **2012**, *33*, 4379.
- [636] J. W. Park, K. H. Bae, C. Kirm, T. G. Park, *Biomacromolecules* **2010**, *12*, 457.
- [637] F. N. Al-Deen, J. Ho, C. Selomulya, C. Ma, R. Coppel, *Langmuir* **2011**, *27*, 3703.
- [638] Y. Tang, D. Wang, C. Zhou, W. Ma, Y. Zhang, B. Liu, S. Zhang, *Gene therapy* **2012**, *19*, 1187.
- [639] M. Chorny, E. Hood, R. J. Levy, V. R. Muzykantov, *J. Controlled Release* **2010**, *146*, 144.
- [640] K. Katagiri, Y. Imai, K. Koumoto, T. Kaiden, K. Kono, S. Aoshima, *Small* **2011**, *7*, 1683.
- [641] N. S. Satarkar, J. Z. Hilt, *Acta biomaterialia* **2008**, *4*, 11.
- [642] a) J. P. May, S.-D. Li, *Expert Opin. Drug Delivery* **2013**, *10*, 511; b) B. Caetano, C. Guibert, R. Fini, J. Fresnais, S. Pulcinelli, C. Ménager, C. Santilli, *RSC Advances* **2016**, *6*, 63291; c) S. Laurent, S. Dutz, U. O. Häfeli, M. Mahmoudi, *Adv. Colloid Interface Sci.* **2011**,

- 166, 8; d) E. Bringas, Ö. Köysüren, D. V. Quach, M. Mahmoudi, E. Aznar, J. D. Roehling, M. D. Marcos, R. Martínez-Máñez, P. Stroeve, *Chem. Commun.* **2012**, 48, 5647.
- [643] A. M. Derfus, G. von Maltzahn, T. J. Harris, T. Duza, K. S. Vecchio, E. Ruoslahti, S. N. Bhatia, *Adv. Mater.* **2007**, 19, 3932.
- [644] a) J. Kost, J. Wolfrum, R. Langer, *J. Biomed. Mater. Res.* **1987**, 21, 1367; b) Z. Lu, M. D. Prouty, Z. Guo, V. O. Golub, C. S. Kumar, Y. M. Lvov, *Langmuir* **2005**, 21, 2042.
- [645] P. Pradhan, J. Giri, F. Rieken, C. Koch, O. Mykhaylyk, M. Döblinger, R. Banerjee, D. Bahadur, C. Plank, *J. Controlled Release* **2010**, 142, 108.
- [646] K. T. Al-Jamal, J. Bai, J. T.-W. Wang, A. Protti, P. Southern, L. Bogart, H. Heidari, X. Li, A. Cakebread, D. Asker, *Nano Lett.* **2016**.
- [647] Y. Wang, Q. Zhao, N. Han, L. Bai, J. Li, J. Liu, E. Che, L. Hu, Q. Zhang, T. Jiang, *Nanomed.: Nanotechnol., Biol. Med.* **2015**, 11, 313.
- [648] a) A. Pourjavadi, Z. M. Tehrani, S. Jokar, *J. Ind. Eng. Chem.* **2015**, 28, 45; b) X.-L. Qiu, Q.-L. Li, Y. Zhou, X.-Y. Jin, A.-D. Qi, Y.-W. Yang, *Chem. Commun.* **2015**, 51, 4237.
- [649] N. K. Mal, M. Fujiwara, Y. Tanaka, *Nature* **2003**, 421, 350.
- [650] Y. Zhu, M. Fujiwara, *Angew. Chem.* **2007**, 119, 2291; *Angew. Chem. Int. Ed.* **2007**, 46, 2241.
- [651] D. He, X. He, K. Wang, J. Cao, Y. Zhao, *Langmuir* **2012**, 28, 4003.
- [652] P. Saint-Cricq, S. Deshayes, J. Zink, A. Kasko, *Nanoscale* **2015**, 7, 13168.
- [653] L. Cao, T. Man, J. Zhuang, M. Kruk, *J. Mater. Chem.* **2012**, 22, 6939.
- [654] S. Mura, J. Nicolas, P. Couvreur, *Nat. Mater.* **2013**, 12, 991.
- [655] S. H. Hu, S. Y. Chen, D. M. Liu, C. S. Hsiao, *Adv. Mater.* **2008**, 20, 2690.
- [656] S. H. Hu, D. M. Liu, W. L. Tung, C. F. Liao, S. Y. Chen, *Adv. Funct. Mater.* **2008**, 18, 2946.
- [657] S.-H. Hu, S.-Y. Chen, X. Gao, *ACS nano* **2012**, 6, 2558.
- [658] M. Zborowski, L. Sun, L. R. Moore, P. S. Williams, J. J. Chalmers, *J. Magn. Magn. Mater.* **1999**, 194, 224.
- [659] H. C. Weng, *J. Biomech. Eng.* **2013**, 135, 034504.
- [660] a) T. Kubo, T. Sugita, S. Shimose, Y. Nitta, Y. Ikuta, T. Murakami, *Int. J. Oncol.* **2000**, 17, 309; b) B. B. Yellen, Z. G. Forbes, D. S. Halverson, G. Fridman, K. A. Barbee, M. Chorniy, R. Levy, G. Friedman, *J. Magn. Magn. Mater.* **2005**, 293, 647.
- [661] E. Furlani, *J. Appl. Phys.* **2006**, 99, 024912.
- [662] R. Cheng, T. Zhu, L. Mao, *Microfluid. Nanofluid.* **2014**, 16, 1143.
- [663] E. M. Cherry, P. G. Maxim, J. K. Eaton, *Med. Phys.* **2010**, 37, 175.
- [664] J.-B. Mathieu, S. Martel, *Biomed. Microdevices* **2007**, 9, 801.
- [665] C. Alexiou, D. Diehl, P. Henninger, H. Iro, R. Rockelein, W. Schmidt, H. Weber, *IEEE Trans. Appl. Supercond.* **2006**, 16, 1527.
- [666] K. D. Sattler, J. Ally, A. Amirfazli, in *Handbook of Nanophysics: Nanomedicine and Nanorobotics*, (Ed: K. D. Sattler), CRC Press, Boca Raton, US **2010**, pp. 1–17.
- [667] S.-i. Takeda, F. Mishima, S. Fujimoto, Y. Izumi, S. Nishijima, *J. Magn. Magn. Mater.* **2007**, 311, 367.
- [668] M. O. Aviles, H. Chen, A. D. Ebner, A. J. Rosengart, M. D. Kaminski, J. A. Ritter, *J. Magn. Magn. Mater.* **2007**, 311, 306.
- [669] a) B. Chertok, A. E. David, Y. Huang, V. C. Yang, *J. Controlled Release* **2007**, 122, 315; b) N. J. Darton, B. Hallmark, X. Han, S. Palit, N. K. Slater, M. R. Mackley, *Nanomed.: Nanotechnol., Biol. Med.* **2008**, 4, 19.
- [670] M. O. Aviles, A. D. Ebner, J. A. Ritter, *J. Magn. Magn. Mater.* **2008**, 320, 2640.
- [671] H. Chen, A. D. Ebner, M. D. Kaminski, A. J. Rosengart, J. A. Ritter, *J. Magn. Magn. Mater.* **2005**, 293, 616.
- [672] M. O. Aviles, A. D. Ebner, J. A. Ritter, *J. Magn. Magn. Mater.* **2007**, 310, 131.
- [673] a) H. Xu, T. Song, X. Bao, L. Hu, *J. Magn. Magn. Mater.* **2005**, 293, 514; b) H. Kempe, M. Kempe, *Biomaterials* **2010**, 31, 9499.
- [674] A. D. Grief, G. Richardson, *J. Magn. Magn. Mater.* **2005**, 293, 455.
- [675] a) J. Dobson, *Drug Dev. Res.* **2006**, 67, 55; b) G. P. Hatch, R. E. Stelter, *J. Magn. Magn. Mater.* **2001**, 225, 262.
- [676] a) J. O. Mangual, S. Li, H. J. Ploehn, A. D. Ebner, J. A. Ritter, *J. Magn. Magn. Mater.* **2010**, 322, 3094; b) R. Tietze, J. Zaloga, H. Unterweger, S. Lyer, R. P. Friedrich, C. Janko, M. Pöttler, S. Dürr, C. Alexiou, *Biochem. Biophys. Res. Commun.* **2015**, 468, 463; c) K. Hournkumnuard, M. Natenapit, *Med. Phys.* **2013**, 40, 062302.
- [677] a) P. Clegg, K. Murphy, A. Mardinoglu, *J. Magn. Magn. Mater.* **2008**, 320, 3272; b) G.-H. Zhang, A.-H. Wang, C. Zhang, C.-Z. Wu, L.-L. Hu, X.-L. Huo, presented at *Annu. Int. Conf. IEEE Eng. Med. Biol. Soc. (EMBC)*, *Design of site-directed magnetic targeting system in acute spinal cord injury*, Milan, Italy, August **2015**.
- [678] a) J. O. Mangual, M. O. Avilés, A. D. Ebner, J. A. Ritter, *J. Magn. Magn. Mater.* **2011**, 323, 1903; b) S. Sharma, U. Singh, V. Katiyar, *Microfluid. Nanofluid.* **2015**, 19, 1061; c) E. Lueshen, I. Venugopal, T. Soni, A. Alaraj, A. Linniger, *J. Biomed. Nanotechnol.* **2015**, 11, 253.
- [679] M. O. Avilés, J. O. Mangual, A. D. Ebner, J. A. Ritter, *Int. J. Pharm.* **2008**, 361, 202.
- [680] M. O. Avilés, A. D. Ebner, H. Chen, A. J. Rosengart, M. D. Kaminski, J. A. Ritter, *J. Magn. Magn. Mater.* **2005**, 293, 605.
- [681] a) A. Nacev, C. Beni, O. Bruno, B. Shapiro, *J. Magn. Magn. Mater.* **2011**, 323, 651; b) P. Clegg, K. Murphy, A. Mardinoglu, A. Prina-Mello, *J. Magn. Magn. Mater.* **2010**, 322, 2087.
- [682] J. A. Ritter, A. D. Ebner, K. D. Daniel, K. L. Stewart, *J. Magn. Magn. Mater.* **2004**, 280, 184.
- [683] O. Rotariu, N. J. Strachan, *J. Magn. Magn. Mater.* **2005**, 293, 639.
- [684] F. Chen, K. A. Smith, T. A. Hatton, *AIChE J.* **2012**, 58, 2865.
- [685] a) J. Zheng, J. Wang, T. Tang, G. Li, H. Cheng, S. Zou, *Chin.-Ger. J. Clin. Oncol.* **2006**, 5, 336; b) P. Clegg, K. Murphy, A. Mardinoglu, *J. Magn. Magn. Mater.* **2009**, 321, 3893.
- [686] N. Pei, Z. Huang, W. Ma, J. Ge, W. Zheng, *J. Magn. Magn. Mater.* **2009**, 321, 2911.
- [687] D. Ortega, Q. A. Pankhurst, in *Nanoscience: Nanostructures through Chemistry*, Vol. 1, (Ed: P. O'Brien), The Royal Society of Chemistry, Cambridge, UK **2013**, pp. 60–88.
- [688] Z. Nemati, J. Alonso, H. Khurshid, M. Phan, H. Srikanth, *RSC Adv.* **2016**, 6, 38697.
- [689] C. Binns, in *Nanostructured Materials for Magnetoelectronics*, Springer, Heidelberg, Germany **2013**, pp. 197–215.
- [690] B. Mehdaoui, A. Meffre, J. Carrey, S. Lachaize, L. M. Lacroix, M. Gougeon, B. Chaudret, M. Respaut, *Adv. Funct. Mater.* **2011**, 21, 4573.
- [691] M. Falk, R. Issels, *Int. J. Hyperthermia* **2001**, 17, 1.
- [692] a) J. van der Zee, *Ann. Oncol.* **2002**, 13, 1173; b) N. Zaffaroni, G. Fiorentini, U. De Giorgi, *Eur. J. Surg. Oncol.* **2001**, 27, 340; c) D. Jia, J. Liu, *Expert Rev. Med. Devices* **2010**, 7, 407.
- [693] a) S. Dutz, R. Hergt, *Nanotechnology* **2014**, 25, 452001; b) R. W. Habash, R. Bansal, D. Krewski, H. T. Alhafid, *Crit. Rev. Bioeng.* **2006**, 34, 491.
- [694] K. Tanaka, A. Ito, T. Kobayashi, T. Kawamura, S. Shimada, K. Matsumoto, T. Saida, H. Honda, *J. Biosci. Bioeng.* **2005**, 100, 112.
- [695] R. Gilchrist, R. Medal, W. D. Shorey, R. C. Hanselman, J. C. Parrott, C. B. Taylor, *Ann. Surg.* **1957**, 146, 596.
- [696] I. Brigger, C. Dubernet, P. Couvreur, *Adv. Drug Delivery Rev.* **2002**, 54, 631.
- [697] R. D. Issels, *Eur. J. Cancer* **2008**, 44, 2546.
- [698] a) A. Jordan, P. Wust, R. Scholz, B. Tesche, H. Fähling, T. Mitrovics, T. Vogl, J. Cervos-Navarro, R. Felix, *Int. J. Hyperthermia* **1996**, 12, 705; b) C. S. Kumar, F. Mohammad, *Adv. Drug Delivery Rev.* **2011**, 63, 789.
- [699] I. Hilger, K. Fröhlauf, W. Andrä, R. Hiergeist, R. Hergt, W. A. Kaiser, *Acad. Radiol.* **2002**, 9, 198.

- [700] a) Q. A. Pankhurst, J. Connolly, S. K. Jones, J. Dobson, *J. Phys. D: Appl. Phys.* **2003**, *36*, R167; b) E. Pollert, K. Závěta, in *Magnetic Nanoparticles: From Fabrication to Clinical Applications*, (Ed: N. T. Thanh), Taylor and Francis group, Boca Raton, US **2012**, pp. 449–479.
- [701] R. W. Rand, H. D. Snow, D. G. Elliott, G. M. Haskins, *Google Patents*, **1985**.
- [702] a) R. Medal, W. Shorey, R. Gilchrist, W. Barker, R. Hanselman, *AMA Arch. Surg.* **1959**, *79*, 427; b) R. Gilchrist, W. Shorey, R. C. Hanselman, F. A. DePeyster, J. Yang, R. Medal, *Ann. Surg.* **1965**, *161*, 890.
- [703] a) M. Johannsen, U. Gneveckow, K. Taymoorian, B. Thiesen, N. Waldöfner, R. Scholz, K. Jung, A. Jordan, P. Wust, S. Loening, *Int. J. Hyperthermia* **2007**, *23*, 315; b) K. Maier-Hauff, F. Ulrich, D. Nestler, H. Niehoff, P. Wust, B. Thiesen, H. Orawa, V. Budach, A. Jordan, *J. Neuro-Oncol.* **2011**, *103*, 317.
- [704] S. Dutz, R. Hergt, *Int. J. Hyperthermia* **2013**, *29*, 790.
- [705] A. E. Deatsch, B. A. Evans, *J. Magn. Magn. Mater.* **2014**, *354*, 163.
- [706] A. Jordan, P. Wust, H. Fähling, W. John, A. Hinz, R. Felix, *Int. J. Hyperthermia* **2009**, *25*, 499.
- [707] a) J.-P. Fortin, C. Wilhelm, J. Servais, C. Ménager, J.-C. Bacri, F. Gazeau, *J. Am. Chem. Soc.* **2007**, *129*, 2628; b) R. Hergt, W. Andra, C. G. d'Amby, I. Hilger, W. A. Kaiser, U. Richter, H.-G. Schmidt, *IEEE Trans. Magn.* **1998**, *34*, 3745.
- [708] J. Carrey, B. Mehdaoui, M. Respaud, *J. Appl. Phys.* **2011**, *109*, 083921.
- [709] C. Dennis, A. Jackson, J. Borchers, P. Hoopes, R. Strawbridge, A. Foreman, J. Van Lierop, C. Grüttner, R. Ivkov, *Nanotechnology* **2009**, *20*, 395103.
- [710] a) G. F. Goya, E. Lima Jr., A. D. Arellano, T. Torres, H. R. Rechenberg, L. Rossi, C. Marquina, M. R. Ibarra, *IEEE Trans. Magn.* **2008**, *44*, 4444; b) K. Bakogiannis, K. Simeonidis, D. Sakellari, G. Stefanou, M. Angelakeris, *IEEE Trans. Magn.* **2012**, *48*, 1320.
- [711] a) W. F. Brown Jr., *J. Appl. Phys.* **1963**, *34*, 1319; b) B. Jeyadevan, *J. Ceram. Soc. Jpn.* **2010**, *118*, 391.
- [712] L. Néel, *J. Phys. Radium* **1952**, *13*, 249.
- [713] a) C. Rivière, C. Wilhelm, F. Cousin, V. Dupuis, F. Gazeau, R. Perzynski, *Eur. Phys. J., E* **2007**, *22*, 1; b) D.-L. Zhao, X.-X. Wang, X.-W. Zeng, Q.-S. Xia, J.-T. Tang, *J. Alloys Compd.* **2009**, *477*, 739.
- [714] a) G. Goya, T. S. Berquó, F. C. Fonseca, M. Morales, *J. Appl. Phys.* **2003**, *94*, 3520; b) J. Wan, G. Tang, Y. Qian, *Appl. Phys. A* **2007**, *86*, 261.
- [715] H. Khurshid, J. Alonso, Z. Nemati, M. Phan, P. Mukherjee, M. Fdez-Gubieda, J. Barandiarán, H. Srikanth, *J. Appl. Phys.* **2015**, *117*, 17A337.
- [716] a) D.-H. Kim, Y. T. Thai, D. E. Nikles, C. S. Brazel, *IEEE Trans. Magn.* **2009**, *45*, 64; b) P. Pradhan, J. Giri, G. Samanta, H. D. Sarma, K. P. Mishra, J. Bellare, R. Banerjee, D. Bahadur, *J. Biomed. Mater. Res., Part B* **2007**, *81*, 12.
- [717] R. Sharma, C. Chen, *J. Nanopart. Res.* **2009**, *11*, 671.
- [718] P. Drake, H.-J. Cho, P.-S. Shih, C.-H. Kao, K.-F. Lee, C.-H. Kuo, X.-Z. Lin, Y.-J. Lin, *J. Mater. Chem.* **2007**, *17*, 4914.
- [719] a) E. Alphandéry, F. Guyot, I. Chebbi, *Int. J. Pharm.* **2012**, *434*, 444; b) Y.-S. Chang, S. Savitha, S. Sadhasivam, C.-K. Hsu, F.-H. Lin, *J. Colloid Interface Sci.* **2011**, *363*, 314.
- [720] a) M. Timko, M. Molcan, A. Hashim, A. Skumił, M. Muller, H. Gojzewski, A. Jozefczak, J. Kovac, M. Rajnak, M. Makowski, *IEEE Trans. Magn.* **2013**, *49*, 250; b) C. Martinez-Boubeta, K. Simeonidis, A. Makridis, M. Angelakeris, O. Iglesias, P. Guardia, A. Cabot, L. Yedra, S. Estradé, F. Peiró, *Sci. Rep.* **2013**, *3*.
- [721] E. Alphandéry, S. Faure, L. Raison, E. Duguet, P. Howse, D. Bazylinski, *J. Phys. Chem., C* **2010**, *115*, 18.
- [722] S. Dutz, R. Hergt, J. Mürbe, R. Müller, M. Zeisberger, W. Andrä, J. Töpfer, M. Bellemann, *J. Magn. Magn. Mater.* **2007**, *308*, 305.
- [723] E. Alphandéry, C. Carvallo, N. Menguy, I. Chebbi, *J. Phys. Chem., C* **2011**, *115*, 11920.
- [724] E. Alphandéry, M. Amor, F. Guyot, I. Chebbi, *Appl. Microbiol. Biotechnol.* **2012**, *96*, 663.
- [725] F. Matsuoka, M. Shinkai, H. Honda, T. Kubo, T. Sugita, T. Kobayashi, *Biomagn. Res. Technol.* **2004**, *2*, 1.
- [726] C. Xu, Y. Zheng, W. Gao, J. Xu, G. Zuo, Y. Chen, M. Zhao, J. Li, J. Song, N. Zhang, *ACS Appl. Mater. Interfaces* **2015**, *7*, 13866.
- [727] a) M. T. Madsen, *J. Nucl. Med.* **2007**, *48*, 661; b) G. D. Luker, K. E. Luker, *J. Nucl. Med.* **2008**, *49*, 1; c) A. Gibson, J. Hebdon, S. R. Arridge, *Phys. Med. Biol.* **2005**, *50*, R1.
- [728] J. Garcia, T. Tang, A. Y. Louie, *Nanomedicine* **2015**, *10*, 1343.
- [729] a) J. H. Lee, Y. W. Jun, S. I. Yeon, J. S. Shin, J. Cheon, *Angew. Chem. 2006*, *118*, 8340; *Angew. Chem. Int. Ed.* **2006**, *45*, 8160; b) X. Cui, D. Mathe, N. Kovács, I. Horváth, M. Jauregui-Osoro, R. Torres Martin de Rosales, G. E. Mullen, W. Wong, Y. Yan, D. Krüger, *Bioconjugate Chem.* **2015**, *27*, 319; c) R. Thomas, I.-K. Park, Y. Y. Jeong, *Int. J. Mol. Sci.* **2013**, *14*, 15910.
- [730] a) J. Kim, Y. Piao, T. Hyeon, *Chem. Soc. Rev.* **2009**, *38*, 372; b) D.-E. Lee, H. Koo, I.-C. Sun, J. H. Ryu, K. Kim, I. C. Kwon, *Chem. Soc. Rev.* **2012**, *41*, 2656.
- [731] a) G. Lamanna, M. Kueny-Stotz, H. Mamlouk-Chauouachi, C. Ghobril, B. Basly, A. Bertin, I. Miladi, C. Billotey, G. Pourroy, S. Begin-Colin, *Biomaterials* **2011**, *32*, 8562; b) E.-J. Cha, E. S. Jang, I.-C. Sun, I. J. Lee, J. H. Ko, Y. I. Kim, I. C. Kwon, K. Kim, C.-H. Ahn, *J. Controlled Release* **2011**, *155*, 152.
- [732] A. J. Sinusas, F. Bengel, M. Nahrendorf, F. H. Epstein, J. C. Wu, F. S. Villanueva, Z. A. Fayad, R. J. Gropler, *Circ.: Cardiovasc. Imaging* **2008**, *1*, 244.
- [733] G. Kandasamy, D. Maity, *Int. J. Pharm.* **2015**, *496*, 191.
- [734] W. R. Hendee, C. J. Morgan, *West. J. Med.* **1984**, *141*, 491.
- [735] P. B. Santhosh, N. P. Ulrich, *Cancer Lett.* **2013**, *336*, 8.
- [736] S. A. Khan, S. Gambhir, A. Ahmad, *Beilstein J. Nanotechnol.* **2014**, *5*, 249.
- [737] a) M. Bartolini, J. Pekar, D. Chettle, F. McNeill, A. Scott, J. Sykes, F. Prato, G. Moran, *Magn. Reson. Imaging* **2003**, *21*, 541; b) F. G. Shellock, E. Kanal, *J. Magn. Reson. Imaging* **1999**, *10*, 477.
- [738] A. S. Wadajkar, J. U. Menon, K. T. Nguyen, *Rev. Nanosci. Nanotechnol.* **2012**, *1*, 284.
- [739] C. Corot, P. Robert, J.-M. Idée, M. Port, *Adv. Drug Delivery Rev.* **2006**, *58*, 1471.
- [740] a) B. Bonnemain, *J. Drug Targeting* **2009**; b) L. Frullano, T. J. Meade, *J. Biol. Inorg. Chem.* **2007**, *12*, 939.
- [741] Y. Gossuin, P. Gillis, A. Hocq, Q. L. Vuong, A. Roch, *Wiley Interdiscip. Rev.: Nanomed. Nanobiotechnol.* **2009**, *1*, 299.
- [742] a) A. J. Cole, V. C. Yang, A. E. David, *Trends Biotechnol.* **2011**, *29*, 323; b) Y.-X. J. Wang, *Quant. Imaging Med. Surg.* **2011**, *1*, 35.
- [743] R. C. Semelka, T. K. Helmberger, *Radiology* **2001**, *218*, 27.
- [744] a) R. a. Weissleder, D. D. Stark, B. L. Engelstad, B. R. Bacon, C. C. Compton, D. L. White, P. Jacobs, J. Lewis, *Am. J. Roentgenol.* **1989**, *152*, 167; b) C.-Y. Yang, M.-F. Tai, S.-T. Chen, Y.-T. Wang, Y.-F. Chen, J.-K. Hsiao, J.-L. Wang, H.-M. Liu, *J. Appl. Phys.* **2009**, *105*, 07B314.
- [745] a) C. T. Farrar, G. Dai, M. Novikov, A. Rosenzweig, R. Weissleder, B. R. Rosen, D. E. Sosnovik, *NMR Biomed.* **2008**, *21*, 453; b) V. Mani, K. C. Briley-Saebo, V. V. Itsckovich, D. D. Samber, Z. A. Fayad, *Magn. Reson. Med.* **2006**, *55*, 126.
- [746] M. C. Pierce, D. J. Javier, R. Richards-Kortum, *Int. J. Cancer* **2008**, *123*, 1979.
- [747] X. Wu, H. Liu, J. Liu, K. N. Haley, J. A. Treadway, J. P. Larson, N. Ge, F. Peale, M. P. Bruchez, *Nat. Biotechnol.* **2003**, *21*, 41.
- [748] a) Q. T. Nguyen, R. Y. Tsien, *Nat. Rev. Cancer* **2013**, *13*, 653; b) E. Sevick-Muraca, *Annu. Rev. Med.* **2012**, *63*, 217.

- [749] H. Kobayashi, M. Ogawa, R. Alford, P. L. Choyke, Y. Urano, *Chem. Rev.* **2009**, *110*, 2620.
- [750] R. Weissleder, M. J. Pittet, *Nature* **2008**, *452*, 580.
- [751] a) X. He, J. Gao, S. S. Gambhir, Z. Cheng, *Trends Mol. Med.* **2010**, *16*, 574; b) V. Ntziachristos, *Annu. Rev. Biomed. Eng.* **2006**, *8*, 1.
- [752] a) T. Heidt, M. Nahrendorf, *NMR Biomed.* **2013**, *26*, 756; b) R. Weissleder, V. Ntziachristos, *Nat. Med.* **2003**, *9*, 123.
- [753] M. J. Pittet, R. Weissleder, *Cell* **2011**, *147*, 983.
- [754] V. Ntziachristos, C. Bremer, R. Weissleder, *Eur. Radiol.* **2003**, *13*, 195.
- [755] a) S. Biju, M. Harris, L. Vander Elst, M. Wolberg, C. Kirschhock, T. N. Parac-Vogt, *RSC Adv.* **2016**, *6*, 61443; b) L. Josephson, M. F. Kircher, U. Mahmood, Y. Tang, R. Weissleder, *Bioconjugate Chem.* **2002**, *13*, 554.
- [756] a) L. Cheng, K. Yang, Y. Li, J. Chen, C. Wang, M. Shao, S. T. Lee, Z. Liu, *Angew. Chem.* **2011**, *123*, 7523; *Angew. Chem. Int. Ed.* **2011**, *50*, 8160; b) E. S. Shibu, K. Ono, S. Sugino, A. Nishioka, A. Yasuda, Y. Shigeri, S.-i. Wakida, M. Sawada, V. Biju, *ACS Nano* **2013**, *7*, 9851.
- [757] Q. Guo, L. Kuang, H. Cao, W. Li, J. Wei, *Colloids Surf., B* **2015**, *136*, 687.
- [758] S. Kim, Y. T. Lim, E. G. Soltesz, A. M. De Grand, J. Lee, A. Nakayama, J. A. Parker, T. Mihaljevic, R. G. Laurence, D. M. Dor, *Nat. Biotechnol.* **2004**, *22*, 93.
- [759] H. Ow, D. R. Larson, M. Srivastava, B. A. Baird, W. W. Webb, U. Wiesner, *Nano Lett.* **2005**, *5*, 113.
- [760] T.-H. Shin, Y. Choi, S. Kim, J. Cheon, *Chem. Soc. Rev.* **2015**, *44*, 4501.
- [761] Y. Piao, A. Burns, J. Kim, U. Wiesner, T. Hyeon, *Adv. Funct. Mater.* **2008**, *18*, 3745.
- [762] a) Z. Medarova, W. Pham, C. Farrar, V. Petkova, A. Moore, *Nat. Med.* **2007**, *13*, 372; b) C.-W. Lu, Y. Hung, J.-K. Hsiao, M. Yao, T.-H. Chung, Y.-S. Lin, S.-H. Wu, S.-C. Hsu, H.-M. Liu, C.-Y. Mou, *Nano Lett.* **2007**, *7*, 149.
- [763] G. Wang, X. Zhang, Y. Liu, Z. Hu, X. Mei, K. Uvdal, *J. Mater. Chem. B* **2015**, *3*, 3072.
- [764] a) C. Chapon, J. S. Jackson, E. O. Aboagye, A. H. Herlihy, W. A. Jones, K. K. Bhakoo, *Mol. Imaging Biol.* **2009**, *11*, 31; b) T. Higuchi, S. G. Nekolla, A. Jankaukas, A. W. Weber, M. C. Huisman, S. Reder, S. I. Ziegler, M. Schwaiger, F. M. Bengel, *J. Nucl. Med.* **2007**, *48*, 288.
- [765] a) A. Kohan, J. Kolthammer, J. Vercher-Conejero, C. Rubbert, S. Partovi, R. Jones, K. Herrmann, P. Faulhaber, *Eur. Radiol.* **2013**, *23*, 3161; b) S. Nagamachi, R. Nishii, H. Wakamatsu, Y. Mizutani, S. Kiyohara, S. Fujita, S. Futami, T. Sakae, E. Furukoji, S. Tamura, *Ann. Nucl. Med.* **2013**, *27*, 554.
- [766] a) M. S. Judenhofer, H. F. Wehr, D. F. Newport, C. Catana, S. B. Siegel, M. Becker, A. Thielscher, M. Kneilling, M. P. Lichy, M. Eichner, *Nat. Med.* **2008**, *14*, 459; b) H.-P. W. Schlemmer, B. J. Pichler, M. Schmand, Z. Burbar, C. Michel, R. Ladebeck, K. Jattke, D. Townsend, C. Nahmias, P. K. Jacob, *Radiology* **2008**, *248*, 1028.
- [767] a) F. Leuschner, M. Nahrendorf, *Circ. Res.* **2011**, *108*, 593; b) S. R. Cherry, A. Y. Louie, R. E. Jacobs, *Proc. IEEE* **2008**, *96*, 416.
- [768] a) D. Chen, C. A. Dougherty, D. Yang, H. Wu, H. Hong, *Tomogr. J. Imaging Res.* **2016**, *2*, 3; b) F. Ai, C. A. Ferreira, F. Chen, W. Cai, *Wiley Interdiscip. Rev.: Nanomed. Nanobiotechnol.* **2015**.
- [769] a) J. Huang, J. Xie, K. Chen, L. Bu, S. Lee, Z. Cheng, X. Li, X. Chen, *Chem. Commun.* **2010**, *46*, 6684; b) M. H. Pablo-Lansigan, S. F. Situ, A. C. S. Samia, *Nanoscale* **2013**, *5*, 4040.
- [770] X. Cui, S. Belo, D. Krüger, Y. Yan, R. T. de Rosales, M. Jauregui-Osoro, H. Ye, S. Su, D. Mathe, N. Kovács, *Biomaterials* **2014**, *35*, 5840.
- [771] H. Y. Ko, J. H. Lee, H. Kang, S. H. Ryu, I. C. Song, D. S. Lee, S. Kim, *J. Nucl. Med.* **2010**, *51*, 98.
- [772] J. S. Kim, Y.-H. Kim, J. H. Kim, K. W. Kang, E. L. Tae, H. Youn, D. Kim, S.-K. Kim, J.-T. Kwon, M.-H. Cho, *Nanomedicine* **2012**, *7*, 219.
- [773] G. Baldi, D. Bonacchi, C. Innocenti, G. Lorenzi, C. Sangregorio, *J. Magn. Magn. Mater.* **2007**, *311*, 10.
- [774] S. R. Cherry, *Semin. Nucl. Med.* **2009**, *39*, 348.
- [775] M. J. Welch, C. J. Hawker, K. L. Wooley, *J. Nucl. Med.* **2009**, *50*, 1743.
- [776] H. S. Choi, W. Liu, P. Misra, E. Tanaka, J. P. Zimmer, B. I. Ipe, M. G. Bawendi, J. V. Frangioni, *Nat. Biotechnol.* **2007**, *25*, 1165.
- [777] B. J. Pichler, A. Kolb, T. Nägele, H.-P. Schlemmer, *J. Nucl. Med.* **2010**, *51*, 333.
- [778] S. M. Ametamey, M. Honer, P. A. Schubiger, *Chem. Rev.* **2008**, *108*, 1501.
- [779] a) F. Chen, P. A. Ellison, C. M. Lewis, H. Hong, Y. Zhang, S. Shi, R. Hernandez, M. E. Meyerand, T. E. Barnhart, W. Cai, *Angew. Chem.* **2013**, *125*, 13561; *Angew. Chem. Int. Ed.* **2013**, *52*, 13319; b) R. Chakravarty, H. F. Valdovinos, F. Chen, C. M. Lewis, P. A. Ellison, H. Luo, M. E. Meyerand, R. J. Nickles, W. Cai, *Adv. Mater.* **2014**, *26*, 5119.
- [780] J. Luo, J. D. Wilson, J. Zhang, J. I. Hirsch, H. C. Dorn, P. P. Fatouros, M. D. Shultz, *Appl. Sci.* **2012**, *2*, 465.
- [781] T. J. Wadas, E. H. Wong, G. R. Weisman, C. J. Anderson, *Chem. Rev.* **2010**, *110*, 2858.
- [782] a) X. Yang, H. Hong, J. J. Grailer, I. J. Rowland, A. Javadi, S. A. Hurley, Y. Xiao, Y. Yang, Y. Zhang, R. J. Nickles, *Biomaterials* **2011**, *32*, 4151; b) S. Aryal, J. Key, C. Stigliano, M. D. Landis, D. Y. Lee, P. Decuzzi, *Small* **2014**, *10*, 2688.
- [783] J. s. Choi, J. C. Park, H. Nah, S. Woo, J. Oh, K. M. Kim, G. J. Cheon, Y. Chang, J. Yoo, J. Cheon, *Angew. Chem.* **2008**, *120*, 6355; *Angew. Chem. Int. Ed.* **2008**, *47*, 6259.
- [784] H.-Y. Lee, Z. Li, K. Chen, A. R. Hsu, C. Xu, J. Xie, S. Sun, X. Chen, *J. Nucl. Med.* **2008**, *49*, 1371.
- [785] S.-H. Moon, B. Y. Yang, Y. J. Kim, M. K. Hong, Y.-S. Lee, D. S. Lee, J.-K. Chung, J. M. Jeong, *Nanomed.: Nanotechnol., Biol. Med.* **2016**, *12*, 871.
- [786] a) O. Schillaci, G. Simonetti, *Cancer Biother. Radiopharm.* **2004**, *19*, 1; b) J. Booij, K. de Bruin, M. M. de Win, C. Lavini, G. J. den Heeten, J. B. Habraken, *Nucl. Med. Biol.* **2003**, *30*, 643.
- [787] S. Deng, W. Zhang, B. Zhang, R. Hong, Q. Chen, J. Dong, Y. Chen, Z. Chen, Y. Wu, *J. Nanopart. Res.* **2015**, *17*, 1.
- [788] P. Bouziotis, D. Psimadas, T. Tsotakos, D. Stamopoulos, C. Tsoukalas, *Curr. Top. Med. Chem.* **2012**, *12*, 2694.
- [789] T. Schurrat, H. Alfke, M. Béhé, T. Maina, B. Nock, H. Mäcke, J. T. Heverhagen, K. J. Klose, H. Halling, T. M. Behr, *Eur. J. Nucl. Med. Mol. Imaging* **2003**, *30*, 800.
- [790] D. Berman, H. Kiat, K. Van Train, J. Friedman, F. Wang, G. Germano, *Cardiol. Clin.* **1994**, *12*, 261.
- [791] a) P. G. Sanches, S. Peters, R. Rossin, E. L. Kaijzel, I. Que, C. W. Löwik, H. Grüll, *Bone* **2015**, *75*, 62; b) M. J. Hamamura, S. Ha, W. W. Roeck, L. T. Muftuler, D. J. Wagenaar, D. Meier, B. E. Patt, O. Nalcioglu, *Phys. Med. Biol.* **2010**, *55*, 1563.
- [792] a) S. W. Zielhuis, J.-H. Seppenwoolde, V. A. Mateus, C. J. Bakker, G. C. Krijger, G. Storm, B. A. Zonnenberg, A. D. v. h. Schip, G. A. Koning, J. F. Nijsen, *Cancer Biother. Radiopharm.* **2006**, *21*, 520; b) R. Madru, P. Kjellman, F. Olsson, K. Wingårdh, C. Ingvar, F. Ståhlberg, J. Olsrud, J. Lätt, S. Fredriksson, L. Knutsson, *J. Nucl. Med.* **2012**, *53*, 459; c) M. Lijowski, S. Caruthers, G. Hu, H. Zhang, M. J. Scott, T. Williams, T. Erpelding, A. H. Schmieder, G. Kiefer, G. Gulyas, *Invest. Radiol.* **2009**, *44*, 15.
- [793] a) C. Goetz, E. Breton, P. Choquet, V. Israel-Jost, A. Constantinesco, *J. Nucl. Med.* **2008**, *49*, 88; b) R. Misri, D. Meier, A. C. Yung, P. Kozlowski, U. O. Häfeli, *Nanomed.: Nanotechnol., Biol. Med.* **2012**, *8*, 1007.

- [794] Q. Meng, Z. Li, *Int. J. Biomed. Imaging* **2013**, 2013, 2.
- [795] J. Wang, H. Zhao, Z. Zhou, P. Zhou, Y. Yan, M.-W. Wang, H. Yang, Y. Zhang, S.-P. Yang, *ACS Appl. Mater. Interfaces* **2016**.
- [796] C. Catana, D. Prociassi, Y. Wu, M. S. Judenhofer, J. Qi, B. J. Pichler, R. E. Jacobs, S. R. Cherry, *Proc. Natl. Acad. Sci. USA* **2008**, 105, 3705.
- [797] B. J. Pichler, H. F. Wehrle, M. S. Judenhofer, *J. Nucl. Med.* **2008**, 49, 55.
- [798] a) Y. Liu, K. Ai, L. Lu, *Acc. Chem. Res.* **2012**, 45, 1817; b) H. Y. Zhao, S. Liu, J. He, C. C. Pan, H. Li, Z. Y. Zhou, Y. Ding, D. Huo, Y. Hu, *Biomaterials* **2015**, 51, 194.
- [799] L. W. Goldman, *J. Nucl. Med. Technol.* **2007**, 35, 115.
- [800] D. Kim, S. Park, J. H. Lee, Y. Y. Jeong, S. Jon, *J. Am. Chem. Soc.* **2007**, 129, 7661.
- [801] K. C.-F. Leung, S. Xuan, X. Zhu, D. Wang, C.-P. Chak, S.-F. Lee, W. K.-W. Ho, B. C.-T. Chung, *Chem. Soc. Rev.* **2012**, 41, 1911.
- [802] a) H. Wang, H. Wang, Z. Liu, *Drug Discoveries Ther.* **2011**, 5; b) K. M. Hasebrook, N. J. Serkova, *Expert Opin. Drug Metab. Toxicol.* **2009**, 5, 403.
- [803] D. Kim, J. W. Kim, Y. Y. Jeong, S. Jon, *Bull. Korean Chem. Soc.* **2009**, 30, 1855.
- [804] a) M. W. Galper, M. T. Saung, V. Fuster, E. Roessl, A. Thran, R. Proksa, Z. A. Fayad, D. P. Cormode, *Invest. Radiol.* **2012**, 47, 475; b) C. Peng, L. Zheng, Q. Chen, M. Shen, R. Guo, H. Wang, X. Cao, G. Zhang, X. Shi, *Biomaterials* **2012**, 33, 1107.
- [805] a) J. Li, Y. Hu, J. Yang, P. Wei, W. Sun, M. Shen, G. Zhang, X. Shi, *Biomaterials* **2015**, 38, 10; b) H. Wang, L. Zheng, C. Peng, R. Guo, M. Shen, X. Shi, G. Zhang, *Biomaterials* **2011**, 32, 2979.
- [806] a) J. Gao, H. Gu, B. Xu, *Acc. Chem. Res.* **2009**, 42, 1097; b) D. Kim, M. K. Yu, T. S. Lee, J. J. Park, Y. Y. Jeong, S. Jon, *Nanotechnology* **2011**, 22, 155101.
- [807] a) D. A. Giljohann, D. S. Seferos, W. L. Daniel, M. D. Massich, P. C. Patel, C. A. Mirkin, *Angew. Chem.* **2010**, 122, 3352; *Angew. Chem. Int. Ed.* **2010**, 49, 3280; b) H. Cai, K. Li, J. Li, S. Wen, Q. Chen, M. Shen, L. Zheng, G. Zhang, X. Shi, *Small* **2015**, 11, 4584.
- [808] L. E. Kelderhouse, V. Chelvam, C. Wayua, S. Mahalingam, S. Poh, S. A. Kularatne, P. S. Low, *Bioconjugate Chem.* **2013**, 24, 1075.
- [809] a) H. Lusic, M. W. Grinstaff, *Chem. Rev.* **2012**, 113, 1641; b) K. Wang, H. Peng, K. J. Thurecht, S. Puttick, A. K. Whittaker, *Polym. Chem.* **2016**, 7, 1059.
- [810] a) J. Li, L. Zheng, H. Cai, W. Sun, M. Shen, G. Zhang, X. Shi, *ACS Appl. Mater. Interfaces* **2013**, 5, 10357; b) Y. Hu, J. Yang, P. Wei, J. Li, L. Ding, G. Zhang, X. Shi, M. Shen, *J. Mater. Chem. B* **2015**, 3, 9098.
- [811] a) Z. Ali, A. Abbasi, F. Zhang, P. Arosio, A. Lascialfari, M. Casula, A. Wenk, W. Kreyling, R. Plapper, M. Seidel, *Anal. Chem.* **2011**, 83, 2877; b) D. P. Cormode, P. C. Naha, Z. A. Fayad, *Contrast Media Mol. Imaging* **2014**, 9, 37.
- [812] a) Y. Hu, R. Wang, S. Wang, L. Ding, J. Li, Y. Luo, X. Wang, M. Shen, X. Shi, *Sci. Rep.* **2016**, 6; b) Y. Cao, Y. He, H. Liu, Y. Luo, M. Shen, J. Xia, X. Shi, *J. Mater. Chem. B* **2015**, 3, 286.
- [813] N. Panagiotopoulos, R. L. Duschka, M. Ahlborg, G. Bringout, C. Debbeler, M. Graeser, C. Kaethner, K. Lüdtke-Buzug, H. Medimagh, J. Stelzner, *Int. J. Nanomed.* **2015**, 10, 3097.
- [814] B. Gleich, J. Weizenecker, *Nature* **2005**, 435, 1214.
- [815] a) H. Arami, K. M. Krishnan, *IEEE Trans. Magn.* **2013**, 49, 3500; b) J. Borgert, J. D. Schmidt, I. Schmale, J. Rahmer, C. Bontus, B. Gleich, B. David, R. Eckart, O. Woywode, J. Weizenecker, *J. Cardiovasc. Comput. Tomogr.* **2012**, 6, 149.
- [816] E. U. Saritas, P. W. Goodwill, L. R. Croft, J. J. Konkle, K. Lu, B. Zheng, S. M. Conolly, *J. Magn. Reson.* **2013**, 229, 116.
- [817] R. M. Ferguson, A. P. Khandhar, K. M. Krishnan, *J. Appl. Phys.* **2012**, 111, 07B318.
- [818] a) B. Zheng, T. Vazin, P. W. Goodwill, A. Conway, A. Verma, E. U. Saritas, D. Schaffer, S. M. Conolly, *Sci. Rep.* **2015**,
- 5; b) B. Zheng, P. Marc, E. Yu, B. Gunel, K. Lu, T. Vazin, D. V. Schaffer, P. W. Goodwill, S. M. Conolly, *Theranostics* **2016**, 6, 291.
- [819] K. Murase, M. Aoki, N. Banura, K. Nishimoto, A. Mimura, K. Hamakawa, T. Kuboyabu, I. Yabata, presented at *Int. Workshop Magn. Part. Imaging (IWMPPI), Usefulness of Magnetic Particle Imaging for Monitoring the Therapeutic Effect of Magnetic Hyperthermia*, Istanbul, Turkey, March **2015**.
- [820] a) J. Rahmer, J. Weizenecker, B. Gleich, J. Borgert, *BMC Med. Imaging* **2009**, 9, 1; b) P. W. Goodwill, G. C. Scott, P. P. Stang, S. M. Conolly, *IEEE Trans. Med. Imaging* **2009**, 28, 1231.
- [821] R. L. Duschka, J. Haegele, N. Panagiotopoulos, H. Wojtczyk, J. Barkhausen, F. M. Vogt, T. M. Buzug, K. Lüdtke-Buzug, *Curr. Cardiovasc. Imaging Rep.* **2013**, 6, 390.
- [822] a) T. Knopp, S. Biederer, T. Sattel, J. Weizenecker, B. Gleich, J. Borgert, T. Buzug, *Phys. Med. Biol.* **2008**, 54, 385; b) J. Weizenecker, B. Gleich, J. Rahmer, H. Dahnke, J. Borgert, *Phys. Med. Biol.* **2009**, 54, L1.
- [823] J. Rahmer, B. Gleich, C. Bontus, I. Schmale, J. Schmidt, J. Kanzenbach, O. Woywode, J. Weizenecker, J. Borgert, presented at *Proc. Intl. Soc. Mag. Reson. Med., Results on Rapid 3d Magnetic Particle Imaging with a Large Field of View*, Canada, May **2011**.
- [824] a) B. Gleich, *Principles and Applications of Magnetic Particle Imaging*, Springer Fachmedien Wiesbaden, **2013**; b) T. Knopp, T. M. Buzug, *Magnetic Particle Imaging: An Introduction to Imaging Principles and Scanner Instrumentation*, Springer Berlin Heidelberg, **2012**; c) T. M. Buzug, J. Borgert, *Magnetic Particle Imaging: A Novel SPIO Nanoparticle Imaging Technique*, Springer Berlin Heidelberg, Germany **2012**; d) T. Knopp, *Effiziente Rekonstruktion und alternative Spulentopologien für Magnetic-Particle-Imaging*, Vieweg+Teubner Verlag, Wiesbaden, Germany **2011**.
- [825] S. Chikazumi, S. H. Charap, *Physics of Magnetism*, R. E. Krieger Pub. Co. **1978**, p. 117.
- [826] a) P. W. Goodwill, S. M. Conolly, *IEEE Trans. Med. Imaging* **2011**, 30, 1581; b) S. Biederer, T. Knopp, T. Sattel, K. Lüdtke-Buzug, B. Gleich, J. Weizenecker, J. Borgert, T. Buzug, *J. Phys. D: Appl. Phys.* **2009**, 42, 205007.
- [827] a) J. Rahmer, J. Weizenecker, B. Gleich, J. Borgert, *IEEE Trans. Med. Imaging* **2012**, 31, 1289; b) T. Knopp, J. Rahmer, T. Sattel, S. Biederer, J. Weizenecker, B. Gleich, J. Borgert, T. Buzug, *Phys. Med. Biol.* **2010**, 55, 1577.
- [828] T. Kuboyabu, I. Yabata, M. Aoki, N. Banura, K. Nishimoto, A. Mimura, K. Murase, *Open J. Med. Imaging* **2016**, 6, 1.
- [829] M. Xu, L. V. Wang, *Rev. Sci. Instrum.* **2006**, 77, 041101.
- [830] C. Li, L. V. Wang, *Phys. Med. Biol.* **2009**, 54, R59.
- [831] a) A. P. Jathoul, J. Laufer, O. Ogunlade, B. Treeby, B. Cox, E. Zhang, P. Johnson, A. R. Pizzey, B. Philip, T. Marafioti, *Nat. Photonics* **2015**, 9, 239; b) P. Beard, *Interface focus* **2011**, 1, 602.
- [832] a) J.-T. Oh, M.-L. Li, H. F. Zhang, K. Maslov, G. Stoica, L. V. Wang, *J. Biomed. Opt.* **2006**, 11, 034032; b) X. Wang, Y. Pang, G. Ku, G. Stoica, L. V. Wang, *Opt. Lett.* **2003**, 28, 1739.
- [833] W. Cai, T. Gao, H. Hong, J. Sun, *Nanotechnol., Sci. Appl.* **2008**, 2008.
- [834] E. V. Shashkov, M. Everts, E. I. Galanzha, V. P. Zharov, *Nano Lett.* **2008**, 8, 3953.
- [835] G. Kim, S.-W. Huang, K. C. Day, M. O'Donnell, R. R. Agayan, M. A. Day, R. Kopelman, S. Ashkenazi, *J. Biomed. Opt.* **2007**, 12, 044020.
- [836] A. De La Zerda, C. Zavaleta, S. Keren, S. Vaithilingam, S. Bodapati, Z. Liu, J. Levi, B. R. Smith, T.-J. Ma, O. Oralkan, *Nat. Nanotechnol.* **2008**, 3, 557.
- [837] G. Ku, L. V. Wang, *Opt. Lett.* **2005**, 30, 507.
- [838] X. Ji, R. Shao, A. M. Elliott, R. J. Stafford, E. Esparza-Coss, J. A. Bankson, G. Liang, Z.-P. Luo, K. Park, J. T. Markert, *J. Phys. Chem., C* **2007**, 111, 6245.